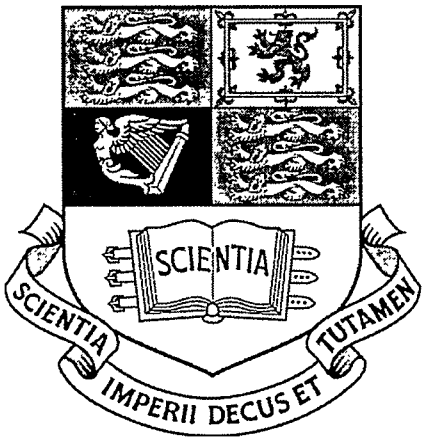
THREE-PHASE GAS/LIQUID/LIQUID SLUG FLOW



Utomi Ayodele Odozi

A thesis submitted in fulfilment of the requirements for
the degree of Doctor of Philosophy of the University of London and for
the Diploma of Imperial College of Science, Technology and Medicine

Department of Chemical Engineering and Chemical Technology
Imperial College of Science Technology and Medicine
London SW7 2BY , United Kingdom

SEPTEMBER 2000

ROY. LONDON UNIV.

ABSTRACT

In this thesis, a study of three-phase air-oil-water flow in horizontal and inclined pipes, with particular emphasis on the slug flow regime is described. Slug flow is one of the most predominant flow patterns that occur in oil pipelines. The experiments described here were all carried out in the WASP Multiphase Flow facility situated in the Department of Chemical Engineering at the Imperial College, London.

The objectives of the project were to generate detailed data on three-phase air-oil-water flow, develop improved analytical frameworks for the prediction of three-phase flows and obtain detailed data on slug parameters such as slug velocity, slug length, slug body holdup and slug frequency. In addition to these, it was the aim of this project to extend CFD techniques from two-phase to the three-phase flow case.

In addressing these objectives, experiments were carried out in which pressure drop and liquid holdup were measured. These data particularly highlighted the anomalous behaviour of air-oil-water slug flow, particularly around the phase inversion region were relatively high pressure gradients and liquid holdups were recorded.

In addition to these, based on a comprehensive database of three-phase air-oil-water slug flow, a new correlation was formulated for the prediction of the phase inversion water-cut. This correlation was shown to improve predictions of the pressure drop and liquid holdup.

Slug parameters were also measured experimentally and these revealed some new findings. Foremost amongst these new findings were the relatively high values recorded for the slug translational velocity in the phase inversion region, a result not predicted by existing two-phase correlations.

A commercially available CFD code has been used to simulate three-phase air-oil-water slug flow in a pipeline and the results obtained have been compared favourably with the experimental data.

ACKNOWLEDGEMENT

I would like to express my gratitude to my supervisors Professor G.F. Hewitt and Dr. M. A. Mendes-Tatsis for giving me the opportunity to carry out research into the subject of Multiphase Flow under their supervision. Furthermore, I extend thanks to them for their support, guidance and encouragement.

I wish to thank my parents Victor and Theresa Odozi for their unceasing support throughout my studies. For this I am truly grateful. I also wish to thank my sister Isioma and brother Nnamdi for their companionship and friendship all through the years.

My colleagues in the Multiphase Flow System Group Consortium both past and present deserve a mention here for their support, advice and camaraderie, which made working with them such a pleasant experience. Special mention here of Colin Hale for his numerous insightful discussions on multiphase flow amongst other matters. I apologise for not mentioning names specifically for lack of space.

Special thanks are deserved by the Workshop (Bob King), Computer Services (Richard Wood and Garry Mohammed), the Electronics Workshop (Malcolm, Peter and Richard), and Technical Services (Pim Amrit) for their support during the experimental work. Mention must be included here of Mr Sid Fisher and Mr Elios Jorisi for their invaluable assistance with the experimental facility. In addition, I would like to thank members of the Library, General Stores and the General Office for their support .

Thanks are also extended to the members of the WASP Consortium for financially supporting this PhD research project.

TABLE OF CONTENTS

Title page		1
Abstract		2
Acknowledgement		3
Table of Contents		4
List of Figures		8
List of Tables		34
Nomenclature		35
CHAPTER 1	**INTRODUCTION**	**40**
CHAPTER 2	**LITERATURE REVIEW**	**43**
2.1	TWO-PHASE GAS-LIQUID FLOW	44
2.1.1	Pressure Drop	44
2.1.1.1	Pressure Drop Correlations	45
2.1.1.1.1	Dukler *et al.* (1964)	46
2.1.1.1.2	Beggs and Brill (1973)	47
2.1.1.1.3	Lockhart and Martinelli (1949)	48
2.1.1.1.4	Chisholm (1967)	50
2.1.1.1.5	Schlichting (1970)	51
2.1.2	Holdup	52
2.1.2.1	Liquid Holdup Correlations	52
2.1.2.1.1	Lockhart and Martinelli (1949)	52
2.1.2.1.2	Guzhov *et al.* (1967)	52
2.1.2.1.3	Beggs and Brill (1973)	53
2.1.2.1.4	Minami and Brill (1987)	54
2.1.3	Slug Flow	55
2.1.3.1	Phenomenological Models	55
2.1.3.1.1	Bonnecaze *et al.* (1971)	56
2.1.3.1.2	Taitel and Barnea (1990)	58
2.1.3.2	Slug Parameters	64
2.1.3.2.1	Slug Length	64
2.1.3.2.2	Slug Velocity	67
2.1.3.2.3	Slug Body Holdup	70
2.1.3.2.4	Slug Frequency	74
2.2	TWO-PHASE LIQUID-LIQUID FLOW	78
2.2.1	Flow Pattern	78
2.2.2	Pressure Drop	79
2.2.2.1	Viscosity Models	79
2.2.3	Holdup	83
2.3	THREE PHASE GAS-LIQUID-LIQUID FLOW	83
2.3.1	Flow Patterns	83
2.3.2	Pressure Drop	91
2.3.3	Holdup	98
2.3.4	Slug Flow	100
2.3.4.1	Slug Frequency	100
2.3.4.2	Slug Velocity	100

2.4 SUMMARY 102

CHAPTER 3 EXPERIMENTAL APPARATUS AND PROCEDURES 121
3.1 THE WASP FACILITY 121
3.2 PROPERTIES OF WASP FLUIDS 122
3.2.1 Oil 122
3.2.2 Water 122
3.2.3 Air 122
3.3 INSTRUMENTATION 123
3.3.1 Pressure Drop Measurement 123
3.3.2 Liquid Holdup Measurement 123
3.3.2.1 Single Beam Dual Energy Gamma Densitometer 124
3.3.3 Slug Velocity Measurement 126
3.3.3.1 Triple Beam Dual Energy Gamma Densitometer 127
3.3.3.2 Cross correlation Method 128
3.4 EXPERIMENTAL CAMPAIGNS
3.4.1 Campaign #1 (January –March 1997) 128
3.4.2 Campaign #2 (August –October 1997) 129
3.4.3 Campaign #3 (September 1998) 130
3.4.4 Campaign #4 (July –September 1999) 130

CHAPTER 4 EXPERIMENTAL RESULTS FOR PRESSURE GRADIENT, LIQUID FRACTIONS AND SLUG CHARACTERISTICS 140
4.1 PRESSURE GRADIENT 140
4.1.1 Effect of Air Superficial Velocity 141
4.1.1.1 Horizontal Flows 141
4.1.1.2 Inclined Flows 144
4.1.2 Effect of Total Liquid Superficial Velocity 145
4.1.2.1 Horizontal Flows 145
4.1.2.2 Inclined Flows 145
4.1.3 Effect of Oil Superficial Velocity 146
4.1.4 Effect of system pressure 147
4.1.5 Effect of flow pattern 147
4.2 MEAN LIQUID HOLDUP 148
4.2.1 Effect of Air Superficial Velocity 149
4.2.2 Effect of Liquid Superficial Velocity 150
4.2.2.1 Horizontal Flows 150
4.2.2.2 Inclined flows 150
4.2.3 Effect of system Pressure 150
4.3 PHASIC HOLDUPS 151
4.3.1 Effect of Air Superficial Velocity 151
4.4 SLIP RATIOS 152
4.5 SLUG FREQUENCY 153
4.5.1 Effect of Air Superficial Velocity 153
4.5.2 Effect of Total Liquid Superficial Velocity 155
4.6 SLUG BODY HOLDUP 155
4.6.1 Effect of Air Superficial Velocity 155
4.6.2 Effect Of Liquid Superficial Velocity 156
4.7 LIQUID FILM HOLDUP 156

4.7.1 Effect of Air Superficial Velocity 156
4.7.2 Effect of Liquid Superficial Velocity 156
4.7.3 Effect of System Pressure 157
4.8 SLUG VELOCITY 157
4.8.1 Effect of Total liquid superficial velocity 158
4.9 SLUG LENGTH 159
4.9.1 Effect of Air Superficial Velocity 159
4.9.2 Effect of Liquid Superficial Velocity 160
4.10 SUMMARY 160

CHAPTER 5 FLOW PATTERN AND FLOW PATTERN MAPS 186
5.1 FLOW REGIMES 186
5.1.1 Terminology 186
5.1.2 Description 188
5.2 FLOW PATTERN MAPS 190
5.2.1 Horizontal Flow Pattern Maps 190
5.2.1.1 Effect of system pressure on Flow pattern in Horizontal flow 193
5.2.2 Inclined Flow Pattern Maps 193
5.2.2.1 Effect of system pressure on flow pattern in downwards inclined flow 194
5.2.3 Effect of Inclination Angle on Flow Pattern Transition 196
5.3 COMPARISON WITH OTHER FLOW PATTERN MAPS 197
5.3.1 Comparisons of Flow pattern data with flow pattern map of Acikgoz *et al.* (1992). 197
5.3.1.1 Horizontal Data 198
5.3.1.2 Inclined Data 198
5.3.2 Comparisons of flow pattern data with flow pattern map of Pan (1996) 199
5.3.2.1 Horizontal Data 199
5.3.2.2 Inclined Data 201
5.4 SUMMARY201

CHAPTER 6 COMPARISON OF DATA WITH PREDICTIVE METHODS 209
6.1 A MODEL FOR MEAN LIQUID VISCOSITY IN THREE PHASE FLOW 211
6.2 COMPARISON OF DATA WITH TWO-PHASE GAS-LIQUID FLOW PRESSURE DROP CORRELATIONS 214
6.2.1 Dukler *et al.* (1964) 215
6.2.2 Chisholm(1967) 216
6.2.3 Beggs and Brill (1973) 216
6.2.4 Lockhart and Martinelli (1949) 217
6.2.5 Schlichting (1970) 217
6.2.6 Statistical Comparisons 218
6.3 PRESSURE DROP PHENOMENOLOGICAL MODELS 219
6.3.1 Bonnecaze *et al.* (1970) 220
6.3.2 Taitel and Barnea (1990) 220
6.4 MEAN LIQUID HOLDUP CORRELATIONS 222
6.4.1 Lockhart and Martinelli (1949) 222

6.4.2 Guzhov *et al.* (1967) 223
6.4.3 Beggs and Brill (1973) 224
6.4.4 Minami and Brill (1987) 224
6.4.5 Statistical comparisons 225
6.5 SLUG FREQUENCY 225
6.5.1 Gregory and Scott (1969) 226
6.5.2 Heywood and Richardson (1979) 226
6.5.3 Tronconi (1990) 227
6.5.4 Hill and Wood (1990) 228
6.5.5 Manolis (1995) 228
6.5.6 Statistical Comparisons 229
6.6 SLUG BODY HOLDUP229
6.6.1 Gregory *et al.* (1978) 229
6.6.2 Ferschneider (1983) 230
6.6.3 Malnes (1983) 230
6.6.4 Gomez *et al.* (2000) 230
6.7 SLUG LENGTH 231
6.8 SLUG VELOCITY 232
6.8.1 Comparison with Bendiksen (1984) 232
6.8.2 CFD Prediction of Translational Velocity 232
6.8.2.1 Previous work on CFD prediction of slug velocity 233
6.8.2.2 Description of the CFX software 233
6.8.2.3 Simulation set-up 236
6.8.2.4 Results 237
6.9 SUMMARY AND OVERVIEW 238

CHAPTER 7 CONCLUSIONS AND RECOMMENDATIONS FOR FUTURE WORK 291
7.1 CONCLUSIONS 291
7.1.1 Steady state results 291
7.1.2 Flow Patterns and Flow Pattern Maps 292
7.1.3 Comparisons with empirical correlations 293
7.1.4 Comparisons with Phenomenological models 294
7.1.5 Comparisons with CFD Code 294
7.2 FUTURE WORK 295
7.2.1 Steady state flows 295
7.2.2 CFD Study 295

REFERENCES 297
APPENDICES 306
APPENDIX A WASP EXPERIMENTAL DATA 306
APPENDIX B DEFINITION OF STATISTICAL ERRORS 326

LIST OF FIGURES

CHAPTER 2

Figure 2.1: Flow Patterns in Horizontal two-phase flow (Hewitt 1982).

Figure 2.2: Gas-Liquid Flow Pattern Map (Mandhane *et al.* 1974).

Figure 2.3 Generalised Gas-Liquid Flow Pattern Map (Taitel and Dukler 1976).

Figure 2.4 Slug Flow Geometry (Taitel and Barnea 1990).

Figure 2.5 Mean slug lengths d=5 cm from air-water slug flow experiments (Nydal, 1991).

Figure 2.6 Mean values of C_o as measured by Nydal (1991).

Figure 2.7 Mean slug body void fraction plotted against total mixture superficial velocity for a range of pipe inclination angles (Andreussi and Bendiksen, 1989).

Figure 2.8 Mean slug body void fraction plotted against total mixture superficial velocity for a range of pipe inclination angles (Andreussi and Bendiksen, 1989).

Figure 2.9 Mean slug body void fraction plotted against total mixture superficial velocity for two different pipe inclination angles Ferschneider (1983)

Figure 2.10 Mean void fraction in the slug. The dotted line is the empirical correlation by Gregory *et al.* (1978) and the solid line is the correlation by Andreussi and Bendiksen (1989)

Figure 2.11 Mean void fraction in the slugs for a range of pipe inclination angles (Andreussi and Bendiksen, 1989)

Figure 2.12 Slug frequency versus total mixture velocity (Nydal, 1991)

Figure 2.13a Oil/Water Flow Patterns (Trallero, 1995).

Figure 2.13b Oil/Water Flow Patterns (Trallero, 1995)

Figure 2.14 Two-phase kerosene-water experimental results of Soleimani (1999) for a horizontal pipe.

Figure 2.15 Plot obtained by Malinowsky (1975) of the Sobosinski(1955) flow pattern data on the revised Beggs and Brill (1973) flow pattern map.

Figure 2.16 Acikgoz *et al.* (1992) three-phase flow pattern map (horizontal pipe: $U_{O,S}$=0.095 m/s; p=0 barg)

Figure 2.17 Pan (1996) three-phase flow pattern map (horizontal pipe: $U_{O,S}$=0.095 m/s; p=0 barg)

Figure 2.18 Pan (1996) three-phase flow pattern map (horizontal pipe: $U_{O,S}$=0.095 m/s; p=5 barg)

Figure 2.19 Pan (1996) three phase flow pattern map (1° upwardly inclined $U_{O,S}$=0.095 m/s; p=5 barg)

Figure 2.20 Comparison of the Pan (1996) three-phase flow pattern data with the three-phase flow map of Acikgoz *et al.* (1992) for 5 barg

Figure 2.21 Comparison of the Pan (1996) three-phase flow pattern data with the three-phase flow map of Acikgoz *et al.* (1992) for 0 barg.

Figure 2.22 Comparison of the Pan (1996) three-phase flow pattern data with the two-phase flow map of Beggs and Brill (1973) for 0 barg.

Figure 2.23 Three-phase air-oil-water experimental results of Pan (1996) for a horizontal pipe.

Figure 2.24 Three-phase air-oil-water pressure gradient experimental results of Donnelly (1997) for liquid superficial velocities 0.0773 m/s and 0.0329 m/s respectively.

Figure 2.25 Three-phase air-oil-water pressure gradient experimental results of Donnelly (1997).

Figure 2.26 Three-phase air-oil-water pressure gradient experimental results of Donnelly for a total liquid flowrate 6L/min for a range of gas flowrates(1997).

Figure 2.27 Three-phase air-oil-water holdup experimental results of Pan for air superficial velocity 2 m/s, oil superficial velocity 2 m/s, oil superficial velocity 0.1 m/s and pressure 0 barg. (1996).

Figure 2.28 Three-phase air-oil-water holdup experimental results of Pan (1996) for air superficial velocity 5.5 m/s, oil superficial velocity 0.1 m/s and pressure 0 barg.

Figure 2.29 Three-phase air-oil-water holdup experimental results of Donnelly (1997) for air superficial velocity 14 m/s and total liquid flowrate 3L/min.

Figure 2.30 Three-phase air-oil-water holdup experimental results of Donnelly (1996) for gas superficial velocity 10 m/s and total liquid flowrate 1.6 L/min.

CHAPTER 3

Figure 3.1 Schematic of the WASP Multiphase Flow Facility.

Figure 3.2 High pressure Air Tanks.

Figure 3.3 WASP Facility Oil and Water storage tanks.

Figure 3.4 Inlet Mixer.

Figure 3.5 WASP test section.

Figure 3.6 Visualisation section.

Figure 3.7 Slug catcher.

Figure 3.8 Silencer.

Figure 3.9 Dump Tank.

Figure 3.10 WASP dual energy gamma densitometer.

Figure 3.11: Calibration data for 31 keV gamma energy.

Figure 3.12 Calibration data for 81 keV gamma energy.

Figure 3.13 Source collimator for single beam dual-energy gamma densitometer.

Figure 3.14 Detector and source collimator for single beam dual-energy gamma densitometer.

Figure 3.15 Electronic components for single beam dual energy gamma densitometer.

Figure 3.16 Measurement methods for single beam dual energy gamma densitometer.

Figure 3.17 Detector and source collimator for triple beam dual energy gamma densitometer.

CHAPTER 4

Figure 4.1 Measured pressure gradient plotted against IWFIL at total liquid superficial velocity 0.5 m/s, system pressure 0 barg, horizontal pipe at two different air superficial velocities 4 m/s and 6 m/s.

Figure 4.2 Measured pressure gradient plotted against IWFIL at oil superficial velocity 0.2 m/s, system pressure 0 barg, horizontal pipe at two different air superficial velocities 10 m/s and 12 m/s.

Figure 4.3 Measured pressure gradient plotted against IWFIL at oil superficial velocity 0.5 m/s, system pressure 5 barg, horizontal pipe at two different air superficial velocities 2 m/s and 5 m/s

Figure 4.4 Measured pressure gradient plotted against IWFIL at oil superficial velocity 0.7 m/s, system pressure 5 barg, horizontal pipe at two different air superficial velocities 2 m/s and 5 m/s.

Figure 4.5 Measured pressure gradient plotted against IWFIL at total liquid superficial velocity 0.35 m/s, system pressure 0 barg, pipe downwardly inclined at an angle of –1.5° to the horizontal, at two different air superficial velocities 10 m/s and 12 m/s.

Figure 4.6 Measured pressure gradient plotted against IWFIL at an air superficial velocity 4 m/s, at 0 barg, horizontal pipe at two different liquid superficial velocities 0.5 m/s and 0.6 m/s.

Figure 4.7 Measured pressure gradient plotted against IWFIL at an air superficial velocity of 10 m/s, at atmospheric pressure, pipe downwardly inclined 1.5° for two different liquid superficial velocities 0.2 m/s and 0.35 m/s.

Figure 4.8 Measured pressure gradient plotted against IWFIL at an air superficial velocity of 10 m/s, at atmospheric pressure, pipe downwardly inclined 1.5° for two different liquid superficial velocities 0.5 m/s and 0.7 m/s.

Figure 4.9 Measured pressure gradient plotted against IWFIL at an air superficial velocity 2 m/s, at 5 barg, horizontal pipe for two different oil superficial velocities 0.5 m/s and 0.7 m/s.

Figure 4.10 Measured pressure gradient plotted against IWFIL at an air superficial velocity of 5 m/s, at 5 barg, pipe horizontal at two different oil superficial velocities 0.5 m/s and 0.7 m/s

Figure 4.11 Measured pressure gradient plotted against IWFIL at an air superficial velocity of 4 m/s, total liquid superficial velocity 0.5 m/s at two different system pressures 0 barg and 5 barg for a horizontal pipe.

Figure 4.12 Measured pressure gradient plotted against IWFIL at an air superficial velocity of 2 m/s, oil liquid superficial velocity 0.5 m/s, at two different system pressures 0 barg and 5 barg for a horizontal pipe.

Figure 4.13 Measured pressure gradient plotted against IWFIL at an air superficial velocity of 5 m/s, oil liquid superficial velocity 0.5 m/s, at two different system pressures 0 barg and 5 barg for a horizontal pipe.

Figure 4.14 Measured pressure gradient plotted against IWFIL at an air superficial velocity of 5 m/s, oil liquid superficial velocity 0.5 m/s, system pressure 0 barg for a horizontal pipe.

Figure 4.15 Pipe geometry illustrating the height of the oil and water layers.

Figure 4.16 A typical total liquid holdup trace from the dual energy gamma densitometer for air superficial velocity 2 m/s, oil superficial velocity 0.5 m/s, water superficial velocity 0.2 m/s, system pressure 5 barg for a horizontal pipe.

Figure 4.17 Measured total liquid holdup plotted against IWFIL at a total liquid superficial velocity 0.5 m/s, at two different air superficial velocities 4 m/s and 6 m/s, system pressure 0 barg, for a horizontal pipe.

Figure 4.18 Measured total liquid holdup plotted against IWFIL at a total liquid superficial velocity 0.5 m/s, at two different air superficial velocities 4 m/s and 6 m/s, system pressure 0 barg, for a horizontal pipe.

Figure 4.19 Measured total liquid holdup plotted against IWFIL at oil superficial velocity 0.7 m/s,. system pressure 5 barg, horizontal pipe for two different air superficial velocities 2 m/s and 5 m/s

Figure 4.20 Measured total liquid holdup plotted against IWFIL at air superficial velocity 0.2 m/s, system pressure 0 barg, horizontal pipe for two different air superficial velocities 8 m/s and 10 m/s.

Figure 4.21 Measured total liquid holdup plotted against IWFIL at total liquid superficial velocity 4 m/s, for two different total liquid superficial velocities 0.5 m/s and 0.6 m/s at 0 barg, horizontal pipe.

Figure 4.22 Measured total liquid holdup plotted against IWFIL at air superficial velocity 10 m/s and 0 barg, pipe downwardly inclined $-1.5°$ for two distinct liquid superficial velocities 0.5 m/s and 0.7 m/s.

Figure 4.23 Measured total liquid holdup plotted against IWFIL at an air superficial velocity 4 m/s and total liquid superficial velocity 0.5 m/s at two different system pressures 0 barg and 5 barg for a horizontal pipe.

Figure 4.24 Measured total liquid holdup plotted against IWFIL at air superficial velocity 2 m/s at two different system pressure 4 barg and 5 barg, for a horizontal pipe.

Figure 4.25 Measured total liquid holdup plotted against IWFIL at air superficial velocity 5 m/s, at oil superficial velocities 5 m/s for a horizontal pipe at system pressures 0 barg and 5 barg.

Figure 4.26 Measured total liquid holdup plotted against IWFIL at air superficial velocity 4 m/s, at total liquid superficial velocity 0.5 m/s for a horizontal pipe at atmospheric pressure.

Figure 4.27 Measured total liquid and phasic holdup plotted against IWFIL at air superficial velocity 6 m/s, at total liquid superficial velocities 0.5 m/s for a horizontal pipe at 0 barg.

Figure 4.28 Measured total liquid and phasic holdup plotted against IWFIL at air superficial velocity 4 m/s, at total liquid superficial velocities 0.6 m/s for a horizontal pipe at 0 barg.

Figure 4.29 Measured in-situ water holdup plotted against IWFIL at oil superficial velocity 0.2 m/s, for a range of air superficial velocities at 5 barg., pipe downwardly inclined –1.5° to the horizontal.

Figure 4.30 Measured in-situ oil holdup plotted against IWFIL at oil superficial velocity 0.2 m/s, for a range of air superficial velocities at 5 barg., pipe downwardly inclined –1.5° to the horizontal.

Figure 4.31 Measured in-situ water fraction in the liquid plotted against IWFIL at air superficial velocity 4 m/s, total liquid superficial velocity 0.5 m/s at 0 barg for a horizontal pipe.

Figure 4.32 Measured in-situ water fraction in the liquid plotted against IWFIL at air superficial velocity 6 m/s, total liquid superficial velocity 0.5 m/s at 0 barg for a horizontal pipe.

Figure 4.33 Measured slug frequency plotted against IWFIL at total liquid superficial velocity 0.5 m/s, for two different air superficial velocities at 0 barg, horizontal pipe.

Figure 4.34 Measured slug frequency plotted against IWFIL at oil superficial velocity 0.2 m/s, at two different air superficial velocities 8 m/s and 10 m/s, at 0 barg, for a horizontal pipe.

Figure 4.35 Measured slug frequency plotted against IWFIL at oil superficial velocity 0.5 m/s, for two different air superficial velocities 2 m/s and 5 m/s, at 5 barg, for a horizontal pipe.

Figure 4.36 Measured slug frequency plotted against IWFIL at oil superficial velocity 0.7 m/s, for two different air superficial velocities 2 m/s and 5 m/s, at 5 barg, for a horizontal pipe.

Figure 4.37 Measured slug frequency plotted against IWFIL at air superficial velocity 4 m/s, for two different total liquid superficial velocities 0.5 m/s and 0.6 m/s, at 0 barg, for a horizontal pipe.

Figure 4.38 Measured average slug holdup plotted against IWFIL at total liquid superficial velocity 0.5 m/s, for two different air superficial velocities 4 m/s and 6 m/s, at 0 barg, for a horizontal pipe.

Figure 4.39 Measured average slug holdup plotted against IWFIL at air superficial velocity 4 m/s, at two different liquid superficial velocities 4 m/s and 6 m/s, at 0 barg, for a horizontal pipe.

Figure 4.40 Measured average liquid film holdup plotted against IWFIL at total liquid superficial velocity 0.5 m/s, at two different air superficial velocities 4 m/s and 6 m/s at 0 barg horizontal pipe

Figure 4.41 Measured average liquid film holdup plotted against IWFIL at air superficial velocity 4 m/s, total liquid superficial velocity 0.6 m/s at 0 barg horizontal pipe

Figure 4.42 Measured average liquid film holdup plotted against IWFIL at air superficial velocity 4 m/s, total liquid superficial velocity 0.5 at different system pressures 0 barg and 5 barg, horizontal pipe

Figure 4.43 Measured slug front velocity plotted against IWFIL at air superficial velocity 6 m/s, total liquid superficial velocity 0.5 m/s at 0 barg, horizontal pipe

Figure 4.44 Measured Co values plotted against IWFIL at air superficial velocity 4 m/s, for a range of total liquid superficial velocities at 0 barg, horizontal pipe

Figure 4.45 Measured average slug lengths plotted against IWFIL at air superficial velocity 4 m/s, at total liquid superficial velocity 0.5m/s at 0 barg horizontal pipe

Figure 4.46 Measured average slug lengths plotted against IWFIL at air superficial velocity 6 m/s, at total liquid superficial velocity 0.5m/s at 0 barg horizontal pipe

Figure 4.47 Measured average slug lengths plotted against IWFIL at air superficial velocity 4 m/s, at total liquid superficial velocities 0.5 m/s and 0.6 m/s at 0 barg for a horizontal pipe

CHAPTER 5

Figure 5.1 WASP Flow pattern Map for Horizontal Pipe at 0 bargPressure at Oil Superficial Velocity 0.5 m/s

Figure 5.2 WASP Flow pattern Map for Horizontal Pipe at 5 barg Pressure at Oil Superficial Velocity 0.2 m/s

Figure 5.3 WASP Flow pattern Map for Horizontal Pipe at Atmospheric Pressure at Oil Superficial Velocity 0.2 m/s

Figure 5.4 WASP Flow pattern Map at 0 barg at Oil Superficial Velocity 0.2 m/s for a Pipe downwardly inclined 1.5° to the horizontal.

Figure 5.5 WASP Flow pattern Map at 5 barg at Oil Superficial Velocity 0.2 m/s for a Pipe downwardly inclined 1.5° to the horizontal.

Figure 5.6 WASP Flow pattern Map at 5 barg at Oil Superficial Velocity 0.2 m/s for a Pipe downwardly inclined 1.5° to the horizontal.

Figure 5.7 WASP horizontal Flow pattern data obtained at oil superficial velocity 0.2 m/s plotted on the horizontal flow pattern map of Acikgoz *et al.*.

Figure 5.8 WASP horizontal Flow pattern data obtained at oil superficial velocity 0.5 m/s plotted on the horizontal flow pattern map of Acikgoz *et al.*

Figure 5.9 WASP horizontal flow pattern data obtained at an oil superficial velocity of 0.2 m/s with the pipe downwardly inclined at an angle of –1.5°to the horizontal plotted on Acikgoz *et al.* horizontal flow pattern map (1992).

Figure 5.10 WASP horizontal flow pattern data obtained at oil superficial velocity 0.2 m/s plotted on the horizontal flow pattern map of Acikgoz *et al.*

Figure 5.11 WASP horizontal flow pattern data obtained at oil superficial velocity 0.5 m/s plotted on Pan's horizontal flow pattern map (1996).

Figure 5.12 WASP horizontal flow pattern data obtained at oil superficial velocity 0.1 m/s with the pipe downwardly inclined at an angle of –1.5°to the horizontal plotted on Pan's horizontal flow pattern map (1996).

CHAPTER 6

Figure 6.1 Graph showing influence of air and total liquid superficial velocity on the phase inversion.water-cut

Figure 6.2 Comparison of WASP three-phase pressure drop experimental data with predictions by the correlation of Dukler *et al.* (1964) ($U_{A,S}$ = 4 m/s, $U_{L,S}$ = 0.5 m/s, p= 0 barg, pipe = horizontal)

Figure 6.3 Comparison of WASP three-phase pressure gradient experimental data with predictions by the correlation of Dukler *et al.* (1964) ($U_{A,S}$ = 4 m/s, $U_{L,S}$ = 0.5 m/s, P= 5 barg, pipe = horizontal)

Figure 6.4 Comparison of WASP three-phase pressure gradient experimental data with predictions by the correlation of Dukler *et al.* (1964) ($U_{A,S}$ = 6 m/s, $U_{L,S}$ = 0.5 m/s, P= 0 barg, pipe = horizontal)

Figure 6.5 Comparison of WASP three-phase pressure gradient experimental data with predictions by the correlation of Dukler *et al.* (1964)

Figure 6.6 Comparison of WASP three-phase pressure gradient experimental data with predictions by the correlation of Chisholm (1967) ($U_{A,S}$= 4 m/s, $U_{L,S}$= 0.5 m/s, p= 0 barg, pipe = horizontal)

Figure 6.7 Comparison of WASP three-phase pressure gradient experimental data with predictions by the correlation of Chisholm (1967) ($U_{A,S}$= 4 m/s, $U_{L,S}$= 0.5 m/s, p= 5 barg, pipe = horizontal)

Figure 6.8 Comparison of WASP three-phase pressure gradient data with predictions by the correlation of Chisholm (1967) ($U_{A,S}$= 6 m/s, $U_{L,S}$= 0.5 m/s, P= 0 barg, pipe = horizontal)

Figure 6.9 Comparison of WASP three-phase pressure gradient data with predictions by the correlation of Chisholm (1967)

Figure 6.10 Comparison of WASP three-phase pressure gradient experimental data with predictions by the correlation of Beggs and Brill (1973) ($U_{A,S}$ = 4 m/s, $U_{L,S}$ = 0.5 m/s, p= 0 barg, pipe = horizontal)

Figure 6.11 Comparison of WASP three-phase pressure gradient experimental data with predictions by the correlation of Beggs and Brill (1973) ($U_{A,S}$= 4 m/s, $U_{L,S}$= 0.5 m/s, p= 5 barg pipe = horizontal)

Figure 6.12 Comparison of WASP three-phase pressure gradient experimental data with the predictions by the correlation of Beggs and Brill (1973) ($U_{A,S}$ = 6 m/s, $U_{L,S}$ = 0.5 m/s, p= 0 barg, pipe = horizontal)

Figure 6.13 Comparison of WASP three-phase pressure gradient experimental data with predictions by the correlation of Beggs and Brill (1973)

Figure 6.14 Comparison of WASP three-phase pressure gradient experimental data with predictions by the correlation of Lockhart and Martinelli (1949) ($U_{A,S}$= 4 m/s, $U_{L,S}$= 0.5 m/s, p= 0 barg pipe = horizontal)

Figure 6.15 Comparison of WASP three-phase pressure gradient experimental data with predictions by the correlation of

Lockhart and Martinelli (1949) ($U_{A,S}$ = 4 m/s, $U_{L,S}$ = 0.5 m/s, p= 5 barg, pipe = horizontal)

Figure 6.16 Comparison of WASP three-phase pressure gradient experimental data with predictions by the correlation of Lockhart and Martinelli (1949) ($U_{A,S}$ = 6 m/s, $U_{L,S}$ = 0.5 m/s, P= 0 barg pipe = horizontal)

Figure 6.17 Comparison of WASP three-phase pressure gradient experimental data with predictions by the correlation of Lockhart and Martinelli (1949)

Figure 6.18 Comparison of WASP three-phase pressure gradient experimental data with predictions by the correlation of Schlichting (1970) ($U_{A,S}$ = 4 m/s, p = 0.5 m/s, p= 5 barg, pipe = horizontal)

Figure 6.19 Comparison of WASP three-phase pressure gradient experimental data with predictions by the correlation of Schlichting (1970) ($U_{A,S}$ = 6 m/s, $U_{L,S}$ = 0.5 m/s, p= 0 barg, pipe = horizontal)

Figure 6.20 Comparison of WASP three-phase pressure gradient experimental data with predictions by the correlation of Schlichting (1970)

Figure 6.21 Comparison of WASP three-phase pressure gradient experimental data with the predictions of the slug model of Bonnecaze *et al.* ($U_{A,S}$ = 4 m/s, $U_{L,S}$= 0.5 m/s, p= 0 barg pipe = horizontal)

Figure 6.22 Comparison of WASP three-phase pressure gradient experimental data with the predictions of the slug model of

Bonnecaze *et al.* ($U_{A,S}$ = 4 m/s, $U_{L,S}$= 0.5 m/s, p= 5 barg pipe = horizontal)

Figure 6.23 Comparison of WASP pressure gradient experimental data with the predictions by the slug model of Taitel and Barnea (1990) ($U_{A,S}$ = 4 m/s, $U_{L,S}$= 0.5 m/s, p= 0 barg pipe = horizontal)

Figure 6.24 Comparison of WASP pressure gradient experimental data with the predictions by the slug model of Taitel and Barnea (1990) ($U_{A,S}$ = 4 m/s, $U_{L,S}$= 0.5 m/s, p= 5 barg pipe = horizontal)

Figure 6.25 Comparison of WASP three-phase total liquid holdup experimental data with predictions by the correlation of Lockhart and Martinelli (1949) ($U_{A,S}$ = 4 m/s, $U_{L,S}$ = 0.5 m/s, p= 0 barg, pipe = horizontal)

Figure 6.26 Comparison of WASP three-phase total liquid holdup experimental data with predictions by the correlation of Lockhart and Martinelli (1949) ($U_{A,S}$ = 4 m/s, $U_{L,S}$ = 0.5 m/s, p= 5 barg, pipe = horizontal)

Figure 6.27 Comparison of WASP three-phase total liquid holdup experimental data with predictions by the correlation of Lockhart and Martinelli (1949) ($U_{A,S}$ = 6 m/s, $U_{L,S}$ = 0.5 m/s, p= 5 barg pipe = horizontal)

Figure 6.28 Comparison of WASP three-phase total liquid holdup experimental data with predictions by the correlation of Lockhart and Martinelli (1949)

Figure 6.29 Comparison of WASP three-phase total liquid holdup experimental data with predictions by the correlation of Guzhov *et al.* (1967) ($U_{A,S}$ = 4 m/s, $U_{L,S}$ = 0.5 m/s, p= 0 barg pipe = horizontal)

Figure 6.30 Comparison of WASP three-phase total liquid holdup experimental data with predictions by the correlation of Guzhov *et al.* (1967) ($U_{A,S}$ = 4 m/s, $U_{L,S}$ = 0.5 m/s, p= 5 barg pipe = horizontal)

Figure 6.31 Comparison of WASP three-phase total liquid holdup experimental data with predictions by the correlation of Guzhov *et al.* (1967) ($U_{A,S}$ = 6 m/s, $U_{L,S}$ = 0.5 m/s, p= 0 barg pipe = horizontal)

Figure 6.32 Comparison of WASP three-phase total liquid holdup experimental data with predictions by the correlation of Guzhov *et al.* (1967)

Figure 6.33 Comparison of WASP three-phase total liquid holdup experimental data with predictions by the correlation of Beggs and Brill (1973) ($U_{A,S}$ = 4 m/s, $U_{L,S}$ = 0.5 m/s, p= 0 barg pipe = horizontal)

Figure 6.34 Comparison of WASP three-phase total liquid holdup experimental data with predictions by the correlation of Beggs and Brill (1973) ($U_{A,S}$ = 4 m/s, $U_{L,S}$ = 0.5 m/s, p= 5 barg pipe = horizontal)

Figure 6.35 Comparison of WASP three-phase total liquid holdup experimental data with predictions by the correlation of Beggs and Brill (1973) ($U_{A,S}$ = 6 m/s, $U_{L,S}$ = 0.5 m/s, p= 0 barg pipe = horizontal)

Figure 6.36 Comparison of WASP three-phase total liquid holdup experimental data with predictions by the correlation of Beggs and Brill (1973)

Figure 6.37 Comparison of WASP three-phase total liquid holdup experimental data with predictions by the correlation of Minami and Brill (1987) ($U_{A,S}$ = 4 m/s, $U_{L,S}$ = 0.5 m/s, p= 0 barg pipe = horizontal)

Figure 6.38 Comparison of WASP three-phase total liquid holdup experimental data with predictions by the correlation of Minami and Brill (1987) ($U_{A,S}$ = 4 m/s, $U_{L,S}$ = 0.5 m/s, p= 5 barg pipe = horizontal)

Figure 6.39 Comparison of WASP three-phase total liquid holdup experimental data with predictions by the correlation of Minami and Brill (1987) ($U_{A,S}$ = 6 m/s, $U_{L,S}$ = 0.5 m/s, p= 0 barg pipe = horizontal)

Figure 6.40 Comparison of WASP three-phase total liquid holdup experimental data with predictions by the correlation of Minami and Brill (1987)

Figure 6.41 Comparison of WASP three-phase slug frequency experimental data with predictions by the correlation of Gregory and Scott (1969) ($U_{A,S}$ = 4 m/s, $U_{L,S}$ = 0.5 m/s, p= 0 barg pipe = horizontal)

Figure 6.42 Comparison of WASP three-phase slug frequency experimental data with predictions by the correlation of Gregory and Scott (1969) ($U_{A,S}$ = 6 m/s, $U_{L,S}$ = 0.5 m/s, p= 0 barg pipe = horizontal)

Figure 6.43 Comparison of WASP three-phase slug frequency experimental data with predictions by the correlation of Gregory and Scott (1969) ($U_{A,S}$ = 4 m/s, $U_{L,S}$ = 0.6 m/s, p= 0 barg pipe = horizontal)

Figure 6.44 Comparison of WASP three-phase slug frequency experimental data with predictions by the correlation of Gregory and Scott (1969)

Figure 6.45 Comparison of WASP three-phase slug frequency experimental data with predictions by the correlation of Heywood and Richardson (1979) ($U_{A,S}$ = 4 m/s, $U_{L,S}$ = 0.5 m/s, p= 0 barg pipe = horizontal)

Figure 6.46 Comparison of WASP three-phase slug frequency experimental data with predictions by the correlation of Heywood and Richardson (1979) ($U_{A,S}$ = 4 m/s, $U_{L,S}$ = 0.6m/s, p= 0 barg pipe = horizontal)

Figure: 6.47 Comparison of WASP three-phase slug frequency experimental data with predictions by the correlation of Heywood and Richardson (1979) ($U_{A,S}$ = 6 m/s, $U_{L,S}$ = 0.5 m/s, p= 0 barg pipe = horizontal)

Figure 6.48 Comparison of WASP three-phase slug frequency WASP experimental data with predictions by the correlation of Heywood and Richardson (1979)

Figure 6.49 Comparison of WASP three-phase slug frequency experimental data with predictions by the correlation of Tronconi (1990) ($U_{A,S}$ = 4 m/s, $U_{L,S}$ = 0.5 m/s, p= 0 barg pipe = horizontal)

Figure 6.50 Comparison of WASP three-phase slug frequency experimental data with predictions by the correlation of Tronconi (1990) ($U_{A,S}$ = 4 m/s, $U_{L,S}$ = 0.5 m/s, p= 5 barg pipe = horizontal)

Figure 6.51 Comparison of WASP three-phase slug frequency experimental data with predictions by the correlation of Tronconi (1990) ($U_{A,S}$ = 6 m/s, $U_{L,S}$ = 0.5 m/s, p= 0 barg pipe = horizontal)

Figure 6.52 Comparison of WASP three-phase slug frequency experimental data with predictions by the correlation of Tronconi (1990)

Figure 6.53 Comparison of WASP three-phase slug frequency experimental data with predictions by the correlation of Hill and Wood (1990) ($U_{A,S}$ = 4 m/s, $U_{L,S}$= 0.5 m/s, p= 0 barg pipe = horizontal)

Figure 6.54 Comparison of WASP three-phase slug frequency experimental data with predictions by the correlation of Hill and Wood (1990) ($U_{A,S}$= 4 m/s, $U_{L,S}$= 0.5 m/s, p= 5 barg pipe = horizontal)

Figure 6.55 Comparison of WASP three-phase slug frequency experimental data with the predictions by the correlation of Hill and Wood (1990) ($U_{A,S}$= 6 m/s, $U_{L,S}$ = 0.5 m/s, p= 0 barg pipe = horizontal)

Figure 6.56 Comparison of WASP three-phase slug frequency experimental data with predictions by the correlation of Hill and Wood (1990)

Figure 6.57 Comparison of WASP three-phase slug frequency data with predictions by the correlation of Manolis (1995) ($U_{A,S}$ = 4 m/s, $U_{L,S}$ = 0.5 m/s, p= 0 barg pipe = horizontal)

Figure 6.58 Comparison of WASP three-phase slug frequency experimental data with the correlation of Manolis (1995) ($U_{A,S}$ = 4 m/s, $U_{L,S}$ = 0.5 m/s, p= 5 barg pipe = horizontal)

Figure 6.59 Comparison of WASP three-phase slug frequency experimental data with predictions by the correlation of Manolis (1995) ($U_{A.S}$ = 6 m/s, $U_{L,S}$ = 0.5 m/s, p= 0 barg pipe = horizontal)

Figure 6.60 Comparison of WASP three-phase slug frequency experimental data with Manolis correlation (1995)

Figure 6.61 Comparison of WASP three-phase slug body holdup experimental data with the predictions by the correlation of Gregory *et al.* (1978) ($U_{A,S}$ = 4 m/s, $U_{L,S}$ = 0.5 m/s, p= 0 barg pipe = horizontal)

Figure 6.62 Comparison of WASP three-phase slug body holdup experimental data with the predictions by the correlation of Gregory *et al.* (1978) ($U_{A,S}$ = 4 m/s, $U_{L,S}$ = 0.5 m/s, p= 5 barg pipe = horizontal)

Figure 6.63 Comparison of WASP three-phase slug body holdup experimental data with the predictions by the correlation of Gregory *et al.* (1978) ($U_{A,S}$ = 4 m/s, $U_{L,S}$ = 0.5 m/s, p= 5 barg pipe = horizontal)

Figure 6.64 Comparison of WASP three-phase slug body holdup experimental data with the predictions by the correlation of Ferschneider (1983) ($U_{A,S}$ = 4 m/s, $U_{L,S}$ = 0.5 m/s, p= 0 barg pipe = horizontal)

Figure 6.65 Comparison of WASP three-phase slug body holdup experimental data with the predictions by the correlation of Ferschneider (1983) ($U_{A,S}$ = 4 m/s, $U_{L,S}$ = 0.5 m/s, p= 5 barg, pipe = horizontal)

Figure 6.66 Comparison of WASP three-phase slug body holdup experimental data with the predictions by the correlation of Malnes (1983) ($U_{A,S}$ = 4 m/s, $U_{L,S}$ = 0.5 m/s, p= 0 barg, pipe = horizontal)

Figure 6.67 Comparison of WASP three-phase slug body holdup experimental data with the predictions by the correlation of Malnes (1983) ($U_{A,S}$ = 4 m/s, $U_{L,S}$ = 0.5 m/s, p= 5 barg pipe = horizontal)

Figure 6.68 Comparison of WASP three-phase slug body holdup experimental data with the predictions by the correlation of Gomez (2000) ($U_{A,S}$ = 4 m/s, $U_{L,S}$ = 0.5 m/s, p= 0 barg pipe = horizontal)

Figure 6.69 Comparison of WASP three-phase slug body holdup experimental data with the predictions by the correlation of Gomez (2000) ($U_{A,S}$ = 4 m/s, $U_{L,S}$ = 0.5 m/s, p= 5 barg pipe = horizontal)

Figure 6.70 Comparison of WASP three-phase average slug length data with the predictions from the correlations of Brill *et al.* (1979), Norris (1982) and Scott *et al.* (1986) ($U_{A,S}$ = 4 m/s, $U_{L,S}$ = 0.6 m/s, p= 0 barg pipe = horizontal)

Figure 6.71 Comparison of WASP three-phase average slug length data with the predictions from the correlations of Brill *et al.* (1979), Norris (1982) and Scott *et al.* (1986) ($U_{A,S}$ = 6 m/s, $U_{L,S}$= 0.5 m/s, p= 0 barg pipe = horizontal)

Figure 6.72 Comparison of WASP three-phase Co ratio experimental data with the predictions by the expression of Bendiksen (1984) ($U_{A,S}$ = 4 m/s, $U_{L,S}$ = 0.5 m/s, p= 0 barg pipe = horizontal)

Figure 6.73 Slug flow in a fixed coordinate system

Figure 6.74 Slug flow in a moving coordinate system

Figure 6.75 Initial conditions for slug tail simulation

Figure 6.76 The Geometry of the Computational Domain

Figure 6.77 The Mesh of the Computational Domain

Figure 6.78 Gas-Liquid Phase Distribution for Horizontal Air-Oil-Water Slug Flow (Mixture Velocity 4.0 m/s Time: 1.0 s Water cut 40 %)

Figure 6.79 Gas Phase Distribution for Horizontal Air-Oil-Water Slug Flow (Mixture Velocity 4.0 m/s Time: 2.0 s Water-cut 40%)

Figure 6.80 Gas Phase Distribution for Horizontal Air-Oil-Water Slug Flow (Mixture Velocity 4.0 m/s Time: 3.0 s. Water-cut 40 %)

Figure 6.81 Gas-Liquid Phase Distribution for Horizontal Air-Oil-Water Slug Flow (Mixture Velocity 4.0 m/s Time: 3.0 s Water-Cut 0%)

Figure 6.82 Gas-Liquid Phase Distribution for Horizontal Air-Oil-Water Slug Flow (Mixture Velocity 4.0 m/s Time: 3.0 s Water-Cut 20%)

Figure 6.83 Gas-Liquid Phase Distribution for Horizontal Air-Oil-Water Slug Flow (Mixture Velocity 4.0 m/s Time: 3.0 s Water-Cut 40%)

Figure 6.84 Gas-Liquid Phase Distribution for Horizontal Air-Oil-Water Slug Flow (Mixture Velocity 4.0 m/s Time: 3.0 s Water-Cut 55%)

Figure 6.85 Gas-Liquid Phase Distribution for Horizontal Air-Oil-Water Slug Flow (Mixture Velocity 4.0 m/s Time: 3.0 s Water-Cut 70%)

Figure 6.86 Gas-Liquid Phase Distribution for Horizontal Air-Oil-Water Slug Flow (Mixture Velocity 4.0 m/s Time: 3.0 s Water-Cut 100%)

Figure 6.87 Comparison of WASP ratio of translational velocity to mixture velocity with the predictions by the CFX code ($U_{A,S}$ = 4 m/s, $U_{L,S}$= 0.5 m/s, p= 0 barg. pipe = horizontal)

LIST OF TABLES

CHAPTER 2

Table 2.1 Values of parameter C for the Lockhart and Martinelli correlation.

Table 2.2 Values of parameters for the Beggs and Brill (1973) correlation.

Table 2.3 Three-phase air-oil-water flow patterns observed by Acikgoz *et al.* (1992).

Table 2.4 Three-phase air-oil-water flow patterns observed by Pan (1996) using the WASP facility.

Table 2.5 Matching three-phase air-oil-water flow patterns observed by Acikgoz *et al.* (1992) and Pan (1996).

CHAPTER 3

Table 3.1 Range of Parameters for WASP Experimental Campaign #1.

Table 3.2 Range of Parameters for WASP Experimental Campaign #2.

Table 3.3 Range of Parameters for WASP Experimental Campaign #3.

CHAPTER 5

Table 5.1 The WASP three-phase flow pattern classification.

Table 5.2 Key for Acikgoz et al's Flow Pattern Map.

Table 5.3 Flow Pattern Map Key for Pan's (1996) Flow Pattern Map.

CHAPTER 6

Table 6.1 Summary of statistical errors for pressure drop correlations when compared to WASP data

Table 6.2 Performance of Dukler *et al.* (1964) correlation when applied to oil-continuous and water-continuous data separately

Table 6.3 Performance of Dukler *et al.* (1964) correlation when applied to atmospheric and pressure data separately

Table 6.4 Statistical errors obtained on comparing the modified Taitel and Barnea model and the correlation of Dukler *et al.* (1964) with the experimental data.

Table 6.5 Summary of statistical errors for empirical liquid holdup correlations when compared to WASP mean liquid hold-up data.

Table 6.6 Table listing the statistical errors for various correlations' performance against slug frequency data.

NOMENCLATURE

Roman Symbols

Symbol	Denotes	Dimensions
A	Pipe cross sectional area	m^2
A_G	Cross sectional area occupied by gas phase	m^2
A_f	Cross sectional area occupied by liquid film	m^2
B	Parameter in the correlation of Chisholm (1967)	-
Bo	Bond Number as defined by Equation (2.114)	-
C	Constant in Chisholm's fit to Lockhart and Martinelli graphical correlation	-
C_1, C_2	Parameters used in Schlichting (1970) correlation	-
C_3, C_4	Governing Coefficient as used by Griffith and Wallis Equation (2.105)	-
C_f	constants used in Blasius Equation (2.81)	-
C_o	Distribution parameter Equation (2.98)	-
C_M	Mixing Degree Coefficient	-
D	Pipe diameter	m
D_h	Hydraulic diameter	m
$\left[\frac{dp_F}{dz}\right]$	Frictional pressure gradient	Nm^{-3}
$\left[\frac{dp}{dz}\right]$	Pressure gradient	Nm^{-3}
$\left[\frac{dp_F}{dz}\right]_G$	Frictional pressure gradient for gas flowing alone in pipe	Nm^{-3}
$\left[\frac{dp_F}{dz}\right]_L$	Frictional pressure gradient for liquid flowing alone in pipe	Nm^{-3}
$\left[\frac{dp}{dz}\right]_{LO}$	Frictional pressure gradient for a fluid with total mass flux and liquid properties	Nm^{-3}
$\left[\frac{dp}{dz}\right]_{GO}$	Frictional pressure gradient for a fluid with total mass flux and gas properties	Nm^{-3}
E	Inclination factor for Beggs and Brill (1973) holdup correlation-	-
f	Friction factor	-
f_f	Liquid–wall friction factor	-
f_i	Interfacial friction factor	-
f_G	Gas-wall interfacial friction factor	-
f_L	Liquid–wall interfacial friction factor	-
f_M	Two-phase friction factor	-
f_{LO}	Liquid-wall friction factor	-
g	Acceleration due to gravity	ms^{-2}
G	Amount of liquid picked up	kgs^{-1}
h	liquid height	m
h_b	liquid volume fraction in the slug bubble	-

$h_f(z)$	Liquid film height as a function of distance	-	m
k	Ratio of oil to water viscosity as used by Donnelly(1997)		-
k_1	Constant in Brinkman equation		-
K_1, K_2	Coefficients in gas entrainment relationship as used by Nydal (1991)		-
K	Pan (1996) correlation constant		-
K_2	Pal and Rhodes (1985) constant		-
k_3	constant in Richardson's expression		-
I	Transmitted Intensity of gamma energy		count/s
I_o	Initial Intensity of gamma energy		count/s
l_s	Slug length		m
l_t	Length of slug unit		m
l_f	Length of slug film region		m
$\dot{m}$	Mass flux		$kgm^{-2}s^{-1}$
$\dot{m}_G$	Gas mass flux		$kgm^{-2}s^{-1}$
$\dot{m}_L$	Liquid mass flux		$kgm^{-2}s^{-1}$
m	Oil region inversion factor Equation 2.14		-
n	Water region inversion factor Equation 2.147		-
p	Pressure		Nm^{-2}
P	Channel periphery		m
S	Parameter in Beggs and Brill (1973) correlation		-
S_f	Liquid film perimeter		m
S_G	Gas phase perimeter		m
S_i	Gas-Liquid interface perimeter		m
S_w	Liquid film perimeter		m
t_s	Time for the passage of one slug body		s
t_f	Time for the passage of one slug film		s
t_u	Time for the passage of one slug unit		s
t	Time		s
T	Absolute Temperature		°C
t	Absolute Temperature		°C
U_b	Average Velocity of gas bubbles within slug body		ms^{-1}
U_d	Drift velocity/Bubble rise velocity		ms^{-1}
$U_f(z)$	Liquid film velocity as a function of axial distance		ms^{-1}
U_t	Slug translational velocity		ms^{-1}
U_f	liquid velocity in the film region		ms^{-1}
$U_{L,S}$	Liquid Superficial velocity		ms^{-1}
U_L	Liquid Velocity		ms^{-1}
$U_{W,S}$	Water Superficial velocity		ms^{-1}
$U_{O,S}$	Oil Superficial velocity		ms^{-1}
$U_{G,S}$	Gas Superficial velocity		ms^{-1}
U_G	Gas Velocity		ms^{-1}
U_M	Mixture Superficial velocity		ms^{-1}
W	Input liquid flowrate as used in model of Taitel and Barnea Equation (2.63)		ms^{-1}
X	Lockhart-Martinelli flow parameter defined by Equation 2.23		-
x	Flow quality		-
x	Medium thickness in gamma measurement		m

y	Parameter in Beggs and Brill (1973) correlation as shown by Equation (2.14)	-
z	Distance	m
Z_e	Parameter used in the Minami and Brill (1987) Correlation as defined in Equation (2.46)	-

Greek Symbols

α	Ratio of slug length to slug unit length	-
α_f	void fraction in the liquid film	-
α_u	average void fraction in the liquid unit	-
ε	holdup	-
ε_L	Liquid holdup	-
ε_{LE}	Equilibrium liquid holdup	-
ε_s	average liquid holdup in slug body	-
ε_f	average liquid holdup in the film region	-
ε_G	void fraction	-
π	pi number	-
θ	pipe inclination angle	degrees
τ_o	Wall Shear Stress	Nm^{-2}
τ_f	Liquid-wall shear stress	Nm^{-2}
τ_G	Gas-wall shear stress	Nm^{-2}
τ	shear stress	Nm^{-2}
μ	viscosity	Pa.s
μ_G	Gas viscosity	Pa.s
μ_{Ha}	Viscosity evaluated using Hatschek Equation 6.9	Pa.s
μ_L	Liquid viscosity	Pa.s
μ_r	Relative viscosity	Pa.s
μ_o	Oil Viscosity	Pa.s
μ_W	Water Viscosity	Pa.s
μ_{LIN}	Viscosity evaluated using Equation 6.3	Pa.s
μ_{Cont}	Viscosity of continuous liquid phase	Pa.s
μ_{NONLIN}	Non Linear Viscosity	Pa.s
λ_{dis}	Volume fraction of dispersed phase	-
λ_F	a constant as used by Bonnecaze *et al.* Equation (2.59)	-
λ_w	Inlet water fraction in total liquid/water-cut	-
$\lambda_{w,i}$	Phase inversion water-cut	-
λ_L	Input liquid volume fraction	-
λ_o	Input oil fraction in total liquid	-
τ	shear stress	Nm^{-2}
ρ	density	kgm^{-3}
ρ_H	Homogeneous density	kgm^{-3}
ρ_L	Liquid Density	kgm^{-3}
ρ_G	Gas Density	kgm^{-3}
ρ_M	Mixture Density	kgm^{-3}
σ	surface tension	$N\ m^{-1}$
ϕ	Disperse phase concentration	-

ϕ_L	Two-phase Multiplier as used in correlation by Lockhart and Martinelli (1949)	-
ϕ_{LO}	Two-phase Multiplier as used in correlation by Chisholm (1967)	-
ψ	Inclination correction factor as used in the Beggs and Brill (1973) Equation (2.43)	-
Δp	Pressure Drop	Pa
Δp_{tot}	Total Pressure Drop	Pa
Δp_{fric}	Frictional Pressure Drop	Pa
Δp_{accel}	Accelerational Pressure Drop	Pa
Δp_u	Pressure drop for a slug unit	Pa
Δp_{slug}	Pressure drop for a slug unit	Pa
Δp_{mix}	Pressure drop in mixing zone	Pa
Δp_{liq}	Pressure drop in the slug body	Pa
Δp_{gas}	Pressure drop in the gas bubble region	Pa
δ	Inclination Parameter used by Bonnecaze *et al.* (1971) Equation (2.57)	-
η_r	ratio of liquid to gas viscosity	-
ν_s	Slug Frequency	Hz
ν_f	Relative film velocity	ms^{-1}
ν_G	Relative gas velocity	ms^{-1}
Ω	Dimensionless slug frequency	-

Dimensionless Number Symbols

E_o	Eotvos Number
F	Dimensionlesss parameter used in Taitel and Dukler (1976) flow regime Map
F_L	Liquid phase Froude Number
F_G	Gas phase Froude Number
N_D	Diameter Number
$N_{L,V}$	Liquid velocity number
N_{GV}	Gas Velocity Number
$N_{L\mu}$	Liquid Viscosity Number
N_f	Viscosity Number
Re	Reynolds Number
Re_L	Liquid Reynolds Number
Re_{GO}	Gas Reynolds Number as defined using total mass flux and gas properties
Re_{LO}	Mixture Reynolds Number as defined using total mass flux and liquid properties
Re_M	Mixture Reynolds Number
Re_s	Slug Body Reynolds Number as defined by Equation (2.62)
Re_{3P}	Three-phase Reynolds Number
We	Weber Number
Z	ratio of inertial to gas phase pressure drop

Abbreviations

AE	Average Error
AAE	Absolute Average Error
ARE	Average Relative Error
AARE	Absolute Average Relative Error
CFD	Computational Fluid Dynamics
D-St.S	Dispersed stratified Smooth Flow
D-St.W	Dispersed stratified Wavy Flow
DWSt.A	Dispersed Water Stratifying Annular Flow
DOSt.A	Dispersed Oil Stratifying Annular Flow
DWSt	Dispersed Water Continuous Stratified Flow
DOSl	Dispersed Oil Continuous Slug Flow
DWSt	Dispersed Water Continuous Stratified Flow
DOSt	Dispersed Oil Continuous Slug Flow
DOA	Dispersed Oil Annular Flow
DWA	Dispersed Water Annular Flow
IWFIL	Input water fraction in the liquid
PDF	Power Spectral Density
PSD	Probability Density Function
SSl	Separated Slug Flow
SSt	Separated Stratified Flow
S.DOSl	Separated-Dispersed Oil-Continuous Slug Flow
S.DWSl	Separated-Dispersed Water-Continuous Slug Flow
SD1	Standard Deviation (based on Average Error)
SD2	Standard Deviation (based on Relative Error)

Chapter 1

INTRODUCTION

In the petroleum industry, in the initial stages of oil well operation, the produced fluids are predominantly oil and gas, but as the well ages, the amount of water produced increases either naturally or as a result of water injection, which is used to boost the diminishing reservoir pressure, and three-phase flow of gas, oil and water occurs.

Usually the multiphase mixture is transported via a pipe along the seabed and then through a vertical riser to the platform for phase separation. However, in the case of marginal reservoirs, it is uneconomical to have fixed or floating platforms and there has been a shift towards multiphase production where untreated oil-well fluids are transported in one pipeline to a central processing platform or to an existing on-shore processing facility. In the case of transporting the multiphase mixture to shore, this could involve distances of hundreds of kilometres. To ensure proper design and operation of these pipelines, it is necessary to have knowledge of some important flow characteristics such as pressure drop and liquid hold-up. These flow characteristics are related to the spatial and temporal distribution of the three phases in the pipe, namely the *flow pattern* or *flow regime*.

The most commonly occurring flow pattern in pipelines is that of slug flow, which consists of liquid slugs filling the whole cross-sectional area of the pipe and separated by elongated gas bubbles. Important aspects of three-phase slug flow are the possibility of formation of liquid emulsions which lead to even higher pressure drops especially close to the phase inversion region i.e. the region in which the liquid/liquid dispersion changes from oil-continuous to water continuous.

For pipeline design, the pressure drop is a very important parameter as it determines the production rate for a given pipe size and source (reservoir) pressure. In some cases, the reservoir pressure is insufficient to overcome the pressure drop at the desired production rate. Increasingly, multiphase pumps are being used to address this problem; clearly, pressure drop is an important factor in designing such pumping

systems. Mean liquid holdup is important in determining gravitational pressure drop in non-horizontal pipelines. Liquid production rate fluctuates with time in slug flow and separation equipment ("slug catchers") must be capable of dealing with such fluctuations. Thus, the characteristics of slug flow (slug frequency, slug length, etc) are also important design parameters.

To be better able to predict important parameters such as pressure drop, liquid holdup and slug parameters in three-phase air-oil water flow, one needs correlations and models which are able to account for the unique interactions which take place between the oil and water phases in the liquid. However, there is a distinct lack of correlations and models which are capable of being applied to the three-phase flow case as they fail to account for the effects of the mixing between the oil and the water. This is because existing models and correlations have been based on data obtained from two-phase data.

In this thesis a study of three-phase air-oil-water flow in horizontal and inclined pipes, with particular emphasis on the slug flow regime, is described

Experiments have been carried out in which pressure drop and liquid hold-up were measured. This data were compared with existing models and correlations and a new improved model for predicting three-phase flows is presented.

This project had the following objectives:

- To generate detailed data on three-phase air-oil-water flow to supplement the database already developed using the Imperial College high pressure multiphase facility (WASP).
- To develop improved analytical frameworks for the prediction of three-phase flows.
- To obtain detailed data on slug parameters such as slug velocity and slug body holdup.
- To extend CFD techniques from two-phase to the three-phase flow case.

In pursuance of the above-mentioned objectives, unique data on slug velocity slug length and slug frequency have been obtained and compared with existing empirical correlations. A new correlation has been devised for the prediction of the phase inversion water-cut which has resulted in improved predictions of the pressure drop and the liquid holdup as well as slug parameters. An existing two-phase flow slug model has been adapted to the three-phase flow case. This model has been used to predict the experimental data and the results are also presented. A commercially available CFD code has been used to simulate slug flow and the results have also been compared with the experimental data.

This thesis is organised as follows: In Chapter 2, a review of the relevant literature is included. In Chapter 3, a description of the WASP Multiphase Flow Facility is given together with the instrumentation used for the experiments. This is then followed by Chapter 4, in which the experimental results obtained are presented and discussed. Data on flow pattern are presented in Chapter 5, together with flow pattern maps, which have been developed from the data. In addition to this, the flow pattern data have been compared with existing flow pattern maps. In Chapter 6, data on pressure gradient, holdup and slug parameters such as slug frequency slug velocity, slug length and slug body holdup have been compared with existing correlations. An existing slug model has been adapted to the three-phase flow case with good results. In this Chapter a new correlation for the prediction of the phase inversion point is also presented. Chapter 6 also presents a brief description of the CFD method used to model three-phase slug tails as well as a presentation of the results obtained. Finally, a conclusion and recommendations for future work are set out in Chapter 7.

Chapter 2

LITERATURE REVIEW

The objective of this Chapter is to present a general review of information relevant to three-phase gas-liquid-liquid flow with particular emphasis on the slug flow regime. The literature on three-phase gas-liquid-liquid flow is relatively sparse (as will be seen from the review of all sources identified in the present work in Section 2.3 below). The normal practice (also followed in the present study) is to relate the three-phase behaviour to that of two-phase flows. Three-phase flows have many features in common with gas-liquid and liquid-liquid flows and the literature on these two-phase systems is reviewed briefly in Section 2.1 and 2.2 below respectively. There is a vast literature on two-phase flows and it is inappropriate to review this here; rather those features of gas-liquid and liquid-liquid flows are highlighted which form an important background to the presentation and analysis of the present results.

In Section 2.1, gas-liquid flow regimes are briefly described and those (selected) correlations for pressure drop and liquid holdup which are used for the analysis of the present three-phase flow data are outlined. Work on gas-liquid slug flow is then described; Section 2.1.3.1 details the phenomenological models of Bonnecaze *et al.* (1971) and Taitel and Barnea (1990) which were used for the three-phase case in the present work. Section 2.1.3.2 discusses relationships for the parameters of two-phase slug flow (slug length, slug velocity, slug body liquid holdup and slug frequency), again to form a basis for the analysis of the present three-phase slug flow data.

Liquid-liquid two-phase flows are important in themselves in oil pipeline transport systems and in chemical plants. In pipelines, a commonly occurring case is that of the transport of mixtures of oil and produced water in hydrocarbon recovery. Again only a brief survey is given here of the liquid–liquid flows. However one aspect is discussed in detail, namely that of the viscosity of liquid-liquid dispersions (Section 2.2.2.1); this forms an important background to the analysis of the present three-phase flow data described in Chapter 6.

2.1 TWO-PHASE GAS-LIQUID FLOW

The simultaneous flow of gas and liquid occurs in many industrial disciplines such as petroleum, chemical, civil and nuclear engineering. In the petroleum industry, two-phase gas-liquid flow occurs in the reservoir, the wells, flow lines, as well as in process equipment used for separating and processing the mixture.

For optimum design and operation of these flowlines and process equipment, knowledge of the flow patterns in the pipelines is essential. Flow patterns in horizontal and near-horizontal two-phase gas-liquid flows have been studied exhaustively in the literature and a consensus has been reached on the fact that seven main flow patterns exist. These are dispersed bubbly flow, stratified flow, stratified wavy flow, plug flow, semi-slug flow, slug flow and annular flow. An illustration of these flow patterns is illustrated in Figure 2.1.

As these flow patterns or regimes have a profound influence on design parameters such as the pressure drop and the liquid holdup, it is essential to be able to predict the transition between the different flow patterns. Flow pattern maps which illustrate these transitions have been formulated by a number of researchers. Examples of these flow pattern maps include those by Mandhane *et al.* (1974) and Taitel and Dukler (1976) illustrated in figures 2.2 and 2.3 respectively. Comprehensive reviews of two-phase gas-liquid flow pattern maps are given by Hewitt (1982, 1999).

2.1.1 Pressure Drop

The pressure drop in gas-liquid flow in pipelines is a very important parameter as it governs the pumping requirement. In order to design pipelines adequately it is necessary to be able to predict the pressure drop.

The most straightforward approach is that in which the gas-liquid mixture behaves as a homogeneous fluid. For this case, carrying out a momentum balance for steady state flow in a constant cross-section duct (Hewitt, 1982) yields the following expression for the pressure gradient:

$$-\frac{dp}{dz} = \frac{\tau_o P}{A} + \frac{\dot{m}^2 d(1/\rho_H)}{dz} + g\rho_H \sin\theta \qquad (2.1)$$

Where A is the channel cross section, P is the channel periphery and τ_o is the wall shear stress, θ is the pipe inclination angle, ρ_H, is the homogeneous mixture density and $\dot{m}$ is the mass flux. An alternative approach (the "separated flow model", Hewitt, 1982) is to consider the two phases as each occupying a separate zone of the channel; in contrast to the homogeneous model, the phases may have different velocities. For steady flow in constant diameter duct, the equation for pressure drop using this model is as follows:

$$-\frac{dp}{dz}=\frac{\tau_o P}{A}+\dot{m}^2\frac{d}{dz}\left[\frac{x^2}{\rho_G\varepsilon_G}+\frac{(1-x^2)}{\rho_L(1-\varepsilon_G)}\right]+g\left[\rho_G\varepsilon_G+(1-\varepsilon_G)\rho_L\right]\sin\theta \quad (2.2)$$

Where ε_G is the void fraction (fraction of the cross section occupied by the gas phase), ρ_G *and* ρ_H are the gas and liquid densities respectively and x is the quality, the ratio of the gas mass flux to the total mass flux. The three terms on the right hand side of Equations (2.1) and (2.2) are the frictional, accelerational and gravitational components of pressure drop respectively. For horizontal flows the gravitational component is equal to zero, and usually the contribution of the accelerational component is negligible. However, for flows with phase change (or where there is a large change of entrained drop fraction in annular flow), the accelerational component may become significant (particularly at low qualities). Thus, the frictional term calculated as the difference between the total pressure gradient and the sum of the accelerational and gravitational components, may have different values if the flow is interpreted in terms of the homogeneous model than the value obtained by interpretation of the data via the separated flow model. To evaluate the frictional component of the pressure gradient, an empirical correlation is usually required.

2.1.1.1 Pressure Drop Correlations

In the course of this work, several empirical gas-liquid pressure drop correlations have been compared with the present three-phase flow experimental data (see Chapter 6). In what follows, a brief review of these correlations is given for completeness. The correlations selected were those of Dukler *et al.* (1964), Beggs and Brill (1973), Lockhart and Martinelli (1949), Chisholm (1967) and Schlichting (1970). The correlation of Dukler *et al.* (1964) is based on the homogeneous model and uses single-phase flow relationships for friction factor. The Beggs and Brill (1973) correlation is also basically of the homogeneous type but uses a friction factor, which

is related to (non-homogeneous) liquid hold-up. The Lockhart and Martinelli (1949), Chisholm (1967) and Schlichting (1970) correlation are all of the separated flow type and relate the frictional pressure gradients to those of flows with one or other phase properties via a "frictional multiplier".

2.1.1.1.1 Dukler *et al.* (1964).

This correlation is of the homogeneous type with the density and the viscosity defined on a volumetric mean basis between the gas and liquid values. The friction factor is calculated from standard single-phase flow relationships.

The frictional pressure gradient $\left[\frac{dp_F}{dz}\right]$ is calculated using the following expression:

$$\left(\frac{dp_F}{dz}\right)=\frac{\tau_o P}{A}=\frac{4\tau_o}{D}=\frac{2f(\dot{m}_G+\dot{m}_L)^2}{D\rho_M}=\frac{2f\dot{m}^2}{D\rho_M} \tag{2.3}$$

Where D is the tube diameter and $\dot{m}_G$ and $\dot{m}_L$ are the mass fluxes of the gas and liquid respectively and f the friction factor is given by the Blasius equation:

$$f=\frac{\tau_o}{\frac{1}{2}\rho_M U_M^{\,2}}=\frac{\tau_o\rho_M}{\frac{1}{2}(\dot{m}_G+\dot{m}_L)^2}=0.079(\mathrm{Re}_M)^{-0.25} \tag{2.4}$$

Where U_M is the mixture superficial velocity (U_M=$U_{G,S}$+$U_{L,S}$) and ρ_M the mixture density. The mixture Reynolds number is defined by the expression:

$$\mathrm{Re}_M=\frac{(\dot{m}_G+\dot{m}_L)D}{\mu_M} \tag{2.5}$$

The gas and liquid mass fluxes are related to the phase superficial velocities $U_{G,S}$ and $U_{L,S}$ as follows:

$$\dot{m}_G=\rho_G U_{G,S} \tag{2.6}$$

$$\dot{m}_L=\rho_L U_{L,S} \tag{2.7}$$

And the mixture density ρ_M is evaluated using the expression:

$$\rho_M=(1-\lambda_L)\rho_G+\lambda_L\rho_L \tag{2.8}$$

Where λ_L is the input liquid volume flow fraction, which is defined as the ratio of the total liquid superficial velocity to the total mixture superficial velocity:

$$\lambda_L = \frac{U_{L,S}}{U_{L,S} + U_{G,S}} \tag{2.9}$$

The mixture viscosity μ_M is calculated using the expression

$$\mu_M = (1 - \lambda_L)\mu_G + \lambda_L \mu_L \tag{2.10}$$

2.1.1.1.2 Beggs and Brill (1973).

The Beggs and Brill (1973) correlation is probably the most widely used method for calculating pressure gradient in two-phase flows in hydrocarbon recovery (the context of the present work).

The air-water experimental data used to formulate the pressure drop correlation were collected over a wide range of conditions using a 27 metre long transparent acrylic pipe with pipe inclinations ranging from -90° to +90°. Two pipe diameters were used with nominal bores 25.4 mm (1 inch) and 38 mm (1.5 inch). A total of 584 data points were collected.

Liquid holdup was measured through the aid of quick-closing ball valves, which were actuated pneumatically. The pressure drop was measured using variable reluctance pressure transducers.

When Beggs and Brill plotted their holdup data against the pipe inclination angle, they observed a strong dependency of the holdup on the pipe angle. In particular, no "segregated flow"(i.e. stratified flow) was observed for angles greater that +3°, whereas in downhill flows the flow was always segregated. The approach taken was to use the homogeneous model but to correlate the friction factor in terms of the actual liquid holdup. A separate correlation was developed for liquid holdup (see Section 2.1.2.1.3).

The pressure drop is calculated using the expression:

$$\left(\frac{dp_F}{dz}\right)_M = \frac{f(\dot{m}_G + \dot{m}_L)^2}{2D\rho_M}\left(\frac{f_M}{f}\right) \tag{2.11}$$

Where f is the friction factor for a smooth pipe given by the expression:

$$f = \left[2\log\left(\frac{\mathrm{Re}_M}{4.5223\log \mathrm{Re}_M - 3.8215}\right)\right]^{-2} \tag{2.12}$$

Re_M is given by Equation (2.5) with the mean density (ρ_M) and viscosity (μ_M) being given by Equations (2.8) and (2.10) respectively and f_M the two-phase friction factor is given by:

$$\frac{f_M}{f} = \exp(S) \tag{2.13}$$

S was correlated as a function of y defined as

$$y = \frac{\lambda_L}{\varepsilon_L^{\,2}} \tag{2.14}$$

Where

$$\lambda_L = \text{no slip holdup}, \frac{U_{L,S}}{U_{L,S} + U_{G,S}} \tag{2.15}$$

$$\varepsilon_L = \text{liquid holdup}$$

S is calculated by applying the following criteria:

$$S = \ln(2.2y - 1.2) \qquad \text{For } 1<y<1.2 \tag{2.16}$$

For other values of y, S is given by:

$$S = \frac{\ln(y)}{\{-0.0523 + 3.182\ln(y) - 0.8725[\ln(y)]^2 + 0.01853[\ln(y)]^4\}} \tag{2.17}$$

The liquid holdup is obtained from the Beggs and Brill correlation, which is described below in Section 2.1.2.1.3.

2.1.1.1.3 Lockhart and Martinelli (1949)

Lockhart and Martinelli (1949) correlated frictional pressure gradient in terms of *multipliers* which are applied to the pressure gradients for the individual phases flowing alone in the channel; For instance, the multiplier ϕ_L is used to calculate the two-phase frictional pressure gradient $\left[\frac{dp_F}{dz}\right]$ from the pressure gradient for the liquid phase flowing alone $\left[\frac{dp_F}{dz}\right]_L$ as follows:

$$\left(\frac{dp_F}{dz}\right) = \phi_L^2 \left(\frac{dp_F}{dz}\right)_L \tag{2.18}$$

This correlation is based on the separated flow approach. The pressure gradient for liquid flowing alone in the pipe is given by:

$$\left(\frac{dp_F}{dz}\right)_L = \frac{2f_L \dot{m}_L^2}{D\rho_L} = \frac{2f_L \dot{m}^2 (1-x)^2}{D\rho_L} \tag{2.19}$$

Where f_L is the friction factor for the liquid phase flowing alone in the channel. Lockhart and Martinelli used the following correlational relationships for the single-phase friction factor:

$$f_L = \frac{16}{Re_L} \; for \; Re_L < 2000 \tag{2.20}$$

$$f_L = 0.046 Re_L^{-0.2} \; for \; Re_L \geq 2000 \tag{2.21}$$

Where Re_L is given by:

$$\mathrm{Re}_L = \frac{\dot{m}_L D}{\mu_L} = \frac{\dot{m}(1-x)D}{\mu_L} \tag{2.22}$$

Lockhart and Martinelli correlated the multipliers in terms of the parameter X defined as follows:

$$X = \left[(dp_F / dz)_L / (dp_F / dz)_G\right]^{1/2} \tag{2.23}$$

Where $\left[\frac{dp_F}{dz}\right]_G$ is the pressure gradient for the gas phase flowing alone in the pipes. This is given by:

$$\left[\frac{dp_F}{dz}\right]_G = \frac{2f_G \dot{m}^2 G}{D\rho_G} = \frac{2f_G \dot{m}^2 x^2}{D\rho_G} \tag{2.24}$$

Where f_G is calculated from Equations (2.20) and (2.21), using gas phase Reynolds number instead. The original Lockhart and Martinelli correlation was in graphical form but Chisholm (1967) provided convenient fits to the curves. For instance, ϕ_L was fitted by the equation:

$$\phi_L^2 = 1 + \frac{C}{X} + \frac{1}{X^2} \tag{2.25}$$

Where the value of C depends on whether the gas or liquid phase flowing alone in the channel would have been turbulent or laminar. Values for C for the four possible combinations are listed in Table 2.1. For all the cases considered in this work, it was

BRL LONDON UNIV.

found that the gas phase was turbulent, i.e. the gas phase Reynolds number always exceeded 2000.

Gas	Liquid	C
Laminar	Laminar	5
Laminar	Turbulent	10
Turbulent	Laminar	12
Turbulent	Turbulent	20

Table 2.1 Values of parameter *C* for the Lockhart and Martinelli correlation.

2.1.1.1.4 Chisholm (1967)

A major problem with the Lockhart and Martinelli (1949) correlation is that it fails to take adequate account of the effect of mass flux; large differences exist between the experimental data and the correlation for high mass fluxes. The complex graphical correlations of Baroczy (1966) were aimed at allowing for the mass flux and other effects. The correlation of Chisholm (1967) was partly based on that of Baroczy but uses more convenient analytical expressions to correlate the data. Again their correlation is based on the separated flow approach.

In the Chisholm (1967) correlation, the pressure gradient is given by:

$$\left(\frac{dp_F}{dz}\right) = \phi_{LO}^2 \left(\frac{dp}{dz}\right)_{LO} \tag{2.26}$$

Where ϕ_{LO}^2 is defined as the ratio of the frictional pressure drop to that for a fluid having the *total* mass flux and the *liquid* properties, $\left[\frac{dp_F}{dz}\right]_{LO}$. It follows that:

$$\left(\frac{dp}{dz}\right)_{LO} = \frac{2 f_{LO} \dot{m}^2}{D \rho_L} \tag{2.27}$$

Where f_{LO} is obtained from the single-phase friction relationships (Equations 2.20 and 2.21) for a Reynolds number defined as follows:

$$Re_{LO} = \frac{\dot{m} D}{\mu_L} \tag{2.28}$$

Chisholm (1967) correlated ϕ_{LO} as a function of system parameters as follows:

$$\phi^2{}_{LO} = 1 + \left(Y^2 - 1\right)\left[Bx^{(2-n/2)}(1-x)^{(2-n)/2} + x^{2-n}\right] \tag{2.29}$$

Where x is the flow quality, n the exponent in the relationship between the friction factor and Reynolds number (e.g. n=0.2 in Equation 2.21) and Y is defined as:

$$Y = \left[(dp_F / dz)_{GO} / (dp_F / dz)_{LO} \right]^{1/2} \tag{2.30}$$

Where f_{GO} is a friction factor calculated for a single-phase flow (from Equation 2.20 and 2.21) with a Reynolds number defined as:

$$\mathrm{Re}_{GO} = \frac{\dot{m}D}{\mu_G} \tag{2.31}$$

The value of the parameter B in Equation (2.29) is dependent on the value of Y as follows:

$$B = \frac{55}{(\dot{m})^{0.5}} \quad \text{For } 0<Y<9.5 \tag{2.32}$$

$$B = \frac{520}{Y(\dot{m})^{0.5}} \quad \text{For } 9.5<Y<28 \tag{2.33}$$

$$B = \frac{15000}{Y^2(\dot{m})^{0.5}} \quad \text{For } 28<Y \tag{2.34}$$

2.1.1.1.5 Schlichting (1970)

The correlation of Schlichting (1970) was selected on the basis of the fact that that it had been modified for gas-oil-water three-phase flows. This separated flow-type correlation is similar to that utilised by Lockhart and Martinelli (1949) with the two-phase multiplier ϕ_L modified to account for oil viscosities ranging from 10 to 6000 mPas.

The pressure gradient of the mixture is calculated using the expression:

$$\left(\frac{dp}{dz}\right)_M = \phi_L^2 \left(\frac{dp}{dz}\right)_L \tag{2.35}$$

Where $$\phi_L^2 = C_1 + \frac{C_2}{X} \tag{2.36}$$

The parameters C_1 and C_2 are dependent on the ratio of the liquid and gas viscosities, η_r, which is defined by:

$$\eta_r = \left(\frac{\eta_L}{\eta_G}\right) \times 10^{-4} \tag{2.37}$$

Thus if $\eta_r < 100$ $C_1 = 1$; $C_2 = 6$

If $\eta_r > 100$ $$C_1 = \frac{1 + 0.65\eta_r^{0.8}}{(1-\lambda_w)^{1.3}}; \qquad C_2 = 6 + 7.5\eta_r^{0.5} \tag{2.38}$$

$\left(\frac{dp_F}{dz}\right)_L$ and X are calculated as in the case of Lockhart and Martinelli using Equations (2.18) and (2.23) respectively.

2.1.2 Holdup

The liquid holdup in two-phase gas-liquid flow is defined as the fraction of the pipe cross sectional area or volume that is occupied by the liquid phase. Again, many correlations are available in the literature for holdup and only selected ones were used for comparisons with the present data. The correlations selected were those of Lockhart and Martinelli (1949), Guzhov *et al.* (1967), Beggs and Brill (1973) and Minami and Brill (1987). The Lockhart and Martinelli (1949) and Beggs and Brill (1973) correlation were selected for consistency with the selection of pressure gradient correlations, and also because the latter correlation has been widely applied in hydrocarbon recovery systems. The other two correlations were selected on the basis also of their extensive use in these industrial systems. For a thorough review of liquid holdup correlations the reader is directed to the review carried out by Pan (1996).

2.1.2.1 Liquid holdup correlations

2.1.2.1.1 Lockhart and Martinelli (1949)

Lockhart and Martinelli (1949) presented their correlation for liquid holdup in the form of a graphical relationship between ε_L and the parameter X, which is defined in Equation (2.23). Pan (1996) presented the following expression as a best fit to this graphical correlation:

$$\varepsilon_L = 0.228255 + 0.111327 \ln X + 0.012566(\ln X)^2 - 0.001085(\ln X)^3 \quad (2.39)$$

And this equation has been used in the present work.

2.1.2.1.2 Guzhov *et al.* (1967)

Guzhov *et al.* (1967) concluded that ε_L was related principally to the Froude number Fr_M, which is defined by the expression in Equation (2.40) and the input liquid fraction λ_L.

$$Fr_M^2 = \frac{U_M}{gD} = \frac{(U_{G,S} + U_{L,S})^2}{gD} \tag{2.40}$$

They developed a correlation for the liquid holdup as follows:

$$\varepsilon_L = 1 - 0.81(1 - \lambda_L)\left[1 - \exp(-2.2\mathrm{Fr}_M^{2.5})\right] \tag{2.41}$$

The expression for the no slip holdup, λ_L, is given by Equation (2.15).

2.1.2.1.3 Beggs and Brill (1973)

Using quick-closing valve holdup data obtained from the facility described in Section 2.1.2.1, Beggs and Brill (1973) formulated a correlation for the liquid holdup. By carrying out regression analysis, Beggs and Brill were able to show (consistent with the findings of Guzhov *et al.*, 1967) that the liquid holdup in horizontal flows was affected most significantly by the Froude number $\mathrm{Fr_M}$ (see Equation 2.40) and the input liquid content λ_L. Beggs and Brill and proposed a relationship of the form:

$$\varepsilon_L(0) = A\lambda_L^{\alpha}\mathrm{Fr_M}^{\beta} \tag{2.42}$$

Where $\varepsilon_L(0)$ is the liquid holdup in horizontal; flow and A, α and β are constants.

This corresponds with the results obtained by Guzhov *et al.* (1967), who also developed a holdup correlation dependent on these two parameters. Further work was carried out to correlate the liquid holdup to the pipe inclination angle through an inclination correction factor ψ which multiplies the holdup value for horizontal flow (i.e. $\varepsilon_L(\theta) = \psi\varepsilon_L(0)$) where $\varepsilon_L(\theta)$ is the holdup in a pipe inclined at an angle θ to the horizontal.

A relationship between ψ and θ (in degrees) of the form as seen in Equation (2.43) was established.

$$\psi = 1 + E(\sin\phi - 1/3\sin^3\phi) \tag{2.43}$$

Where $\phi = 1.8\theta$

The experimental data were then subdivided into three regimes segregated, intermittent and distributed and it was seen that it was possible to correlate the E values with the input liquid content λ_L, the Froude number Fr and the liquid velocity number N_{LV}.

$$N_{LV} = U_{L,S}\left(\frac{\rho_L}{g\sigma}\right)^{0.25} \tag{2.44}$$

A summary of the results obtained for each flow pattern is shown in Table 2.2.

Horizontal flow pattern	Horizontal holdup $\varepsilon_L(\theta)$	Upward flow E	Downward flow E
Segregated	$\frac{0.98\lambda_L^{0.4846}}{Fr_M^{0.0868}}$	$(1-\lambda_L)\ln\left(\frac{0.011N_{LV}^{3.539}}{\lambda_L^{3.768}Fr_M^{1.614}}\right)$	$(1-\lambda_L)\ln\left(\frac{4.7N_{LV}^{0.1244}}{\lambda_L^{0.3692}Fr_M^{0.5056}}\right)$
Intermittent	$\frac{0.845\lambda_L^{0.5351}}{Fr_M^{0.0173}}$	$(1-\lambda_L)\ln\left(\frac{2.96\lambda_L^{0.305}Fr_M^{0.0978}}{N_{LV}^{0.4473}}\right)$	(same as the above)
Distributed	$\frac{1.065\lambda_L^{0.5824}}{Fr_M^{0.0609}}$	0	(same as the above)

Table 2.2 Values of parameters for the Beggs and Brill (1973) correlation

2.1.2.1.4 Minami and Brill (1987)

Minami and Brill (1987) carried out two-phase air-kerosene experiments and measured the liquid holdup using quick-closing valves. They produced a correlation for the liquid holdup expressed in terms of the parameter Z_e:

$$\varepsilon_L = 1 - \exp\left\{-\left[(\ln Z_e + 9.21)/8.7115\right]^{4.3374}\right\} \tag{2.45}$$

Where the parameter Z_e is defined by the expression:

$$Z_e = \frac{1.84N_{LV}^{0.575}N_{L\mu}^{0.1}}{N_{GV}N_D^{0.0277}}\left(\frac{p}{p_b}\right)^{0.05} \tag{2.46}$$

Where $N_{GV}, N_{LV}, N_{L\mu}$ and N_D are defined by the following expressions:

$$N_{GV} = U_{G,S}\left(\frac{\rho_L}{g\sigma}\right)^{0.25} \tag{2.47}$$

$$N_{LV} = U_{L,S}\left(\frac{\rho_L}{g\sigma}\right)^{0.25} \tag{2.48}$$

$$N_{L,\mu} = \mu_L\left(\frac{g}{\rho_L\sigma^3}\right)^{0.25} \tag{2.49}$$

$$N_D = D\left(\frac{\rho_L g}{\sigma}\right)^{0.5} \tag{2.50}$$

Where p is the system pressure and p_b is a reference pressure corresponding to atmospheric pressure.

2.1.3 Slug Flow

Slug flow is arguably the most dominant flow regime in multiphase pipelines and can have a significant influence on the performance of the phase separation equipment (slug-catcher). The pressure gradient occurring in this flow regime is significantly greater than those in the other flow regimes. In the present work, the predominant regime was slug flow and this Section presents aspects of earlier work on this type of flow in two-phase gas-liquid systems. The discussion starts in Section 2.1.3.1 with the presentation of two phenomenological models for slug flow, namely those of Bonnecaze *et al.* (1971) and Taitel and Barnea (1990). These models were used in the analysis of the present three-phase flow data (see Chapter 6). Section 2.1.3.2 discusses results from the literature on the detailed parameters of gas-liquid slug flow (slug velocity, slug body holdup, slug frequency and slug length); again the relationships reported form the basis for the comparisons with the present data for slug flow characteristics given in Chapter 6.

2.1.3.1 Phenomenological Models

There is an increasing tendency to prefer phenomenological models for specific flow regimes to the use of the traditional empirical-type correlation. Though such models may not always predict given sets of data more accurately than the empirical correlations, it is often argued that they offer a more secure route for extrapolations.

For slug flow, a number of phenomenological models have been developed. One of the earliest (and simplest) was that of Bonnecaze *et al.* (1971). A more detailed model was developed by Dukler and Hubbard (1975) and a more recent model (which essentially extends the Dukler and Hubbard treatment) is that of Taitel and Barnea (1990).

The present experimental data obtained on pressure drop and liquid holdup in the three-phase flow have been compared against two-phase gas-liquid phenomenological slug models (see Chapter 6). The models selected were those of Bonnecaze *et al.* (1971) and Taitel and Barnea (1990), the first for its simplicity and the second since it

is the most complete published model. These two models are described in what follows.

2.1.3.1.1 Bonnecaze *et al.* (1971)

Bonnecaze *et al.* (1971) developed a model for slug flow for horizontal and inclined pipes. In this model, the pressure drop across a slug unit was given as a sum of three terms: the pressure drop in the mixing zone (Δp_{mix}), at the slug front, the pressure drop in the slug body (Δp_{liq}) and the pressure drop in the gas bubble (Δp_{gas}). Thus

$$\Delta p_{slug} = \Delta p_{mix} + \Delta p_{liq} + \Delta p_{gas} \tag{2.51}$$

Bonnecaze *et al.* made the assumption that the pressure drop in the mixing zone was zero and that the pressure drop across the slug bubble was negligible. As a result of these assumptions, the expression for the pressure drop across the slug "unit" (i.e. the combined slug and bubble zones) reduces to:

$$\Delta p_{slug} = \Delta p_{liq} \tag{2.52}$$

Since the pressure drop in the liquid slug arises primarily due to the wall shear and gravitational forces acting on the liquid, it can be expressed using a Fanning friction factor type equation. Thus the pressure gradient for slug flow is defined by the expression below, which is essentially a sum of the gravitational and frictional forces respectively:

$$\left[\frac{dp}{dz}\right] = \alpha[g\rho_L \sin\theta + \frac{2f_L\rho_L U_M^{\ 2}}{D}] \tag{2.53}$$

Where θ is the pipe inclination angle, D is the pipe diameter, ρ_L is the liquid density, f_L is the Fanning friction factor calculated for liquid flow at a velocity U_M and liquid physical properties. α is the fraction of the pipe occupied by liquid slugs and is given by the ratio of the slug length l_s to the slug unit length l_t:

$$\alpha = \frac{l_s}{l_t} \tag{2.54}$$

By equating the total liquid in the slug unit to the liquid in the slug and in the film, Bonnecaze *et al.* were able to arrive at the following expression for α:

$$\alpha = \frac{l_s}{l_t} = \frac{\varepsilon_L - \varepsilon_f}{1 - \varepsilon_f} \tag{2.55}$$

Where ε_f is the average liquid holdup in the gas bubble and ε_L is the average holdup.

For horizontal flows, Bonnecaze *et al.* were able to show that α is approximately equal to the liquid volume fraction of liquid entering the pipe and is given by:

$$\alpha = \frac{U_{L,S}}{U_{L,S} + U_{G,S}} \tag{2.56}$$

Where $U_{L,S}$ and $U_{G,S}$ are the liquid and gas superficial velocities respectively.

For uphill and downhill flows, α is calculated using Equation (2.55) where ε_L and ε_F are evaluated below. A correlation for the average holdup was developed by Bonnecaze *et al.* and is defined by the expression:

$$\varepsilon_L = 1 - \frac{(1-\lambda_L)}{1.20 + \frac{0.35(1-\frac{\rho_G}{\rho_L})}{\delta\sqrt{Fr_M}}} \tag{2.57}$$

Where $\delta = +1$ for uphill flow, $\delta = -1$ for downhill flow, λ_L is the liquid volume fraction entering the pipeline given by Equation (2.15) and Fr_M is the Froude number as defined in Equation (2.40). The liquid holdup ε_F in the film is calculated from the following expression:

$$\frac{\varepsilon_F{}^3}{\frac{1}{\pi}\cos^{-1}(1-\frac{2h}{D})} = \frac{2 f_L Fr_M \lambda_F{}^2}{|\sin\theta|} \tag{2.58}$$

Where λ_F, a constant is defined by Equation (2.59)

$$\lambda_F = \delta\left[\frac{U_t}{U_{L,S}}(1-\varepsilon_F) - 1\right] \tag{2.59}$$

Where U_t is the slug translational velocity (See Section 2.1.3.2.2), $U_{L,S}$ is the superficial liquid velocity and ε_F is given by the expression.

$$\varepsilon_F = \frac{1}{\pi}\left[\cos^{-1}\left[1-\frac{2h}{D}\right] - \left[1-\frac{2h}{D}\right]\left[\frac{2h}{D}\right]^{0.5}\left[2-\frac{2h}{D}\right]^{0.5}\right] \tag{2.60}$$

Where h is the height of stratified liquid layer in the pipe and D is the pipe diameter. Equation (2.58) is solved iteratively by guessing values of h.

Because the velocity profile in the slug flow was likely to be unsymmetrical, Bonnecaze *et al.* developed a new friction factor correlation from their experimental measurements by correlating their pressure drop measurements with the following friction factor:

$$f_L = 0.0048 + \frac{3980}{\mathrm{Re}_s^{1.285}} \tag{2.61}$$

Where Re_s, the slug body Reynolds number is given by the expression

$$\mathrm{Re}_s = \frac{\rho_L U_M D}{\mu_L} \tag{2.62}$$

And U_M is the total gas and liquid mixture superficial velocity.

Bonnecaze *et al.* compared predictions from their model with oil-gas field data and reported good agreement.

2.1.3.1.2 Taitel and Barnea (1990)

Taitel and Barnea (1990) developed a mechanistic unit cell model to calculate the average pressure gradient over a slug unit. An illustration of the slug unit is shown in Figure 2.4.

Here the slug unit consists of two main sections: the slug film region of length l_f, which consists of an elongated gas bubble and a liquid film below it, and the slug body having a length l_s consisting of liquid with or without dispersed gas within it. The slug unit length which is the sum of the slug body length and the slug film length is denoted by the symbol l_u. The average velocity of the gas bubbles entrained within the slug body is U_b and the average velocity of the liquid within the liquid slug body is U_L. The velocity of the liquid in the film is denoted by U_f while the velocity of the gas is given by U_G.

The slug model was developed by carrying out mass and momentum balances. However, a few assumptions were made to simplify this process. It is assumed that the density of the liquid and the gas phases do not vary over the length of the entire slug unit (incompressible).

A liquid mass balance over the entire slug unit can be carried out in two ways:

(1) The first method is carried out by integrating the fluid flow rate at a fixed cross section over the time t_u, taken for the passage of one slug unit. This yields the following expression:

$$W_L = \frac{1}{t_u}\left(U_L A \varepsilon_s \rho_L t_s + \int_0^{t_f} U_f A \varepsilon_f \rho_L dt \right) \tag{2.63}$$

Where W_L is the input liquid flowrate, U_L is the average liquid velocity in the slug body, U_f is the liquid velocity in the film region, ε_s and ε_f are the average liquid holdup in the slug body and the film region respectively, A is pipe cross sectional area and t_s, t_f and t_u are the times taken for the passage of the slug body, the film region and the entire slug unit respectively.

Equation (2.63) can be expressed in another way by making use of the following expressions:

$$t_s = \frac{l_s}{U_t} \tag{2.64}$$

$$t_f = \frac{l_f}{U_t} \tag{2.65}$$

$$t_u = \frac{l_u}{U_t} \tag{2.66}$$

Where U_t is the translational velocity of the elongated bubble. Substituting expressions (2.64-2.66) into equation (2.63) leads to:

$$W_L = U_L A \varepsilon_s \rho_L \frac{l_s}{l_u} + \frac{1}{l_u}\int_0^{l_f} U_f A \varepsilon_f \rho_L dz \tag{2.67}$$

(2) The second method of carrying out a liquid mass balance over a slug unit consists of considering the volume of fluid in a slug unit.

This mass balance yields the following expression:

$$W_L = \frac{1}{t_u}\left(\rho_L A \varepsilon_s l_s + \int_0^{l_f} \rho_L A R_f dz \right) - G \tag{2.68}$$

The term in the brackets represents the mass of liquid in a slug unit. However, as the slug unit propagates in the pipe, some liquid is picked up at the front of the slug and is

shed at the rear of the slug. G represents the amount of liquid picked up and is given by the expression:

$$G = (U_t - U_L)\rho_L A\varepsilon_s = (U_t - U_f)\rho_L A\varepsilon_f \tag{2.69}$$

Equations (2.68) and (2.69) can then combined in the following manner yielding the expression:

$$W_L = \frac{1}{t_u}\left[\rho_L A\varepsilon_s l_s + \int_0^{l_f} \rho_L A\varepsilon_f dz\right] - (U_t - U_L)\rho_L A\varepsilon_s \tag{2.70}$$

$$\text{Now, } \frac{W_L}{\rho_L A} = U_{L,S} \tag{2.71}$$

And

$$\alpha_f = (1 - \varepsilon_f) \tag{2.72}$$

Where $U_{L,S}$ is the superficial liquid velocity and α_f is the void fraction in the liquid film. Substituting Equations (2.71) and (2.72) in Equation (2.70) gives

$$U_{L,S} = U_L\varepsilon_s - U_t\varepsilon_s + \frac{\varepsilon_s l_s}{t_u} + \frac{l_f}{t_u} - \frac{U_t}{l_u}\int_0^{l_f} \alpha_f dz \tag{2.73}$$

Further simplification of this expression leads to:

$$U_{L,S} = U_L\varepsilon_s + U_t(1 - \varepsilon_s)\frac{l_f}{l_u} - \frac{U_t}{l_u}\int_o^{l_f} \alpha_f dz \tag{2.74}$$

Applying a mass balance on both the liquid and gas phases on a cross section of the liquid slug zone yields the following expression:

$$U_M = U_{L,S} + U_{G,S} = U_L\varepsilon_s + U_b\alpha_s \tag{2.75}$$

Where U_M is the total mixture superficial velocity, U_L is the velocity of the liquid in the slug body and U_b is the gas in the slug body.

In order to calculate the pressure drop in slug flow, it is important to calculate the length of the liquid film l_f, its shape $h_f(z)$ and the velocity profile along the liquid film $U_f(z)$. To obtain solutions for the film velocity profile $U_f(z)$ and the film holdup profile $\varepsilon_f(z)$ momentum balances on the film zone are carried out. Equations (2.76) and (2.77) represent the momentum equations for the liquid film and the gas above it relative to a coordinate system moving with velocity U_t.

$$\rho_L v_f \frac{\partial v_f}{\partial z} = -\frac{\partial P}{\partial z} + \frac{\tau_f S_f}{A_f} - \frac{\tau_i S_i}{A_f} + \rho_L g \sin\theta - \rho_L g \cos\theta \frac{\partial h_f}{\partial z} \quad (2.76)$$

$$\rho_G v_G \frac{\partial v_G}{\partial z} = -\frac{\partial P}{\partial z} + \frac{\tau_G S_G}{A_G} + \frac{\tau_i S_i}{A_G} + \rho_G g \sin\theta - \rho_G g \cos\theta \frac{\partial h_f}{\partial z} \quad (2.77)$$

Where h_f is the height of the liquid film, the relative gas and liquid velocities are given by the expressions $\upsilon_f = U_i - U_f$, $\upsilon_G = U_i - U_G$ respectively and θ is the angle the pipe makes with the horizontal plane.

The shear stresses are given by the following expression:

$$\tau_f = \frac{f_f(\rho_L |U_f| U_f)}{2} \quad (2.78)$$

$$\tau_G = \frac{f_G(\rho_G |U_G| U_G)}{2} \quad (2.79)$$

$$\tau_i = \frac{f_i(\rho_G |U_G - u_f| (U_G - U_f))}{2} \quad (2.80)$$

Where f_i is the friction factor at the gas-liquid interface, f_f is the friction factor between the liquid film and the wall and f_G is the friction factor between the gas and the wall. These friction factors can be evaluated, for smooth pipes, using the Blasius correlation:

$$f_f = C_f (D_h U_f / \upsilon_l)^n \quad (2.81)$$

$$f_G = C_G (D_h U_G / \upsilon_G)^n \quad (2.82)$$

Where C_f=16 and n =-1 for laminar flow, C_f=0.046 and n =-0.2 for turbulent flow and D_h the hydraulic diameter for the liquid and gas phase respectively is given by the following expressions:

$$D_h = \frac{4A_f}{S_f} \quad (2.83)$$

$$D_h = \frac{4A_G}{(S_G + S_i)} \quad (2.84)$$

Where A_G, and A_f, the cross sectional area occupied by the gas and liquid phase are defined by:

$$A_G = \frac{D^2}{4}\left[\cos^{-1}\left(\frac{2h_f}{D} - 1\right) - \left(\frac{2h_f}{D} - 1\right)\sqrt{1 - \left(\frac{2h_f}{D} - 1\right)^2}\right] \quad (2.85)$$

$$A_f = D^2\left[\frac{\pi}{4} - \frac{A_G}{D^2}\right] \tag{2.86}$$

S_g, S_f, and S_i the perimeters for the gas phase, liquid film and the gas-liquid interface are given by:

$$S_G = D\left[\cos^{-1}\left(\frac{2h_f}{D} - 1\right)\right] \tag{2.87}$$

$$S_f = D\left[\left(\pi - D\cos^{-1}\left(\frac{2h_f}{D} - 1\right)\right)\right] \tag{2.88}$$

$$S_i = D\sqrt{1 - \left(\frac{2h_f}{D} - 1\right)^2} \tag{2.89}$$

For low liquid and gas velocities the interfacial friction factor f_i can be determined using the smooth surface friction factor, thus f_i/f_G=1 and for higher gas velocities when the gas-liquid interface is wavy a value of 15 is used for this ratio.

From the momentum conservation Equations (2.76) and (2.77), equating the pressure gradient in the gas and liquid phases yields the following expression:

$$\rho_L v_f \frac{\partial v_f}{\partial z} - \rho_G v_G \frac{\partial v_G}{\partial z} = \frac{\tau_f S_f}{A_f} - \frac{\tau_G S_G}{A_G} - \tau_i S_i\left(\frac{1}{A_f} + \frac{1}{A_G}\right) + (\rho_L - \rho_G)g\sin\theta - (\rho_L - \rho_G)g\cos\theta\frac{\partial h_f}{\partial z} \tag{2.90}$$

From equation (2.69) the relative velocity v_f can be expressed by:

$$\upsilon_f \equiv (U_t - U_f) = (U_t - U_l)\varepsilon_s / \varepsilon_f \tag{2.91}$$

For the gas this can be expressed as:

$$\upsilon_g \equiv (U_t - U_G) = (U_t - U_b)\alpha_s / \alpha_f \tag{2.92}$$

Substituting Equations (2.91) and (2.92) into (2.90) gives a differential equation for h_f as a function of z:

$$\frac{dh_f}{dz} = \frac{\frac{\tau_f S_f}{A_f} - \frac{\tau_G S_G}{A_G} - \tau_i S_i\left(\frac{1}{A_f} + \frac{1}{A_G}\right) + (\rho_L - \rho_G)g\sin\theta}{(\rho_L - \rho_G)g\cos\theta - \rho_L v_f \frac{(u_t - u_l)\varepsilon_s}{\varepsilon_f^2}\frac{d\varepsilon_f}{dh_f} - \rho_G v_G \frac{(U_t - U_b)(1-\varepsilon_s)}{(1-\varepsilon_f)^2}\frac{d\varepsilon_f}{dh_f}} \tag{2.93}$$

This differential equation can be solved numerically to yield the film height $h_f(z)$. The corresponding film velocity $u_f(z)$ is calculated by using the mass balance described by Equation (2.91).

To evaluate the length of the liquid film l_f, Equation (2.74) is used and the integration is carried out until this mass balance is satisfied.

The pressure drop for a slug unit can now be evaluated by carrying out a global force balance over a slug unit yielding:

$$\Delta p_u = \rho_u g \sin\theta_u + \frac{\tau_s \pi D}{A} l_s + \int_0^{l_f} \frac{\tau_f S_f + \tau_G S_G}{A} dz \tag{2.94}$$

Where the first term on the right hand side of Equation (2.94) represents the gravitational component of the pressure drop and the second and third terms are the frictional components of the pressure drop in the slug body and liquid film region respectively.

The average density of the slug unit is given by:

$$\rho_u = \alpha_u \rho_G + (1-\alpha_u)\rho_L \tag{2.95}$$

α_u the average void fraction of the slug unit is defined as :

$$\alpha_u = \frac{(\alpha_s l_s + \int_0^{l_f} \alpha_f dz)}{l_u} \tag{2.96}$$

Using Equations (2.74) and (2.75), Equation (2.96) can be simplified to:

$$\alpha_u = (-U_{G,S} + U_b \alpha_s + U_t \alpha_s)/U_t \tag{2.97}$$

From the above analysis, it can be seen that in order to calculate the pressure gradient in slug flow, closure laws for certain parameters need to be obtained. Taitel and Barnea (1990) give general guidance on these closure laws (though the model can be used with any reasonable set of laws) as follows:

1) Translational velocity

Taitel and Barnea note that the translational velocity is often expressed as:

$$U_t = C_o U_M + U_d \tag{2.98}$$

Where U_d is the drift velocity and U_M is the total superficial velocity. Taitel and Barnea cite typical values for C_o=1.2 and U_d =0.54gD and these values are used in the present implementation of the model.

(2)Slug body holdup

There are a number of correlations available for slug body hold-up. These are reviewed in Section 2.1.3.2.3 below. Taitel and Barnea also review these correlations and cite amongst others the correlation of Gregory *et al.* (1978). This correlation was used in the present implementation of the Taitel and Barnea model.

(3) Slug length

Taitel and Barnea review work on slug lengths (further information is given in Section 2.1.3.2.1 below) and concluded that (from the work of Nicholson (1978), a value of 30D was typical. Again this value has been used in the present implementation of the Taitel and Barnea model.

2.1.3.2 Slug Parameters

Although comprehensive phenomenological models for horizontal two-phase slug flow exist as exemplified in Section 2.1.3.1, these models still require closure relationships in the form of slug frequency (or slug length), slug translational velocity and liquid volume fraction within the slug. For two-phase gas-liquid flow, extensive work has been carried out on these parameters (though there is practically no reported data on three-phase flow- a deficiency addressed in the present work). This present section of the review highlights the work that has been carried out in the area of two-phase gas-liquid slug flow parameters, namely slug length (Section 2.1.3.2.1), slug velocity (Section 2.1.3.2.2), slug body holdup (Section 2.1.3.2.3) and slug frequency (Section 2.1.3.2.4).

2.1.3.2.1 Slug Length

The slug length is an important parameter, particularly for the sizing of downstream separation facilities. Because of the unsteady nature of slug flow, a critical quantity is

the maximum possible slug length, as it is this parameter upon which the slug catcher design is based. In what follows, a brief review is carried out on the most commonly used correlations and models of slug length in the literature.

Dukler and Hubbard (1975) observed stable slug lengths to be about 12-30D (where D is the pipe diameter) where a stable slug was defined as one, which is long enough for the velocity profile at the back of the slug to be fully developed.

Based on field data obtained from the Prudhoe Bay field, Alaska, Brill *et al.* (1981) developed a correlation for the mean slug length as a function of the pipe diameter and mixture velocity. This correlation is given by the expression:

$$\ln(3.2808 l_s) = -2.663 + 5.445(\ln(39.37D))^{0.5} + 0.059\ln(3.2808 U_M) \qquad (2.99)$$

Where l_s is the mean slug length, D is the pipe diameter and U_M is the total mixture superficial velocity.

Norris (1982) modified the above expression in Equation (2.99) using further data from the Prudhoe Bay Field and produced the following expression:

$$\ln(3.2808 l_s) = -2.099 + 4.589(\ln(39.37D))^{0.1} \qquad (2.100)$$

Crawley *et al.* (1984) made measurements of slug length for refrigerant-water and for refrigerant-glycerine systems and observed that the average slug length for the refrigerant-glycerine system was about 2.4 m (14 diameters) while that of the refrigerant-water was 1.2 m (7 diameters). They also observed that the slug lengths decreased with increasing gas velocity and increased with increasing gas density.

Barnea and Brauner (1985) extended an existing model for slug length in vertical flow by Taitel *et al.* (1980) to the horizontal case and obtained a stable slug length of 32D, which compared favourably with the experimental results of Gregory *et al.* (1978).

Scott *et al.* (1986), using a much wider range of flowrates were able to put forward the following relationship for predicting the slug length in large diameter pipelines.

$$\ln(3.2808 l_s) = -25.4134 + 28.4948(\ln(39.37D))^{0.1} \qquad (2.101)$$

Using the residence time and velocity of slug bubbles at a conductance probe measuring station; Nydal (1991) was able to calculate slug lengths in air-water two-phase flow. He observed that the lengths of the slugs were independent of the mixture velocities over a wide range. His results are illustrated in Figure 2.5, where the mean slug lengths are plotted against the total mixture superficial velocity. For a 48 mm (1.9 inch) internal diameter tube, slug lengths in the range of 15-20D were observed, whereas in the case of an 89 mm (3.5 inch) internal diameter pipe, the lengths of the slugs were in the region of 12-16 D where D is the tube diameter.

Manolis (1995) using the WASP Facility carried out two-phase air-oil and air-water slug flow experiments. By analysing the traces from a pair of conductivity probes, the slug length was obtained. For the set of conditions he investigated, Manolis observed that the slug length varied between 10 and 25D. He also investigated the effects of gas and liquid superficial velocities on the slug length and concluded that increasing the water superficial velocity led to an increase in the slug length, while increasing the air superficial velocity resulted in a decrease in the slug length. In addition to this, the effect of system pressure on the slug length was studied, and this led to the result that the slug length decreased as the system pressure increased. Manolis compared his experimental data with the slug length correlations of Brill *et al.* (1981), Norris (1982) and Scott *et al.* (1986). The comparisons showed that all the correlations significantly over-predicted his experimental data. Manolis attributed this finding, to the fact that the correlations had been derived from pipeline field data, which were more likely to have incorporated slug growth and decay, two factors likely to have an effect on the slug length.

Goncalves *et al.* (1996) measured slug lengths in a 200 m long 152 mm (6 inch) internal diameter, pipeline for a gas-oil system. They obtained the slug characteristics by cross-correlating the signals from a pair of differential pressure transducers arranged in a top-to-bottom configuration. They obtained a log-normal distribution for the slug lengths in agreement with the findings obtained by Brill *et al.* (1981) although the average slug lengths measured were in excess of the 30D value that had been postulated by earlier researchers.

Marcano *et al.* (1998) using a 76 mm (3 inch) internal diameter horizontal pipeline carried out two-phase air-kerosene experiments and obtained data on slug length by using two capacitance probes to track the propagation of slugs through the pipeline. They obtained a lognormal slug length distribution. They developed a new correlation for slug length using the parameters of Hill and Wood (1994) and compared the prediction of the new correlation with that of the original Hill and Wood (1994) correlation and observed a better prediction with their correlation.

2.1.3.2.2 Slug Velocity

The slug velocity is a key parameter in the modelling of slug flow and therefore has been studied extensively by several researchers. It is important, because it is one of the several closure relationships required by existing pressure drop prediction models.

Dumitrescu (1943) studied the rise velocity of bubbles through a stagnant liquid in a vertical tube. He then showed both theoretically (by assuming potential flow around the bubble nose) and experimentally that the rise velocity of the bubble was:

$$U_d = 0.35\sqrt{gD} \tag{2.102}$$

Davies and Taylor (1949) also arrived at the same result. They carried out experiments to measure the rate at which long glass vertical tubes of different diameters were emptied. They obtained values of $\frac{U_d}{gD}$ ranging from 0.33 to 0.346 (for the largest tube), which compares favourably with the theoretical figure of 0.328, which they had derived earlier.

Zukoski (1966) measured the effect of viscosity, surface tension and tube inclination angle on the velocity of large bubbles propagating into closed horizontal and upward sloping pipes. He found that as the surface tension increased, the bubble rise velocity decreased. For horizontal pipes with large diameters, where surface tension effects are negligible he found that:

$$U_d = 0.54\sqrt{gD} \tag{2.103}$$

Benjamin (1968) carried out a theoretical analysis for the case of a horizontal tube filled with liquid in one end and open at the other end. By applying mass and momentum conservation equations across a control volume moving with the bubble as well as the Bernoulli equation along the interfacial streamline, Benjamin was able to derive the following expression for the bubble rise velocity:

$$U_d = 0.542\sqrt{\left(\frac{\rho_L - \rho_G}{\rho_L}\right)gD} \tag{2.104}$$

This expression concurs with the experimental results of Zukoski (1966).

While all of the above work had been carried out for bubbles passing into stagnant liquids, Griffith and Wallis (1959) extended this to encompass the propagation of bubbles in non-stationary liquid by carrying out slug flow experiments using an 18-ft vertical tube. They showed that the bubble-rise velocities in slug flow were quite sensitive to the velocity profile in the water ahead of the bubbles and proposed the following relationship to account for this:

$$U_d = C_3 C_4 \sqrt{gD} \tag{2.105}$$

Where C_3 is the governing coefficient in stagnant water and C_4 is a function of the water velocity.

Nicklin *et al.* (1962) carried out experiments in which the rise velocity of the large bubbles (Taylor bubbles) in slug flow was measured in upward and downward flowing streams of water. He proposed a relation for the slug propagation velocity in a stagnant liquid, which consisted of the rise velocity U_d, plus a component due to the motion of the fluid:

$$U_t = C_o(U_{G,S} + U_{L,S}) + U_d \tag{2.106}$$

Where $U_{G,S}$ and $U_{L,S}$ and the gas and liquid superficial velocities. For the vertical pipe used:

$$U_d = 0.35\sqrt{gD} \tag{2.107}$$

The following values for C_o were found:

$C_o \approx 1.2$ for fully developed turbulent flow
≈ 2 for laminar flow
< 1.0 for downward slug flow

Crawley *et al.* (1984) carried out two-phase gas-liquid slug flow experiments in a horizontal 171-mm (6.75-inch) internal diameter pipe at high pressure. They measured a number of slug characteristics, slug velocity being included among these. Using an air/water system and refrigerant-water system they obtained a value of 1.35 for C_o, which compared favourably with the result obtained by Gregory and Scott (1969). Replacing the water with a glycerine solution of high viscosity of 0.4 Pas (400 cP) they obtained a value of 2.0 for C_o. They then concluded that there was little effect of gas density on the slug velocity whereas the effect of liquid viscosity was very evident.

Bendiksen (1984) carried out a series of experimental investigations of the bubble propagation rate as a function of several parameters including the pipe inclination angle, the Froude number, the Reynolds number and the surface tension for both stagnant liquid and non-stagnant liquid systems.

Bendiksen's results showed that for Fr ≥ 3.5, C_o has a value of between 1.19 and 1.20 for all inclination angles. The results obtained by Bendiksen can be summarised as follows:

$$\begin{aligned} &C_o = 1.05 + 0.15\sin^2\theta, \; U_d = \sqrt{gD(0.35\sin\theta + 0.54\cos\theta)} && \text{for } Fr^2 = \frac{U_{L,S}{}^2}{gD} < 3.5^2 \\ &C_o = 1.2, && \text{for } Fr^2 = \frac{U_{L,S}{}^2}{gD} > 3.5^2 \end{aligned} \qquad (2.108)$$

Nydal (1991) carried out experiments to measure slug bubble velocities in two-phase air-water flow using conductance probes. He plotted the slug bubble velocity against the mixture velocity, and by assuming the Nicklin *et al.* (1962) relationship (Equation (2.106)) between the slug bubble velocity and the mixture velocity, he was able to calculate mean values for C_0. A graphical representation of his results is shown in Figure 2.6.

The values of C_0 from his experiments are higher than the 1.2 value obtained by earlier workers. Nydal attributed this to several factors, particularly the presence of bubbles within the liquid slugs.

Manolis (1995) using the WASP High Pressure Multiphase Facility, carried out an extensive study of slug velocity in two-phase air-water flow by cross-correlating the signals from conductivity probes and obtained the following result for the slug translational velocity:

$$U_t = U_M(0.00648p + 1.2031) \tag{2.109}$$

Where p is the system pressure in barg.

It is interesting to note that at atmospheric pressure the above equation collapses to:

$$U_t = 1.21U_M \tag{2.110}$$

Similar to the result obtained by previous researchers.

2.1.3.2.3 Slug Body Hold-Up

The slug body holdup i.e. the volume fraction of liquid in the slug body, is also required in slug models as a closure relationship. A significant amount of research has been devoted to the slug body holdup in air-water and air-oil two-phase slug flow systems, but the effect of liquid viscosity on the slug body holdup has not been studied extensively.

Gregory *et al.* (1978) using capacitance sensors measured slug body hold-up for an air-light oil fluid system and arrived at the following correlation:

$$\varepsilon_s = 1 - \frac{1}{1 + \left(\frac{U_M}{8.66}\right)^{1.39}} \tag{2.111}$$

This equation is widely used on the basis of its simplicity, although it fails to account for the influence of the physical properties of the liquid on the slug body holdup.

Malnes (1983) proposed a correlation based on the data obtained by Gregory et al. as follows:

$$\varepsilon_s = \frac{U_M}{83\left(\frac{g\sigma}{\rho_L}\right) + U_M} \tag{2.112}$$

Where σ is the liquid surface tension.

Barnea and Brauner (1985) put forward a model for the prediction of the liquid slug void fraction. The method is based on the assumption that the liquid hold-up in the slug body is equal to the liquid hold-up of fully dispersed bubble flow on the transition boundary with the same mixture velocity.

Ferschneider (1989) proposed the following correlation, based on experiments carried out using natural gas and condensate as the test fluids in a 142 mm (5.6 inch) internal diameter pipe for inclination angles ranging from 0 to 4°.

$$\varepsilon_s = 1 - \frac{1}{\left\{1 + \left[\frac{U_M}{\sqrt{\left(1-\frac{\rho_G}{\rho_L}\right)gD}}\right]^2 \div \left(\frac{A}{\mathrm{Bo}^{\beta}}\right)^2\right\}^2} \tag{2.113}$$

Where σ is the surface tension and Bo the Bond number is defined by:

$$\mathrm{Bo} = \frac{(\rho_L - \rho_G)gD^2}{\sigma} \tag{2.114}$$

No information was given on the value of the coefficients A and β.

Andreussi and Bendiksen (1989) investigated the effect of pipe diameter and pipe inclination angle on slug body void fraction using 48 mm (1.9 inch) and 89 mm (3.5 inch) internal diameter pipes and using air and water as their test fluids. They measured the void fractions by using conductance probes. They observed that the pipe diameter had a significant effect on the slug body void fraction.

Andreussi and Bendiksen also measured slug body void fractions for different pipe inclinations -3°, -0.5°, 0° and 0.3°. As can be seen from Figures 2.7 and 2.8, where the slug body void fraction has been plotted against the total superficial velocity, two trends are clear. For downflow, a decrease in the slug body void fraction was observed for the downwardly inclined angle of -3° with respect to the horizontal case.

Andreussi and Bendiksen attributed this to the diminished bubble production in downflow arising from decreases in the relative slug and film velocity.

For upflows, an increase in the slug body void fraction was observed. This trend was found to be even more pronounced in the data of Ferschneider shown in Figure 2.9.

Nydal (1991) carried out a detailed experimental investigation into the void fraction in the slug body. His experiments were carried out with air and water using one 52.9-mm internal diameter stainless steel pipe and a 90-mm internal diameter acrylic pipe. The slug void fraction was measured with the aid of conductance probes.

Nydal's results indicated that for gas to be entrained within the slug body, a minimum superficial mixture velocity must be exceeded. In addition he compared his experimental results with two correlations, Gregory *et al.* (1978) and Andreussi and Bendiksen (1989). His comparisons showed that the correlation of Andreussi and Bendiksen matched his data more closely than that of Gregory *et al.* (1978). The reason for this is probably due to the fact that the Gregory *et al.* correlation is based on experiments carried out with air and oil, a system which has a higher void fraction, whereas the Andreussi and Bendiksen correlation is based on air-water data and accounts for the physical properties of the fluids. Nydal's experimental results and the comparisons with the above-mentioned correlations are shown in Figure 2.10.

Nydal proposed a relationship for the void fraction in the slug body incorporating the effects of gas entrainment due to dispersed gas in the liquid layer as well as surface entrainment from the gas bubble. This relationship is given by:

$$\alpha_s\left[1+\left(\frac{K_1 S_i}{h_b D}+\frac{\alpha}{1-\alpha}\right)\right]=\left(\frac{K_1 S_i}{h_b D}+\frac{\alpha_f}{1-\alpha_f}\right)-\frac{K_2}{(C_0-1)U_M+U_d} \qquad (2.115)$$

Where U_M is the mixture velocity, U_d slug bubble drift velocity, S_i the interface parameter, h_b the liquid volume fraction in the slug bubble, K_1 and K_2 are coefficients in gas entrainment relations, D is the pipe diameter, C_o is the dimensionless distribution parameter, α_f is the void fraction in the liquid film and α_s the void fraction within the liquid slug.

Nydal compared the predictions from Equation (2.115) with his experimental results and obtained good agreement. Nydal also examined the effect of pipe inclination on the void fraction within the slug body using an air-water system. It can be seen from Figure 2.11, that increasing the pipe inclination angle from -7° to 90° leads to an increase in the slug void fraction.

The effect of fluid properties on the slug void fraction was investigated. Using a gamma densitometer, Nydal (1991) measured slug void fraction for air-oil slug flow and reported that the slug body void fraction in air-oil slug flow was much higher than that for air-water flow.

Nadler *et al.* (1995) carried out experiments to study the effect of liquid viscosity on the phase distribution in horizontal gas-liquid slug flow. The liquids used for the experiments were water and oil. The viscosity of the oil was varied between 0.014 to 0.037 Pas and density in the range of 834 to 848 kg/m^3. The slug body holdup was measured through the use of a multi-beam gamma densitometer. The results obtained showed that the liquid holdup in the film region for two-phase air-oil slug flow was greater than that of two-phase air-water slug flow. For the slug body, the opposite was the case, with the liquid holdup in the slug body for two-phase air-water slug flow being greater than that for two-phase air-oil slug flow.

Manolis (1995) measured average slug body holdup in air-water and air-oil two-phase flow using the WASP High Pressure Multiphase Facility. For both flows, he observed that increasing the air superficial velocity led to a decrease in the average slug body holdup for a constant liquid superficial velocity. In addition, Manolis also showed that increasing the system pressure led to a decrease in the average slug body holdup. The water superficial velocity had no discernible influence on the average slug body holdup.

Marcano *et al.* (1998) measured slug body holdup using capacitance probes. Based on his experimental results, he was able to formulate a correlation for the slug body holdup:

$$\varepsilon_S = \frac{1}{1.001 + 0.0179U_M + 0.0011U_M^{\ 2}} \tag{2.116}$$

Where U_M is the mixture superficial velocity. He compared this correlation with his experimentally measured slug body holdup and observed a relative error of 8%. Marcano *et al.* applied this correlation as well as the correlations of Gregory *et al.* (1978), Yang (1995) to a combined data set, consisting of two-phase slug flow data from the experimental work of Kouba (1986), Roumazeilles (1994) and Yang (1995). Marcano *et al.* observed that their correlation was the most accurate in predicting the data. In addition to this, Marcano *et al.* observed that the liquid holdup in the slug body decreased with increasing gas velocity and increased with increasing liquid superficial velocity.

From an experimental database containing the slug body holdup data of Schmidt (1977), Kouba (1986), Rothe *et al.* (1986), Kokal (1987), Brandt and Fuchs (1989) and Felizola (1992), Gomez *et al.* (2000) were able to develop a correlation for the slug body holdup as a function of the slug Reynolds number and the inclination angle of the pipe. The correlation is given by the expression:

$$\varepsilon_S = 1.0e^{-(0.45\theta + 2.48\times10^{-6}\, Re_S)} \qquad 0 \le \theta \le 1.57 \tag{2.117}$$

Where Re_s is the slug Reynolds number defined as:

$$Re_S = \frac{\rho_L U_M D}{\mu_L} \tag{2.118}$$

and θ is the inclination angle in radians.

2.1.3.2.4 Slug Frequency

Gregory and Scott (1969) proposed a correlation for slug frequency from data they had obtained in a CO_2-water system.

$$\upsilon_S = 0.0226\left[\frac{U_{L,S}}{gD}\left(\frac{19.75}{U_M} + U_M\right)\right]^{1.2} \tag{2.119}$$

Greskovich and Shrier (1972) combining their data with those of Hubbard (1965) obtained the following correlation:

$$\upsilon_s = 0.0226\left[\frac{U_{L,S}}{U_M}\left(\frac{2.02}{D}+\frac{U^2{}_M}{gD}\right)\right]^{1.2} \tag{2.120}$$

Taitel and Dukler (1977) introduced the concept of slug formation as an entrance phenomenon. They then applied the conservation equations for mass and momentum and modelled the entrance phenomenon assuming open channel flow. By reducing the problem to one of determining the characteristic time (the time taken for the liquid to rebuild from its lowest value to the equilibrium value) they calculated the slug frequency by assuming it to be equivalent to the inverse of the characteristic time. Predictions of the model were compared with the data of Dukler and Hubbard (1975), Gregory and Scott (1969) and Vermeulen and Ryan (1971). Good results are obtained in comparison with the data of Dukler and Hubbard (1975). Less satisfactory results were obtained with the data of Gregory and Scott (1969) and Vermeulen and Ryan (1971). The model predicts an increase of frequency with increasing liquid superficial velocity at constant gas superficial velocity as well as a minimum in the plot of slug frequency versus gas velocity at constant liquid superficial velocity.

Heywood and Richardson (1979) were able to estimate the average slug frequency and length by calculating the probability density function and power spectral density of the hold-up. Based on this they proposed the following relationship for the slug frequency:

$$\upsilon_s = 0.0434\left[\lambda_L\left(\frac{2.02}{D}+\frac{U_M^2}{gD}\right)\right]^{1.02} \tag{2.121}$$

Where λ_L is the no slip liquid holdup.

Jepson and Taylor (1988) proposed a correlation based on data obtained from a 30-cm diameter horizontal pipe:

$$\frac{\upsilon_s D}{U_{L,S}} = 4.76\times10^{-3}U_M + 0.035 \tag{2.122}$$

By assuming that the slug frequency was half the frequency of unstable waves precursors of slugs, Tronconi (1990) presented a semi-mechanistic model for slug frequency in horizontal pipes. The expression for the slug frequency was derived as:

$$\upsilon_s = 0.61 \frac{\rho_G}{\rho_L} \frac{U_G}{h_G} \tag{2.123}$$

Predictions from Equation (2.123) were compared with data from Hubbard (1965), Dukler and Hubbard (1975), Heywood and Richardson (1979), Gregory and Scott (1969), Kago *et al.* (1987), Knervold *et al.* (1984) and Vermeulen and Ryan (1971). In all cases except in the case of the data produced by Gregory and Scott (1969) and Vermeulen and Ryan (1971) the model obtained satisfactory results both quantitatively and qualitatively.

Tronconi also investigated the effect of gas and liquid flowrates, pipe diameter, gas density and liquid viscosity on the slug frequency and put forward explanations for these. The Tronconi model was able to predict the increasing slug frequency with decreasing pipe diameter as well as the maxima appearing on the frequency vs. gas superficial velocity plots at low gas rates in small diameter pipes, a trend that had been reported by Taitel and Dukler (1977) and Nicholson *et al.* (1978). The model was also capable of dealing with the effect of gas and liquid properties (particularly the viscosity) on the slug frequency. This is confirmed by the agreement obtained with the data of Kago *et al.* (1987) and Knervold *et al.* (1984). The reason for the enhancement of the slug frequency in the case of more viscous liquids was attributed to the higher equilibrium level of the entry stratified flow.

Hill and Wood (1990) formulated a correlation for the slug frequency based on data obtained from a 50 mm diameter pipe using air and water. The correlation is given by the expression:

$$\Omega = \frac{\upsilon_s D}{(U_G - U_L)} = \frac{2.74 \varepsilon_{LE}}{1 - \varepsilon_{LE}} \tag{2.124}$$

Where Ω is the dimensionless slug frequency and ε_{LE} is the equilibrium liquid holdup.

Nydal (1991) measured slug frequencies in a 59-mm (2-inch) internal diameter pipe and results obtained are shown in Figure 2.12. All results show the characteristic minimum in the slug frequency versus mixture velocity plot reported by several researchers. Nydal compared his data with that of Gregory and Scott (1969) and obtained good agreement for the range $U_{G,S} < 10$ m/s and $U_{L,S}$ 1.3 m/s. At higher gas

and liquid flowrates, there is some discrepancy between the correlation and the data of Nydal. While the data shows a fairly constant slug frequency at these conditions, the correlation of Gregory and Scott shows a strong increase with $U_{G,S}$.

Because of the inadequacy of existing slug frequency correlations in predicting his data, Manolis (1995) developed a new slug frequency correlation based on seven non-dimensional numbers. The expression for the slug frequency is given by:

$$\left[\frac{\upsilon_s D}{U_{G,S}}\right]^{260\left(\frac{1}{N_f}\right)+0.85} = 0.0363\frac{F_L}{F_G}\frac{Z}{X}\left(\frac{1}{Eo}\right)^{0.2} \tag{2.125}$$

Where the inverse of the viscosity number is given by the expression:

$$\frac{1}{N_f} = \frac{\mu_L}{D^{1.5}\left[\rho_L\left(\rho_L-\rho_g\right)g\right]^{0.5}} \tag{2.126}$$

F_L and F_G the liquid phase and gas phase Froude numbers are denoted by the expressions:

$$F_L = \frac{U_{L,S}}{\sqrt{gD}} \tag{2.127}$$

$$F_G = \frac{U_{G,S}}{\sqrt{gD\left(\frac{\rho_L}{\rho_L-\rho_G}\right)}} \tag{2.128}$$

Z the ratio of inertial to gas phase pressure drop is given by the Equation (2.129):

$$Z = \left[\frac{\frac{\rho_L U_{L,S}{}^2}{2D}}{\left(\frac{\mathrm{dp}}{\mathrm{dz}}\right)_G}\right]^{0.5} = \left[\frac{\frac{\rho_L U_L{}^2}{2D}}{\frac{4}{D}C_f Re_G{}^{-m}\frac{\rho_G U_G{}^2}{2}}\right]^{0.5} \tag{2.129}$$

And X the ratio of the liquid to gas pressure gradient flowing alone in the pipe is given by:

$$X = \left[\frac{\left(\frac{dp}{dz}\right)_L}{\left(\frac{dp}{dz}\right)_G}\right]^{0.5} = \left[\frac{\frac{4}{D}C_f Re_L{}^{-m}\frac{\rho_l U_{L,S}{}^2}{2}}{\frac{4}{D}C_f Re_G{}^{-m}\frac{\rho_G U_{G,S}{}^2}{2}}\right]^{0.5} \tag{2.130}$$

E_o the Eotvos number is given by:

$$E_o = \frac{(\rho_L - \rho_G)}{\sigma} gD^2 \qquad (2.131)$$

Manolis compared slug frequency data from the published literature as well as those obtained from the WASP facility with his correlation and concluded that the correlation predicted all the experimental data reasonably well.

2.2 TWO-PHASE LIQUID-LIQUID FLOW

Two-phase liquid-liquid flow occurs in a number of industrial processes such as liquid-liquid extraction as well as multiphase pipelines. This type of flow is considerably different from two-phase gas-liquid flow due to a number of factors. Firstly, the viscosity ratio in liquid-liquid flow is much higher than that occurring in gas-liquid flow, meaning that the slip velocities and drag between the phases are likely to be considerably different from that of gas-liquid flow. Secondly, the ratio of the fluid densities in liquid-liquid flow is also higher than that prevailing in gas-liquid flow. As a result of this, the separating out of the phases in liquid-liquid flow is less pronounced, thus increasing the tendency for the formation of dispersions.

2.2.1 Flow Pattern

As in the case of two-phase gas-liquid flow, the two fluids in two-phase liquid-liquid flow can distribute themselves in a wide number of forms, known as flow patterns or flow regimes. Trallero (1995) delineated the flow patterns occurring in two-phase liquid-liquid flow under the following:

(1) Segregated flow: consisting of Stratified flow (ST) and Stratified flow with mixing at the interface (ST&MI)

(2) Water-dominated Dispersed flow: consisting of dispersion of oil in water and water (Do/w&w) and Oil in water dispersions (o/w)

(3) Oil-dominated Dispersed flow: consisting of dispersions of water in oil and oil in water (Dw/o&Do/w).

Illustrations of these flow patterns can be seen in figure 2.13a and Figure 2.13b.

A detailed description of these flow patterns can be obtained from the review of Valle (1999).

2.2.2 Pressure Drop

The pressure drop in liquid-liquid two-phase flow is a very important parameter. The drive behind the research of pressure gradient in liquid-liquid flow arose from the idea of injecting water into pipelines to reduce the pressure drop and therefore the pumping capacity. The behaviour of the pressure drop in two-phase liquid-liquid flow depends essentially on the flow pattern.

For dispersed flows, it was observed by Hardin (1995) and Soleimani (1999) that the pressure drop increases gradually from single phase oil flow, reaching a maximum at the phase inversion point and decreased thereafter to single phase water flow.

Soleimani (1999) observed a fall in the measured pressure gradient as shown in Figure 2.14. More importantly, a peak on the pressure gradient versus water-cut was observed for around 40%. This peak was explained by the fact that it coincided with the phase inversion point where there was a change in the flow pattern from oil-continuous to water continuous. This peak in the pressure gradient versus water-cut plot is attributed to the formation of emulsions between the liquid phases.

2.2.2.1 Viscosity models

Attempts to obtain correlations and expressions for predicting the pressure gradient in liquid-liquid flows have been hindered by the difficulty in producing expressions capable of describing the effective viscosity of the liquid-liquid mixture adequately. Initially, researchers used a method of linear interpolation to predict the viscosity of a liquid-liquid mixture. This approach is denoted by the expression:

$$\mu_L = (1-\lambda_W)\mu_O + \lambda_W \mu_W \tag{2.132}$$

Where μ_L is the effective viscosity of the liquid mixture, λ_w is the input water fraction in the liquid, which is given by: $\frac{U_{W,S}}{U_{W,S}+U_{O,S}}$ where $U_{W,S,}$ and $U_{O,S}$ are the water and oil superficial velocities respectively and μ_o and μ_w are the viscosities of the oil and water phases respectively.

Equation (2.132) is based on the assumption that the effective viscosity of the oil and water liquid mixture lies somewhere between the water viscosity and the oil viscosity.

Results of experiments carried out by Mkpadi *et al.* (1990) show that the viscosity of the mixture may lie outside the range suggested by Equation (2.132) and may even be several times the viscosity of oil.

Furthermore, this approach has been shown to produce very large discrepancies in the prediction of pressure gradients in two-phase liquid-liquid flows for cases where there is a dispersion of one of the liquid into the other.

Attempts have been made by several researchers to find a suitable viscosity expression capable of describing the emulsion viscosity. A brief outline of the various viscosity expressions available to predict the behaviour of oil-water emulsions is presented below.

This review of viscosity expressions for liquid-liquid flow is by no means exhaustive. Focus has been placed on expressions used by multiphase flow researchers. Some earlier studies have been included for background purposes only.

Einstein (1906) was one of the earliest researchers to notice that in a suspension of solid particles in a liquid, an increase in the amount of the dispersed phase (in this case the solid particles) led to an increase in the viscosity of the suspension. He suggested the following expression for the relative viscosity of the suspension:

$$\mu_r = 1 + 2.5\lambda_{dis} \tag{2.133}$$

Where μ_r the relative viscosity is defined as the ratio of the viscosity of the suspension to the viscosity of the continuous phase and λ_{dis} is the volume fraction of the dispersed particles.

Hatschek (1928) obtained the following relationship for the viscosity of emulsions:

$$\mu_L = \frac{\mu_{cont}}{\left(1 - \lambda_{dis}^{\ k_2}\right)} \tag{2.134}$$

Where μ_{cont} is the viscosity of the continuous liquid phase and the constant k_2 has a recommended value of 0.33

However Richardson (1950) showed that the Einstein expression, Equation (2.133) was applicable to liquid-liquid systems, by carrying out experiments using a benzene-water system. He noticed that the viscosity of the benzene-water dispersion increased exponentially with the concentration of the dispersed phase (in this case, water). He later derived a theoretical explanation for this phenomenon, tested it with his data and those of other workers, and found that it agreed well with his theory. His expression for the mixture viscosity is given by:

$$\mu_L = \mu_{cont} e^{k_3 \lambda_{dis}} \tag{2.135}$$

Where μ_{cont} is the viscosity of the continuous liquid phase and k_3 is a constant with a recommended value of 2.5.

Mooney (1950) extended Einstein's equation for infinitely dilute suspensions to a suspension of finite concentration and accounted for the space crowding effect of the suspended particles on each other. From this he derived the following expression for the relative viscosity of an emulsion system:

$$\mu_r = exp\left(\frac{2.5\lambda_{dis}}{1 - k\lambda_{dis}}\right) \tag{2.136}$$

Where the constant k has a value between 1.35 and 1.91.

Vand (1948) carried out some experiments, which validated the theory of Mooney (1950) and found that a value of 1.43 was suitable for k.

Brinkman (1952) developed a method for estimating the viscosity dependence on concentration. He derived an expression for the relative viscosity and the expression agreed well with the measurements carried out by Eilers (1941) on asphalt emulsions. This expression is given by:

$$\mu_L = \frac{\mu_{cont}}{(1 - \lambda_{dis})^{k_1}} \tag{2.137}$$

Where k_1 is a constant with a recommended value of 2.5.

Pal and Rhodes (1985) also noticed that as the concentration of the dispersed phase was increased, the viscosity of the emulsion increased almost exponentially in all the emulsion systems that they investigated. They then introduced a parameter to

incorporate the effect of particle size distribution and particle size. They arrived at the expression:

$$\mu_r = \left[1 + \frac{\frac{\phi}{K_2}}{1.187 - \frac{\phi}{K_2}}\right]^{2.5} \tag{2.138}$$

Where μ_r is the relative viscosity, ϕ is the disperse phase concentration at which the relative viscosity is equal to 100 and K_2 is a constant with a value ranging from 0.5 to 1.2 depending on the system.

The drawback of the Pal and Rhodes method is that it entails measuring the dispersed phase fraction at the point where the relative viscosity becomes 100. This is difficult to do for a flowing system in a pipe and an alternative approach would involve back calculation of the viscosity using the pressure drop measurements. However the problem with back calculating the effective viscosity from the measured pressure drop, is the possibility of introducing further errors through the pressure drop expression.

Urdahl *et al.* (1997) carried out a review of existing viscosity expressions for liquid-liquid systems and reported that most of them neglected the effect of droplet size and droplet size distribution. Attention was drawn to a set of correlations developed by Rϕnningsen (1995), for water-in-crude oil emulsions based on experimental data. These correlations account for droplet sizes and shear rate. The equation is denoted by the expression:

$$\ln \mu_L = k_1 + k_2 T + k_3 \phi + k_4 T \phi \tag{2.139}$$

Where $k_1 - k_4$ are correlation constants and T is the temperature.

However, as in the case of the expression derived by Pal and Rhodes (1985), the Urdahl *et al.* expression depends on a parameter (in this case drop size), which is difficult to measure in a flowing system.

2.2.3 Holdup

Experimental studies have been carried out on the slip ratio between the liquids in two-phase liquid-liquid flow and have shown this to be dependent on the flowrates, flow patterns as well as physical properties.

For stratified two-phase liquid-liquid flow, work carried out by Russel *et al.* (1959) revealed some interesting results. It was found that for a constant no-slip water fraction increasing the mixture velocity leads to a decrease in the slip ratio. This was attributed to the thinner turbulent boundary layer prevalent at higher mixture velocities.

In the case of dispersed liquid-liquid flows, for water to oil fraction ratios close to unity, Angeli (1996) observed that the mean oil velocity was slightly below the water velocity. This was attributed to the fact that the viscosity in the oil-continuous layer was significantly higher than that in the water-continuous layer.

2.3 THREE PHASE GAS-LIQUID-LIQUID FLOW

2.3.1 Flow Patterns

In the case of three-phase gas-liquid-liquid flows, due to the scarcity of studies carried out, an established nomenclature for the description of the flow patterns does not yet exist. However, several researchers have carried out experiments on three-phase flow patterns in order to address this issue specifically.

In this section, work published on three-phase flow pattern maps for horizontal and slightly inclined pipes is reviewed. Emphasis is placed on the terminology used by the various researchers in describing the flow patterns.

Malinowsky (1975) carried out three-phase gas-liquid-liquid experiments using air, oil and water in a 38.1 mm bore (1.5 inch), 29.7 mm long transparent acrylic resin horizontal pipe. The flows studied were in the slug flow regime and the data points from his experiments as well as the slug flow data points of Sobocinski (1955) were plotted on the revised two-phase flow pattern map derived by Beggs and Brill (1973). All these slug flow data points fell in the intermittent region of the map as shown in Figure 2.15. Malinowsky concluded that the two-phase flow pattern map of Beggs

and Brill was suitable for three-phase gas-liquid-liquid flows. However his conclusion is debatable for two main reasons. Firstly, as most of his data points were obtained in the slug flow regime, the suitability of the Beggs and Brill flow pattern map for other flow regimes remains to be seen. Secondly, the number of data points (33) plotted on the map prevents a generalisation from being made.

Laflin and Oglesby (1976) using the same experimental facilities as Malinowsky (1975), obtained three-phase slug flow data and plotted these on the flow pattern maps of Beggs and Brill (1973) and that of Mandhane *et al.* (1974). All their data coincided with the slug flow region of the Mandhane *et al.* map and the intermittent flow region of the revised Beggs and Brill map so they concluded that these two-phase flow pattern maps were adequate for depicting three-phase flow patterns. However since the results obtained were for the intermittent flow pattern only, the suitability of these maps for other flow regimes is still questionable.

Açikgoz *et al.* (1992) carried out a detailed and comprehensive analysis of three-phase flow regimes and produced three flow pattern maps for three-phase air-oil-water flow in a 25.4 mm bore (1 inch) horizontal pipeline for three different oil superficial velocities: 0.043, 0.09 and 0.24 m/s. Their flow pattern map for the case of oil superficial velocity 0.09 m/s is depicted in Figure 2.16. This flow pattern map shows an interesting new feature, not seen in two-phase flow pattern maps; starting in the annular or slug flow regimes, an increase in the water superficial velocity at a fixed air superficial velocity could lead to the occurrence of stratified wavy flow. In the Açikgoz *et al.* flow pattern maps, the oil superficial velocity was shown to have an effect on the transition between the flow regimes, although the order of the flow regimes is preserved in all the three cases.

Acikgoz *et al.* also introduced a new method of classifying the three-phase flow patterns. Their method of classifying the flow patterns consists of three-parts:

Part 1 describes the nature of the continuous liquid phase if the two liquid phases are mixed. Thus **oil-based** indicates that oil would be the continuous phase and **water-based** indicates that water would be the continuous phase.

Part 2 describes the relationship between the two liquid phases. There are three possibilities here: *Separated* meaning that the liquid layers are flowing in a stratified manner according to their densities, *Dispersed*, where the oil and water layers are fully mixed and are flowing as one dispersed liquid mixture and *Separated-Dispersed* where there is a presence of both separated and dispersed liquid layers.

Part 3 consists of the gas-liquid relationship and this is identical to the six standard flow patterns obtained for gas-liquid two-phase flow namely: plug, slug, stratified, stratified wavy, annular and dispersed bubbly flow.

Using the nomenclature described above, Acikgoz *et al.* obtained ten different three-phase flow patterns and these are summarised in Table 2.3

Pattern #	Flow Pattern	Symbol
1	***Oil-based Dispersed Plug Flow***	***O-D-Pl***
2	***Oil-based Dispersed Slug Flow***	***O-D-Sl***
3	***Oil-based Dispersed Stratified Wavy Flow***	***O-D-St.W***
4	***Oil-based Separated Stratified Wavy Flow***	***O-S-St.W***
5	***Oil-based Separated Annular Flow***	***O-S-A***
6	***Oil-based Separated Dispersed Annular Flow***	***O-S.D-A***
7	***Water-based Slug Flow***	***W-D-Sl***
8	***Water-based Dispersed Stratified Wavy Flow***	***W-D-St.W***
9	***Water-based Separated Dispersed Annular Flow***	***W-S.D-A***
10	***Water-based Dispersed Annular Flow***	***W-D-A***

Table 2.3: Three-phase air-oil-water flow patterns observed by Acikgoz *et al.* (1992)

Lee *et al.* (1993) produced flow pattern maps for two and three-phase gas-oil-water flow in a 10-m long, 102 mm bore (4-inch) acrylic resin pipe using carbon dioxide as the gaseous phase. Two types of oil were used: Conoco LVT 200 oil with a viscosity of 2 cP and Arcopak 90 with a viscosity of 15 cP.

Lee *et al.* documented seven different flow patterns: smooth stratified, wavy stratified, rolling wave, slug, pseudo slug, plug and annular flow. It is worth mentioning that in the slug flow regime, they reported that the distribution of the oil in the water was never homogeneous. They compared the three-phase flow pattern maps with their own two-phase flow pattern maps as well as with the two-phase flow pattern predictions of Taitel *et al.* (1976). Lee *et al.* observed that although the configuration of the flow patterns was similar, the transition lines occurred in different regions. In particular, they found the transition lines for stratified to slug flow to be influenced by both the water-cut and the viscosity of the oil.

For the less viscous oil (LVT 200), Lee *et al.* found that slug flow occurred at a lower liquid velocity than the case for the gas-water and gas-oil two-phase flow pattern map. However, for the heavier oil, it was observed that the stratified slug transition for three-phase flow took place between those for the gas-water and gas-oil two-phase flow systems. Lee *et al.* show results for water cuts 25%, 50% and 75% for both oil systems, and observed that as the water-cut increased, the transition to slug flow occurred at higher liquid velocities.

Pan (1996) generated flow pattern maps for three-phase air-oil-water flow in a 38 m long (3 inch) internal diameter stainless steel pipeline and obtained eight distinct flow patterns as shown in Table 2.4.

Flow Pattern #	Flow Pattern	Abbreviation
1	*Separated Slug Flow*	*SSl*
2	*Separated Stratified Flow*	*SSt*
3	*Dispersed Water Continuous Slug Flow*	*DWSl*
4	*Dispersed Water-Continuous Stratified Flow*	*DWSt*
5	*Dispersed Water-Continuous Annular Flow*	*DWA*
6	*Dispersed Oil Continuous Slug Flow*	*DOSl*
7	*Dispersed Oil-Continuous Stratified Flow*	*DOSt*
8	*Dispersed Oil-Continuous Annular Flow*	*DOA*

Table 2.4: Three-phase air-oil-water flow patterns observed by Pan (1996) using the WASP facility

The flow pattern maps of Pan are illustrated in Figures 2.17–2.19. On comparing the above named flow patterns with those of Acikgoz *et al.* (1992), Pan observed that the descriptions of six of them matched those of Acikgoz *et al.* These matching patterns are listed in Table 2.5

Pan (1996) Flow Pattern	Acikgoz *et al.* (1992)
SSt	*O-S-St.W*
DWSt	*W-D-St.W*
DWSl	*W-D-Sl*
DOSl	*O-D-Sl*
DWSt	*W-D-St.W*
DOSt	*O-D-St.W*

Table 2.5: Matching three-phase air-oil-water flow patterns observed by Acikgoz *et al.* (1992) and Pan (1996)

By specifically obtaining data at an oil superficial velocity of 0.1 m/s for the purpose of comparing his flow pattern map with that of Acikgoz *et al.* (1992), Pan was able to plot his data on the flow pattern map of Acikgoz *et al.* and this is shown in Figures 2.20-2.21. From Figures 2.20 and 2.21, it can be seen that with the exception of the DWA (Dispersed Water-Continuous Annular) flow pattern, none of Pan's flow patterns fall in the corresponding region of the Acikgoz *et al.* map. Pan attributed this to the fact that the maps had been obtained under different experimental conditions (pipe diameters and fluid properties) and therefore were not generic to all experimental data.

In addition to these, Pan, by obtaining flow pattern data at different system pressures (0, 5 and 10 barg) was able to comment on the effect of pressure on the flow pattern map. He observed that the system pressure had a significant effect on the flow pattern map as well as on the flow pattern transitions. Two important results were also obtained

(1) That the region of separated stratified flow (SSt) increased with the system pressure.
(2) The area occupied by the dispersed oil-continuous slug flow (DOSl) regime decreased with increased pressure.

The suitability of two-phase gas-liquid flow pattern maps was another area tackled by Pan. He plotted his three-phase gas-liquid-liquid data on the two-phase flow pattern maps of Beggs and Brill (1973), Mandhane *et al.* (1975). The plot of Pan's data on the two-phase map of Beggs and Brill is illustrated in Figure 2.22; it was concluded that two-phase flow pattern maps could not be applied to three-phase gas-liquid-liquid flow.

Donnelly (1997) obtained flow pattern data in 25.4 (1 inch) and 50.8 mm (2-inch) pipelines. He described each three-phase flow pattern using existing two-phase gas-liquid flow pattern terminology, with emphasis on the effect of the water-cut.

He proposed a new flow regime mapping system which was aimed at minimising the diameter effects observed in the flow regime transitions by choosing the Weber (We), Reynolds (Re) and Froude (Fr) groups as the mapping parameters instead of the gas and liquid superficial velocities. The slug data of Hall (1992), Malinowsky (1975), Lahey *et al.* (1992) and Laflin *et al.* (1976), and the separated and semi-annular flow data of Donnelly, Lunde *et al.* (1993) and Sobocinski (1955) (all obtained from pipelines of different diameters) were all plotted on a single flow pattern map. The proposed map performed satisfactorily in all cases except in the case of the Lahey *et al.* (1992) data set where the performance of the map was poor and this was attributed to the highly viscous oil used in the experiments.

Chen *et al.* (1997) produced flow pattern maps for three-phase air-oil-water flow using oil with viscosity of 13.7 cp. and density of 871.7 kg/m^3, using a 22.9 mm (0.9 inch) and a 43.2 mm bore (1.7 inch) horizontal pipeline. The flow pattern maps were produced at specific input water fractions of 50%, 60%, 70% and 100%. In all the flow patterns observed, water formed the continuous liquid phase. They compared their experimentally derived flow regime transitions with the theoretical one proposed by Taitel and Dukler (1976) and found that for the case of a water fraction of 90%, good agreement with the theoretical prediction of Taitel and Dukler (1976) was obtained, but some deviations were observed as the water fraction decreased towards 50%.

Mantripragada (1998) carried out an investigation of the effect of inclination angles, and water-cut on the flow pattern map and transition lines in three-phase gas-oil-water flow. The fluid used consisted of carbon dioxide, Conoco LVT 200 oil (density 800kg/m^3 and viscosity 0.002 Pas (2 cP) at 40°C) and seawater. The test facility consisted of a 102-mm (4-inch) internal diameter 16-m long acrylic resin pipe. The inclination angles used to obtain the data were ± 2°, ± 5° and ± 15°. Slug flow, stratified flow and annular flow were the flow patterns observed.

For upwardly inclined flows, Mantripragada observed that all the transition lines were shifted to the left of the flow regime map i.e. less gas was required to cause the transitions from stratified flow to slug flow and from slug flow to annular flow at higher upward inclination angles. This is as expected as the region occupied by slug flow would increase at the expense of the stratified flow regime in upwardly inclined flow.

For downwardly inclined flows, the transition lines were shifted to the right with increasing downward angles from –2° to - 15°. This is again expected as the tendency for slug flow is greatly reduced due to increased gravitational component of the flow.

Mantripragada also investigated the effect of water-cut on the flow pattern maps as well as on the flow pattern transition lines. He concluded that there was no discernible effect of water-cut on the flow pattern map for both upwardly inclined and downwardly inclined flows. He attributed this to the fact that the oil used for the experiments had almost the same physical properties as the water.

Cai *et al.* (1999) carried out an investigation into the effect of pressure, water-cut and inclination angle on flow pattern transitions. The facility used consisted of a 102 mm (4 inch) internal diameter 18m long stainless steel test section. The test fluids consisted of carbon dioxide, water and oil of viscosity 26 cP (at 40°C). For the experiments, two inclination angles were used: -2° and +2°.

The results obtained indicated that the system pressure had a significant effect on the stratified-slug transition. Results were obtained at four distinct system pressures: 0.13

MPa, 0.27 MPa, 0.45 MPa and 0.79 MPa, and showed that an increase in the pressure led to an increase in the liquid superficial velocity at which the stratified-slug transition occurred. This is in agreement with the conclusion reached by Manolis (1995) for air-water and air-oil two-phase flow. However, these results are contrary to the theoretical predictions of Taitel and Dukler (1976), which suggest that an increase in pressure shifts the transition from stratified to slug flow towards lower liquid superficial velocities.

In the case of the slug-annular transition, keeping the same liquid superficial velocity, as the system pressure increased, the transition from slug to annular flow took place at lower gas superficial velocities.

Contrary to the results of Mantripragada (1998), Cai *et al.* (1999) observed that the water-cut had an effect on the stratified-slug transition. When the water-cut was increased, the transition from stratified to slug flow occurred at higher liquid superficial velocities for the same gas superficial velocity. The water-cut was found to have little effect on the slug-annular transition.
It was also observed that for the same liquid superficial velocity the transition from slug to annular flow occurred at a lower gas superficial velocity, when the inclination angle was changed from -2° and+2°. This concurs with the results obtained by Mantripragada (1998).

The observed transitions between the flow regimes were compared by Cai *et al.* with the models of Taitel and Dukler (1976) and Wilkens (1997). For the stratified-slug transition, there was good agreement between the Taitel and Dukler prediction and the experimental results at gas superficial velocities less than 3 m/s. At velocities above this, the prediction was poor. The Wilkens model performed well against the data for the same range of gas velocities. In the case of the slug-annular transition, there was no agreement between the experimental data and the Taitel and Dukler prediction, while the Wilkens (1997) prediction compared favourably with the experimental results.

2.3.2 Pressure Drop

Most of the work that is mentioned in this review involves experimental studies on the effect of adding the water phase on the pressure gradient of two-phase air-oil flow or the effect of adding oil to the two-phase air-water flow. Another aspect covered is the location of the phase inversion region, which is usually accompanied by a marked increase in the pressure gradient.

The pressure gradient in slug flow usually consists of a frictional, a gravitational and an accelerational term:

$$\Delta p_{tot} = \Delta p_{fric} + \Delta p_{grav} + \Delta p_{accel} \tag{2.140}$$

For horizontal slug flow, the contributions of the gravitational term is zero and the contribution of the acceleration terms are usually small, relative to the frictional term and hence can be ignored. Thus in the present study of slug flows, the pressure drop consists mainly of a loss due to friction in the slug body and the slug film region. It is common to neglect the frictional pressure drop in the film region except where long slug films are present.

Sobocinski (1955) carried out three-phase gas-liquid-liquid flow experiments in a horizontal 76 mm (3 inch) internal diameter plastic pipe of length 12.7 m using oil of viscosity 0.0028 Pas (2.8 cP) and density 840 kg/m^3 at 38°C.

Pressure gradient data were obtained and it was observed that the pressure gradient increased as water cut increased, reaching a maximum at an input water fraction in the liquid of 77%. This peak coincides with the phase inversion point where a change in the liquid flow pattern from a water-in-oil emulsion to an oil-in -water emulsion was observed. Another point of interest is that when oil was added to the two-phase air-water mixture, the pressure drop was reported to have increased five fold.

Malinowsky (1975) carried out three-phase air-oil-water experiments in a 29-m transparent acrylic pipe of internal diameter 38 mm (1.5 inch) using oil of viscosity 0.003 Pas (3 cP) and density 840 kg/m3 (at 40°C) and measured the pressure gradients. He obtained 34 data points, most of them in the slug flow regime and compared his data with the two-phase correlations of Dukler (1969) and Beggs and Brill (1973). He observed large discrepancies between the predicted and measured

values and this he attributed to the use of the linear viscosity relationship for the oil-water mixture. He also observed that the pressure gradient in three-phase gas-liquid-liquid flow was dependent on the input water fraction in the liquid at which the phase inversion occurred as well as on which of the liquids was the continuous phase.

Laflin and Oglesby (1976) using the same experimental facilities as Malinowsky (1975), also carried out three-phase experiments and reported on the flow patterns observed and the pressure drops measured. They observed that the introduction of air into an oil-water mixture shifted the phase inversion point from 0.4 to 0.5.

Stapelberg *et al.* (1994) measured pressure drop for three-phase gas-liquid-liquid flow experiments carried out in a 35-m long horizontal pipeline using two different pipes with diameters of 23 mm (0.9 inch) and 58 mm (2.3 inch) respectively. These measurements were made with oil of viscosity 0.031 Pas and density of 858 kg/m^3 (at ambient conditions). They compared values of three-phase pressure drop with values of two-phase pressure drop of air-oil flow and those of air-water flow and found that at low gas superficial velocities, the three-phase pressure drops were greater than those for two-phase air-water slug flow, but less than that of two-phase air-oil slug flow. At higher gas velocities they observed that the measured pressure drops in three-phase flow were lower than those of both air-oil and air-water slug flows.
Their findings are summarised as follows:

$$Low\,U_{G,S}: \quad \left(\frac{dp}{dz}\right)_{2P_{Air-water}} < \left(\frac{dp}{dz}\right)_{3P_{Air\text{-}water\text{-}oil}} < \left(\frac{dp}{dz}\right)_{2P_{Air-oil}}$$

$$High\,U_{G,S}: \quad \left(\frac{dp}{dz}\right)_{3P_{Air-water-oil}} < \left(\frac{dp}{dz}\right)_{2P_{Air\text{-}water}} < \left(\frac{dp}{dz}\right)_{2P_{Air-oil}}$$

They attributed the result for high gas superficial velocity case, to be due to a change in the slug parameters. In particular, they observed that the void fraction in the liquid slug for two-phase air-water flows was greater than that for three-phase air-oil-water flows.

Comparisons of the predictions of pressure gradient, using the two-phase slug flow models of Dukler and Hubbard (1975) and Aziz *et al.* (1978) with experimental data were made. To carry out these comparisons, they treated the oil and water as one

homogeneous fluid and closure relationships in the form of the slug frequency and the void fraction in the slug body were provided for the models.

At low gas flow rates good agreement was found between both slug models and the experimental data and the results were not very sensitive to the calculated slug frequency. However at higher gas flowrates, poor agreement was observed between the calculated and measured pressure drop and there was a tendency for the models to over-predict the experimental data. This discrepancy was attributed to the slug body hold-up correlation used. This was confirmed when a significant improvement in the predictive capabilities of the models was observed when the measured slug length was used as a closure relationship instead of the void fraction in the slug.

Details of the liquid mixture viscosity relationship used in the calculations were not given by Stapelberg *et al.* so it is likely that a volume weighted viscosity expression, similar to Equation (2.132) was used. It has been shown that this viscosity relationship gives poor results where emulsions are present, which was likely to be the case for the data obtained at the higher gas velocities and this might go a long way towards explaining the discrepancies, observed by Stapelberg *et al.*, between the predictive models and the experimental data at high gas velocities.

Hall (1992), using the Imperial College WASP Facility, carried out measurements of pressure drop and liquid hold-up in three-phase air-oil-water slug flow. This facility consists of a 38-m long 77.92 mm (3 inch) internal diameter stainless steel pipe. The fluids used were air, water and oil. The oil used was Shell Tellus 22 with viscosity 0.050 Pa.s (50 cP) and density 872 kg/m^3 (at 20°C). He compared his data with the existing two-phase pressure drop correlations of Dukler *et al.* (1964), Schlichting (1971), Beggs and Brill (1973), Friedel (1979) and Lockhart and Martinelli. (1949). Based on these comparisons, he found that he obtained the best agreement with his data using the Beggs and Brill (1973) correlation. He also noticed a significant improvement in the prediction of the pressure gradient, when he substituted the linear volume fraction weighted viscosity expression Equation (2.132) with the non-linear viscosity expression of Brinkman (1952) Equation (2.137).

Lunde *et al.* (1993) carried out three-phase gas-liquid-liquid experiments in a closed loop flow rig with dimensions 20 m in length and internal diameter 0.1 m. Pressure drop was measured using gas filled differential pressure cells over a distance of 2 m. Two dense gases, refrigerant and sulphur-hexafluoride, both having densities of 6 kg/m^3, were used to simulate conditions in high-pressure pipelines. The liquid phases were made up of Exxol D80 (density 800 kg/m^3 and viscosity 0.002 Pas at atmospheric conditions) and tap water. A modest increase in the pressure gradient was observed in the intermittent flow regime as the water-cut was increased at a constant gas and total liquid velocity. However, these observations were confined to a water-cut range of 0 to 15%.

Experiments on three-phase gas-liquid-liquid three-phase flow in a 53 mm (2.1 inch) internal diameter acrylic resin pipe of length 48 m were carried out by Nadler *et al.* (1995). Maxima in the measured pressure drop were observed in the elongated bubble flow regime, between water-cuts of 20% and 50%. Nadler *et al.* attributed this increase to be due to the formation of viscous water-in-oil emulsions. It was also observed that between water-cuts of 10% and 20%, the pressure gradient of the three-phase flow is similar to the pressure drop of two phase air-oil flow whereas for water-cuts between 20% and 30% where the phase inversion was observed, the pressure drop is higher than that for two-phase air-oil flow. For water-cuts greater than 30%, where the continuous liquid phase is water, the pressure drop is close to that obtained in two-phase air-water flow. Their results are in good agreement with the results obtained by Stapleberg *et al.* (1994).

Pan (1996) also using the Imperial College WASP facility and the same fluids as Hall (1992), measured pressure gradient in three-phase air-oil-water flows over a wide range of flow patterns and compared his data against existing two-phase pressure drop correlations. He found that the best combination of correlations was the model of Dukler *et al.* (1964) used in conjunction with the Brinkman (1952) viscosity model. Since his data was collected over a wide range of flow patterns, Pan grouped his data points into oil and water continuous flows and observed that the Dukler *et al.* (1964) correlation was the best for water-continuous flow while the Beggs and Brill (1973) correlation was the best for oil-continuous flow.

In addition, Pan (1996) also investigated the effect of input water fraction in the liquid on the pressure gradient, and observed significant increases in the measured pressure gradients for water-cuts in the region of 40%-60%. An example of the results obtained by Pan is illustrated in Figure 2.23. In Figure 2.23, where the measured pressure gradient is plotted against the water-cut, significant increases in the pressure gradient can be observed for the cases of gas velocity 5.5 m/s and 7.9 m/s.

Pan also observed from his experimental results that the linear interpolation method of predicting the liquid mixture viscosity was inadequate, when used in two-phase pressure drop correlations, when there was intense mixing. In addition to this, Pan (1996) also showed that in the absence of mixing, the Brinkman expression, Equation (2.137) performed badly. Therefore he proposed a model for calculating the effective viscosity of a liquid-liquid mixture, which would take into account the degree of mixing present in the liquid-liquid mixture. This new model incorporated a new parameter $C_{M,}$ called the *mixing degree coefficient*, which described the level of mixing in the mixture, with values ranging from 0 (for the no-mixing case) to 1 (for the fully mixed case). This new model which is a combination of the linear and Brinkman viscosity expressions is denoted by the expression:

$$\mu_L = (1-C_M)[(1-\lambda_W)\mu_O + \lambda_W \mu_W] + C_M \mu_{cont}(1-\lambda_{dis})^{-k} \qquad (2.141)$$

The value of k is taken to be 2.5. The above expression reduces to the linear viscosity when there is no mixing present (C_m=0), and in the case of full mixing (C_m=1), the expression reduces to the Brinkman expression.

Based on experimental observations, Pan was able to identify the major factors, which contributed to the mixing degree coefficient and proposed a mixing degree correlation for smooth pipes:

$$C_m = 1 - exp\left(\frac{-Re_{3p}}{K}\right) \qquad (2.142)$$

Where K is a constant with a recommended value of 15 000 based on Pan's experiments and Re_{3p} is a three-phase Reynolds number defined by the expression:

$$Re_{3p} = \frac{\dot{m}_M D U_M}{(U_{G,S}\mu_G + U_{O,S}\mu_O + U_{W,S}\mu_W)} \qquad (2.143)$$

Where D is the pipe diameter, $\dot{m}_M$ is sum of the individual mass fluxes and U_M is the total mixture superficial velocity.

Donnelly (1997) also carried out three-phase air-oil-water pressure gradient measurements in two pipelines, with internal diameters of 25 mm (1 inch) and 51 mm (2 inch) respectively. Donnelly. observed that there was a maximum in the plot of pressure gradient vs. water cut, the location of which was dependent on both the air and liquid superficial velocities. Figure 2.24 shows some of the pressure gradient results obtained by Donnelly. From Figure 2.24, it can be seen that the maximum pressure gradient occurs at a water-cut of around 60%.

In the case of a constant liquid superficial velocity, Donnelly noticed that when the air superficial velocity was increased, the phase inversion point shifted towards lower water-cut values. This result is shown in Figures 2.25 and 2.26, where the pressure gradient results of Donnelly are plotted against the water-cut.

For a constant air velocity with varying liquid superficial velocity, two trends were noticed:

1. At low gas velocities, increasing the total liquid velocity shifted the phase inversion towards lower water-cut values
2. At high gas superficial velocities, the converse happened.

Donnelly attributed these trends to the fact that for high gas velocities, as the liquid flow rate is increased, the amount of gas present in the liquid mixture decreases thus leading to an increase in the liquid viscosity thereby requiring an increasing amount of water to invert the mixture. In addition to these observations, he proposed a model for pressure drop prediction which made use of Oliemans (1987) expression for the dimensionless film height in the Taitel and Barnea (1995) three phase momentum balance and reported that 78% of his data points were predicted within a $\pm 30\%$ error band.

In addition to this, Donnelly (1997) proposed an expression for the effective viscosity based on his experimental observations. He observed from his experiments that the

position of the phase inversion was very important in determining the viscosity of the liquid mixture. He derived an expression, which accounts for the effects of phase inversion:

In the oil-continuous region, Donnelly proposed the following expressions for the effective viscosity:

$$\mu_L = \frac{\mu_O}{(\lambda_O)^{mk\left(\frac{\mu_W}{\mu_O}\right)}} \tag{2.144}$$

Where the oil region inversion factor m is given by:

$$m = \frac{\lambda_W{}^{y}}{y\left(1-\lambda_W{}^{\frac{1}{k}}\right)^{\left(\frac{y}{k}\right)} y^{1-y^{\frac{1}{k}}}} \tag{2.145}$$

The effective viscosity μ_L in the water-continuous region is given by:

$$\mu_{L=} \frac{\mu_W k^n}{(\lambda_w)^{k^{\left(\frac{0.2}{k}\right)^{\lambda_W}}}} \tag{2.146}$$

Where the water region inversion factor, n, is given by:

$$n = \left[\frac{(\lambda_W)^{\left(\frac{(1-y)^2}{\lambda_W}\right)}}{(1-y)^y}\right]^{0.4} \tag{2.147}$$

And k is the viscosity ratio of oil to water denoted by the expression (μ_O/μ_W), μ_O is the viscosity of the oil, μ_W is the viscosity of the water, λ_O is the oil fraction in the total liquid defined by $\frac{U_{O,S}}{U_{O,S}+U_{W,S}}$ and y is the phase inversion fraction (% v/v water).

By carrying out experiments in three-phase air-oil-water flow, Cai *et al.* (1998) were able to produce a correlation for predicting the effective viscosity of oil-water emulsions. The experiments were carried out in a 4.5-m long (1.7 inch) internal diameter steel pipeline. As a result the two following correlations were produced:
For water-in-oil emulsions, the effective viscosity of the oil-water mixture was given by:

$$\mu_L = 0.4526\left[1+\frac{\lambda_W/0.687}{1.187-\lambda_W/0.687}\right]^{2.5} e^{-0.05748t} p^{-0.06} \qquad (2.148)$$

And for oil-in-water emulsions:

$$\mu_L = 0.002\left[1+\frac{(1-\lambda_W)/0.687}{1.187-(1-\lambda_W)/0.687}\right]^{2.5} e^{-0.0458t} p^{-0.06} \qquad (2.149)$$

Where λ_w is the input water fraction as defined by Equation (2.9), μ_L is the effective viscosity of the oil-water emulsion, t is the temperature of the system (in °C) and p the system pressure (in MPa).

2.3.3 Holdup

Lahey *et al.* (1992) developed a three-phase drift flux model from their experimental data in an attempt to predict global volumetric phase fractions in horizontal three-phase gas-oil-water flows. They observed that there was a significant variation in the drift-flux parameters from one flow regime to another. Nevertheless, they found that the data were well correlated with the drift flux model.

Pan (1996) using the WASP Facility measured liquid holdup in three-phase air-oil-water flows using a traversing single-beam dual-energy gamma densitometer. He compared various two-phase liquid hold-up correlations with his data and found that the Premoli *et al.* (1971) correlation was the best for oil-continuous flow while the correlation by Hughmark (1962) was the best for water-continuous flow. He also observed the trends in total liquid hold-up, water hold-up and oil hold-up with increasing water-cut.

For a *constant oil superficial velocity*, Pan noticed that as the water cut increased, the total liquid hold-up increased to a maximum and then fell sharply to a minimum before increasing again. The first maximum was attributed to the phase inversion phenomena while the second rise was due to the fact that the total liquid flowrate was increasing. The oil hold-up was observed to decrease continuously with increasing water cut with the greatest rate of decrease observed around the phase inversion point; the converse applied to the water hold-up. Pan's results are illustrated in Figures 2.27

and 2.28, in which the experimentally measured phasic holdups of the oil and the water and the total liquid are plotted against the input water fraction in the liquid.

Pan (1996) also found that at *constant liquid flowrate*, once the phase inversion region had been passed, the total liquid hold-up decreased continuously with water-cut; the increase with water cut observed for the case of a fixed oil flowrate did not occur. No differences were observed between the hold-up trends reported for atmospheric and 5 bar (g) although it was noticed that the higher the pressure, the smaller the hold-up of the oil and water.

Donnelly (1997) measured liquid hold-up using quick closing valves. He investigated the effect of water cut on water and oil hold-up over a range of liquid flowrates and superficial gas velocities. Like Pan (1996), he also observed a peak in the total liquid hold-up on a plot of liquid holdup versus water-cut. Donnelly also observed a minimum in the total liquid hold-up immediately after the maximum. This is shown in Figures 2.29 and 2.30; where the measured total liquid holdup increases to a maximum at water-cut of around 30% and then a decreases to a minimum at a water-cut of around 60%. This results echo the trends observed by Pan (1996). Donnelly also noticed that the point of maximum liquid holdup on the holdup versus water-cut plot was dependent on the gas and total liquid superficial velocities.

Malhotra (1998) carried out three-phase gas-oil-water flow experiments in a 102 mm (4 inch) 10-m long horizontal acrylic resin pipeline at the University of Ohio. The fluids used in the experiments were carbon dioxide, Britol 50T oil (viscosity 0.1 Pas (100 cP) and density 848 kg/m^3 at 40°C) and water. Experiments were carried out at atmospheric pressure and at 1.7bar(g).

Although Malhotra obtained data on flow patterns, the emphasis on this work was on measurements of the thickness of the oil and water film layers between the slugs as well as calculations of the velocities of the two liquid phases. The composition of the liquid phases was determined by the use of an iso-kinetic sampling probe. These measurements, coupled with video recordings of the total film height enabled the phasic heights to be determined.

Malhotra reported several interesting results, particularly the result that the total liquid film thickness decreased at higher pressures in stratified three-phase flow. Malhotra explained the findings by attributing the increase in the film thickness to be due to the denser gas sweeping away the oil layer more effectively than at lower pressures.

Another interesting result was the fact that the total film height increased with an increase in the input water percentage. Malhotra (1998) reports that at water-cuts as high as 80%, the total film height is higher than those recorded at 20%, 40% and 60%. It would be expected that as the water-cut increased beyond 60%, the apparent viscosity of the liquid mixture would decrease, leading to lower film heights at 80% than those recorded at 20% water-cut. This would persist until a phase inversion occurred. A possible explanation for this could be that, with the highly viscous oil used by Malhotra, the phase inversion point occurred at a higher water-cut leading to an anomalous viscosity and a larger liquid layer thickness.

2.3.4 Slug Flow

2.3.4.1 Slug Frequency

Nadler and Mewes (1992) measured slug frequencies in three-phase slug flow of air, oil and water by cross and auto correlation of pressure signals in an horizontal pipe of internal diameter 59 mm and compared their results to those obtained for two-phase air-oil and air-water slug flows. They noticed that the slug frequency for three-phase slug flow was always less than that of the corresponding two-phase air-water flow and air-oil flow. They attributed this to the lower kinetic energy possessed by the three-phase mixture when compared to a corresponding two-phase mixture with equal gas flowrate and total liquid volumetric flowrate. Unfortunately this does not explain why the slug frequencies for air-oil flow were observed to be greater than air-water flow. The slug frequency in three-phase flow was found to increase both with increasing air and liquid superficial velocity.

Wilkins and Jepson (1996) measured slug frequencies in two and three-phase gas-oil-water system using carbon dioxide, water and oil as their test fluids in an 18 m long,

97 mm diameter pipe with the pipe being horizontal and upwardly inclined at 5 degrees. They observed that the slug frequency increased with water superficial velocity for the two-phase and three-phase flow tests at constant gas velocities. In the case of plots of slug frequency versus gas velocity at constant liquid velocities, the behaviour of the slug frequency was erratic, sometimes a minimum was observed and sometimes the slug frequency decreased monotonically with the gas velocity. The effect of pressure and pipe inclination angle on the slug frequency was studied and the effect of these parameters was negligible.

Hall (1997) measured slug frequencies in three-phase nitrogen-oil-water flow in 102 mm (4 inch) and 152 mm (6 inch) internal diameter pipelines. The frequencies were obtained visually through the aid of a video camera. Hall compared his data to the correlation proposed by Hill and Wood (1994) and found that there was good agreement of the data from the 152 mm pipeline with the correlation while poor agreement was obtained in the case of the 102 mm pipe data. This was attributed to the fact that the correlation was based on data collected from pipes of diameters greater than 152 mm thus highlighting the importance of obtaining data from large pipe diameters in other to avoid the errors introduced by scaling data from small pipelines.

Mantripragada (1998) observed the effect of pipeline inclinations, water-cut, superficial liquid and gas velocities on the slug frequency in three-phase gas-oil-water flow. The experiments were carried out using light oil of viscosity 0.002 Pas (2 cP) in a 10-m long, 102 mm (4 inch) acrylic resin pipe. The slug frequency was measured with the aid of a video camera, observing the number of slugs passing through two fixed points. He concluded that while an increase in the gas superficial velocity led to a decrease in the slug frequency, an increase in the liquid superficial velocity resulted in an increase in the slug frequency. By carrying out experiments at two distinct water-cuts, he was able to conclude that the water-cut had no discernible effect on the slug frequency. This was because the oil used had a viscosity close to that of the water.

2.3.4.2 Slug Velocity

Mantripragada (1998) studied the effect of pipeline inclination, water-cut, gas and liquid superficial velocities on the slug translational velocity in three-phase gas-oil-water flow in a 10 m long 102 mm (4 inch) acrylic resin pipe. The slug translational velocities were measured with the aid of a video camera, counting the number of frames taken by the slug front to pass between two fixed points. He found the slug translational velocity to be independent of the inclination angles in both upward and downward flows. The slug translational velocities were found to be directly proportional to the gas and liquid superficial velocities. There was no discernible effect of the water-cut on the slug translational velocities, and the translational velocity were observed to be 1.2 times the mixture velocity.

2.4 SUMMARY

From the above review, it is apparent that the existing two-phase flow pattern maps cannot be applied to the three-phase flow case, because of the strong part played by the physical properties of the liquids, particularly the viscosity, on the flow pattern transitions. This view point is backed up by the work of Pan (1996) and Cai *et al.* (1999).

On the subject of evaluating the viscosity for liquid-liquid flow systems, several expressions exist and a trade-off exists between complexity and the practicality of the expressions. Several researchers have derived expressions that take into account factors such as droplet-droplet interaction as well as droplet size distribution, which affect the viscosity of the liquid-liquid system. However the difficulty in obtaining these parameters for flows in pipelines necessitates the use of the simpler expressions of which one good example is that of Brinkman (1952). Several researchers have shown this expression by Brinkman to be the most accurate when applied in two-phase pressure drop prediction models.

The experimental data on pressure gradient and liquid holdup all reveal the significant increases in both parameters around the phase inversion point, especially for flow regimes where intense mixing is present (for example slug flow).

Existing models for the modelling of three-phase slug flow still utilise correlations based on two-phase air-water flow for closure relationships. However this review shows the importance played by the viscosity and how the liquid viscosity affects these parameters significantly.

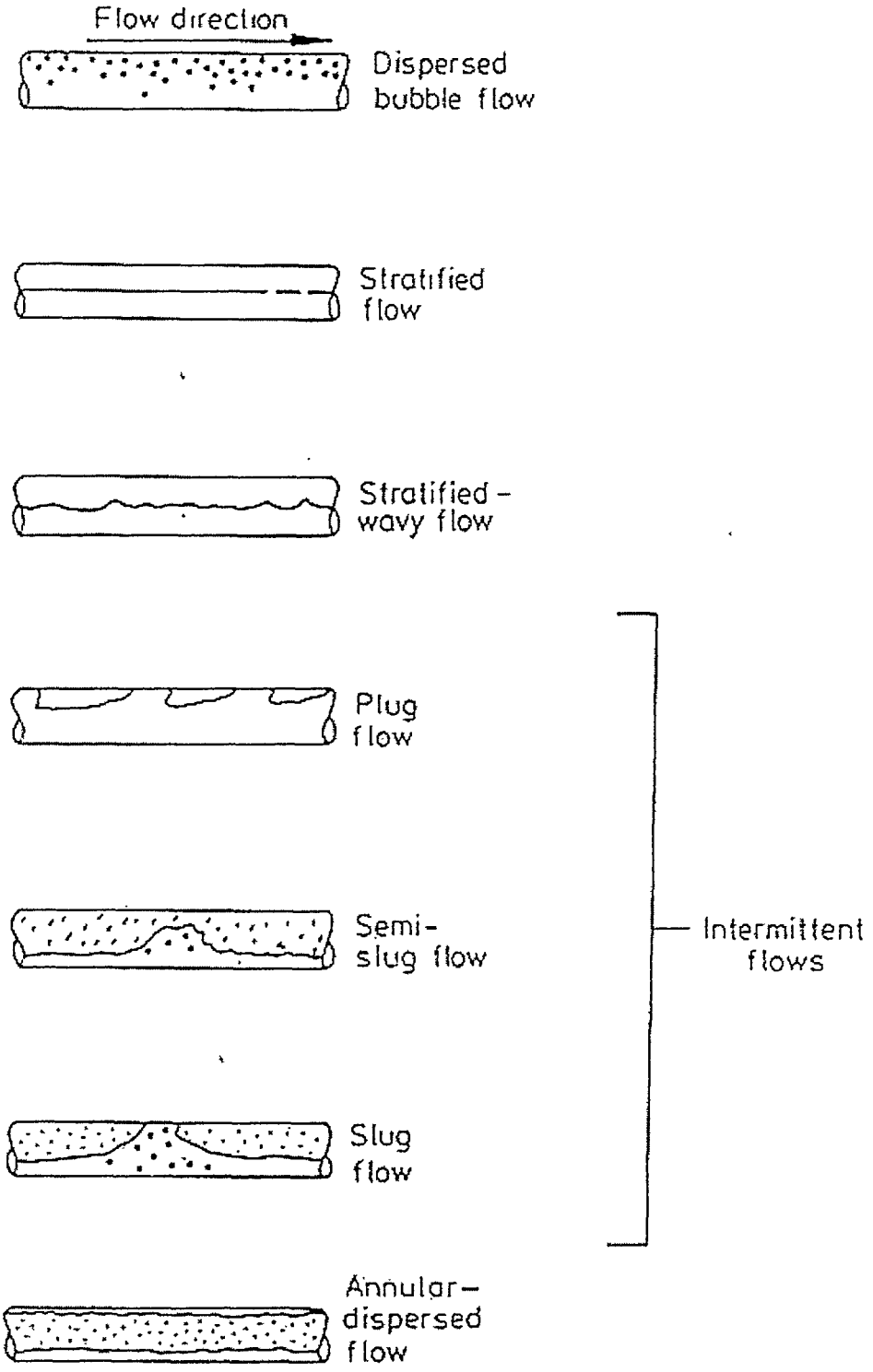


Figure 2.1: Flow patterns in horizontal two-phase flow (Hewitt 1982)

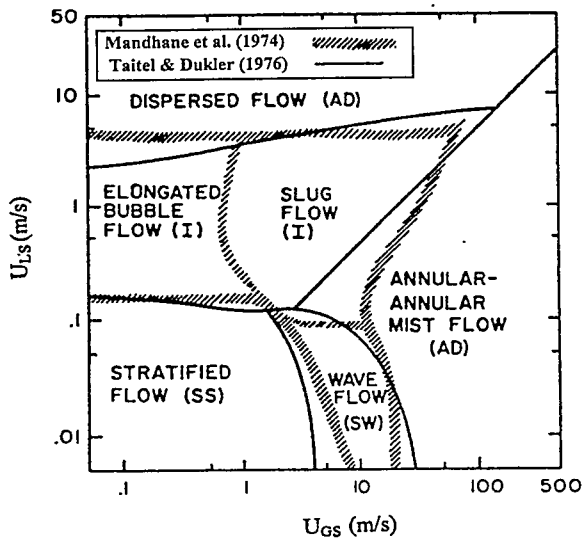


Figure 2.2: Gas-Liquid Flow Pattern Map (Mandhane *et al.* 1974) in terms of superficial velocities (volume flows divided by cross sectional area of the channel) of the gas ($U_{G,S}$) and the liquid ($U_{L,S}$)

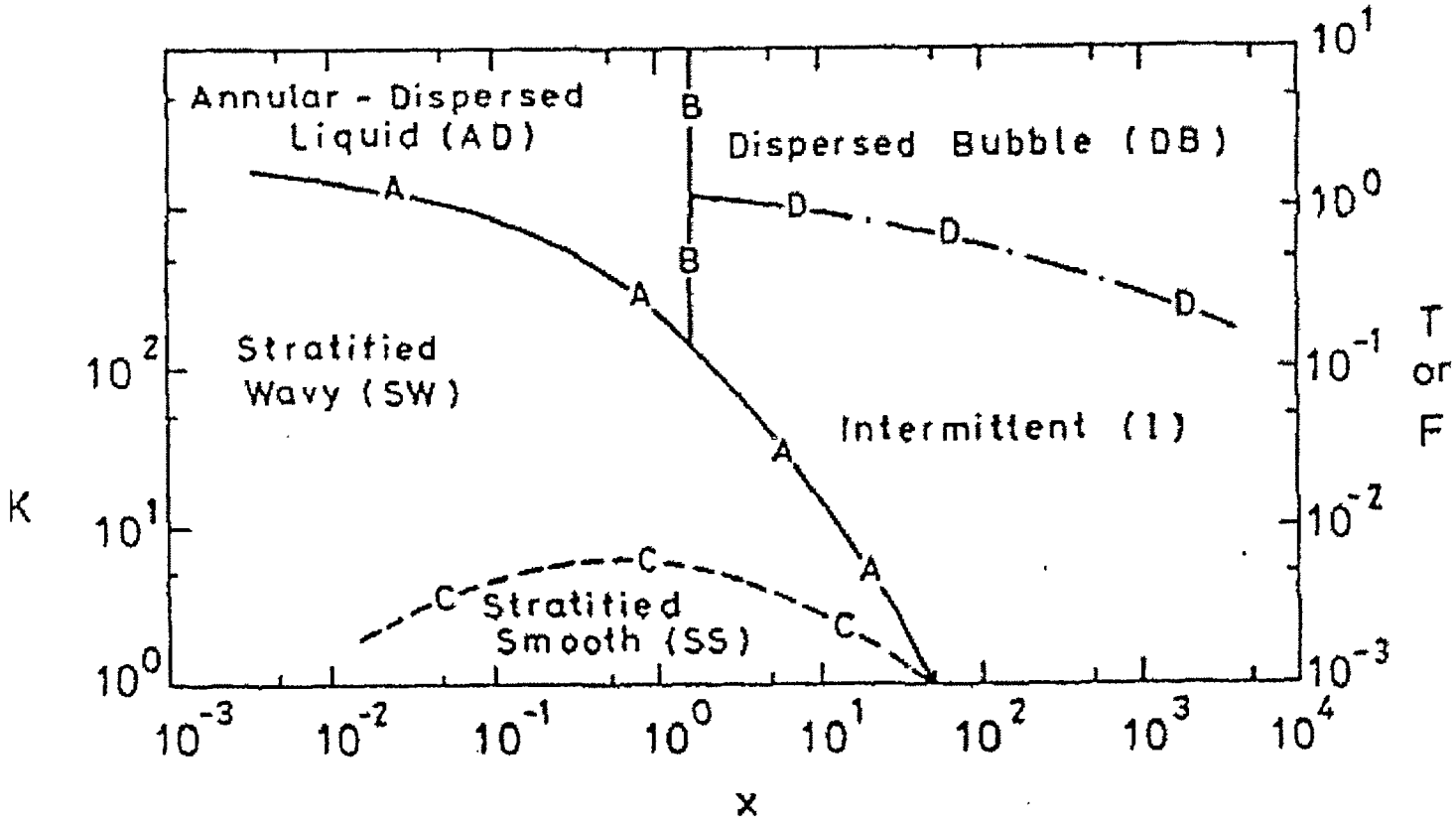


Figure 2.3: Generalised Gas-Liquid Flow Pattern Map (Taitel and Dukler 1976)
The dimensionless groups used by Taitel and Dukler are defined as follows:

$$F = U_{G,S}\left(\frac{\rho_G}{(\rho_{L-}\rho_G)Dg\cos\theta}\right) \tag{2.150}$$

$$T = \left(\frac{|(dp/dz)_L|}{(\rho_L - \rho_G)g\cos\theta}\right)^{0.5} \tag{2.151}$$

$$K = F\left(\frac{\rho_L D U_{L,S}}{\mu_L}\right)^{0.5} \tag{2.152a}$$

$$X = \left[\frac{[dp/dz]_L}{[dp/dz]_G}\right]^{0.5} \tag{2.152b}$$

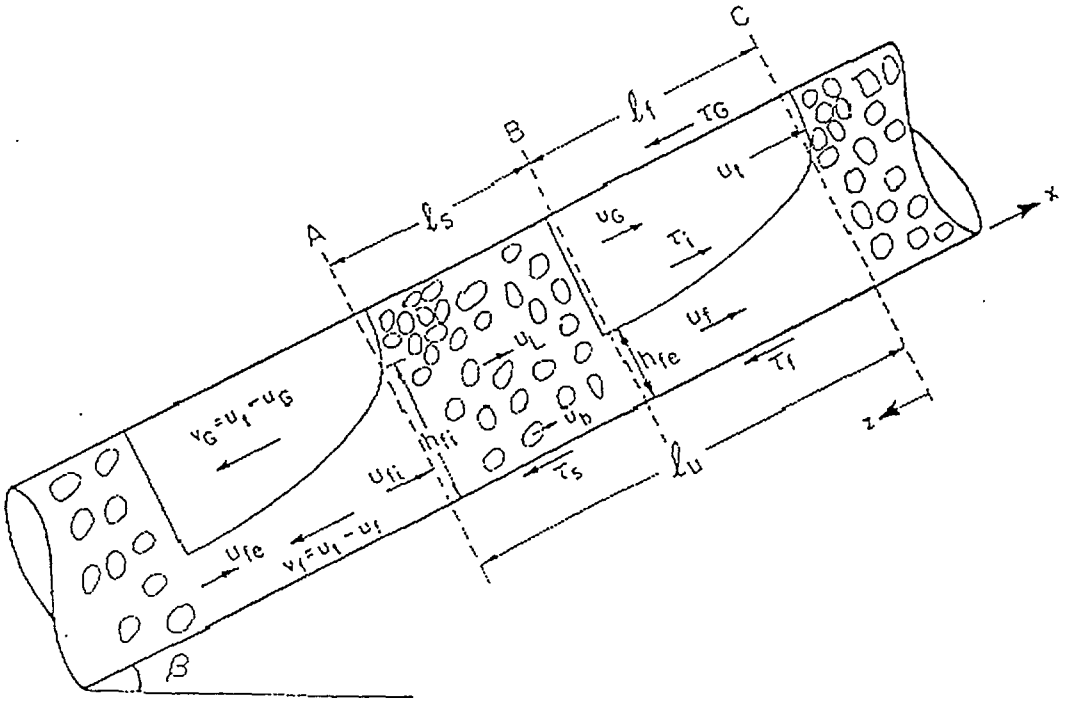


Figure 2.4: Slug Flow Geometry (Taitel and Barnea 1990)

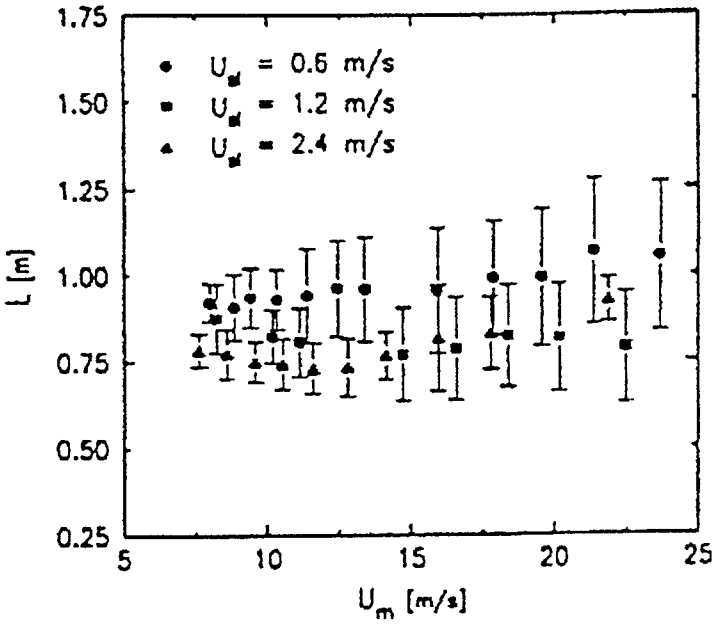


Figure 2.5: Mean slug lengths d=5cm from air-water slug flow experiments.(Nydal, 1991)

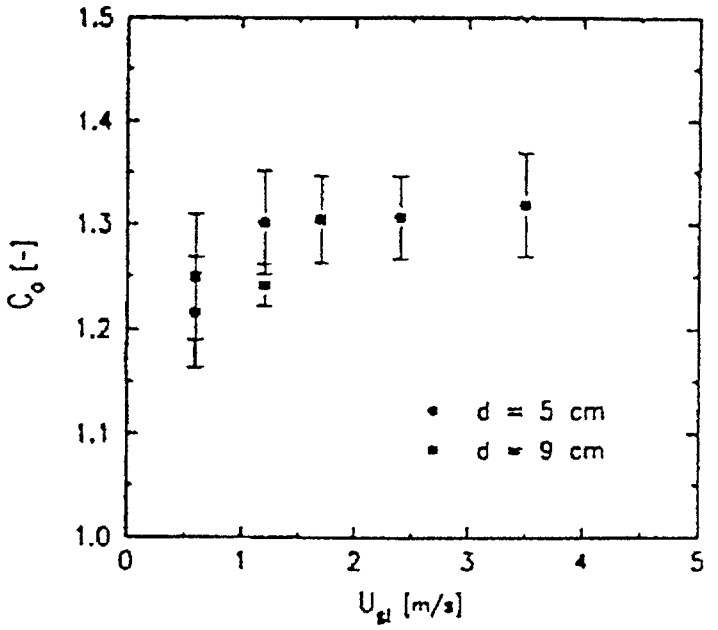


Figure 2.6: Mean values of C_o as measured by Nydal (1991)

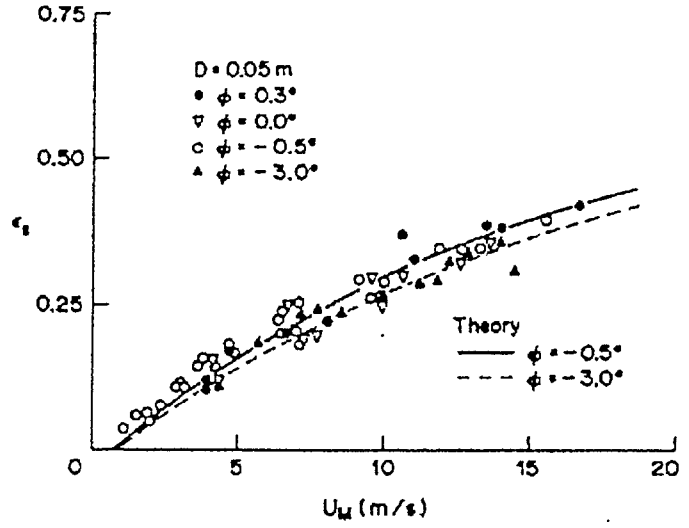


Figure 2.7: Mean slug body void fraction plotted against total mixture superficial velocity for a range of pipe inclination angles (Andreussi and Bendiksen, 1989)

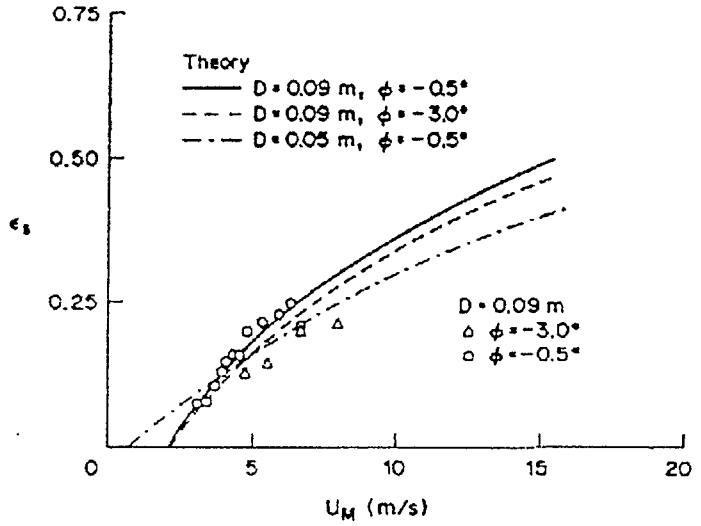


Figure 2.8: Mean slug body void fraction plotted against total mixture superficial velocity for a range of pipe inclination angles. (Andreussi and Bendiksen 1989)

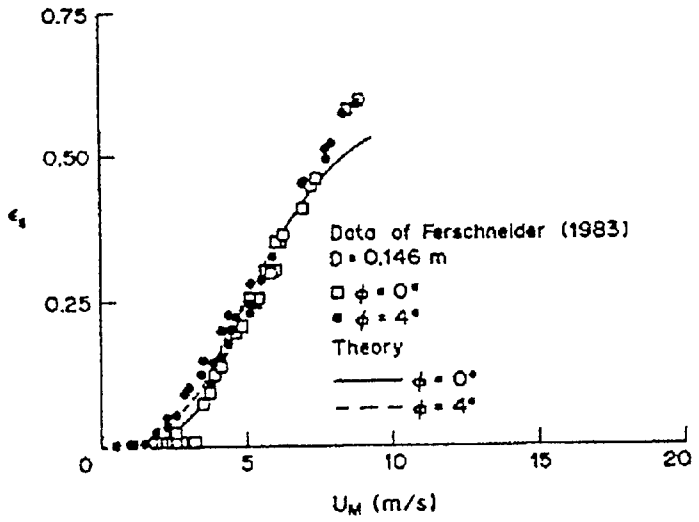


Figure 2.9: Mean slug body void fraction plotted against total mixture superficial velocity for two different pipe inclination angles (Ferschneider, 1983).

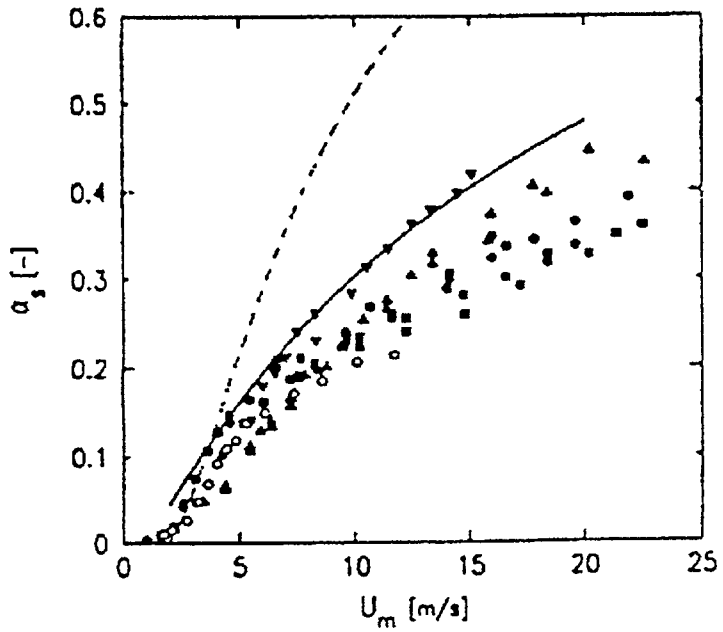


Figure 2.10: Mean void fraction in the slugs. The dotted line is the empirical correlation by Gregory *et al.* (1978) and the solid line is the correlation by Andreussi and Bendiksen (1989)

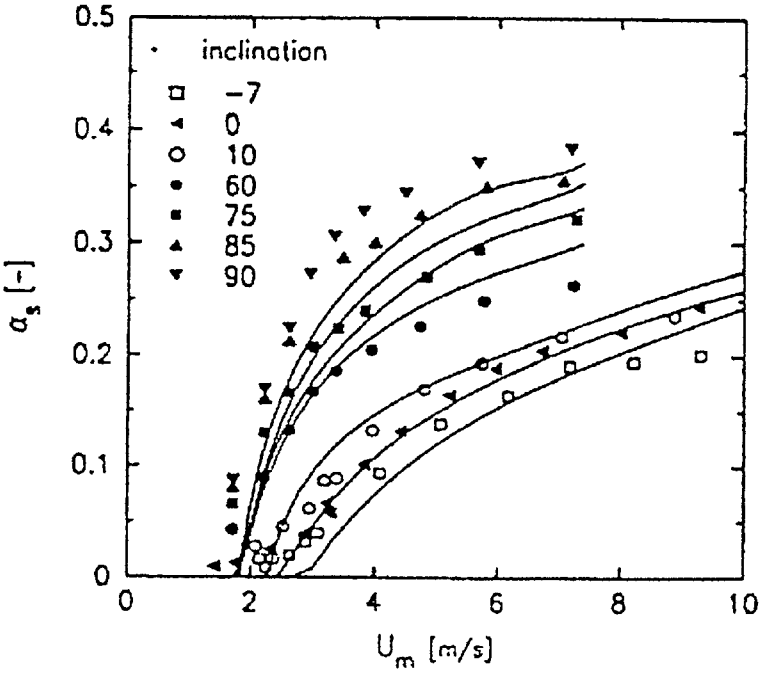


Figure 2.11: Mean void fraction in the slugs for a range of pipe inclination angles (Andreussi and Bendiksen, 1989)

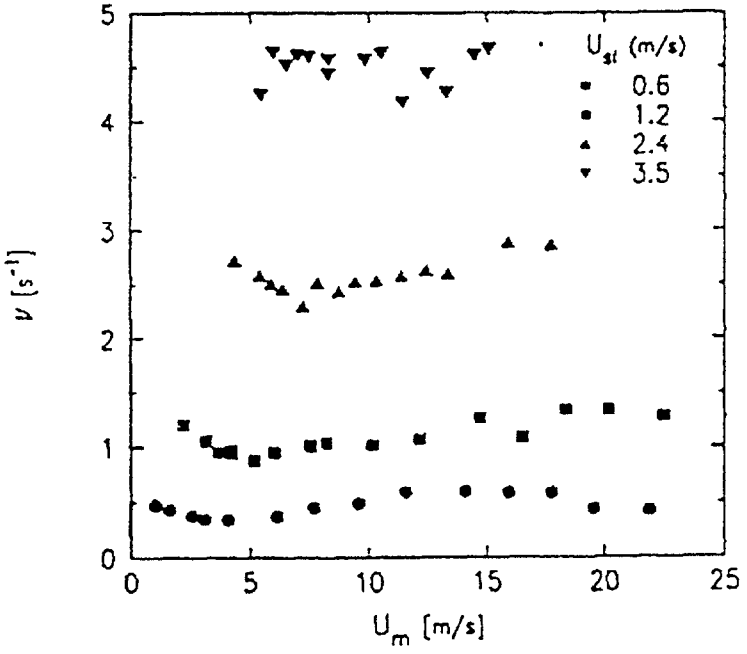


Figure 2.12: Slug frequency versus total mixture velocity (Nydal, 1991)

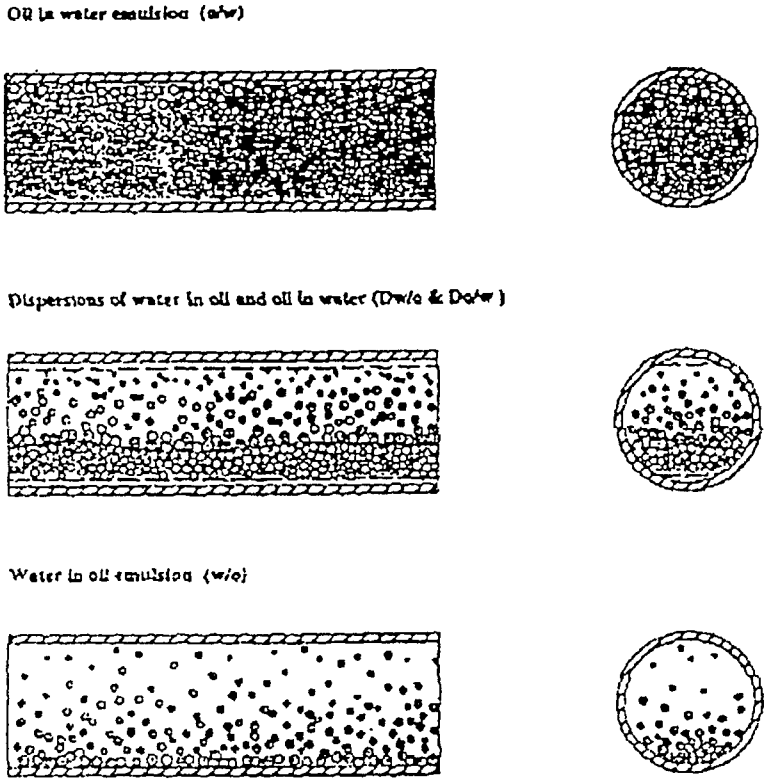


Figure 2.13a: Oil/Water Flow Patterns (Trallero, 1995)

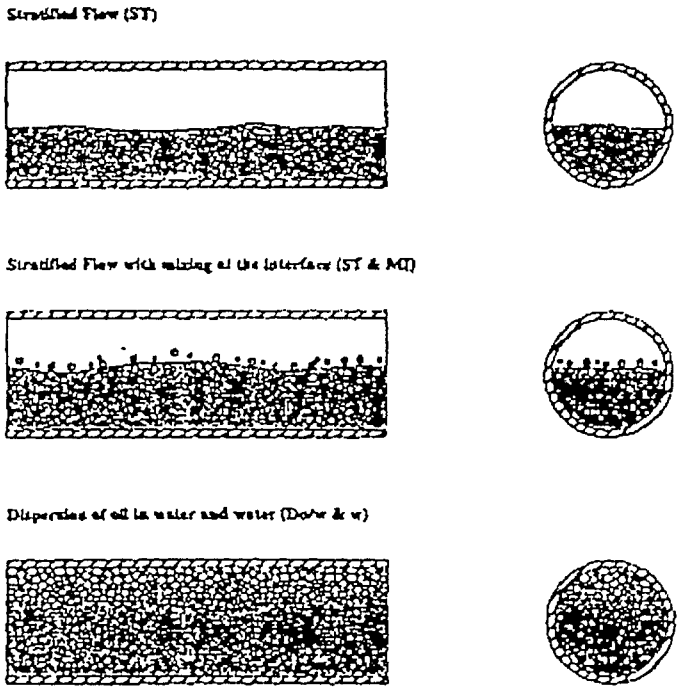


Figure 2.13b: Oil/Water Flow Patterns (Trallero, 1995)

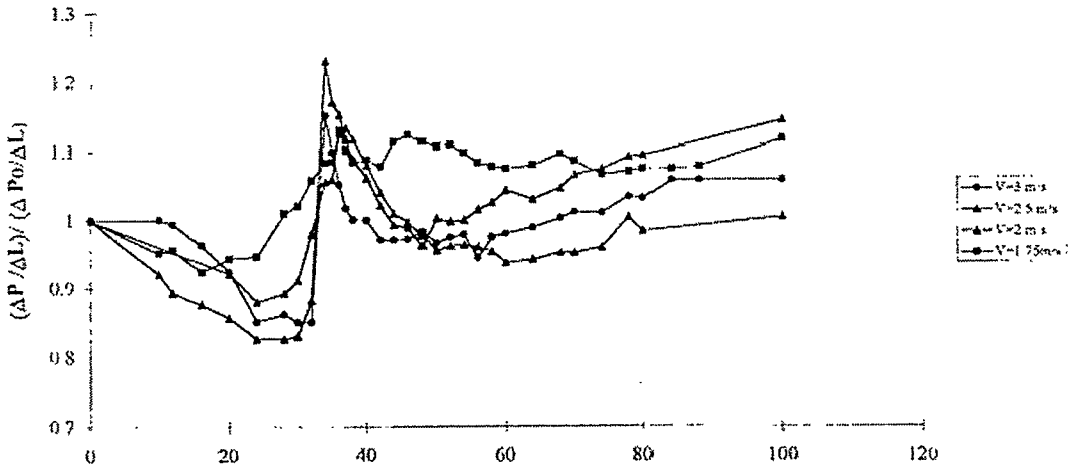


Figure 2.14: Two-phase kerosene-water experimental results of Soleimani (1999) for a horizontal pipe

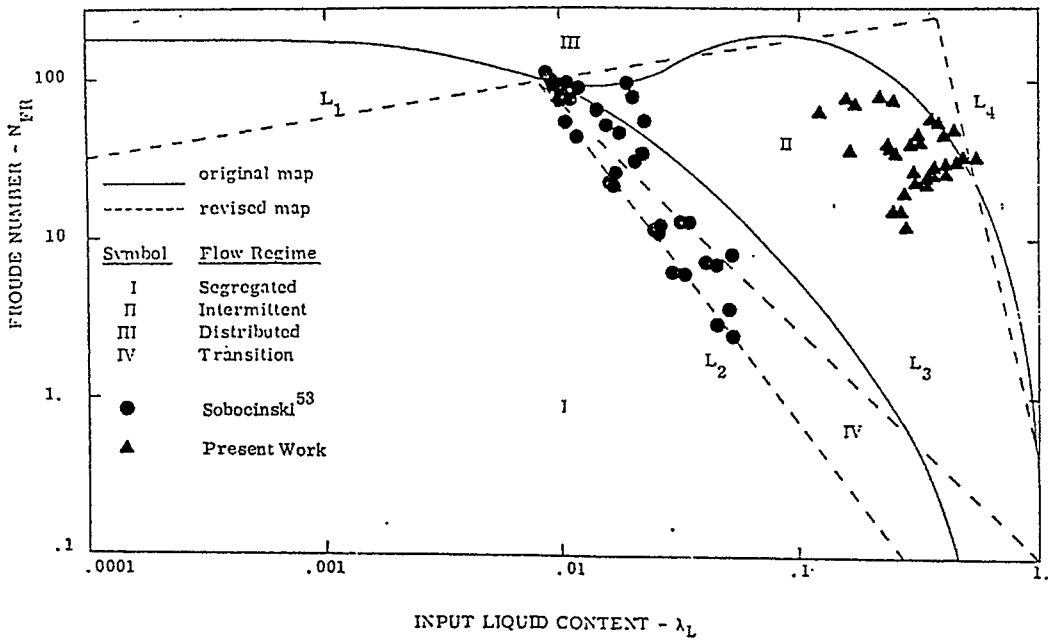


Figure 2.15: Plot obtained by Malinowsky (1975) of the Sobocinski (1955) and Malinowsky (1975) flow pattern data on the revised Beggs and Brill (1973) flow pattern map

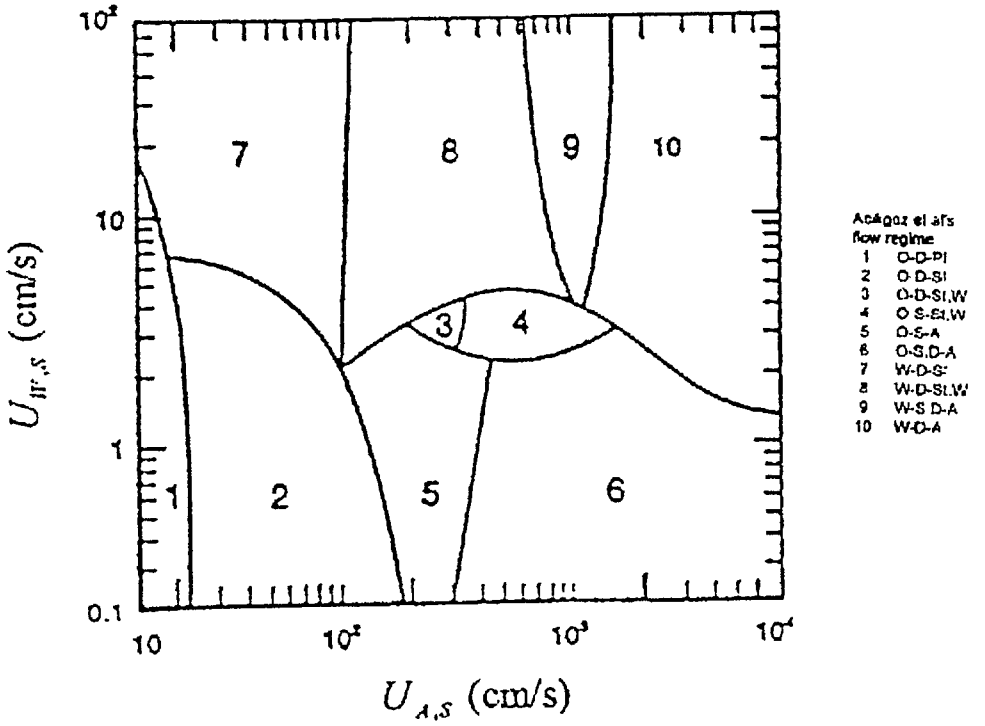


Figure 2.16: Acikgoz *et al.* (1992) three-phase flow pattern map (horizontal pipe; $U_{O,S}$=0.09m/s ; p=0 barg)

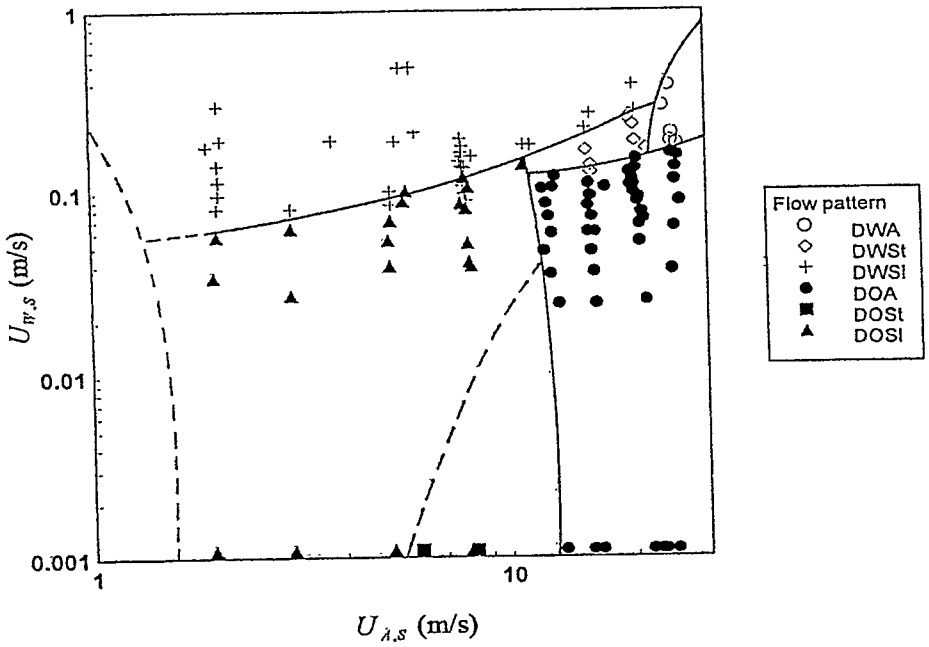


Figure 2.17: Pan (1996) three-phase flow pattern Map (horizontal pipe; $U_{O,S}$=0.095; p=0 barg)

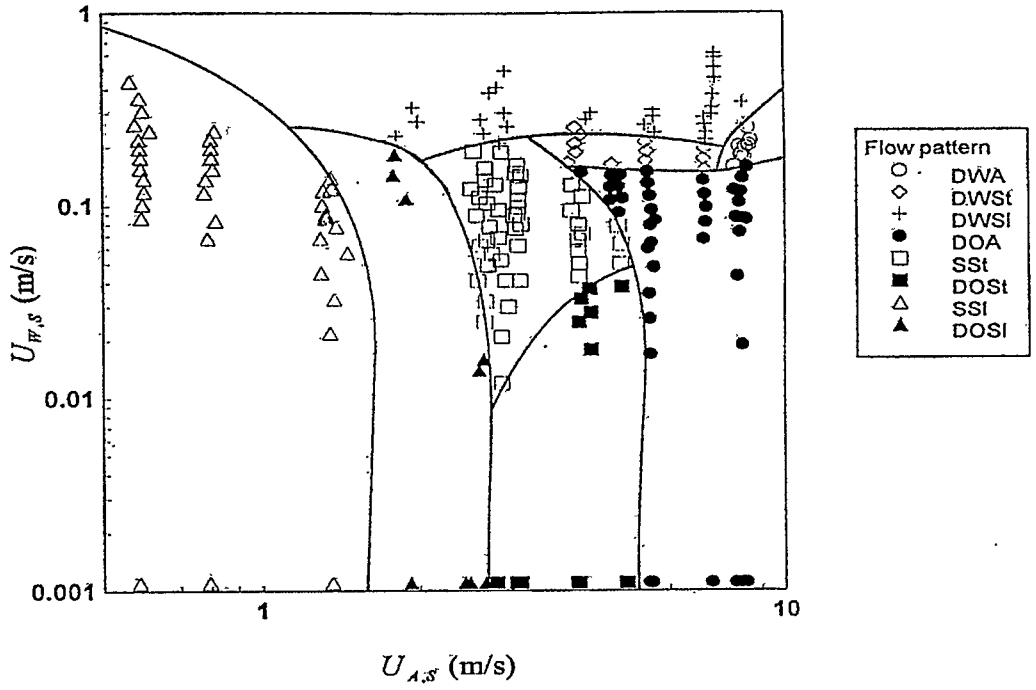


Figure 2.18: Pan (1996) three-phase flow pattern Map (horizontal pipe; $U_{O,S}$=0.095; p=5 barg)

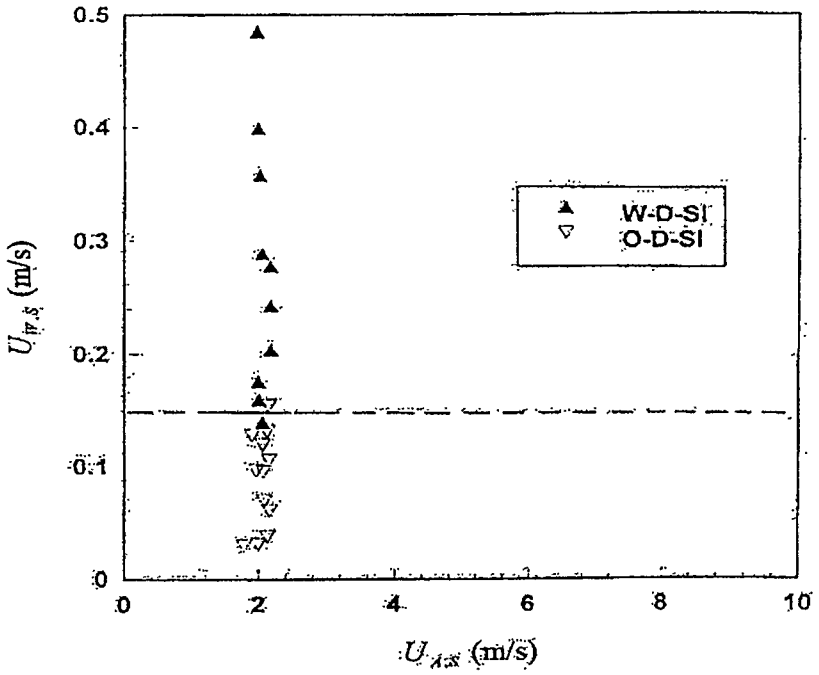


Figure 2.19: Pan (1996) three-phase flow pattern Map (1° Upwardly Inclined; $U_{O,S}$=0.095; p=5 barg)

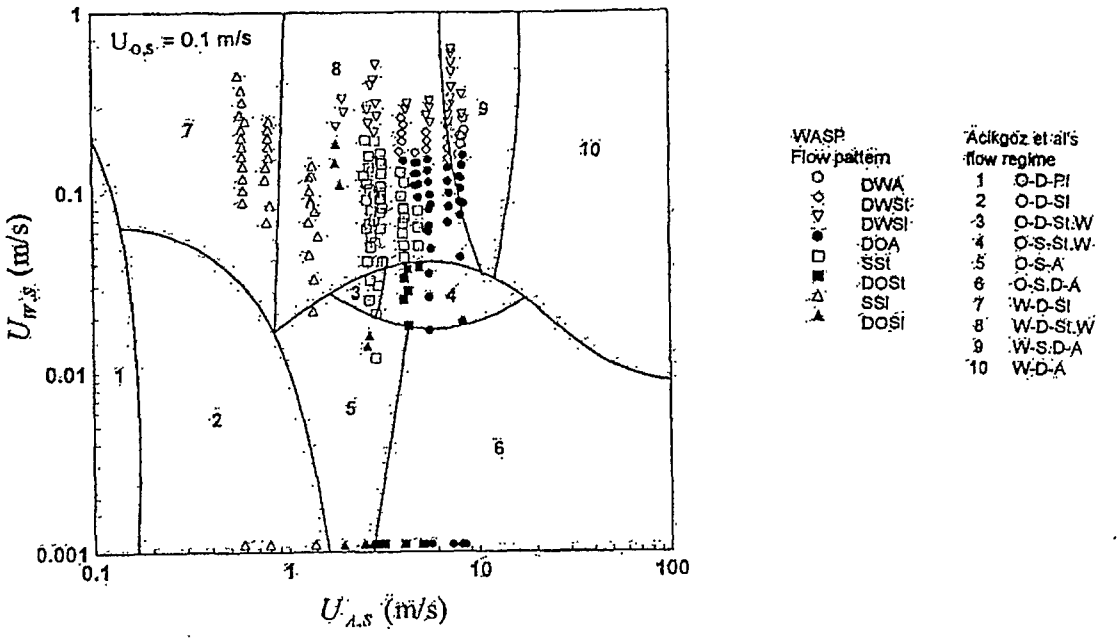


Figure 2.20: Comparison of the Pan (1996) three-phase flow pattern data with the three–phase flow map of Acikgoz *et al.* (1992) for 5 barg

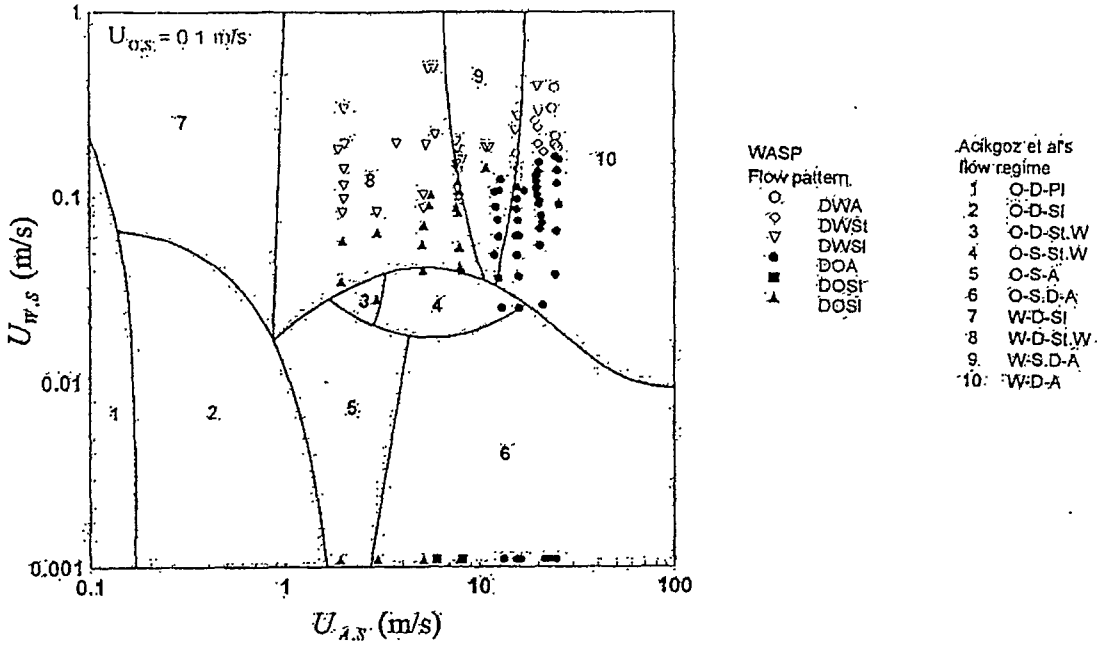


Figure 2.21: Comparison of the Pan (1996) three-phase flow pattern data with the three–phase flow map of Acikgoz *et al.* (1992) for 0 barg

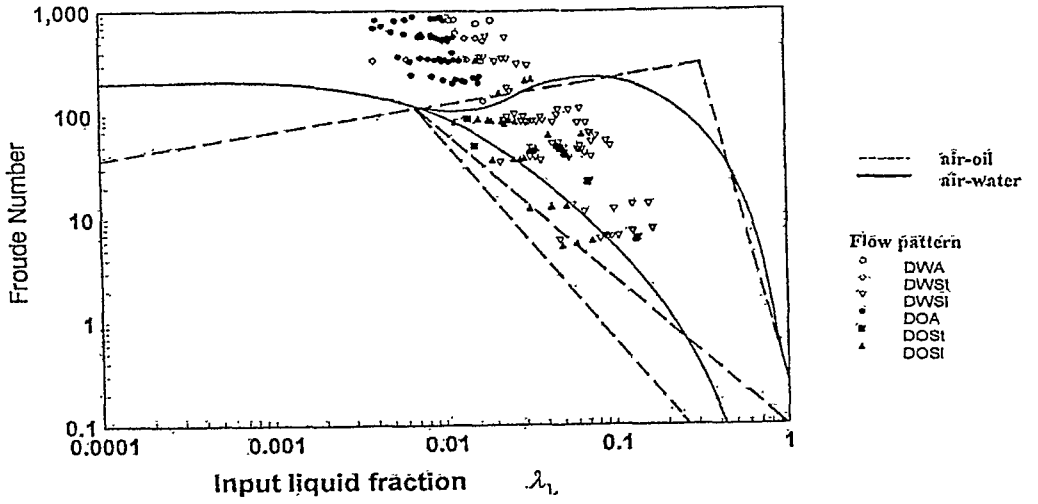


Figure 2.22: Comparison of the Pan (1996) three-phase flow pattern data with the two–phase flow map of Beggs and Brill (1973) for 0 barg

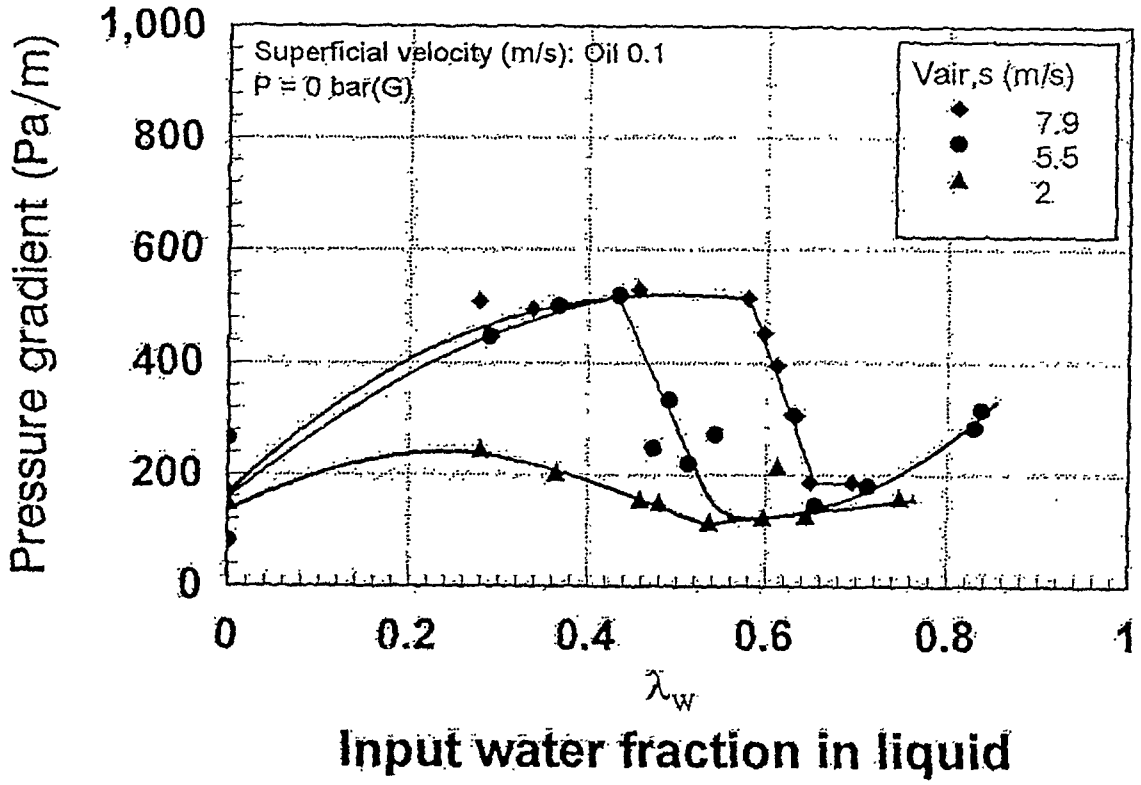


Figure 2.23: Three-phase air-oil-water experimental results of Pan (1996) for a horizontal pipe.

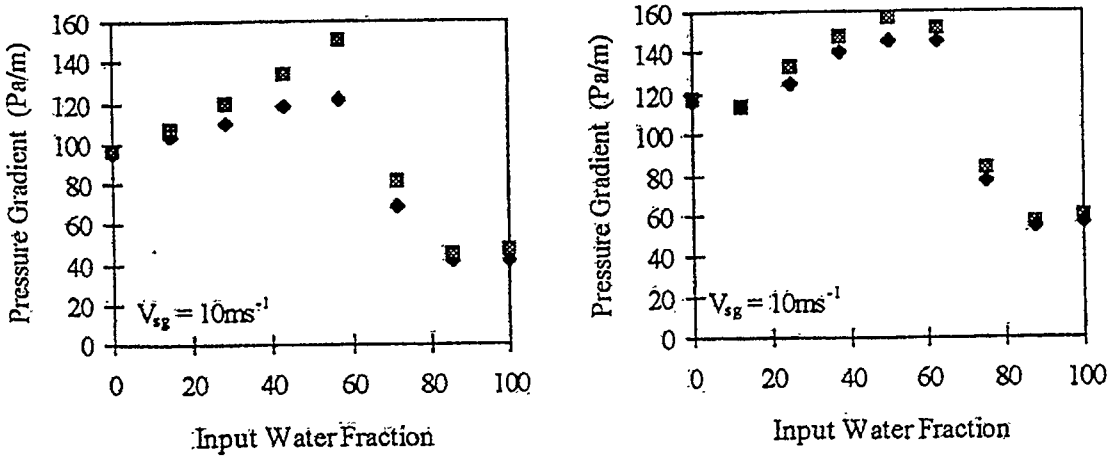


Figure 2.24: Three-phase air-oil-water pressure gradient experimental results of Donnelly (1997) for liquid superficial velocities 0.0773 m/s and 0.0329 m/s respectively.

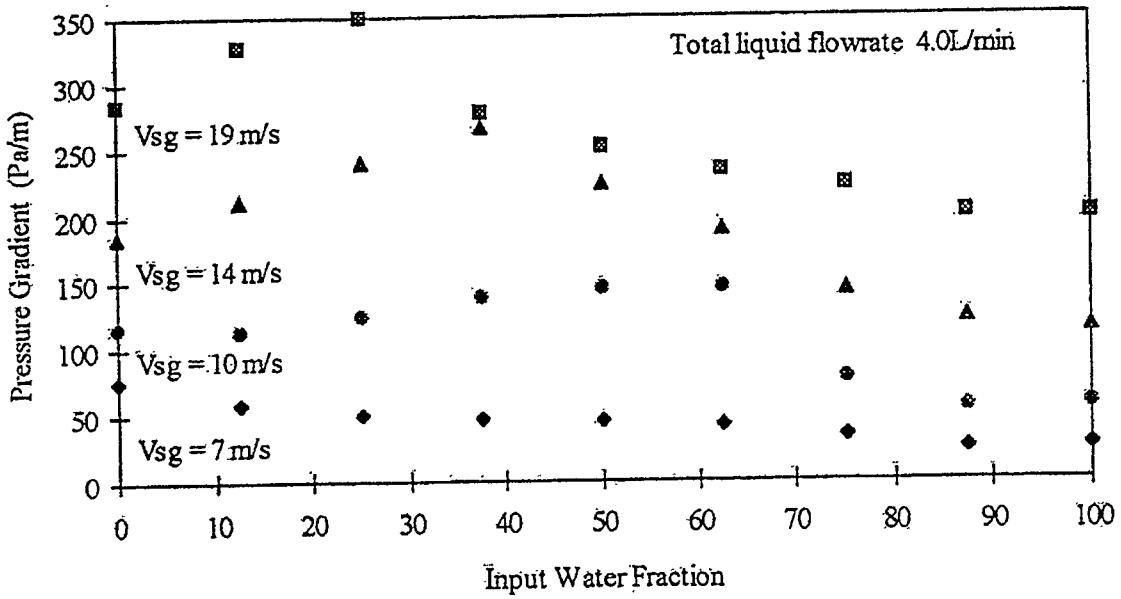


Figure 2.25: Three-phase air-oil-water pressure gradient experimental results of Donnelly (1997) for total liquid flowrate 4L/min for a range of gas flowrates.

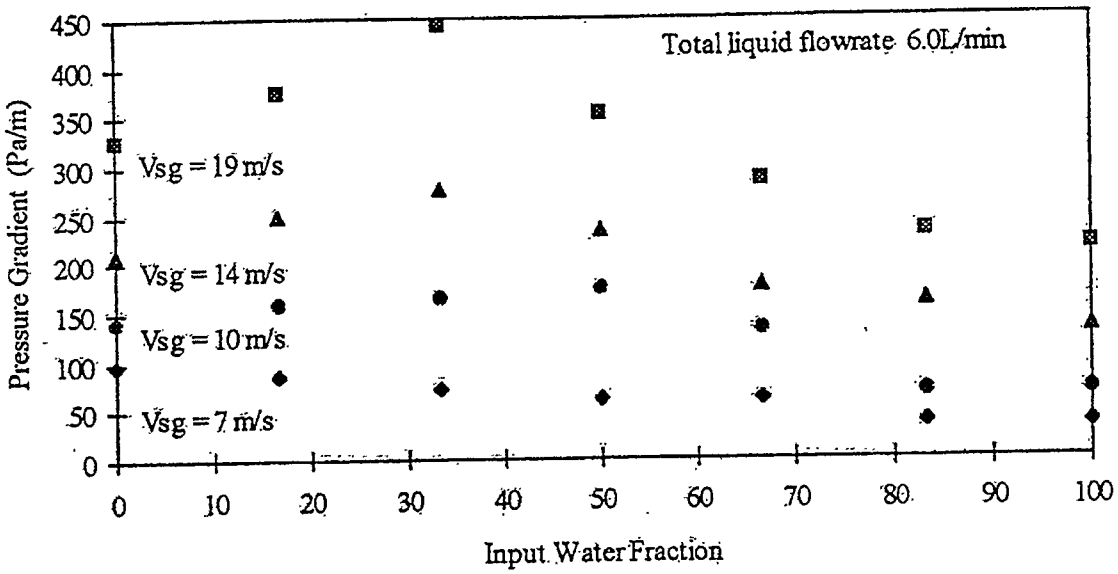


Figure 2.26: Three-phase air-oil-water pressure gradient experimental results of Donnelly (1997) for total liquid flowrate 6L/min for a range of gas flowrates.

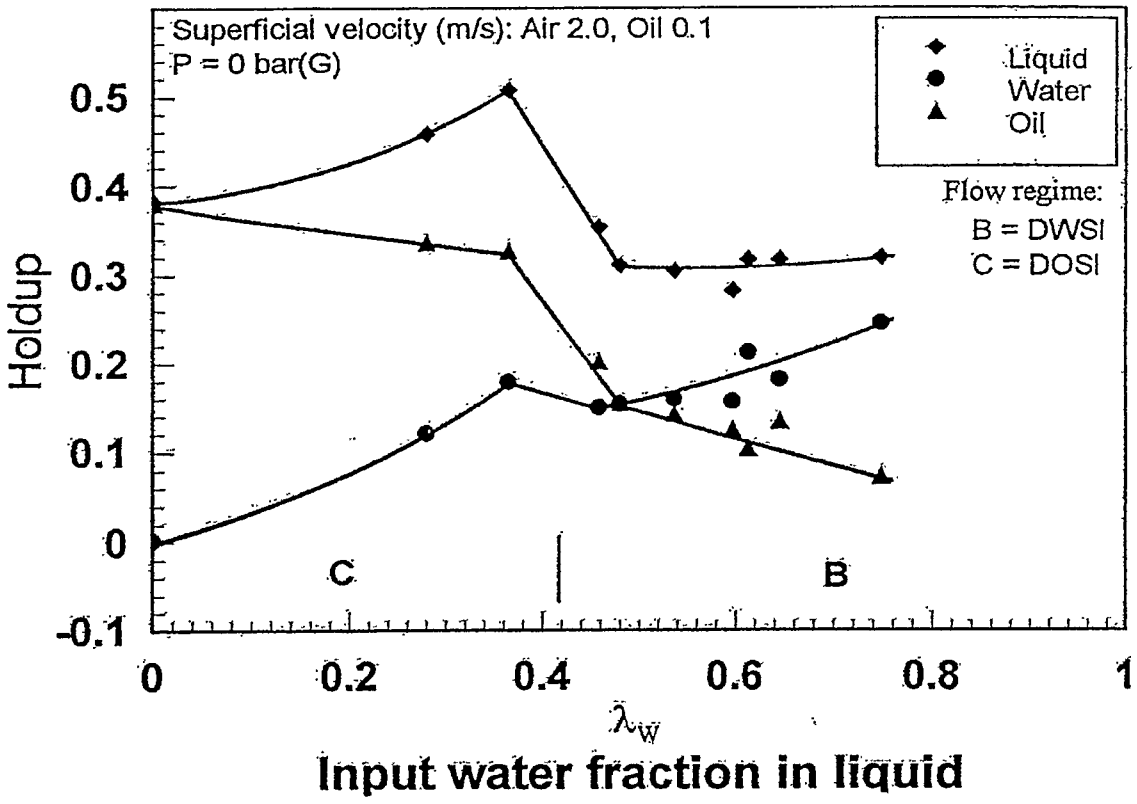


Figure 2.27: Three-phase air-oil-water holdup experimental results of Pan (1996) for air superficial velocity 2 m/s, oil superficial velocity 0.1 m/s and pressure 0 barg.

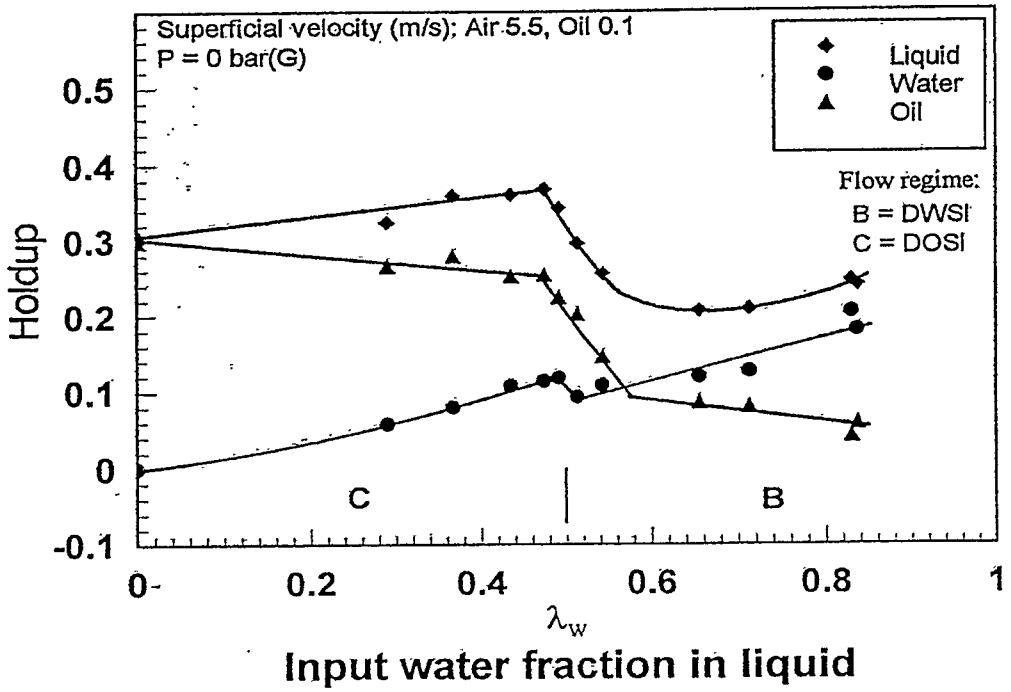


Figure 2.28: Three-phase air-oil-water holdup experimental results of Pan (1996) for air superficial velocity 5.5 m/s, oil superficial velocity 0.1 m/s and pressure 0 barg.

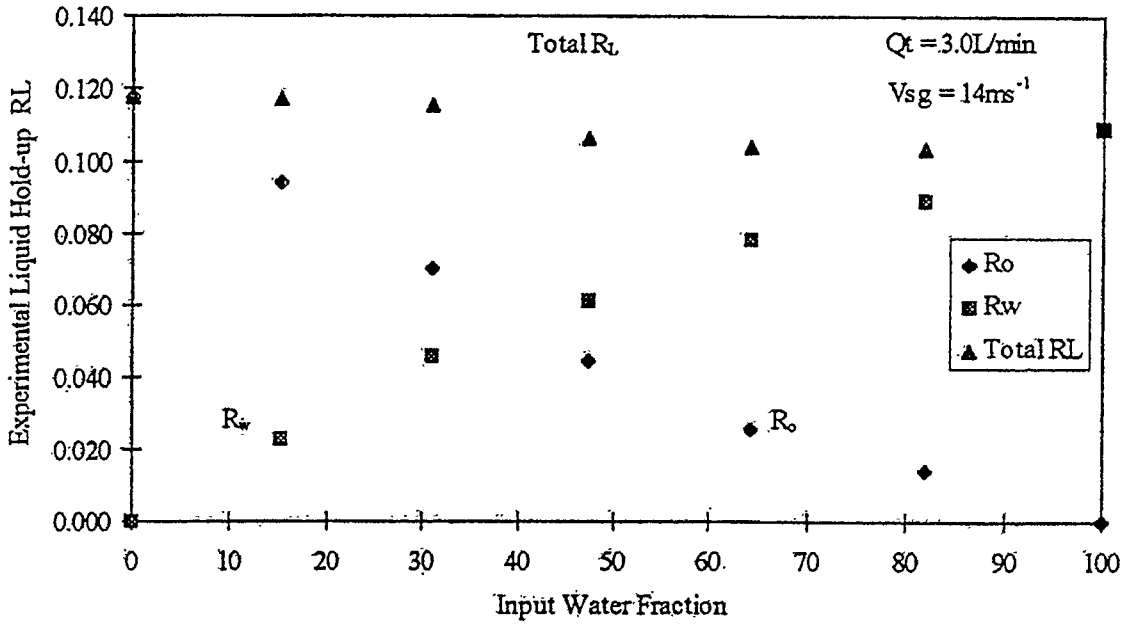


Figure 2.29: Three-phase air-oil-water holdup experimental results of Donnelly (1997) for air superficial velocity 14 m/s and total liquid flowrate 3L/min.

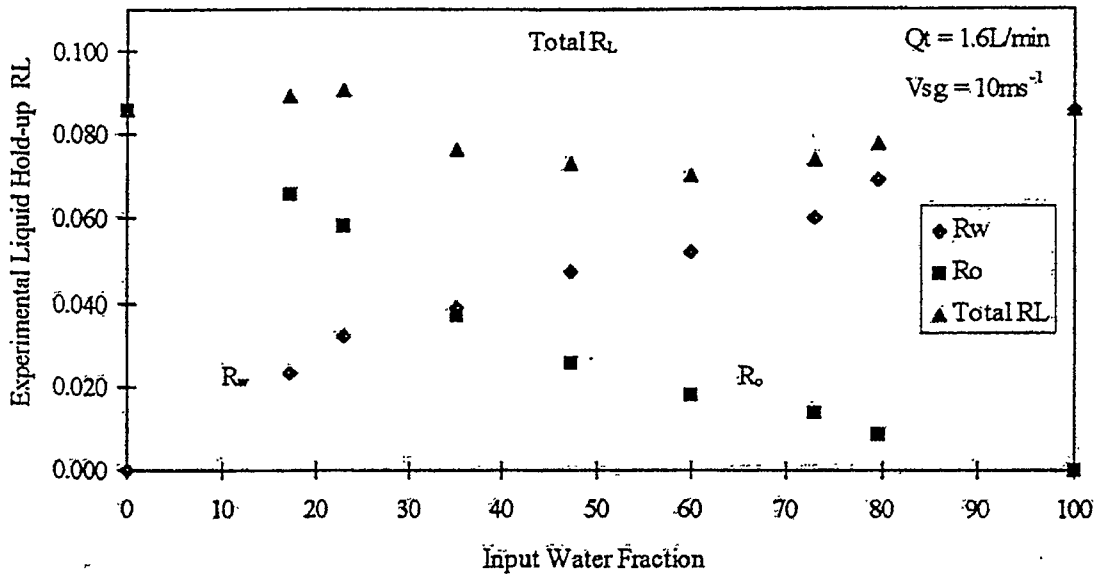


Figure 2.30: Three-phase air-oil-water holdup experimental results of Donnelly (1996) for gas superficial velocity 10 m/s and total liquid flowrate 1.6L/min.

Chapter 3

EXPERIMENTAL APPARATUS AND PROCEDURES

In this Chapter, the WASP facility and associated instrumentation used in the course of the experiments are described and the experimental procedures employed are explained.

3.1 THE WASP FACILITY

The WASP (Water, Air, Sand and Petroleum) High Pressure Multiphase Flow Facility is located at the Department of Chemical Engineering and Chemical Technology at the Imperial College, London and a schematic diagram is shown in Figure 3.1. The test section consists of a 38 m long stainless steel pipe with internal diameter of 77.92 mm (nominal 3 inch). The facility was specifically designed to enable experimental studies on two-phase air-water, oil-water and air-oil flow as well as three-phase air-oil-water flow to be carried out at pressures up to 50 bar and the test section is capable of being inclined from the horizontal, at angles ranging from -3° to +3°.

The air supply is drawn from the high-pressure supply tanks in the neighbouring Aeronautical Department which are illustrated in Figure 3.2. The water and oil are transported from high-pressure storage tanks (Figure 3.3) into the pipeline via the mixer, using centrifugal pumps. The fluids are introduced into the test section as three stratified layers in order of increasing density (water, oil and gas). This form of entrance device, as illustrated in Figure 3.4, avoids spurious effects due to slug formation in the entrance zone; the slugs, which may occur, are formed naturally from these initially stratified layers. Air and oil flowrates are measured using orifice plates built to BS1042 and the water flow rate is measured by an electromagnetic flow meter (MAGFLO 381). The flow then proceeds along test section which is illustrated in Figure 3.5. Close to the end of the test section, there is a visualisation section seen in Figure 3.6, where the flow patterns are observed with the aid of a video camera. After leaving the test section, the multiphase flow mixture passes through a separator (slug catcher) (Figure 3.7) where the air is separated from the liquids. The air leaves

through a silencer (Figure 3.8) where it is vented to the atmosphere and the liquids are discharged from the bottom of the separator into the dump tank (Figure 3.9) where they separate by gravity before being pumped back to their individual storage tanks.

3.2 PROPERTIES OF WASP FLUIDS

3.2.1 Oil

The oil used for all the experiments described in this thesis was Shell Tellus 22. The viscosity and density of the oil, determined experimentally by Hall (1992) are related to the temperature t (in °C) by the expressions:

$$\mu_O = (153 - 11.2t + 0.457t^2 - 0.0103t^3 + 0.0001t^4) \times 10^{-3} \quad (0 \le t \le 35^\circ C) \quad (3.1)$$

$$\rho_O = 860.5 + 0.46(24.7 - t) \qquad (0 \le t \le 35^\circ C) \quad (3.2)$$

The viscosity of the oil was monitored on a daily basis throughout the experimental campaigns with the aid of a Bohlin rheometer. In addition to this, the water content in the oil was not allowed to exceed 3 % of water in oil, thus ensuring that the oil properties were preserved.

3.2.2 Water

The water used to carry out the experiments was tap water and its viscosity as a function of the temperature was obtained using the viscosity correlation of Van Wingen (1950):

$$\mu_W = \left(\exp\left[1.003 - 0.01479t' + 1.928 \times 10^{-5} t'^2 \right] \right) \times 10^{-3} \quad (3.3)$$

Where t' (in °F) is given by the expression

$$t' = 1.8t + 32 \quad (3.4)$$

3.2.3 Air

The air viscosity as a function of its temperature was evaluated using the source (National Research Council "International Critical Tables of Numerical Data" (1928) Vol. 5 No. 2 McGraw Hill Book Company) and was given as:

$$\mu_A = \left(0.01622 + 2.7083 \times 10^{-5} t'\right) \times 10^{-3} \quad (3.5)$$

Where t' is given by Equation (3.4)

The density of air was evaluated using the expression from Perry and Green (1997):

$$\rho_G = 348.5966\left(\frac{p}{t+273}\right) \tag{3.6}$$

Where p is the pressure in bars (absolute)

3.3. INSTRUMENTATION

The main instrumentation used in the course of the experiments was the pressure transducer, which was employed to measure the pressure drop along the pipe and the γ ray densitometer, which was used to measure the in-situ liquid holdup. Detailed descriptions of these devices are given in the following section.

3.3.1 Pressure Drop Measurement

A Rosemount 3051CD differential pressure transducer of maximum range 0.12-13800kPa was used to measure the pressure drop along the test section. Both ports of differential pressure transducer were mounted flush to the bottom of the test section and were placed 3.5 m and 6.0 m upstream of the exit of the test section. The lines of the pressure transducer were filled with silicone fluid to avoid the infiltration of air bubbles into the lines.

The accuracy of the transducer was specified as ±0.5% of the full span. For the experiments reported in this thesis, the maximum range utilised was –4000 Pa to +4000 Pa, which translates into a maximum error in the pressure drop of ±40 Pa. However, the measurements were carried out over a length of 2.5m, thus the error in the pressure gradient measurement is ±16 Pa/m.

3.3.2 Liquid Holdup Measurement

The liquid holdup was measured using a single-beam dual-energy gamma densitometer. The gamma densitometer operates on the principle of the attenuation of the gamma ray beam through a medium. When a gamma ray beam of initial intensity I_o is incident on a medium, the transmitted intensity is given by the expression:

$$I = I_o \exp(-\gamma x) \tag{3.7}$$

Where γ is the linear absorption coefficient of the medium and x is the thickness of the medium. For three-phase air-oil-water flow, Pan (1996) showed that the phasic holdups of the three phases could be given by the following expressions:

$$\varepsilon_1 = \frac{\left[\frac{\ln\frac{I_A}{I_{2a}}}{\ln\frac{I_{3A}}{I_{2A}}}\right] - \left[\frac{\ln\frac{I_B}{I_{2B}}}{\ln\frac{I_{3B}}{I_{2B}}}\right]}{\left[\frac{\ln\frac{I_{1A}}{I_{2A}}}{\ln\frac{I_{3A}}{I_{2A}}}\right] - \left[\frac{\ln\frac{I_{1B}}{I_{2B}}}{\ln\frac{I_{3B}}{I_{2B}}}\right]} \tag{3.8}$$

$$\varepsilon_2 = \frac{\left[\frac{\ln\frac{I_A}{I_{3A}}}{\ln\frac{I_{1A}}{I_{3A}}}\right] - \left[\frac{\ln\frac{I_B}{I_{3B}}}{\ln\frac{I_{1B}}{I_{3B}}}\right]}{\left[\frac{\ln\frac{I_{2A}}{I_{3A}}}{\ln\frac{I_{1A}}{I_{3A}}}\right] - \left[\frac{\ln\frac{I_{2B}}{I_{3B}}}{\ln\frac{I_{1B}}{I_{3B}}}\right]} \tag{3.9}$$

$$\varepsilon_3 = 1 - (\varepsilon_1 + \varepsilon_2) \tag{3.10}$$

Where ε_1, is defined as the holdup of oil, ε_2 is the holdup of water and ε_3 is the void fraction.

The constants I_{1A}, I_{2A}, I_{3A}, I_{1B}, I_{2B}, I_{3B}, are referred to as calibration constants and are obtained by a calibration procedure which involves filling the test section with oil, water and air separately and determining the count rate for each case for each of the two energies, A and B. Typical calibration data for 31 keV and 81 keV gamma energy can be seen in Figures 3.11 and 3.12.

3.3.2.1 Single Beam Dual Energy Gamma Densitometer

The gamma densitometer system consisted of four main parts: the gamma source, the detection system, the positioning system and the computer control & acquisition

system. Full details for this gamma densitometer can be found in the thesis of Pan (1996); here, only a brief summary is presented.

(a) Gamma source

The gamma ray source for this gamma densitometer consists of a Ba-133 isotope of strength 20 mCi. The two energy levels 31 keV and 81 keV were selected on the basis of optimisation studies carried out by Pan (1996). The gamma source, encased within a lead block, was positioned beneath a 76.2 mm internal diameter acrylic resin (Perspex^{TM}) tube which was situated 35m downstream of the inlet section and mounted between the flanges of the main (stainless steel) test section. The lead block was machined with an aperture of dimension 4 mm × 10 mm, so as to collimate the beam from the source. An illustration of the gamma source holder collimation is shown in Figure 3.13.

(b)The detection system

The gamma radiation emitted from the source and passing through the contents of the Perpex pipe is detected by a NaI (sodium iodide) crystal coupled to a photomultiplier tube (PMT) fitted with a pre-amplifier. The details of the detector collimation are shown in Figure 3.14. The NaI crystal scintillates when a gamma photon enters it, giving pulses of light, which are subsequently amplified by the photomultiplier tube and the pre-amplifier. A delay line amplifier (DLA) was used to further amplify the signals obtained from the PMT. Since the electronic detection system is of the pulse mode variety, two single channel analyzers (SCAs), one for each of the energy levels (31 keV and 81 keV) were employed to sort the pulses induced by gamma photons of the respective energies. The output from the SCAs was then passed on to a dual-counter/timer for counting the number of scintillations over a given time period corresponding to the respective energies. A schematic of the electronic components for the single-beam dual-energy gamma densitometer is shown in Figure 3.15.

(c) The positioning system

The positioning system consists of two stepper motors, one for horizontal traversing of both the gamma source and detector system, and a second one for traversing the gamma system vertically. The positioning system is controlled by computer with the

aid of a QUICK BASIC program. For horizontal traversing (using a vertical beam), there are a number of modes in which the gamma densitometer may be used, and these modes are illustrated in Figure 3.16. The full-pipe scan mode involves traversing the gamma beam over 15 chordal positions across the diameter of the pipe, using the PC controlled stepper motor, and this mode was utilised for the calibrations.

When it is not necessary to use all of the fifteen chordal positions in the course of the measurements, the gamma densitometer can also be used in a "half-pipe scan" mode, where only 8 chordal positions across the pipe radius are scanned. This was found to give the same measurement accuracy as the full-pipe scan mode and was adopted for the majority of the data presented in this thesis. In addition to these, a centre pipe scan can also be used. This involves fixing the gamma beam at the pipe center, and is useful for carrying out cross-correlation measurements.

(d)The computer control and acquisition system

A personal computer was used with a QUICK BASIC program to specify options for operation of the gamma densitometer such as scanning times, controlling the positioning system and writing the data.

The gamma densitometer was set to acquire data at a frequency of 25 Hz over a time period of 160s. The measurement accuracy for the gamma densitometer was estimated (Pan 1996) as around 1.5 % for two-phase flows and around 3 % for three-phase flows.

3.3.3 Slug Velocity Measurements

To measure the slug translational velocity, two gamma densitometers were used to track the slugs as they propagated through the test section. In addition to the single beam dual-energy gamma densitometer described above, another gamma densitometer was employed for this purpose. This gamma densitometer is a triple-beam dual- energy type utilizing a 30 mCi Ba-133 source. It is situated at a distance of 7.6 m from the exit of the test section.

3.3.3.1 Triple-Beam Dual Energy Gamma densitometer

Unlike the previously described gamma densitometer, this gamma densitometer was not traversible and thus consisted of three main parts, the source, the detector system and the PC control and data acquisition system. The three-beam gamma densitometer was developed for another project on the WASP facility, one involving mainly transient three-phase flows. The use of the three beams allows some information to be gained on transient cross-sectional distributions of the phases; clearly, in a transient flow, the mechanical traversing method used in the single-beam gamma densitometer described in Section 3.3.2.1 above would not operate quickly enough to obtain the required information on transient spatial distribution. In the present work, the three-beam gamma densitometer was used in single-beam mode with the beam passing vertically through the tube axis being selected. The main objective of using this second densitometer was to provide a signal which could be cross-correlated with that from the single baem densitometer in order to measure slug velocities.

(a) Gamma source and collimation

The three beam gamma densitometer had as its source a 30 mCi Ba-133 isotope. The gamma photons arising from the source were collimated with three apertures in the lead block so as to allow the emission of three beams.

b)The detection system

The details of the detector collimation for the dual-energy triple beam gamma densitometer are shown in Figure 3.17. The dimensions of the detector-side collimation are 52mm by 15 mm, 52 mm being the distance between the detector tube and the top of the acryllic resin (Perspex^{TM}) tube. The width of the aperture, 15 mm is considerably greater than the corresponding width for the single beam dual energy gamma densitometer, and this led to significantly higher count rate. However the down side to this was that the detector was over-saturated with counts thus reducing the ability of this system to distinguish between oil and water accurately. As a result of this, the triple beam dual-energy gamma densitometer was used mainly for cross-correlation.

3.3.3.2 Cross correlation Method

Slug translational velocities were obtained by cross-correlating the liquid holdup readings from the vertical beams of both gamma densitometers.

The slug velocities obtained from cross correlating the gamma densitometers are averaged over all the slugs. To evaluate the time delay between the two gamma densitometers, use was made of the cross correlation function $R_{xy}(\tau)$ which is given by the expression below:

$$R_{xy}(\tau) = \lim_{T\to\infty} \frac{1}{T} \int_0^T x(t-\tau).y(t)dt \qquad (3.11)$$

Where T is the total sample time, τ is the time delay, $x(t-\tau)$ is the time trace of the upstream densitometer and $y(t)$ is the time trace of the downstream densitometer. The time delay between the two gamma densitometer signals is defined as the time delay that corresponds to a maximum in the cross correlation function.

3.4 EXPERIMENTAL CAMPAIGNS

In the WASP facility, a number of experimental projects are pursued in parallel. The programme of the facility is arranged in a series of successive "campaigns", each from one of the constituent projects. This allows periods of preparations and analysis between the campaigns in a given project and makes the most efficient use of the facility. In what follows, the four experimental campaigns carried out over the course of this project are discussed along with the aims and objectives of each of the campaigns.

3.4.1 Campaign #1 (January–March 1997)

This campaign was carried with the aim of obtaining flow pattern data for the construction of flow pattern maps for oil superficial velocities of 0.1 m/s, 0.5 m/s and 0.7 m/s for a horizontal pipe to supplement the data already obtained by Pan (1996) at an oil superficial velocity of 0.1 m/s. In addition, the influence of the water-cut on the pressure gradient and the total liquid holdup as well as the individual phasic holdups of water and oil around the phase inversion region were also investigated.

Most of the tests were carried out at 0.5 m/s superficial oil velocity though tests were initially carried out at 0.1 m/s superficial velocity to investigate the reproducibility of the data obtained by Pan (1996). These tests showed good agreement with his data. The range of the parameters used for Campaign # 1 are given in Table 3.1

Parameter	Range
Air superficial velocity	2-15m/s
Oil superficial velocity	0.1, 0.5 &0.7 m/s
Water superficial velocity	0.05-0.5m/s
System pressure	0 & 5 barg
Pipe configuration	Horizontal

Table 3.1:Range of Parameters for WASP Experimental Campaign #1

When the experiments were carried out, the air flow rate was first set, and then the oil and water flowrates were selected and their respective valves opened. A period of two minutes was allowed to elapse before data acquisition was commenced to allow steady state to be reached. The experiments were carried out for duration of 160s.

The flowrates of oil, water and air were sampled at an acquisition frequency of 10 Hz, while the acquisition frequency for the single-beam dual energy gamma densitometer was set at 25 Hz throughout the duration of data acquisition. The triple-beam dual-energy densitometer was not used in these tests.

Video recordings of the flows were made with the aid of the video camera, so that slug frequency could be measured and flow patterns could be obtained.

3.4.2 Campaign #2 (August-October 1997)

The aim of this set of experiments was to obtain unique data on three-phase air-oil water flow with the pipe downwardly inclined at an angle of $-1.5°$ to the horizontal. Foremost amongst the objectives, was obtaining a flow pattern map at an oil superficial velocity of 0.2 m/s for system pressures of 0, 5 and 10 barg.

The range of parameters investigated during campaign 2 are shown in table 3.2:

Parameter	Range
Air superficial velocity	2-24 m/s
Water superficial velocity	0-0.5m/s
Oil superficial velocity	0-0.5m/s
System pressure	0, 5 & 10 barg,
Pipe configuration	Pipe downwardly inclined –1.5° from the horizontal

Table 3.2:Range of Parameters for WASP Experimental Campaign #2

The same mode of operation as described for Campaign #1 was employed here.

3.4.3 Campaign #3 (September 1997)

The objective of this campaign was to extend the existing database and to investigate the parameters which have an influence on the position of the phase inversion such as the air superficial velocity as well as the liquid superficial velocity.

Data for the construction of a horizontal flow pattern map for a constant oil superficial velocity of 0.2 m/s were collected to enable a comparison with results from Campaign #2 so that the effects of pipe inclination angle on flow patterns could be determined.

Parameter	Range
Air superficial velocity	2-24 m/s
Water superficial velocity	0-0.5m/s
Oil superficial velocity	0-0.5m/s
System pressure	0, 5 & 10 barg,
Pipe configuration	horizontal

Table 3.3: Range of Parameters for WASP Experimental Campaign #3

3.4.4 Campaign #4 (July-September 1999)

The aim of carrying out this set of experiments, was to obtain slug characteristics such as slug velocity, slug length as well as slug body holdup by cross correlating the total liquid holdup signals from both gamma densitometers which were situated 6.4 m apart. The same range of parameters as utilised in Campaign #3 were employed for campaign #4.

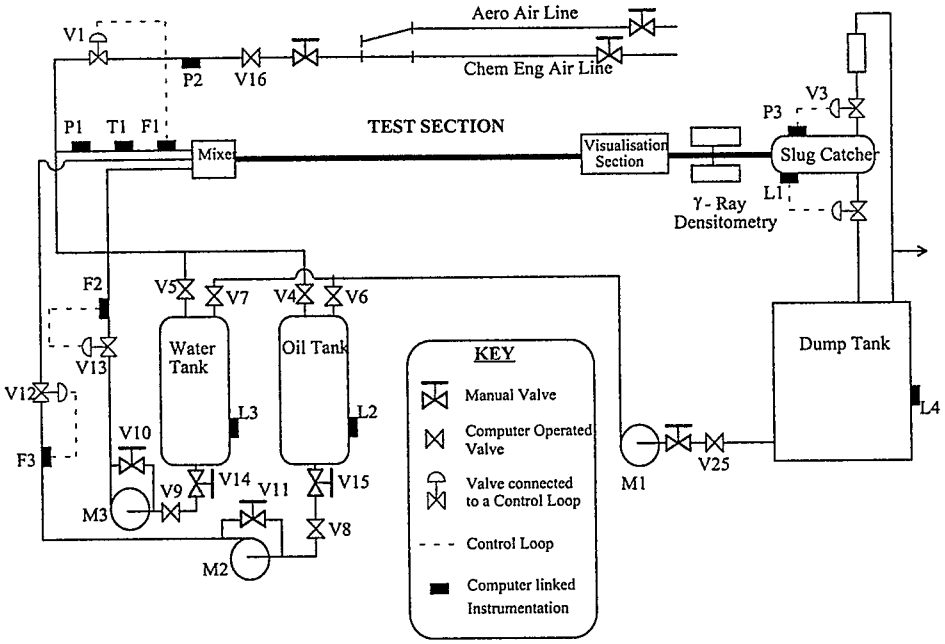


Figure 3.1: Schematic of the WASP multiphase flow facility

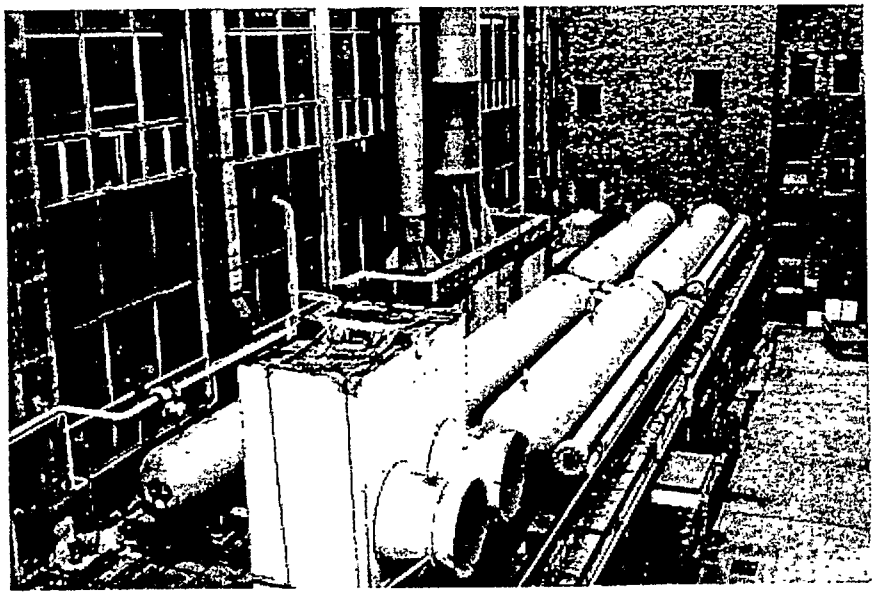


Figure 3.2: High pressure air tanks

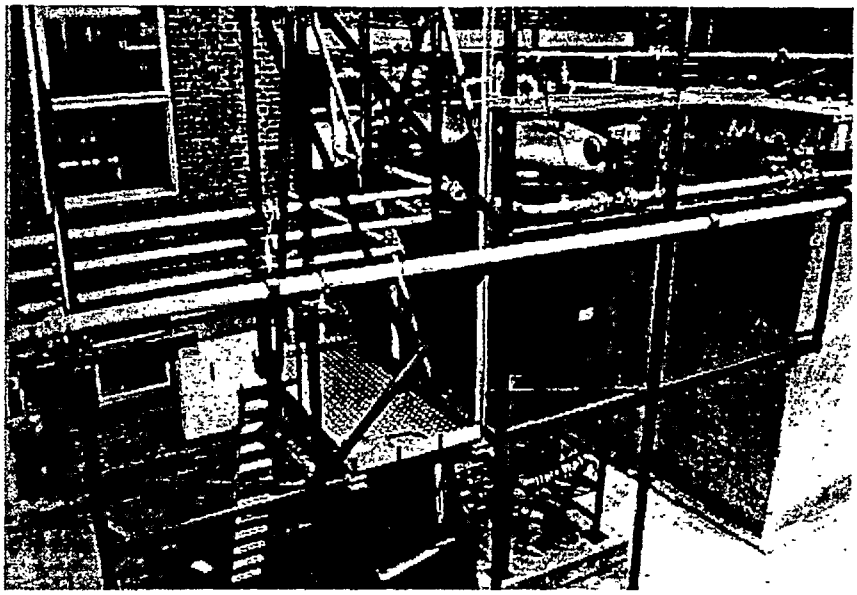


Figure 3.3: WASP Facility oil and water storage tanks

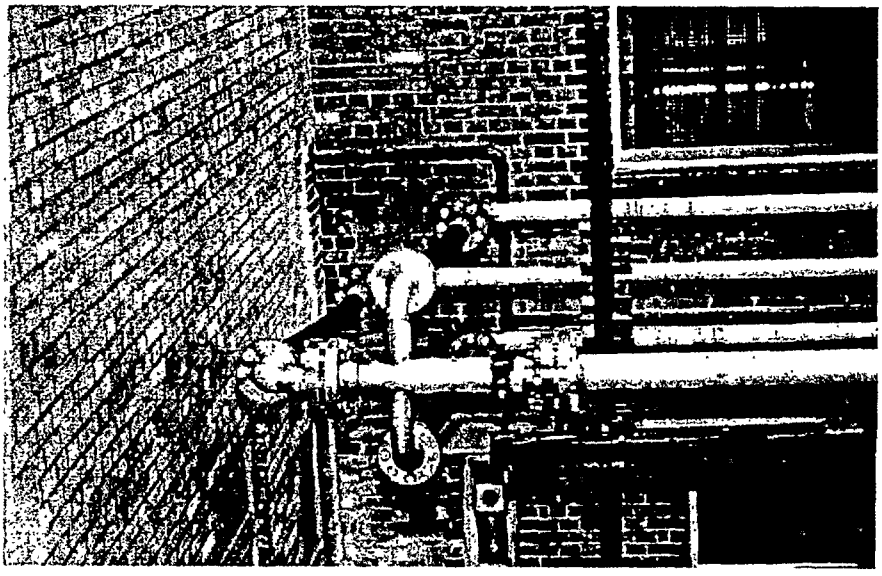


Figure 3.4: Inlet mixer



Figure 3.5: WASP test section

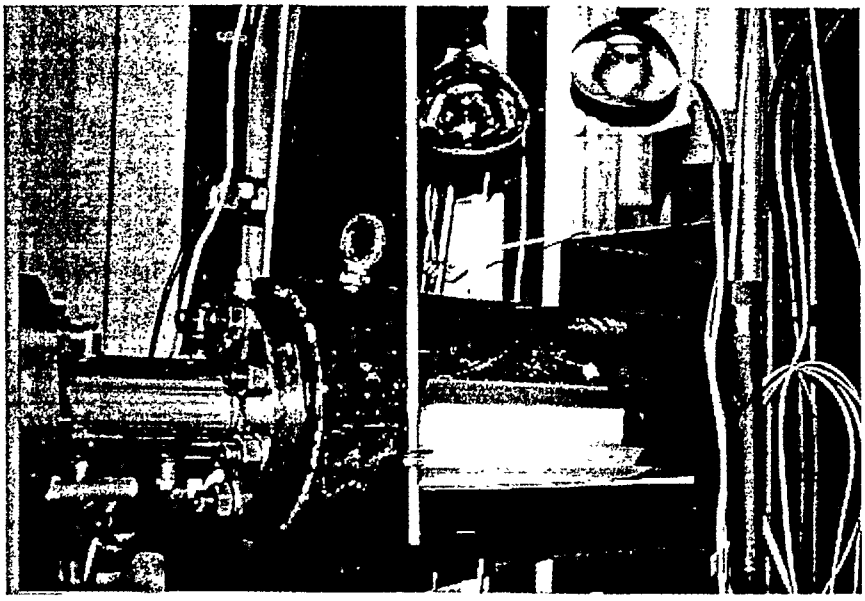


Figure 3.6: Visualization section

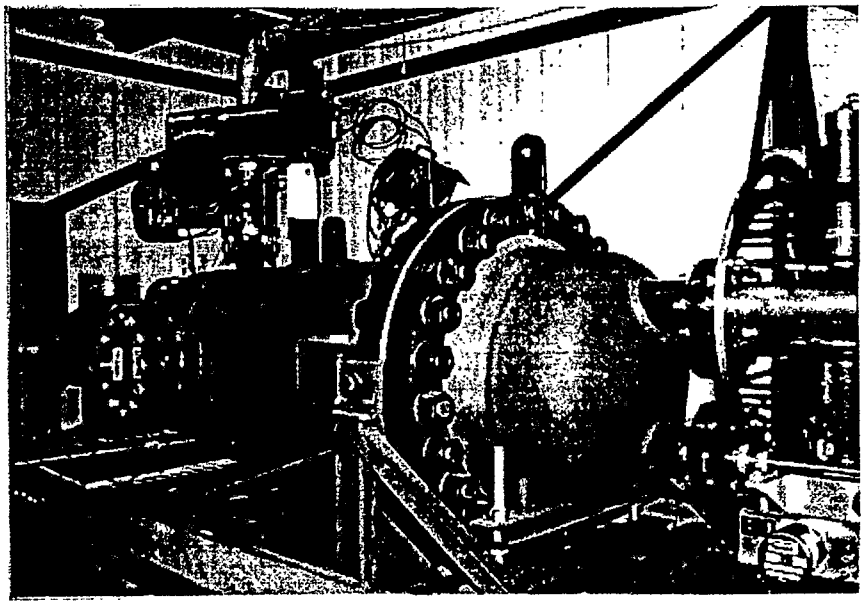


Figure 3.7: Slug catcher

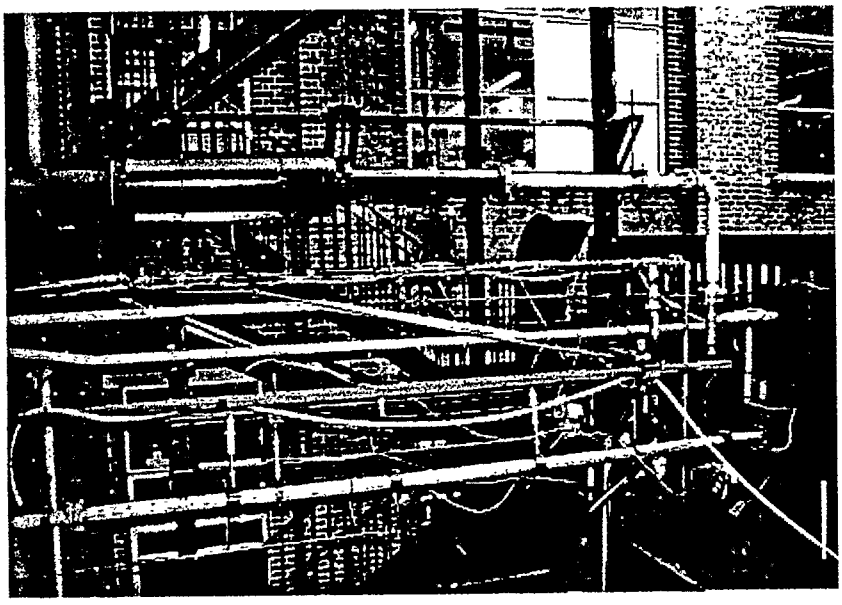


Figure 3.8: Silencer

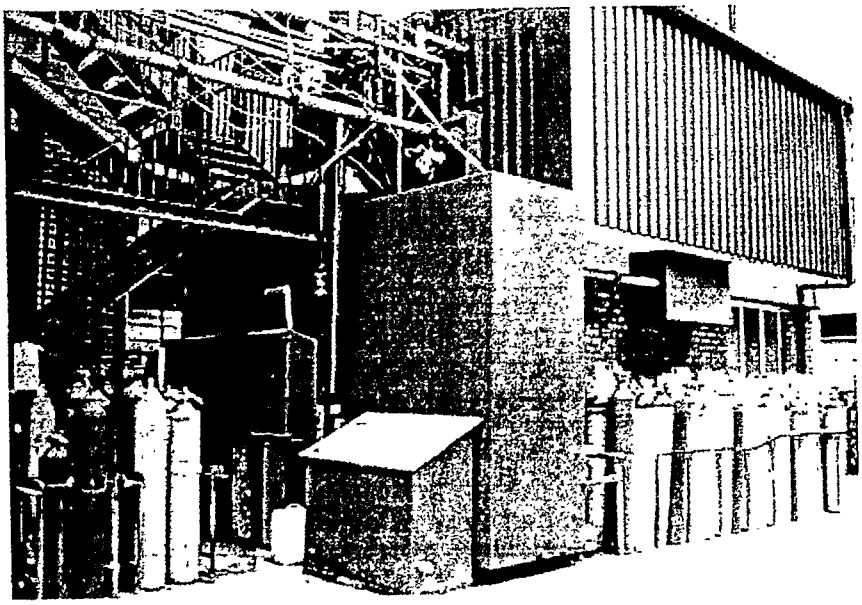


Figure 3.9:Dump Tank

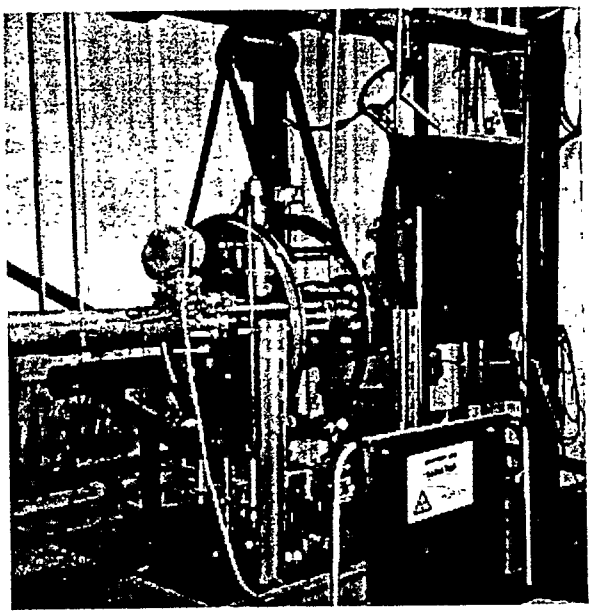


Figure 3.10: WASP single-beam dual-energy gamma densitometer

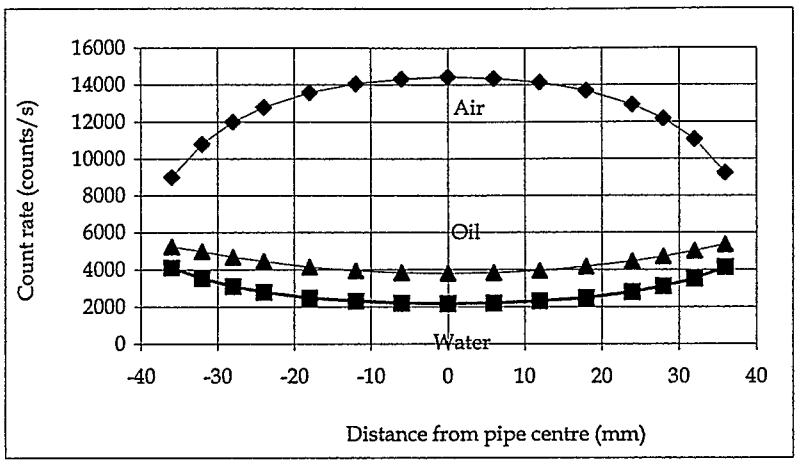


Figure 3.11: Calibration data for 31 keV gamma energy

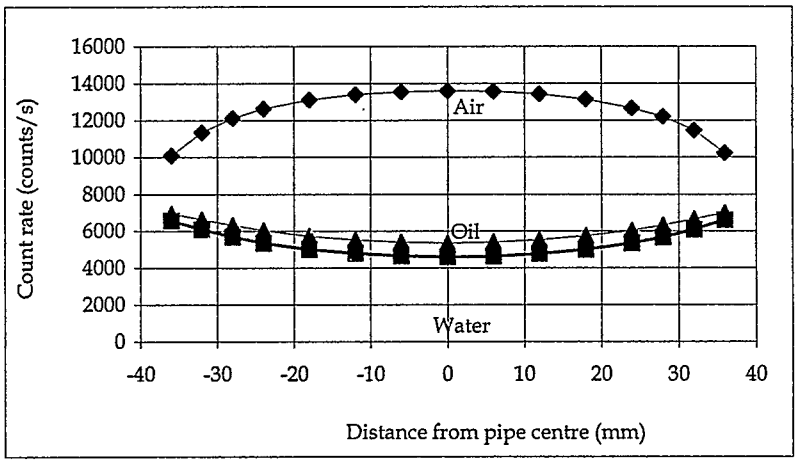


Figure 3.12: Calibration data for 81 keV gamma energy

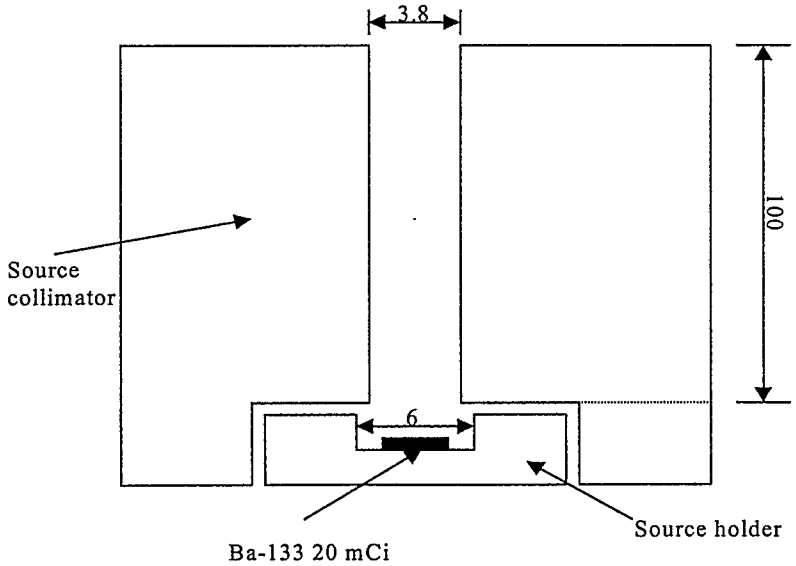
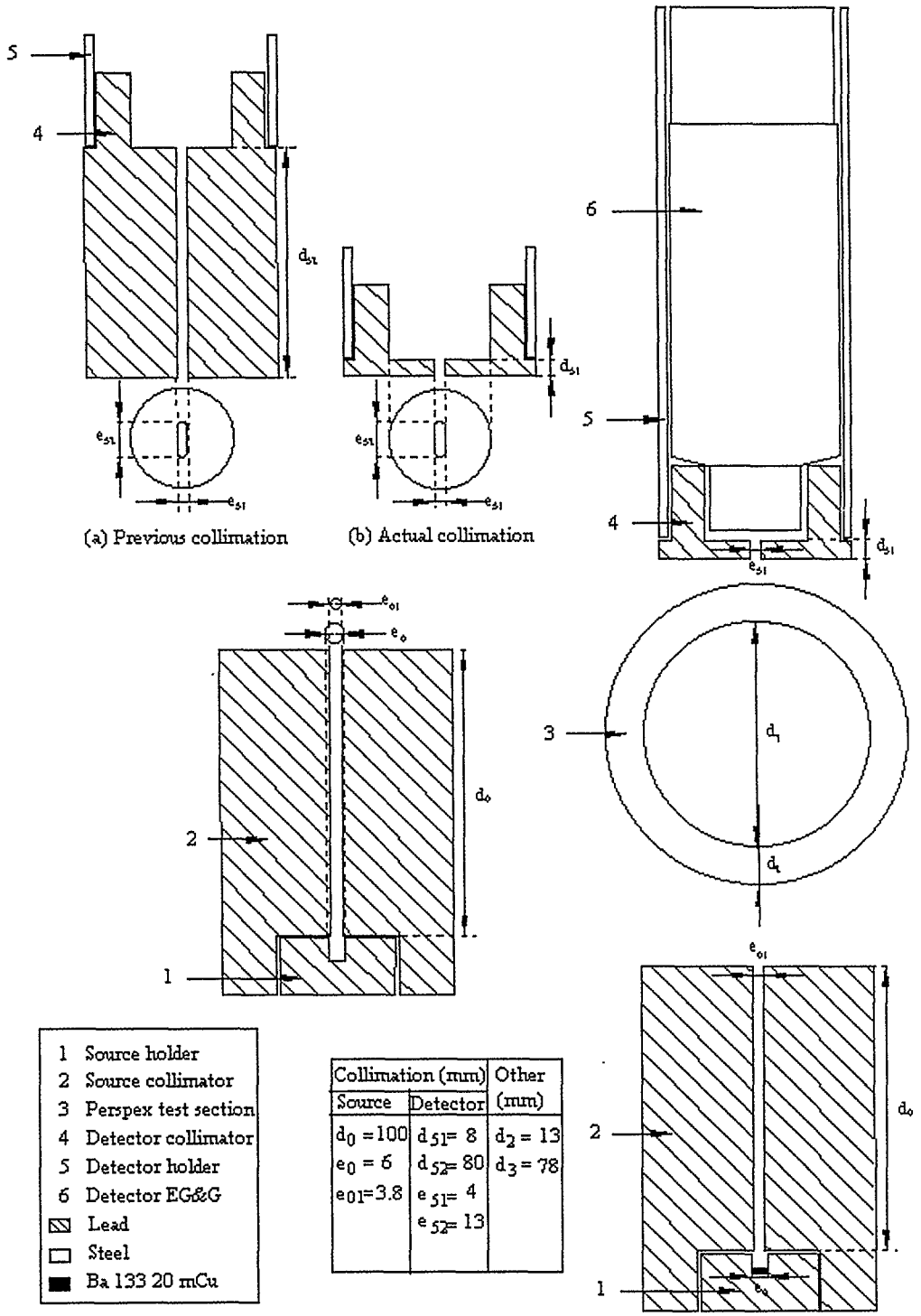


Figure 3.13: Source collimator for single beam dual-energy gamma densitometer

Figure 3.14: Detector and source collimator for single beam dual-energy gamma densitometer



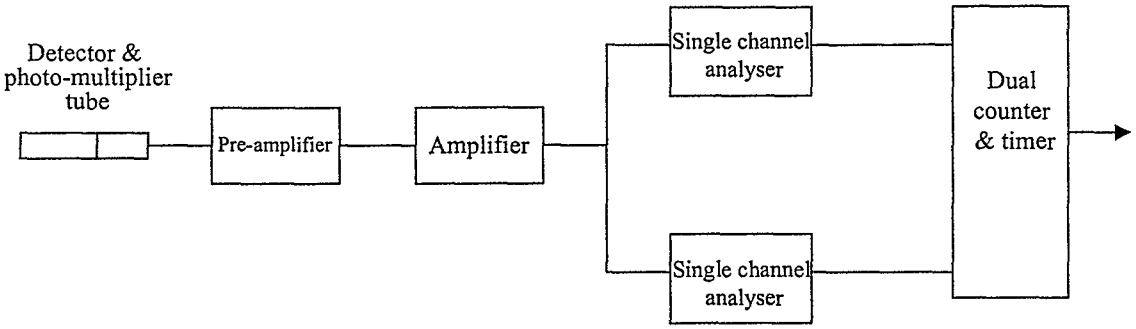


Figure 3.15: Electronic components for single beam dual energy gamma densitometer

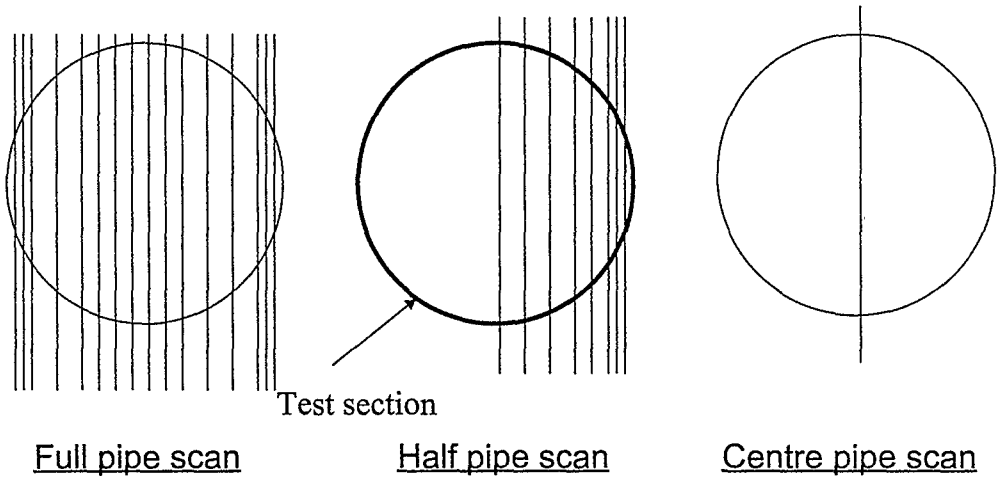


Figure 3.16: Measurement methods for single beam dual-energy gamma densitometer

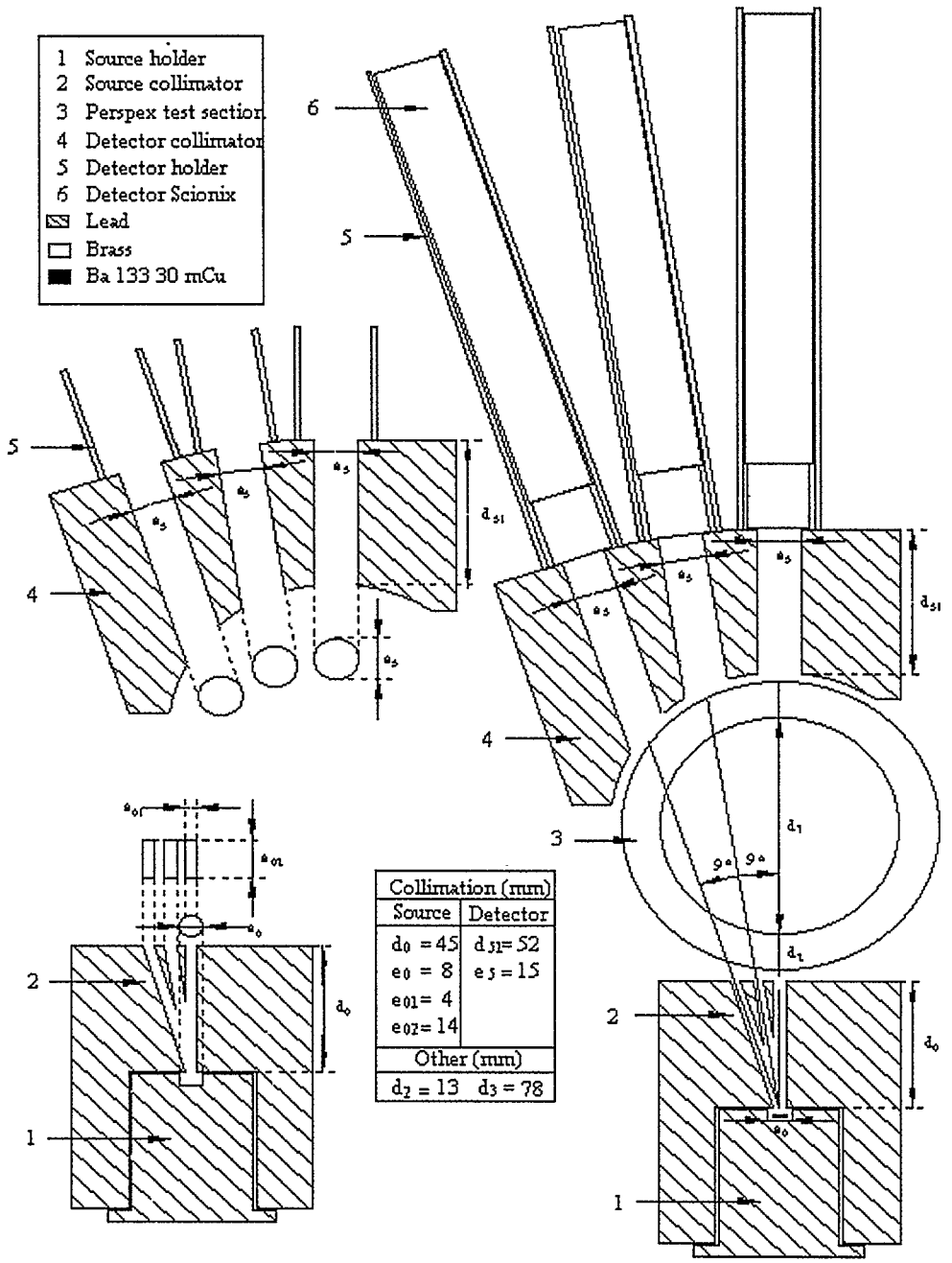


Figure 3.17: Detector and source collimator for triple beam dual-energy gamma densitometer

Chapter 4

EXPERIMENTAL RESULTS FOR PRESSURE, LIQUID FRACTIONS AND SLUG CHARACTERISTICS

To model the slug flow regime, knowledge of certain parameters such as pressure gradient, average liquid holdup as well as slug frequency, slug body holdup, slug length and slug velocity is fundamental. However, there is a distinct lack of data for these parameters for three-phase gas-liquid-liquid slug flow.

In this Chapter the new experimental data on pressure gradient, holdup and slug parameters for three-phase gas-liquid-liquid flow are presented. The effects of various variables such as the gas superficial velocity, liquid superficial velocity, system pressure and input water fraction in the liquid (water-cut) on these parameters are also presented and discussed. The data obtained cover a wide range of conditions and include measurements of pressure gradient, oil, water and total holdups, flow pattern and slug velocity, slug lengths. To ensure an archival record of this data, the results are tabulated in Appendix A. In what follows, data are presented from the respective campaigns to illustrate the effect of various system parameters. The data on flow pattern are presented separately in Chapter 5 and Chapter 6 presents detailed analysis of the data with respect to prediction methods.

4.1: PRESSURE GRADIENT

The pressure gradient is a very important parameter in the design of multiphase pipelines since it governs the pressure and/or pumping capacity required to transport the multiphase mixture from the reservoir to the separators. Furthermore, Bhongale (1995) showed that the pressure gradient is one of several parameters that influence the pipe corrosion rate. The pressure gradient itself is influenced by several factors such as the gas superficial velocity, liquid superficial velocity, system pressure, pipe inclination and the water-cut.

In what follows, the effect of the gas superficial velocity, liquid superficial velocity, system pressure and water-cut on the measured pressure gradient is examined. It should be recalled that in this project, experiments have been carried out both at

constant liquid superficial velocity (i.e. where the oil and water superficial velocities have been adjusted to give a constant total value over the range of water-cuts covered) and at constant oil superficial velocity where the total liquid superficial velocity increases with water cut. Results from these respective scenarios are presented.

4.1.1.Effect of Air Superficial Velocity

Results obtained on the effect of the air superficial velocity on the measured pressure gradient have been sub-divided into horizontal and inclined flows so as to isolate the effects of the change in pipe inclination.

4.1.1.1Horizontal flows

(a) Constant liquid superficial velocity

Figure 4.1 illustrates the effect of the air superficial velocity on the measured pressure gradient at a constant total liquid superficial velocity. In Figure 4.1, the measured pressure gradient has been plotted against input water fraction in the liquid (IWFIL) also known as the water-cut, for a constant total liquid superficial velocity of 0.5 m/s at two distinct air superficial velocities 4 m/s and 6 m/s and at atmospheric pressure, for a horizontal pipe. The water cut (IWFIL) is defined by:

$$\lambda_W = \frac{U_{W,S}}{U_{W,S} + U_{O,S}} \tag{4.1}$$

Where $U_{W,S}$ is the superficial water velocity and $U_{O,S}$ is the superficial oil velocity.

From Figure 4.1, it can be seen that as the water-cut is increased from 0% to about 40%, the measured pressure gradient increases monotonically, reaching a maximum around a water-cut of around 40%. This increase in the measured pressure gradient for this range of water-cuts is as a result of the increasing effective liquid viscosity caused by the intense mixing of the oil and water within the liquid phase.

As the water-cut is increased further beyond 40%, the measured pressure gradient falls significantly. This sudden drop in the measured pressure gradient marks the change in the flow pattern from dispersed oil-continuous slug (DOSl) flow to

dispersed water-continuous slug (DWSl) flow. These flow patterns were observed by monitoring the flow with the aid of a video camera, directed at the visualization section, which was situated 35 m downstream of the pipe inlet.

For water-cuts greater than 50%, there is a gradual decrease in the measured pressure gradient as the water-cut increases from 50% to 100%. This progressive decrease as the water cut increases, is due to the decreasing percentage of oil in the liquid mixture, thus decreasing the effective liquid mixture viscosity.

The decrease in the measured pressure gradient with increasing water-cut for water-cuts ranging from 50 % to 100 % is not as steep as the increase in the pressure gradient for water-cuts between 0 % and 40 % for the 4 m/s case. The reason for this is that the apparent viscosity of the liquid mixture does not change significantly within the water-continuous region. However, in the oil-continuous region, small changes in the water-cut lead to significant changes in the apparent liquid mixture viscosity.

Two points are worth noting:

(1) The two-phase air-oil slug flow pressure gradient is greater than the two-phase air-water slug flow pressure gradient. For the case of air superficial velocity 6 m/s (filled circles on the graph), the pressure gradient for two-phase air-oil slug flow is 600 Pa/m, while the corresponding value for two-phase air-water slug flow is 280 Pa/m. This is expected since the viscosity of water is significantly lower than the oil, (approximately 40 times less at room temperature) yielding a much lower pressure gradient.

(2) The maximum three-phase air-oil-water slug flow pressure gradient for the case of air superficial velocity 6 m/s is almost one and a half times as great as that for two-phase air-oil slug flow.

In Figure 4.1, increasing the air superficial velocity from 4 m/s to 6 m/s leads to an increase in the water cut corresponding to the peak in the measured pressure gradient from 42% to 46%.

This shift in the pressure gradient peak observed in Figure 4.1, is in agreement with the results obtained by Laflin and Oglesby (1976), who observed that on introducing air into an oil-water mixture, the peak in the measured pressure gradient shifted towards higher water-cuts. The reason put forward for this phenomenon is that as the gas superficial velocity is increased, the amount of entrained gas within the slug body increases leading to a dilution and reduction in the overall viscosity of the slug body. This in turn means more water is required to invert the oil-water mixture.

In addition to this, Pan (1996) who carried out three-phase air-oil-water three-phase experiments for low liquid superficial velocities, observed a slight increase in the position of the pressure gradient peak to higher water-cuts for increasing air superficial velocities.

(b) Constant oil superficial velocity

The effect of the air superficial velocity on the measured pressure gradient when the oil superficial velocity is held constant instead of the total liquid superficial velocity is illustrated in Figures 4.2-4.4.

In Figure 4.2, the results depicted were obtained at an oil superficial velocity of 0.2 m/s, system pressure of 0 barg with the pipe horizontal. From this Figure, it can be seen that increasing the air superficial velocity from 10 m/s to 12 m/s, leads to an increase in the measured pressure gradient as expected.

In addition, increasing the air superficial velocity from 10 m/s to 12 m/s leads to an increase in the water-cut at which the peak in the measured pressure gradient occurs from 50 % to 54%.

A similarity with Figure 4.1, is that the maximum three-phase pressure gradient is about two times greater than that of two-phase air-oil slug flow.

A feature of Figure 4.2 which is not present in Figure 4.1, is that after the pressure gradient reaches a peak, and decreases in the water-continuous region, there is a subsequent increase in the measured pressure gradient for water-cuts ranging from

60% to 70 %. The reason for this occurrence is that although the oil superficial velocity has been held constant, the total liquid superficial velocity is still increasing and thus causes an increase in the measured pressure gradient for this range of water-cuts. This was also noticed by Pan (1996) in his experimental results.

In Figure 4.3, where the measured pressure gradient has been plotted against water-cut for a constant oil superficial velocity of 0.5 m/s and for two different air superficial velocities 2 m/s and 5 m/s at a system pressure of 5 barg, the influence of the air superficial velocity on the measured pressure gradient can be observed.

Increasing the air superficial velocity from 2 m/s to 5 m/s, leads to an increase in the measured pressure gradient as expected. A similar trend is observed in Figure 4.4, where the measured pressure gradient has been plotted against the water-cut for a case of a constant oil superficial velocity of 0.7 m/s and system pressure 5 barg. Increasing the air superficial velocity leads to an increase in the measured pressure gradient.
Figures 4.3 and 4.4 were obtained for a limited range of water-cuts 10% to 40%, so the effect of the air superficial velocity on the position of the peak in the measured pressure gradient cannot be discerned from these Figures.

4.1.1.2 Inclined flow

(a)constant total liquid superficial velocity

For flow with the pipe downwardly inclined at an angle of –1.5° to the horizontal, the effect of the air superficial velocity on the measured pressure gradient was also investigated and this is illustrated in Figure 4.5. In Figure 4.5 the measured pressure gradient has been plotted against the water-cut for a total liquid superficial velocity of 0.35 m/s at 0 barg.

Increasing the air superficial velocity from 10 m/s to 12 m/s, increases the measured pressure gradient. In addition to this there is a slight increase in the position at which the peak in the measured pressure gradient occurs.

For the case of air superficial velocity 12 m/s, there is a decrease in the measured pressure gradient for water-cuts ranging from 0% to 15 %. This can be attributed to the fact that these data was obtained at a velocity quite close to the slug-annular transition, where the slugs were not stable.

4.1.2 Effect of Total liquid superficial velocity

4.1.2.1 Horizontal Flows

In Figure 4.6, the measured pressure gradient has been plotted against water-cut at two different constant total liquid superficial velocities of 0.5 m/s and 0.6 m/s respectively, at a constant air superficial velocity of 4 m/s and system pressure of 0 barg, to observe the effect the total liquid velocity on the measured pressure gradient.

In Figure 4.6, an increase in the total liquid superficial velocity from 0.5 m/s to 0.6 m/s leads to an increase in the measured pressure gradient as expected.

From Figure 4.6, it can also be seen that increasing the total liquid superficial velocity from 0.5 m/s to 0.6 m/s leads to a decrease in the water-cut at which the peak in the measured pressure gradient occurs from 42 % to 38 %. An explanation for this effect, is that at higher liquid superficial velocities, due to the more intense mixing, there is more shearing action which tends to reduce the size of the droplets of the liquid phases. This leads to an increase in the apparent viscosity of the oil-water mixture, which in turn increases the pressure gradient. This is agreement with the results of Pan (1996) who observed that the position of the pressure peak moves slightly towards lower water-cuts with increasing oil flowrate.

4.1.2.2 Inclined flows

In Figures 4.7 and 4.8, the effect of the total liquid superficial velocity on the pressure gradient in inclined flows is depicted.

It can be seen from Figure 4.7, where the measured pressure gradient has been plotted at a constant air superficial velocity of 10 m/s and system pressure of 0 barg for two

different total liquid superficial velocities of 0.2 m/s and 0.3 m/s, with the pipe downwardly inclined at an angle of –1.5 °to the horizontal, that increasing the total liquid superficial velocity from 0.2 m/s to 0.35 m/s leads to an increase in the measured pressure gradient.

The same result is evident in Figure 4.8, where increasing the total liquid superficial velocity from 0.5 m/s to 0.7 m/s leads to an increase in the measured pressure gradient for water-cuts ranging from 0% to 50%. However, for a water-cut of 58%, the measured pressure gradient for the lower superficial velocity (0.5 m/s) is greater than that of the case of 0.7 m/s. This can be explained by considering the effect of the total liquid superficial velocity on the peak in the measured pressure gradient. Increasing the total liquid superficial velocity leads to an increase in the position at which the peak occurs. So for a water-cut of 50 %, a change has occurred in the continuous phase of the liquid from oil to water for the case of total liquid superficial velocity 0.7 m/s whereas this change has not occurred for the 0.5 m/s case, which still has an oil continuous liquid phase.

4.1.3.Effect of Oil superficial velocity

Figures 4.9 and 4.10 illustrate the effect of the oil superficial velocity on the pressure gradient. In Figure 4.9, the measured pressure gradient has been plotted for a case of air superficial velocity 2 m/s, system pressure 5 barg and for two different oil superficial velocities 0.5 m/s and 0.7 m/s.

Increasing the oil superficial velocity from 0.5 m/s to 0.7 m/s for water-cuts in the range 10 % to 30%, leads to an increase in the measured pressure gradient. However, for water-cuts greater than 30 %, the measured pressure gradient is greater for the case of 0.5 m/s. The reason is due to the earlier switch in the continuous phase of the liquid (from oil to water) for the case of oil superficial velocity 0.7 m/s. This is similar to the result obtained in Figure 4.8. In Figure 4.10, an increase in the oil superficial velocity also leads to an increase in the measured pressure gradient for the range of water-cuts covered.

4.1.4.Effect of System Pressure

(a) Constant total liquid superficial velocity

In Figure 4.11, the effect of increasing the system pressure on the measured pressure gradient can be observed for a case of constant total liquid superficial velocity. For water-cuts less than 50 %, in the oil continuous region, increasing the system pressure, from 0 barg to 5 barg, leads to a slight increase in the measured pressure gradient. However, in the water-continuous region (water-cut > 50%), there is no discernible effect of the system pressure on the measured pressure gradient.

The results at lower water-cut are in agreement with the results of Pan (1996) who observed that the higher the pressure, the larger the pressure gradient for the range of flow rates covered by his experiments.

(b) Constant oil superficial velocity

In Figures 4.12 and 4.13, the measured pressure gradient is plotted against water-cut at a constant air superficial velocity and oil superficial velocity. Figure 4.12 shows that for an increase in the system pressure from 4 barg to 5 barg, only a slight increase in the pressure gradient is observed. However, in the case of Figure 4.13, it can be seen more clearly that increasing the system pressure leads to an increase in the measured pressure gradient.

4.1.5 Effect of Flow Pattern

In Figure 4.14, the flow patterns are illustrated alongside the data points. This Figure illustrates the reason for the sudden drop in the measured pressure gradient observed around the phase inversion region. Figure 4.14 has been plotted for a case of air superficial velocity 5 m/s, oil superficial velocity 0.5 m/s at atmospheric pressure with the pipe horizontal.

As the water-cut is increased from 12 % to 38 %, the measured pressure gradient increases accordingly, while the flow pattern is dispersed oil-continuous slug flow (D-O-Sl). When the water-cut is increased beyond 38 %, there is a sudden drop in the measured pressure gradient. This sudden drop in the measured pressure gradient is also accompanied by a change in the continuous liquid phase from oil to water, thus

marking the a change in the flow pattern from dispersed oil-continuous slug flow (D-O-Sl) to dispersed water-continuous slug flow (D-W-Sl).

4.2 Mean Liquid Holdup

The mean liquid holdup is a very important parameter in slug flow as it plays a big part in the design of the primary separation equipment 'slug catcher'. The results for the mean liquid holdup presented here have been obtained from the dual-energy gamma densitometer in a traversing mode where the beam is traversed horizontally over 8 chordal positions. The values of the average holdup over each of the chordal positions are then summed up to yield a mean liquid holdup.

In some cases, the gamma densitometer has been used in a central pipe scan mode where the beam is left stationary at the centre of the pipe. The main advantage of this mode over the traversing mode is that it enables the slugs to be tracked, thus enabling better cross correlation of the gamma holdup signals. In this case, the dimensionless liquid height has been converted into a total liquid holdup by assuming that the total liquid holdup can be collapsed into stratified liquid layers of oil and water. The *in-situ* liquid holdup has been calculated using the geometrical relationships in Equations 4.2-4.4, an illustration of the pipe geometry used to derive this relationships is given in Figure 4.15:

The *in-situ* hold-up for the total liquid is given by the expression below:

$$\varepsilon_L = \frac{1}{4}\left[\pi - \cos^{-1}\left(\frac{2h_L}{D} - 1\right) + \left(\frac{2h_L}{D} - 1\right)\sqrt{1 - \left(\frac{2h_L}{D} - 1\right)^2}\right] \tag{4.2}$$

To obtain the individual holdup for the oil and the water, the *in-situ* holdup of the water is calculated using the equation:

$$\varepsilon_w = \frac{1}{4}\left[\pi - \cos^{-1}\left(\frac{2h_W}{D} - 1\right) + \left(\frac{2h_W}{D} - 1\right)\sqrt{1 - \left(\frac{2h_W}{D} - 1\right)^2}\right] \tag{4.3}$$

And the *in-situ* oil holdup is calculated using the following relationship:

$$\varepsilon_o = \varepsilon_L - \varepsilon_w \tag{4.4}$$

Where h_L is the total liquid height, D is the pipe diameter and h_w is the water height. A typical total liquid holdup trace from the dual-energy gamma densitometer is illustrated in Figure 4.16.

4.2.1 Effect of Air Superficial velocity

(a)Constant total liquid superficial velocity

In Figure 4.17, the measured total liquid holdup has been plotted against the water-cut at a constant total liquid superficial velocity of 0.5 m/s, and atmospheric pressure, for two different air superficial velocities. It is seen that as the water-cut is increased, the total liquid holdup increases gradually until a peak is reached at a water-cut of 40%. The total liquid holdup decreases once the water fraction in the liquid exceeds 44% as this marks the change in the continuous liquid phase from oil to water.

The effect of air superficial velocity on the measured total liquid holdup can also be observed from Figure 4.17. Increasing the air superficial velocity from 4 m/s to 6 m/s leads to a decrease in the total liquid holdup, as expected. In addition, the peak observed in Figure 4.17 is similar to those observed in the pressure gradient results presented in the previous section. This is further illustrated in Figure 4.18 where both the measured pressure gradient and the measured total liquid holdup are plotted on the same graph for the same set of conditions.

It can be seen in Figure 4.18 that the peaks in the measured pressure gradient and the total liquid holdup occur at the same water-cut value of 40 %. Since both measurements have been obtained independently, this confirms that the reason for the unusually high pressure gradient observed around the water-cut value of 40 % is due to a significant increase in the total liquid holdup. This increase in the total liquid holdup can be attributed to the increase in the effective viscosity of the liquid mixture around a water-cut value of 40 %.

(b) Constant oil superficial velocity

In Figures 4.19 and 4.20, although the total liquid superficial velocity has not been held constant, the effect of increasing the air superficial velocity on the total liquid

holdup can be clearly seen. In Figure 4.19, increasing the air superficial velocity from 2 m/s to 5 m/s leads to a decrease in the measured total liquid holdup as expected.

The same result is observed in Figure 4.20, where the measured average in-situ total liquid holdup has been plotted against the water-cut for a case of oil superficial velocity 0.2 m/s, atmospheric pressure (0 barg), with the pipe horizontal. Increasing the air superficial velocity from 8 m/s to 10 m/s leads to a decrease in the average in-situ total liquid holdup as expected.

4.2.2 Effect Of Liquid Superficial Velocity

4.2.2.1Horizontal flows

In Figure 4.21, the experimentally determined average in-situ total liquid holdup is plotted against the water cut for two different total liquid superficial velocities, at a constant air superficial velocity of 4 m/s and system pressure of 0 barg. It can be seen that, increasing the total liquid superficial velocity from 0.5 m/s to 0.6 m/s leads to an increase in the measured total liquid holdup in the oil continuous region (water-cuts between 0% and 40%), whereas in the water-continuous region, no generalization can be made on the basis of the data presented here.

4.2.2.2 Inclined flows

For inclined flows, increasing the total liquid superficial velocity also leads to an increase in the average total liquid holdup as can be seen in Figure 4.22. However, this increase in the total liquid holdup with total liquid superficial velocity is confined to the oil-continuous region alone.

4.2.3 Effect of System Pressure

The effect of pressure on the total liquid holdup is shown in Figures 4.23-4.25, where the measured total liquid holdup is plotted against input water fraction in the liquid at different system pressures and for different air superficial velocities.

(a) Constant total liquid superficial velocity

In Figure 4.23, where the total liquid superficial velocity has been held constant, it can be seen that on increasing the system pressure from 0 barg to 5 barg, the measured total liquid holdup in the water-continuous region (water-cut >50%), increases, whereas in the oil continuous region, there appears to be no effect of the system pressure on the total liquid holdup.

(b) Constant oil superficial velocity

In Figures 4.24 and 4.25, where the total liquid holdup has been plotted against the water-cut for a constant oil superficial velocity, increasing the system pressure leads to an increase in the measured total liquid holdup.

4.3 PHASIC HOLDUPS

The holdups for the oil and water phase are also important as they tell us whether any phase is being preferentially accumulated within the system. The measurements are derived directly from the gamma densitometer output.

In Figures 4.26-4.28, the total liquid hold-up and the *in-situ* holdup of the water and oil phases have been plotted together against the water-cut, for a range of conditions. From the plots it can be seen that as the water-cut is increased from 0 % to 40 %, the water *in-situ* holdup increases monotonically. For water-cuts greater than 40 %, the increase in *in-situ* water holdup with water-cut is less steep.

For the *in-situ* oil holdup, as the water cut is increased between 0 % and 40%, there is a steady decrease in the oil *in-situ* holdup. However, after water-cuts greater than 40%, the decrease in the *in-situ* oil holdup is more rapid with increasing water-cut.

4.3.1 Effect of Air superficial velocity

In Figures 4.29 and 4.30, the effect of the air superficial velocity on the *in-situ* water holdup and oil holdup is shown for an inclined pipe. In Figure 4.29, the *in-situ* water

holdup has been plotted against water cut at constant oil superficial velocity 0.2 m/s, and a system pressure of 5 barg. It can be seen that increasing the air superficial velocity leads to a decrease in the *in-situ* water holdup as expected. The same trend is shown in Figure 4.30 where the in-situ oil holdup has been plotted against the water cut for the same set of conditions.

In Figure 4.29, increasing the water cut from 25% to 50%, leads to gradual increases in the *in-situ* water holdup. For water-cuts greater than 50 %, further increases in the water-cut lead to a decrease and then an increase in the *in-situ* water holdup.

It would be expected that the in-situ water holdup would increase monotonically with water-cut. However this is not the case, because beyond the phase inversion point, there is a sudden drop in the total liquid holdup, which also leads to a sudden drop in the in-situ water holdup.

Another possible explanation for the peak observed in the *in-situ* water holdup in Figure 4.29, is that because the liquid mixture is fully dispersed, an increase in the total liquid holdup leads to an increase in the *in-situ* water hold up because the water is inextricably well mixed with the oil within the liquid mixture.

In Figure 4.30, where the in situ oil holdup has been plotted against water cut for a constant oil superficial velocity of 0.2 m/s, the effect of air superficial velocity can also be seen. Increasing the air superficial velocity leads to a decrease in the *in-situ* oil holdup. Initially as the water cut is increased, the *in-situ* oil holdup decreases gradually. However, for water-cuts greater than 50%, the decrease in *in-situ* oil holdup is more rapid.

4.4 SLIP RATIOS

A good indication of the magnitude of the slip ratio between the oil and water ($S_{ow} = U_O / U_W$ where $U_O = U_{O,S} / \varepsilon_o$ and $U_W = U_{W,S} / \varepsilon_w$) can be observed by plotting the measured *in-situ* water fraction in the liquid, against the water-cut.
Here, slip ratio is defined as the ratio of the oil velocity to the water velocity. The *in-situ* water fraction in the liquid is defined by:

$$\lambda_w = \frac{\varepsilon_W}{\varepsilon_W + \varepsilon_O} = \frac{1}{1 + \frac{U_{O,S}}{S_{ow} U_{W,S}}} \tag{4.5a}$$

Where ε_w is the in-situ water holdup and ε_o is the in-situ oil holdup.

The input water-cut is given by:

$$\text{IWFIL} = \frac{U_{W,S}}{U_{W,S} + U_{O,S}} = \frac{1}{1 + \frac{U_{O,S}}{U_{W,S}}} \tag{4.5b}$$

Comparing Equations 4.5a and 4.5b, it is seen that $\lambda_W < IWFIL$ for $S_{ow}<1$ and $\lambda_W > IWFIL$ when $S_{ow}>1$.

From Figures 4.31 and 4.32 where the *in-situ* water fraction in the liquid has been plotted against the input water fraction in the liquid, it can be seen that the oil-water slip ratio deviates significantly from unity. For water-cuts between 0% and 40 %, $\lambda_w > IWFIL$ and the slip ratio is greater than one. Above 40% the slip ratio approaches unity.

4.5 SLUG FREQUENCY

The slug frequency was obtained by observing the slugs through the visualization section with the aid of a video camera. In addition to this, the liquid holdup traces from the gamma densitometer were also used to identify the frequency of slug occurrence. The two methods gave good agreement.

In Figures 4.33-4.37, the experimentally observed slug frequency has been plotted against the input water fraction in the liquid for a range of conditions.

4.5.1 Effect of Air superficial Velocity

(a) Constant total liquid superficial velocity

In Figure 4.33, the observed slug frequency has been plotted against the water cut, at constant total liquid superficial velocity for two distinct air superficial velocities: 4 and 6m/s. It can be seen from the plot that for water-cuts between 0 % and 30 %, the slug frequency is higher for the case of air superficial velocity 6 m/s.

From Figure 4.33, it can also be seen that for the case of air superficial velocity 6 m/s, as the water-cut is gradually increased from 0%, there is little effect on the slug frequency, which maintains a value around 0.4 Hz, whereas in the case of air superficial velocity 4 m/s, the slug frequency increases monotonically with increasing water-cut from a value of 0.3 Hz at water-cut 0 % to a value of 0.4 Hz at a water-cut of 38 %. At water-cuts greater than 40%, the slug frequency begins to decrease rapidly, before settling at a Figure of 0.25 Hz for two-phase air-water flow.

(b) Constant oil superficial velocity

In Figure 4.34 where the measured slug frequency has been plotted against water cut, for a constant oil superficial velocity of 0.2 m/s and for air superficial velocities 8 m/s and 10 m/s, it can be seen that the effect of the air superficial velocity on the slug frequency is not clearly discernible. However, for both air superficial velocities, as the water-cut is increased from 0%, the measured slug frequency increases, before reaching a peak around water-cuts of 50% to 60%. Subsequent increases in the water-cut lead to a decrease in the measured slug frequency.

The decrease in slug frequency is due to a change in the continuous phase of the liquid. When there is a change in the liquid continuous phase from oil to water, the slug frequency decreases because the slug frequency decreases with decreasing liquid viscosity.

Another important feature in Figure 4.34, is that there are two peaks in the plot. The first peak occurs as the continuous phase changes from oil to water. The second peak occurs in the water-continuous region and is due to the fact that although the oil superficial velocity has been held constant, the water superficial velocity has not been held constant.

In Figures 4.35 and 4.36, increasing the air superficial velocity leads to a decrease in the measured slug frequency for the range of water-cuts covered.

4.5.2 Effect of Liquid Superficial Velocity

In Figure 4.37, the effect of the total liquid superficial velocity on the slug frequency can be clearly observed. When the total liquid superficial velocity is increased from 0.5 to 0.6m/s, the slug frequency increases. This is expected as increasing the total liquid superficial velocity, leads to an increase in the height of waves, making it more likely that the waves will eventually bridge the pipe, leading to the formation of slugs. It is worth noting that the slug frequency for the two-phase air-oil slug flow case (water-cut 0%) is shown to be significantly greater than that observed in the two-phase air-water slug flow case (water-cut 100%).

4.6 SLUG BODY HOLDUP

By analyzing the traces of the gamma densitometer, it was possible to obtain the average slug body holdup, which is defined as the volume fraction of liquid contained within the slug body.
From Figures 4.38 and 4.39, where the average slug body holdup has been plotted against the input water fraction in the liquid, distinct trends can be observed.

In all the three plots, the average slug body holdup decreases gradually as the water cut is increased from 0%. However, beyond a water-cut of 40%, the slug body holdup begins to increase with the water-cut. At water-cuts greater than 60%, there is little effect of the water-cut on the average slug body hold-up. Another point of note is that the average slug body holdup for the two extreme cases, two-phase air-water and two-phase air-oil slug flow are similar.

4.6.1 Effect of Air Superficial velocity

To examine the effect of air superficial velocity on the average slug body holdup, Figure 4.38 was plotted. Here the average slug body holdup at two distinct air superficial velocities is depicted with all other parameters being held constant.

It can be seen clearly from Figure 4.38, that increasing the air superficial velocity leads to a decrease in the value of the average slug body holdup as expected. Between water-cuts 0 % and 40 %, the average slug body holdup decreases with

increasing water-cut. The reason for this is that as the water-cut is increased from 0% to 40% the effective viscosity of the liquid mixture increases. This trend in the average slug body holdup agrees with the result of Stapelberg *et al.* (1992) who showed that increasing the liquid viscosity leads to a decrease in the slug body holdup.

4.6.2 Effect of Liquid Superficial velocity

In Figure 4.39, the average slug body holdup has been plotted at a constant air superficial velocity and system pressure for two different total liquid superficial velocities, it can be seen that the total liquid superficial velocity does not have a significant effect on the average slug body holdup for the range presented.

4.7 LIQUID FILM HOLDUP

The liquid film holdup is the volume occupied by the liquid in the film region between successive slug bodies. In Figures 4.39-4.41, the average liquid film holdup has been plotted against the water-cut for different conditions.

4.7.1 Effect of air superficial velocity

From Figure 4.40, it can be seen that as the water-cut is increased from 0%, the average liquid film holdup increases gradually from a value of 0.2, reaching a maximum around a water-cut of 44%, for the case of air superficial velocity 6 m/s. For water-cuts greater than 44%, the average liquid film holdup decreases as the water cut decreases.

In addition to this, the trends in the average liquid film holdup mirror those observed in the pressure gradient described in previous sections. The increase in the average liquid film holdup around the water-cut of 40% is due to the rise in the apparent viscosity of the liquid mixture around the phase inversion region.

It is clear from Figure 4.40, that increasing the air superficial velocity leads to a decrease in the average liquid film holdup as expected.

4.7.2 Effect of total liquid superficial velocity

In Figure 4.41 the measured average liquid film holdup has been plotted against the water-cut at constant air superficial velocity, for two different liquid superficial velocities 0.5 m/s and 0.6 m/s. It can be seen that increasing the total liquid superficial velocity does not have any significant influence on the average liquid film holdup.

4.7.3 Effect of system pressure

The effect of the system pressure on the average liquid film height is seen in Figure 4.42, where the average liquid film holdup has been plotted against water-cut at two different system pressures 0 barg and 5 barg. It can be seen that on increasing the system pressure the liquid film holdup increases.

On comparing the results for both the slug body holdup and the liquid film holdup it can be seen that the results obey the law of conservation of mass. As the liquid content in the slug body decreases for water-cuts of between 0% and 40%, the liquid content in the liquid film between the slugs increases for the same set of conditions. For water-cuts greater than 40% the liquid content in the slug body increases with increasing water cut, while the average liquid film holdup decreases with increasing water cut.

4.8 SLUG VELOCITY

Slug translational velocities were obtained by cross-correlating the liquid holdup readings from the vertical beams of both gamma densitometers. The slug velocities obtained from cross correlating the gamma densitometers are averaged over all the slugs. The slug velocity is usually related to the total mixture velocity by the relationship:

$$U_t = C_o U_M + U_d \tag{4.6}$$

Where U_t is the slug translational velocity, U_M is the total mixture superficial velocity, C_o is a distribution parameter and U_d is a "drift velocity". U_d represents the effect of local relative velocity between the bubble and the surrounding fluid whereas C_o represents the effect of differences between the void and velocity distributions. In

vertical slug flow, the value of U_d is commonly taken as being equal to the rise velocity of a Taylor bubble in stagnant liquid in the tube, namely $0.35\sqrt{gD}$ where g is the acceleration due to gravity and D is the tube diameter. C_o for this case has a value around 1.2 (Nicklin *et al.* 1962).

There has been some controversy about the value of U_d in horizontal flows. Clearly, in contrast to the vertical flow case, a bubble would be stationary in a stagnant fluid in a closed tube. If the tube were full of liquid and one end were opened to, say the atmosphere then the tube would empty as a result of the propagation of a bubble front along it; the velocity of the bubble front of this "Benjamin bubble" (Benjamin, 1968) is $0.54\sqrt{gD}$. At low mixture velocities, Bendiksen (1984) suggests that this value (i.e. $0.54\sqrt{gD}$) be used for U_d with C_o being taken as 1.05.

However, Bendiksen (1984) suggests that when the Froude number (defined as $Fr^2 = U_M^2 / gD$) is greater than 3.5, the value of U_d should be taken as zero and C_o assumes a constant value of 1.2. Thus in this region for Fr> 3.5, the translational velocity may be calculated using the relationship:

$$U_t = C_o U_M = 1.2 U_M \tag{4.7}$$

For all the results presented here, the Froude number was greater than 3.5 (values were typically in the range 10-140) and the drift term U_d would, therefore, be expected to be essentially zero, according to Bendiksen's findings. However, as we shall see below, the value of Co may take a value very different in the flows considered here to the 1.2 value suggested by Bendiksen. A typical plot of the slug translational velocity against water-cut is shown in Figure 4.43.

4.8.1 Effect of Total liquid superficial velocity

From Figure 4.44, it can be seen that for the case of a total liquid superficial velocity of 0.5 m/s, as the water cut increases, the value of C_o increases from a value of 1.7 for two-phase air-oil slug flow to a maximum value of 1.8 at an input water cut value of around 40%. Subsequent to that, C_o decreases slowly ending up with a value of around 1.2 for the two-phase air-water slug flow case. When the total liquid

superficial velocity is increased to 0.6 m/s, C_o increases to a maximum of approximately 2 and decreases subsequently. Possible reasons for this result are discussed in Chapter 6.

4.9 SLUG LENGTH

Knowledge of the translational velocity of the slug as well as the time taken for the slug to pass the monitoring station enables the slug length to be calculated. The slug length is plotted against water cut in Figure 4.45 for a case of air superficial velocity 4 m/s, total liquid superficial velocity 0.5 m/s and system pressure 0 barg for a horizontal pipe.

In Figure 4.45, the average measured slug lengths range from 1m (water-cut 24 %) to 2.8 m (water-cut 100%). This corresponds to a slug length range of 13D to 36D (where D is the WASP pipe diameter of 0.07792m). At 0% water-cut, the measured average slug length is 1.9m. However, increasing the water-cut from 0% to 24 % leads to a decrease in the slug length to 1 m. For water-cuts ranging from 20% to 80%, increasing the water-cut leads to an increase in the slug length. Increasing the water-cut above 80 %, does not have any significant effect on the slug length.

In Figure 4.46, obtained at an air superficial velocity of 6 m/s, total liquid superficial velocity of 0.5 m/s and system pressure 0 barg, a similar trend as observed in Figure 4.45, is noticed. The slug length increases with increasing water-cut reaching a maximum at a water-cut of 100% (two-phase air-water slug flow), with a minimum occurring at a water-cut of 10 %. The slug lengths measured range from 16D (where D is the pipe diameter) for a water-cut of 10 % to a maximum of 37D for a water-cut of 66%.

As can be seen from Figure 4.46, the slug lengths for water-continuous flow are almost twice those occurring in oil-continuous flow.

4.9.1 Effect of Air Superficial Velocity

There appears to be no significant effect of the air superficial velocity on the measured average slug length for the range of air superficial velocities investigated.

4.9.2 Effect of Total liquid superficial velocity

In Figure 4.47, it can be seen that increasing the total liquid superficial velocity does not seem to have a significant effect on the measured average slug length.

4.10 SUMMARY

New three-phase air-oil-water flow data obtained on pressure gradient, hold-up, as well as slug parameters (slug frequency, slug body hold-up, liquid film hold-up, slug velocity and slug length) have been presented and trends inherent in the results have been discussed for a variety of flow conditions, pipe configurations and system pressures.

For a given total superficial velocity, a peak in pressure gradient occurs with increasing water-cut at constant total liquid superficial velocity. It was shown that the air superficial velocity had a significant effect on the position of the pressure gradient peak. Increasing the air superficial velocity leads to an increase in the water-cut at which the peak in the measured pressure gradient occurs.

The effect of the total liquid superficial velocity on the position of the pressure gradient peak was contrary to the effect of the air superficial velocity, an increase in the total liquid superficial velocity leads to a decrease in the position of the peak in the pressure gradient.

The trends in the measured total liquid holdup were found to mirror those observed in the measured pressure gradient, with the peaks occurring at the same water-cuts.

Data obtained on slug frequency revealed that slug frequency for oil-continuous flows exceeded those measured in water-continuous flows for the same set of conditions.

Unique data on the slug body holdup in three-phase air-oil-water flow was presented and this showed that the water-cut has a significant effect on the slug body holdup, particularly for water-cuts in the phase inversion region. The results of the average liquid film holdup showed significant increases in the phase inversion region.

Data on the C_o (ratio of the slug velocity to the mixture velocity) showed that its value was a strong function of the water-cut in the phase inversion region, reflecting the high mixture viscosities in this region. Maximum values of C_o of around 2 were observed in the phase inversion region.

Results obtained on slug length compare well with those postulated in the literature. The slug lengths in water-continuous flows were found to be greater than those for oil-continuous flows.

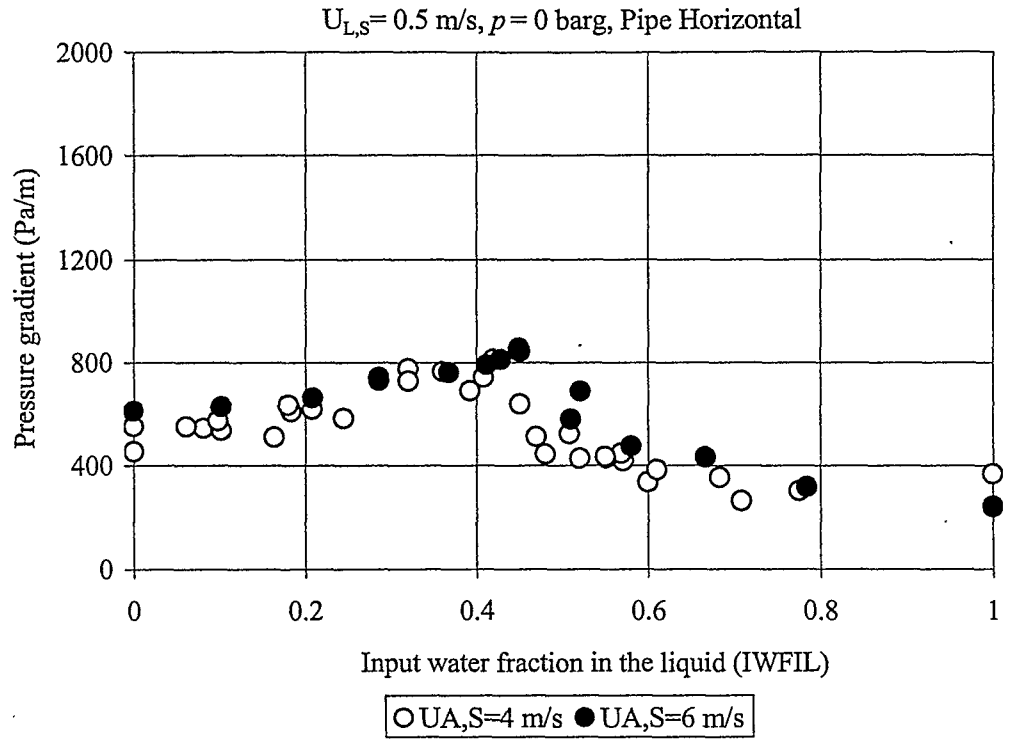


Figure 4.1: Measured pressure gradient plotted against IWFIL at total liquid superficial velocity 0.5 m/s, system pressure 0 barg, horizontal pipe at two different air superficial velocities 4 m/s and 6 m/s

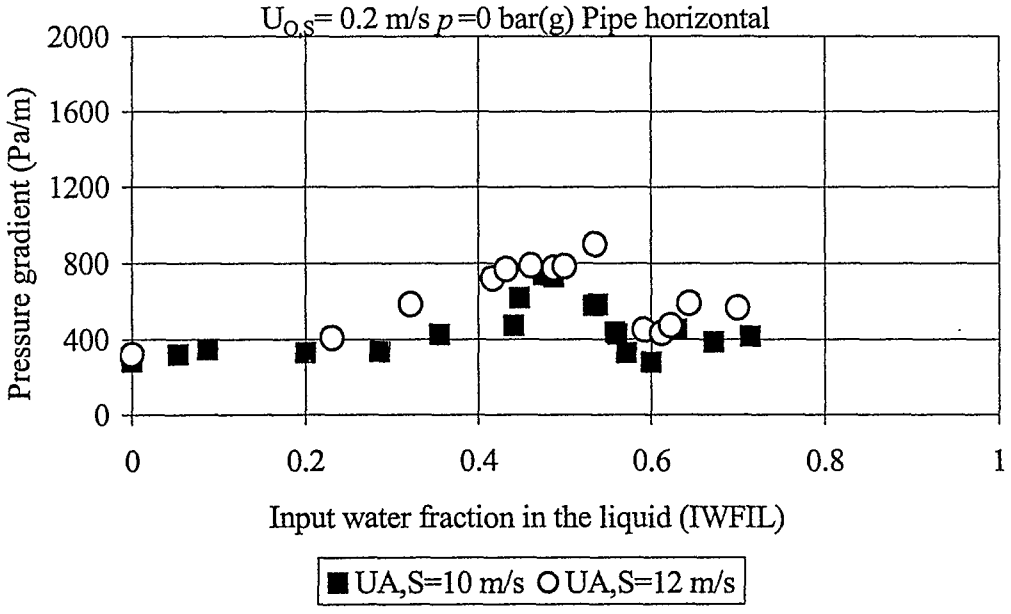


Figure 4.2: Measured pressure gradient plotted against IWFIL at oil superficial velocity 0.2 m/s, system pressure 0 barg, horizontal pipe at two different air superficial velocities 10 m/s and 12 m/s

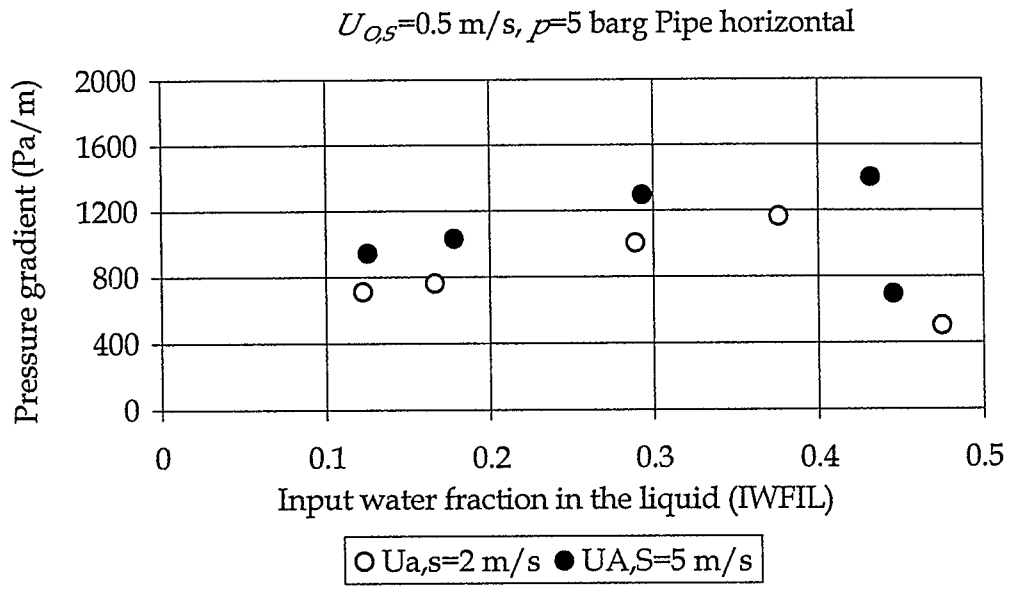


Figure 4.3: Measured pressure gradient plotted against IWFIL at oil superficial velocity 0.5 m/s, system pressure 5 barg, horizontal pipe at two different air superficial velocities 2 m/s and 5 m/s

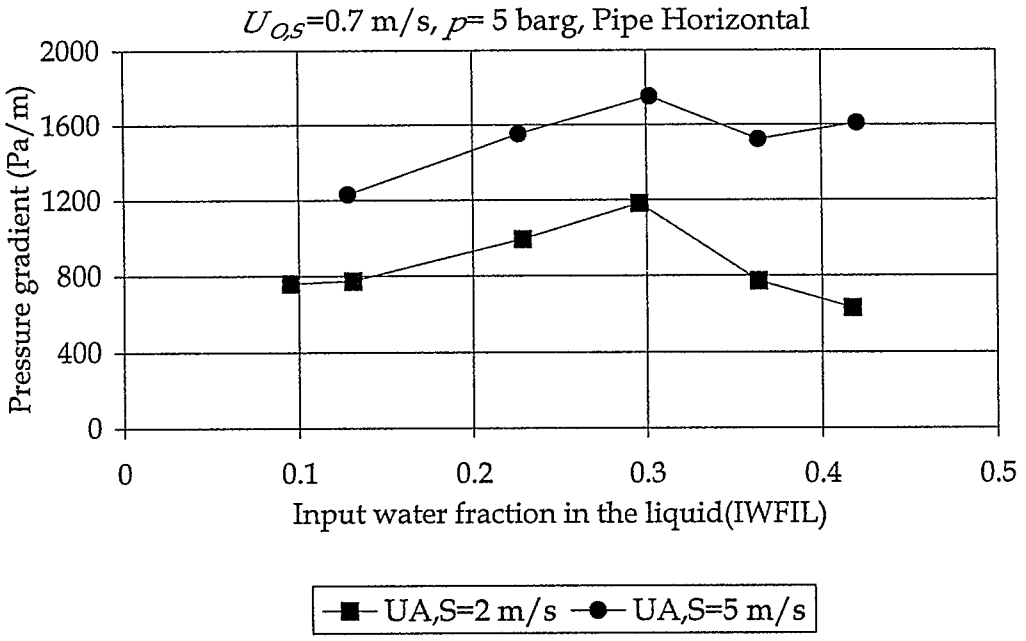


Figure 4.4: Measured pressure gradient plotted against IWFIL at oil superficial velocity 0.7 m/s, system pressure 5 barg, horizontal pipe at two different air superficial velocities 2 m/s and 5 m/s

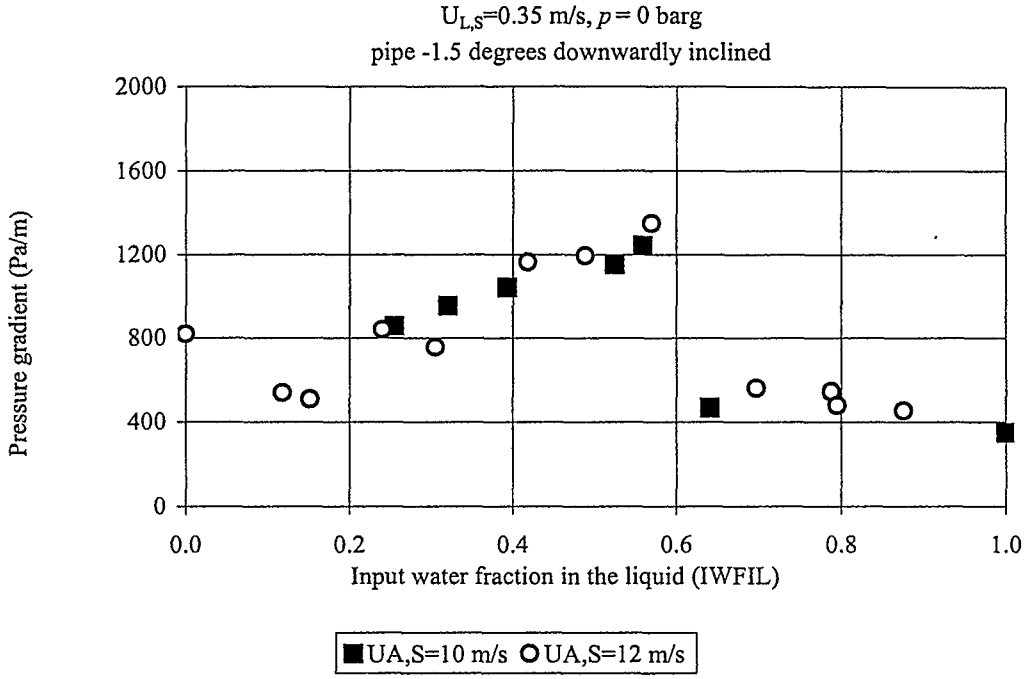


Figure 4.5: Measured pressure gradient plotted against IWFIL at total liquid superficial velocity 0.35 m/s, system pressure 0 barg, pipe downwardly inclined at an angle of –1.5° to the horizontal, at two different air superficial velocities 10 m/s and 12 m/s.

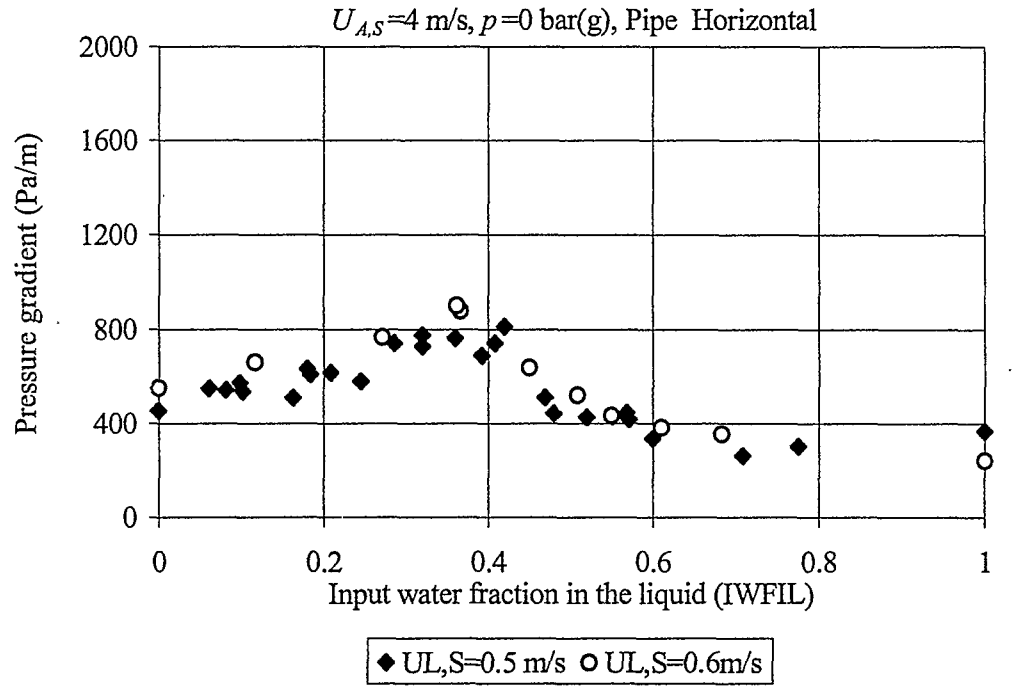


Figure 4.6: Measured pressure gradient plotted against IWFIL at an air superficial velocity of 4 m/s at 0 barg at two different liquid superficial velocities 0.5 m/s and 0.6 m/s.

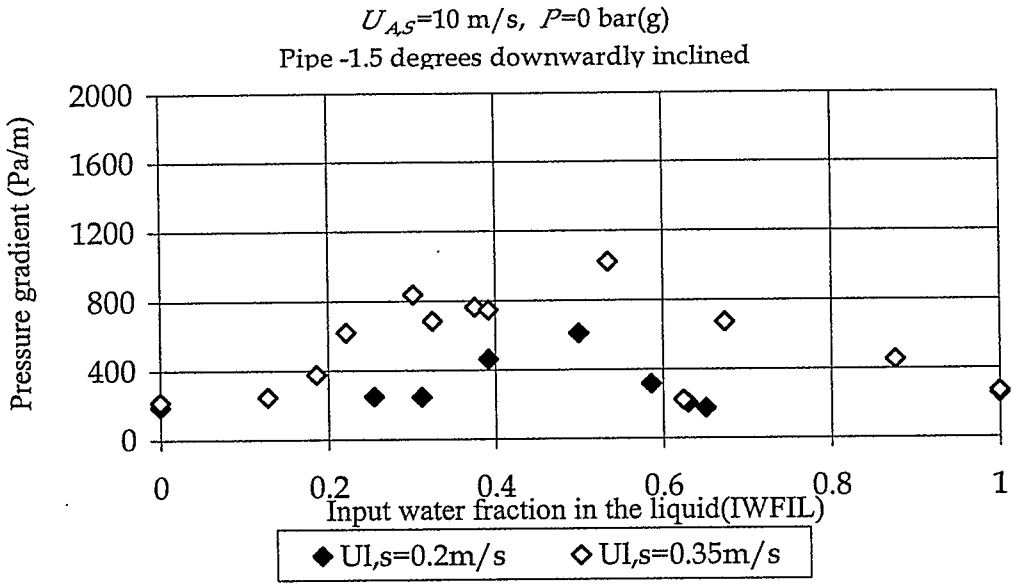


Figure 4.7: Measured pressure gradient plotted against IWFIL at an air superficial velocity of 10 m/s, at atmospheric pressure, pipe downwardly inclined 1.5° for two different liquid superficial velocities 0.2 m/s and 0.35 m/s.

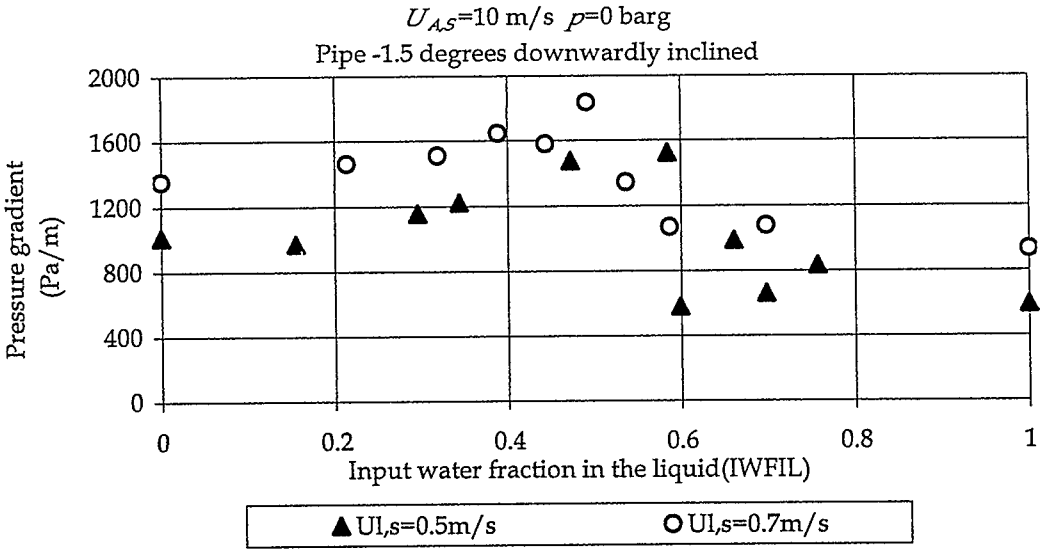


Figure 4.8: Measured pressure gradient plotted against IWFIL at an air superficial velocity of 10m/s, at atmospheric pressure, pipe downwardly inclined 1.5° at two different liquid superficial velocities 0.5 m/s and 0.7 m/s.

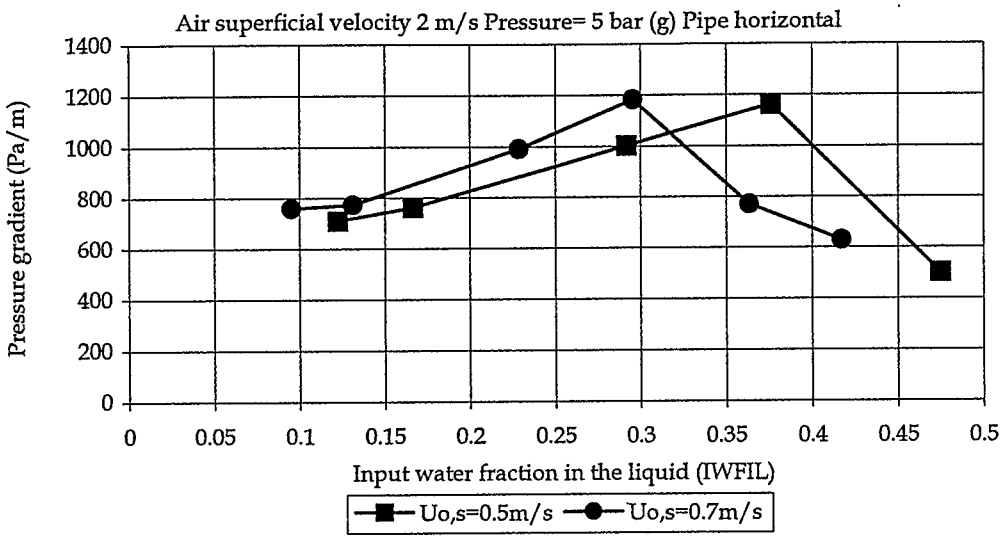


Figure 4.9: Measured pressure gradient plotted against IWFIL at an air superficial velocity of 2m/s, at 5 barg, horizontal for two different oil superficial velocities 0.5 m/s and 0.7 m/s.

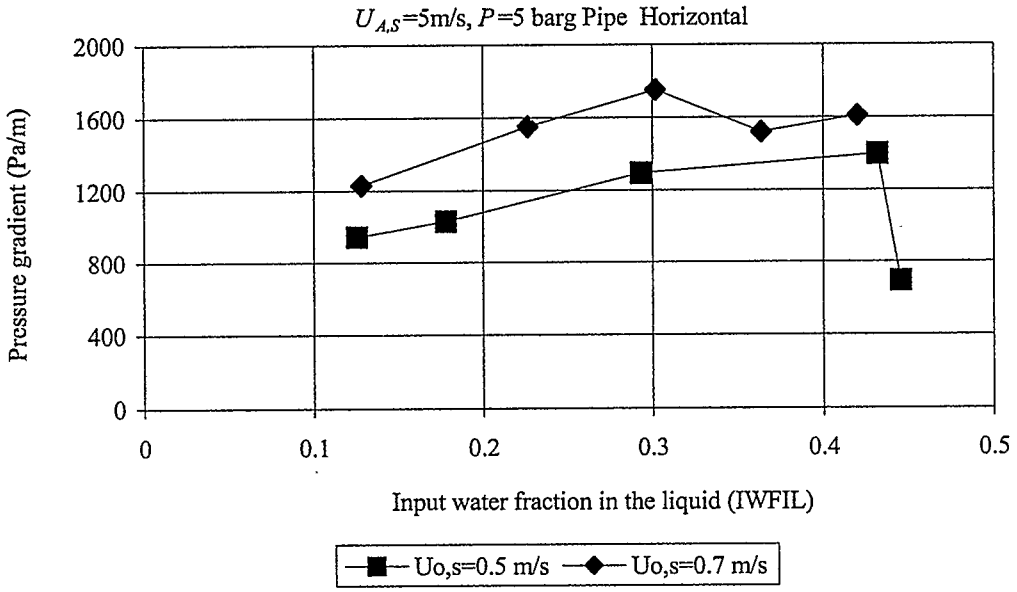


Figure 4.10: Measured pressure gradient plotted against IWFIL at an air superficial velocity of 5m/s, at 5 barg, pipe horizontal for two different oil superficial velocities 0.5 m/s and 0.7 m/s.

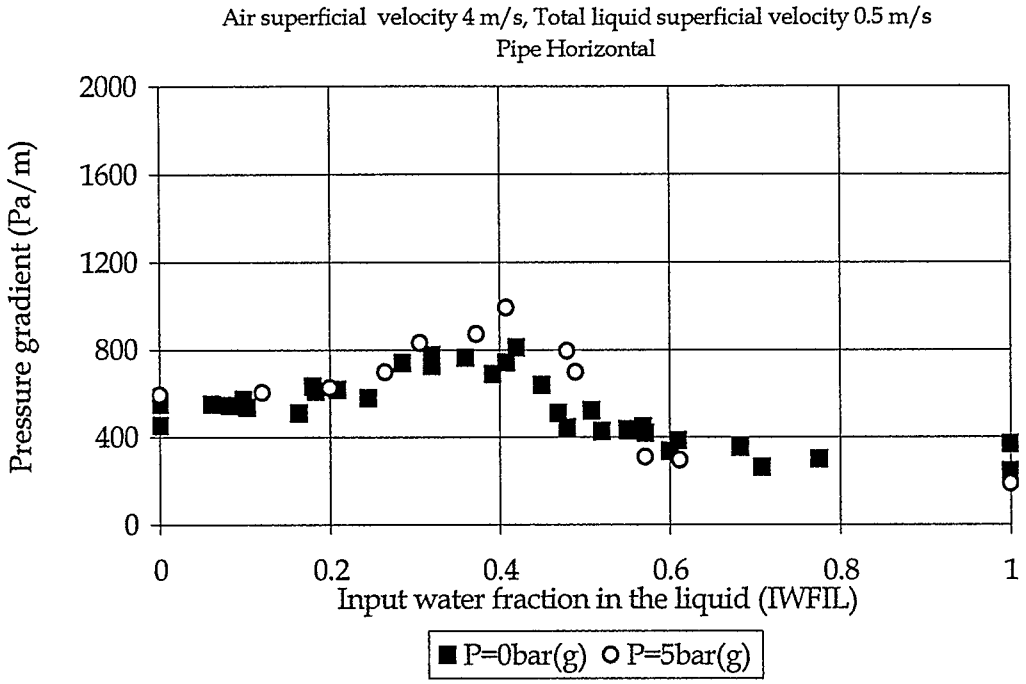


Figure 4.11: Measured pressure gradient plotted against IWFIL at an air superficial velocity 4m/s, total liquid superficial velocity 0.5 m/s at two different system pressures 0 barg and 5 barg for a horizontal pipe.

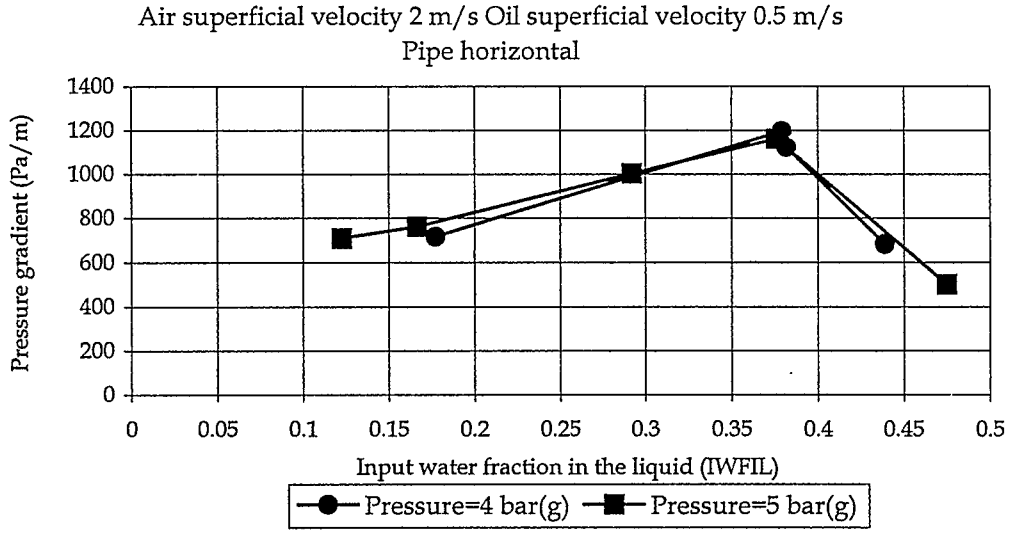


Figure 4.12: Measured pressure gradient plotted against IWFIL at an air superficial velocity 2m/s, oil superficial velocity 0.5 m/s at two different system pressure 4 barg and 5 barg for a horizontal pipe

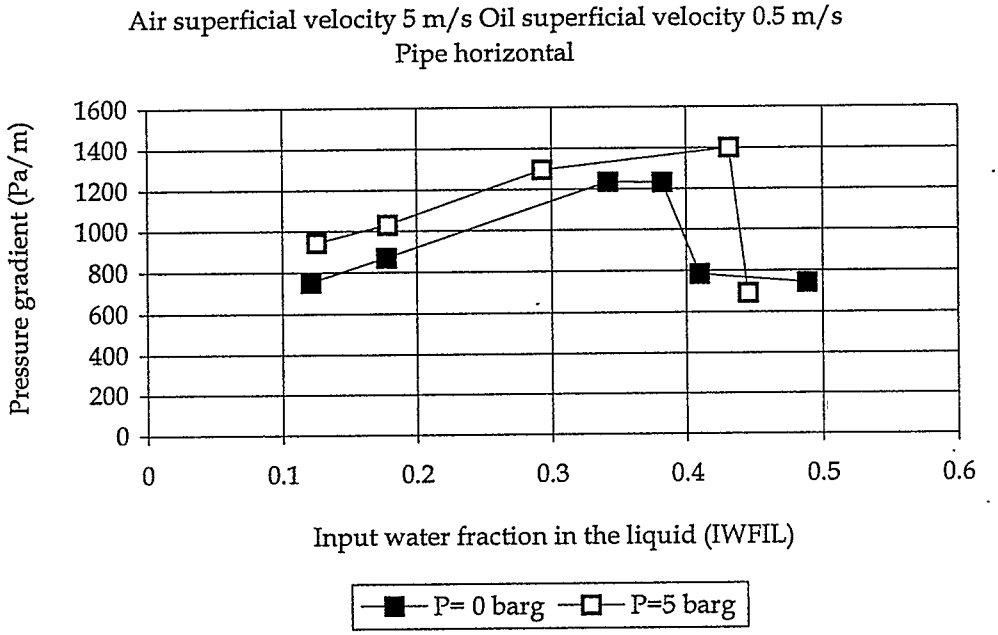


Figure 4.13: Measured pressure gradient plotted against IWFIL at an air superficial velocity 5m/s, oil superficial velocity 0.5 m/s at two different system pressure 0 barg and 5 barg for a horizontal pipe

U_{AS}= 5 m/s, U_{OS}= 0.5 m/s

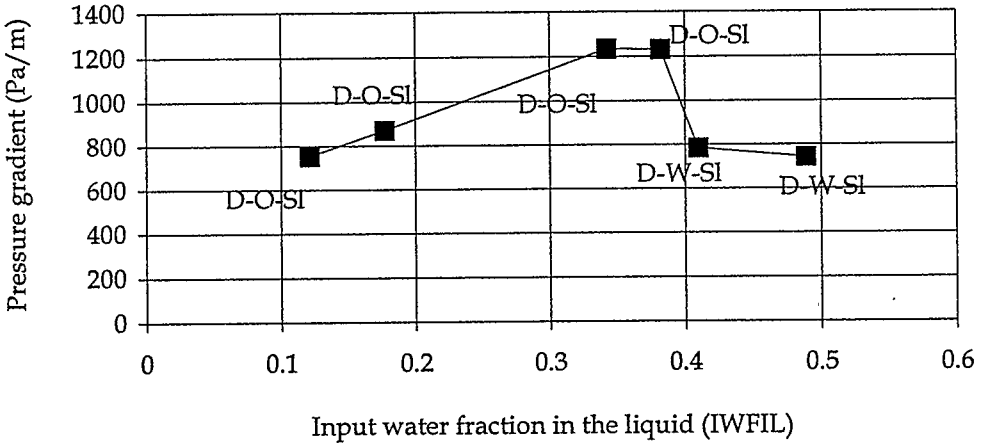


Figure 4.14: Measured pressure gradient plotted against IWFIL at an air superficial velocity 5m/s, oil superficial velocity 0.5 m/s at system pressure 0 barg and 5 barg for a horizontal pipe, illustrating the flow patterns

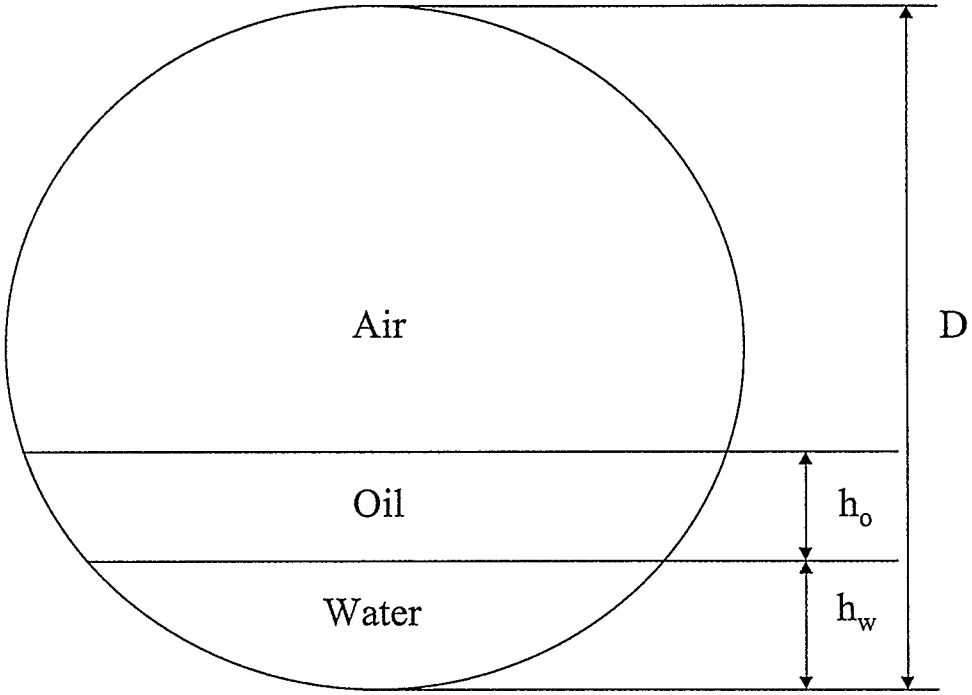


Figure 4.15. Pipe geometry illustrating the height of the oil and water layers.

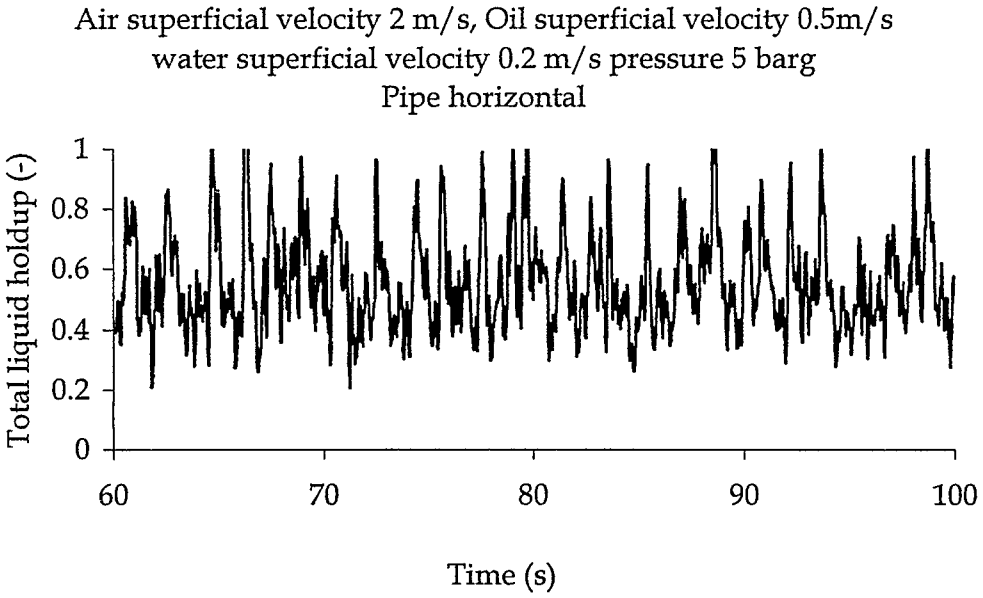


Figure 4.16: A typical total liquid holdup trace from the dual energy gamma densitometer for air superficial velocity 2 m/s, oil superficial velocity 0.5 m/s, water superficial velocity 0.2 m/s, system pressure 5 barg for a horizontal pipe.

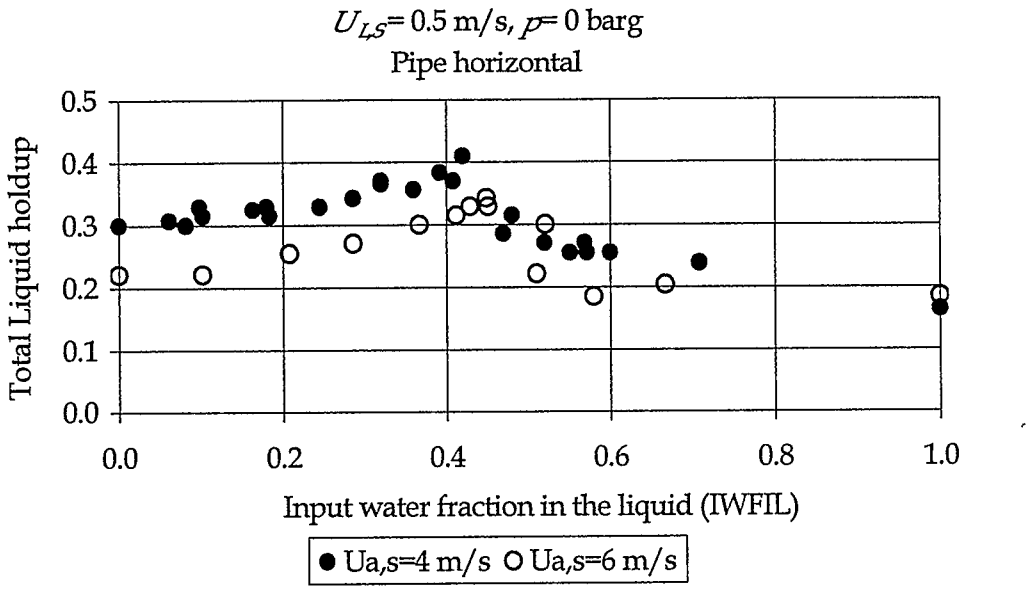


Figure 4.17. Measured total liquid holdup plotted against IWFIL at a total liquid superficial velocity 0.5 m/s, at two different air superficial velocities 4 m/s and 6 m/s for a horizontal pipe

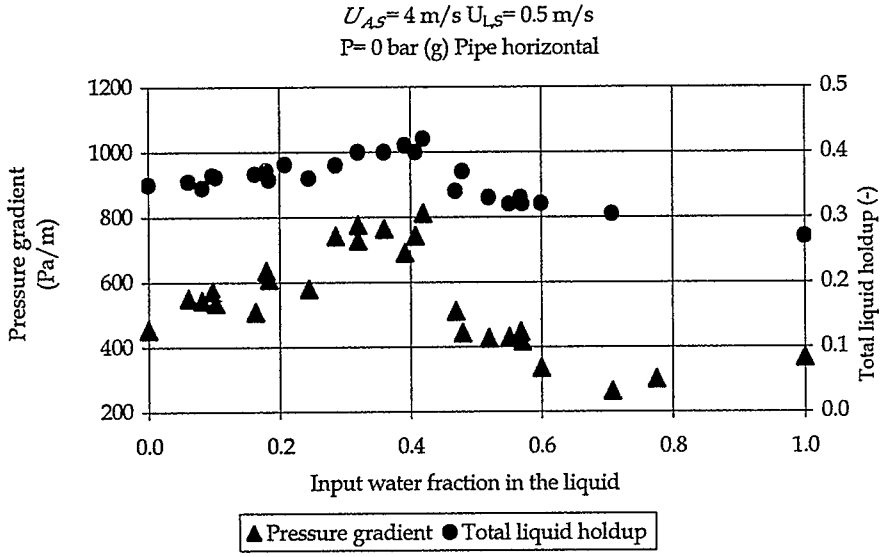


Figure 4.18. Measured total liquid holdup plotted against IWFIL at a total liquid superficial velocity 0.5m/s, at two different air superficial velocities 4m/s and 6 m/s for a horizontal pipe

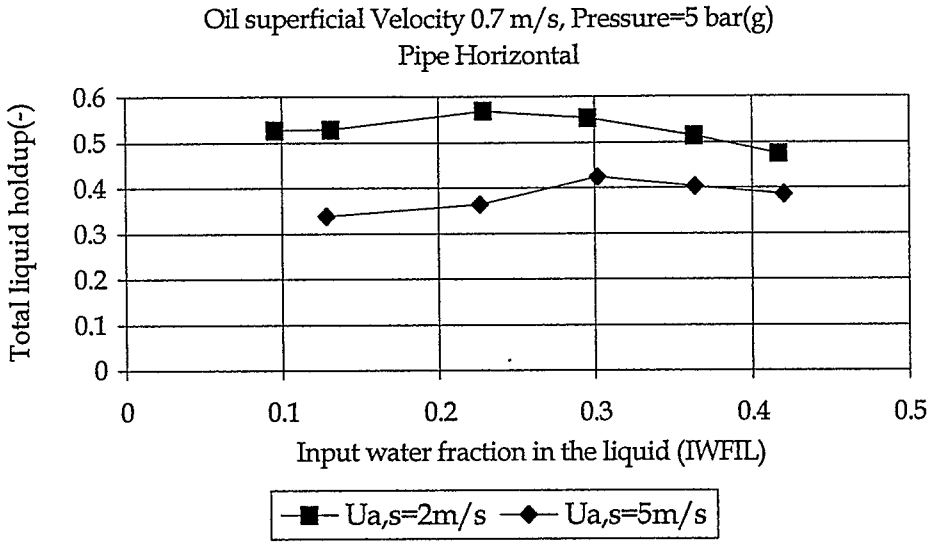


Figure 4.19: Measured total liquid holdup plotted against IWFIL at oil superficial velocity 0.7 m/s at 5 barg, horizontal pipe for two different air superficial velocities 2m/s and 5 m/s.

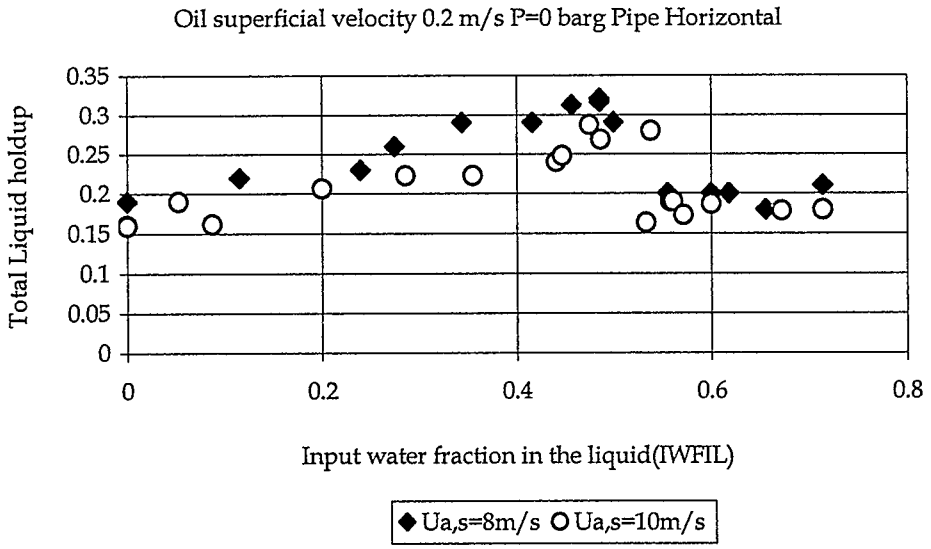


Figure 4.20 Measured total liquid holdup plotted against IWFIL at oil superficial velocity 0.2 m/s for two different air superficial velocities 8 and 10 m/s at 0 barg, horizontal pipe.

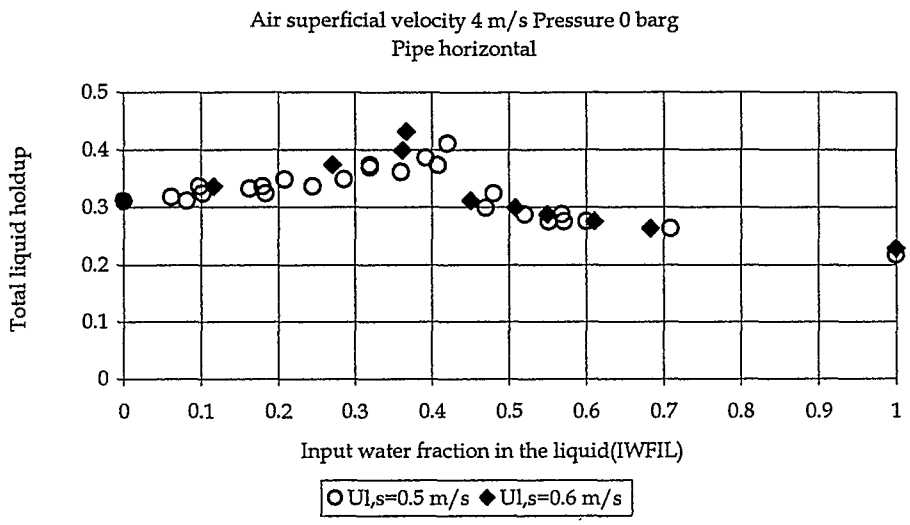


Figure 4.21 Measured total liquid holdup plotted against IWFIL at air superficial velocity 4 m/s for two different total liquid superficial velocities 0.5 m/s and 0.6 m/s at 0 barg, horizontal pipe

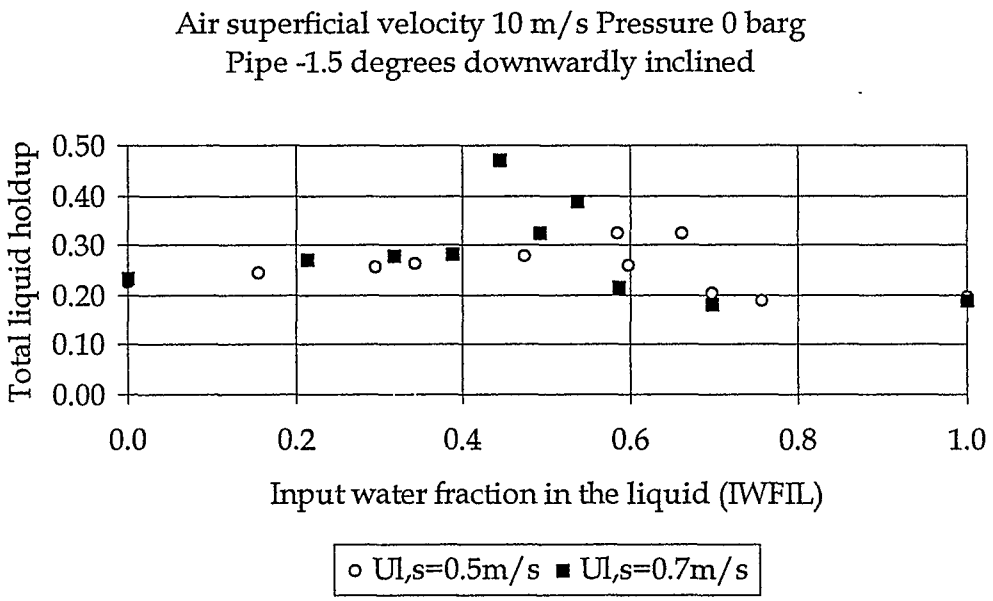


Figure 4.22: Measured total liquid holdup plotted against IWFIL at air superficial velocity 10 m/s and 0 barg, pipe downwardly inclined -1.5° for two distinct liquid superficial velocities 0.5 m/s and 0.7 m/s.

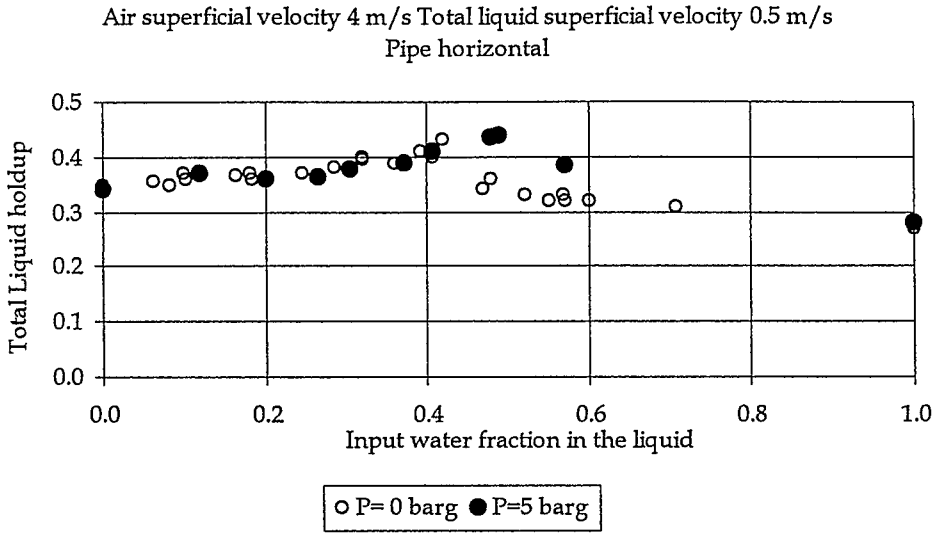


Figure 4.23: Measured total liquid holdup plotted against IWFIL at oil superficial velocity 4 m/s and total liquid superficial velocity 0.5 m/s at 0 barg, horizontal pipe

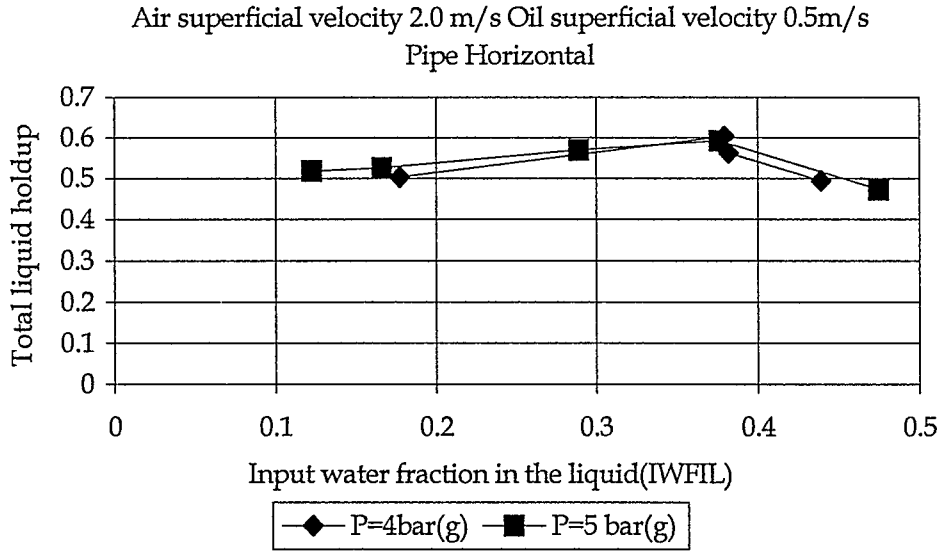


Figure 4.24: Measured total liquid holdup plotted against IWFIL at oil superficial velocity 0.5 m/s at two different system pressures 4 barg and 5 barg for a horizontal pipe .

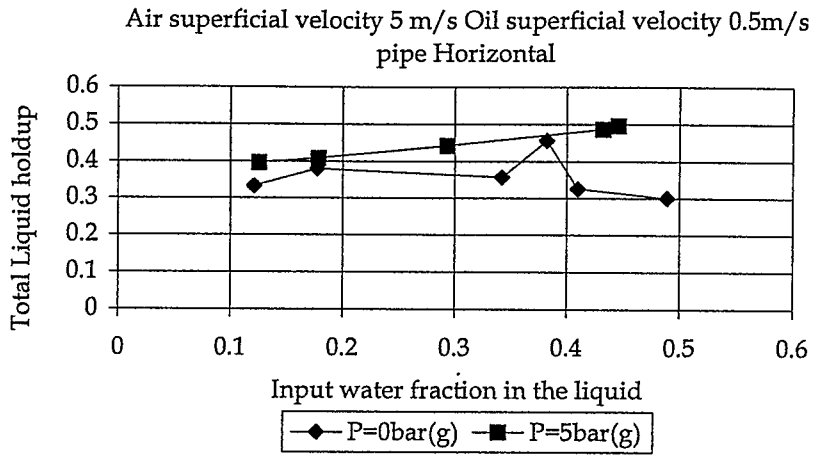


Figure 4.25: Measured total liquid holdup plotted against IWFIL at air superficial velocity 5 m/s at air superficial velocity 5m/s for a horizontal pipe at system pressures 0 barg and 5 barg.

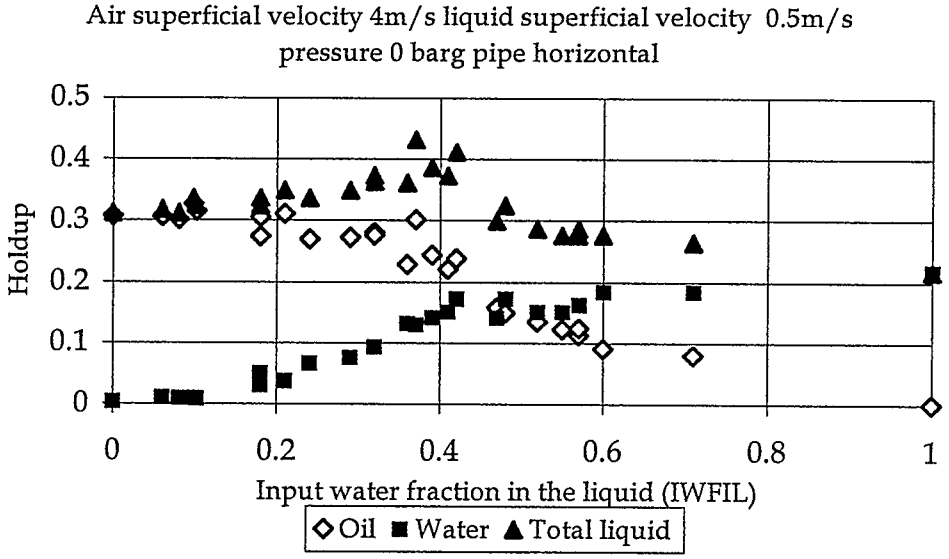


Figure 4.26: Measured total liquid and phasic holdup plotted against IWFIL at air superficial velocity 4 m/s at total liquid superficial velocity 0.5m/s for a horizontal pipe at atmospheric pressure.

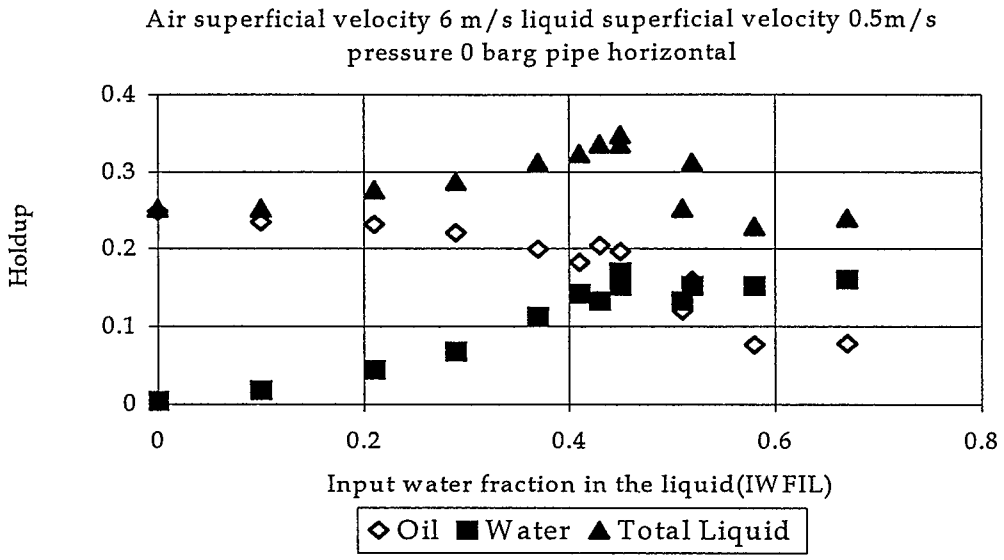


Figure 4.27: Measured total liquid and phasic holdup plotted against IWFIL at air superficial velocity 6 m/s at total liquid superficial velocity 0.5m/s for a horizontal pipe at atmospheric pressure

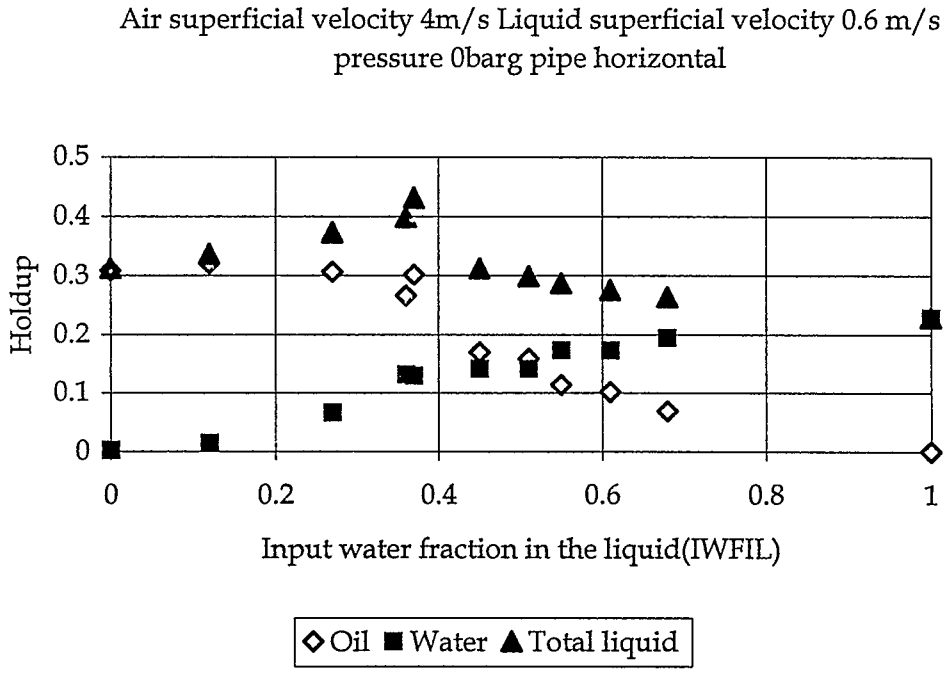


Figure 4.28: Measured total liquid and phasic holdup plotted against IWFIL at air superficial velocity 4 m/s at total liquid superficial velocity 0.6m/s for a horizontal pipe at atmospheric pressure.

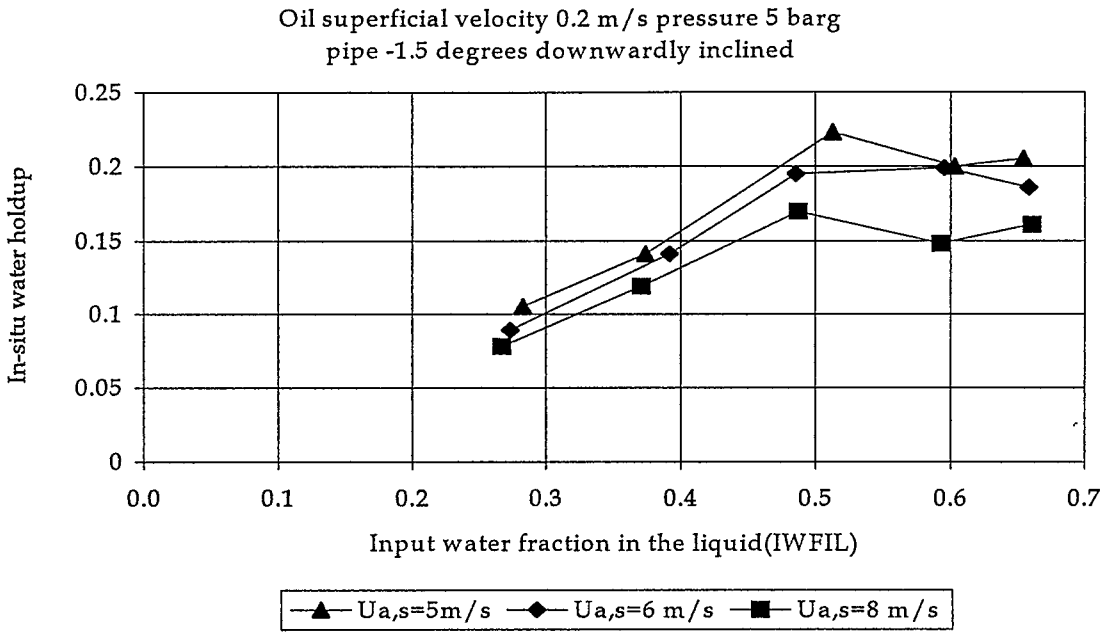


Figure 4.29: Measured *in-situ* water holdup plotted against IWFIL at oil superficial velocity 0.2 m/s for a range of air superficial velocities at 5 barg, pipe downwardly inclined –1.5° to the horizontal.

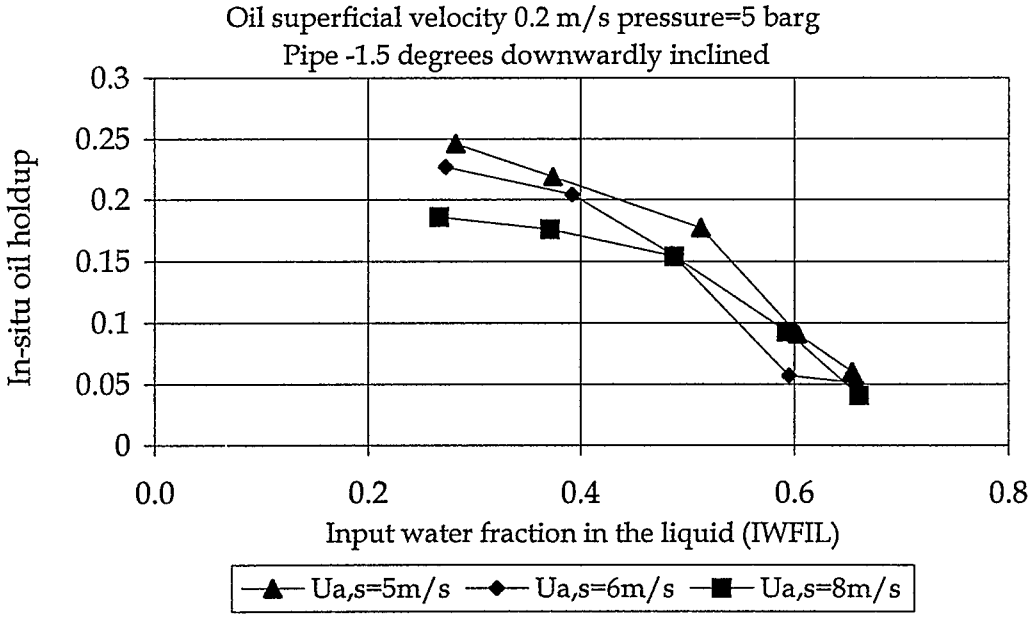


Figure 4.30: Measured *in-situ* oil holdup plotted against IWFIL at oil superficial velocity 0.2 m/s for a range of air superficial velocities at 5 barg, pipe downwardly inclined –1.5° downwardly inclined to the horizontal.

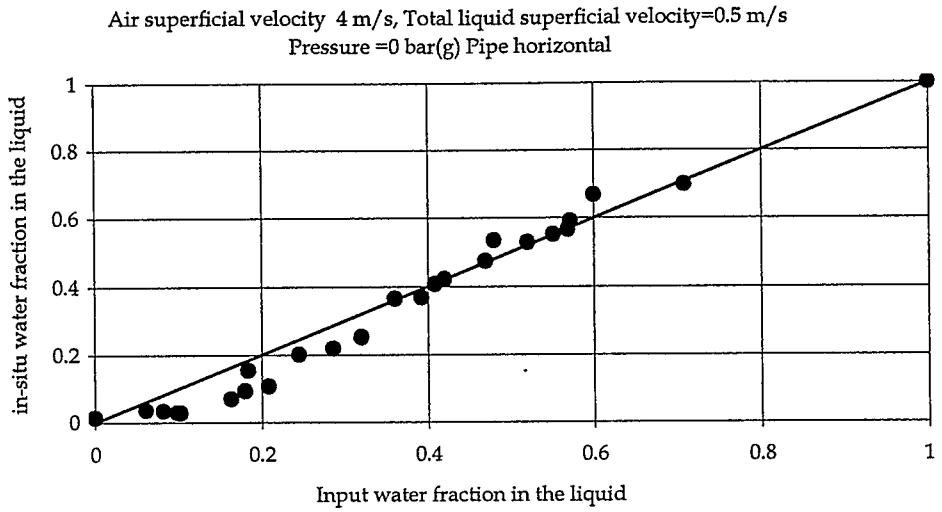


Figure 4.31: Measured in-situ water fraction in the liquid plotted against IWFIL at air superficial velocity 4 m/s, total liquid superficial velocity 0.5 m/s at 0 barg, for a horizontal pipe

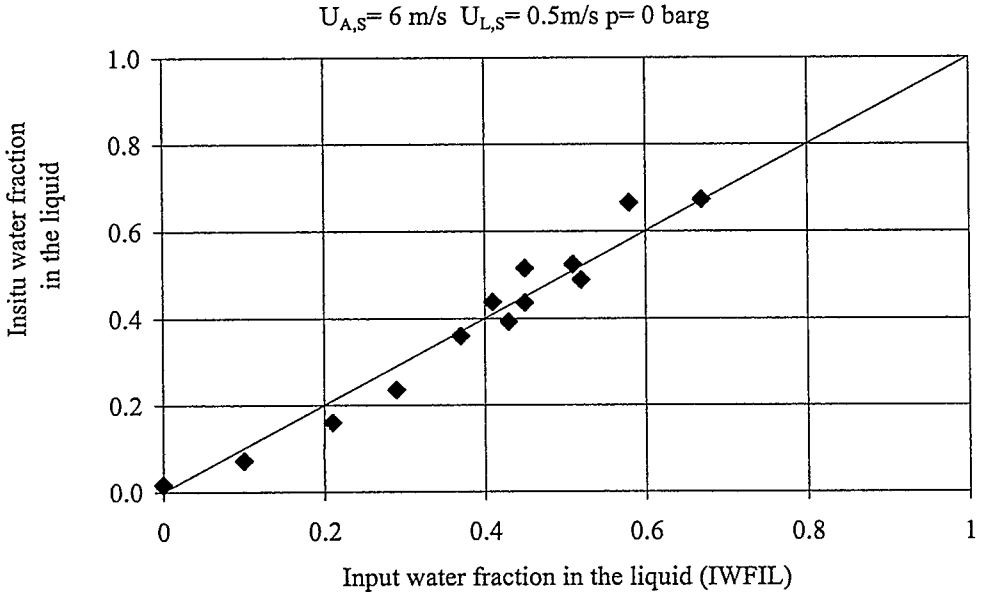


Figure 4.32: Measured in-situ water fraction in the liquid plotted against IWFIL at air superficial velocity 6m/s, total liquid superficial velocity 0.5 m/s at 0 barg, for a horizontal pipe

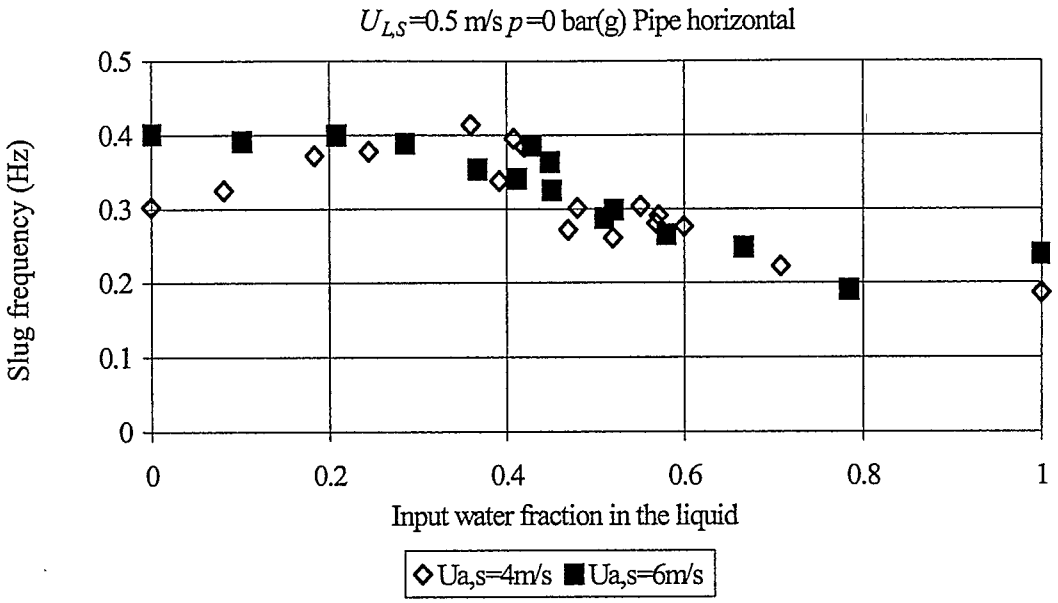


Figure 4.33: Measured slug frequency plotted against IWFIL at total liquid superficial velocity 0.5 m/s, for two different gas superficial velocities at 0 barg, horizontal pipe.

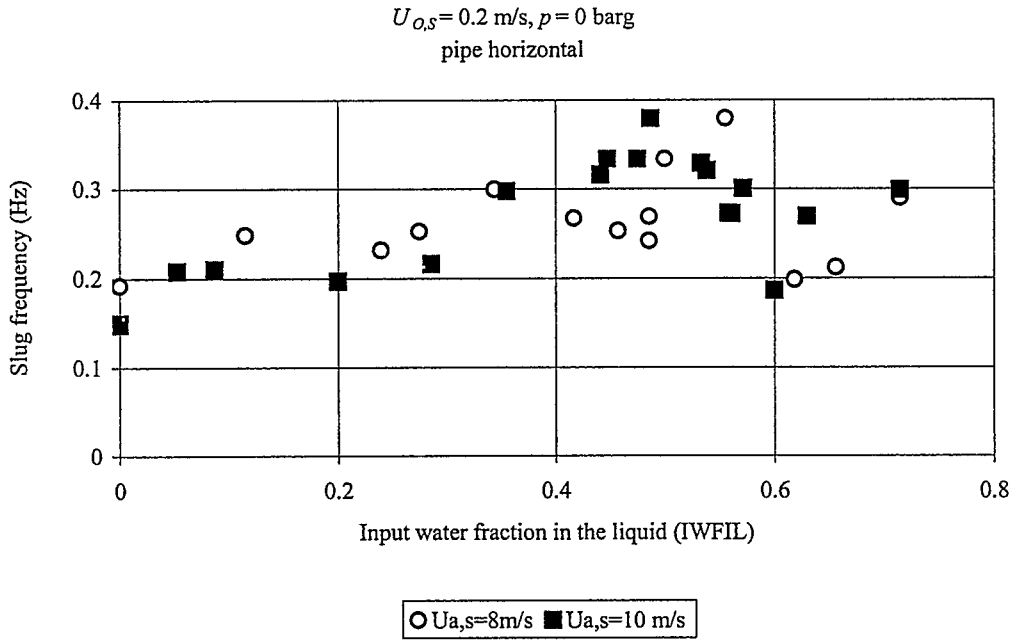


Figure 4.34: Measured slug frequency plotted against IWFIL at oil superficial velocity 0.2 m/s at two different air superficial velocities 8 m/s and 10 m/s at 0 barg, for a horizontal pipe.

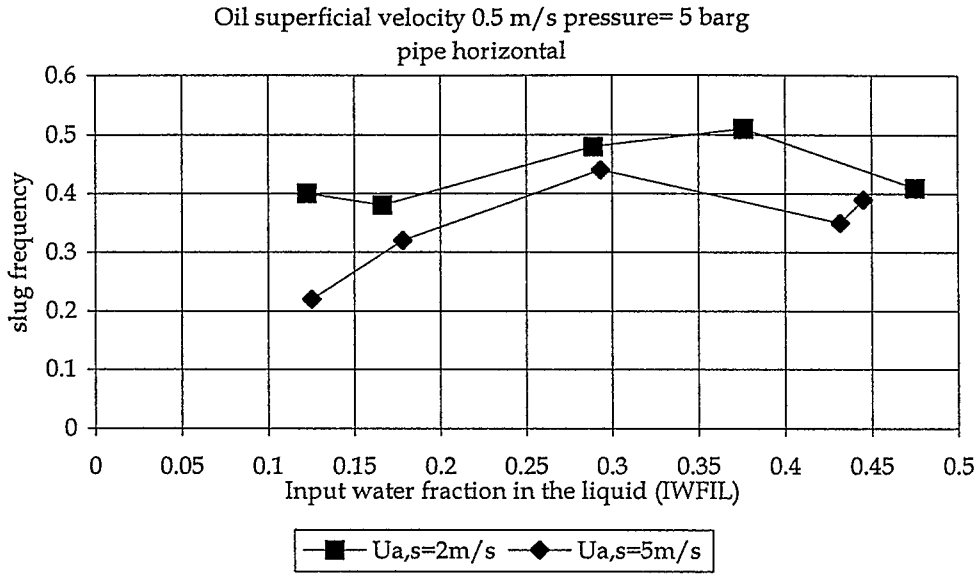


Figure 4.35: Measured slug frequency plotted against IWFIL at oil superficial velocity 0.5 m/s for two different air superficial velocities 2m/s and 5m/s at 5 barg, horizontal pipe.

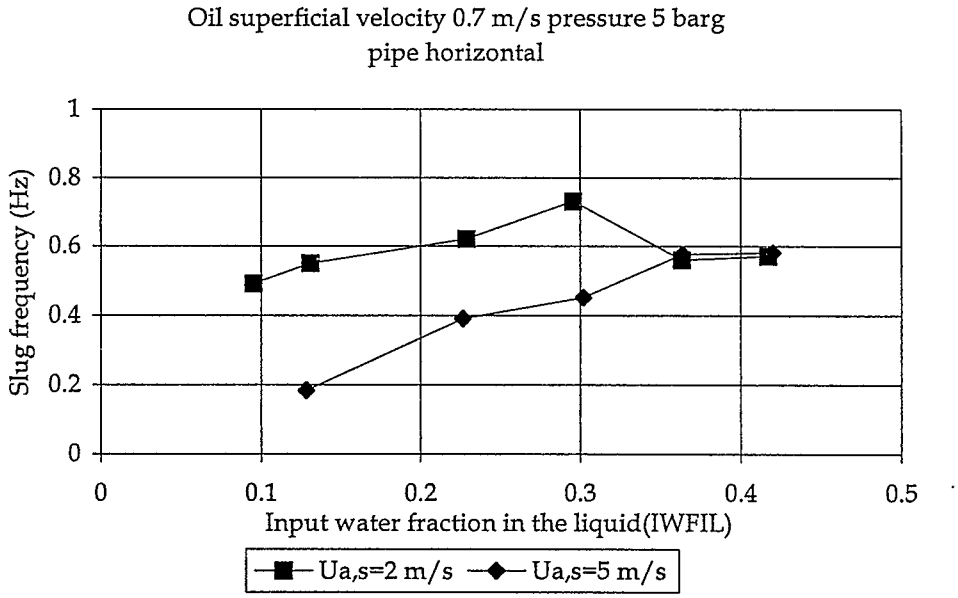


Figure 4.36: Measured slug frequency plotted against IWFIL at oil superficial velocity 0.7 m/s for two different air superficial velocities at 5 barg, horizontal pipe

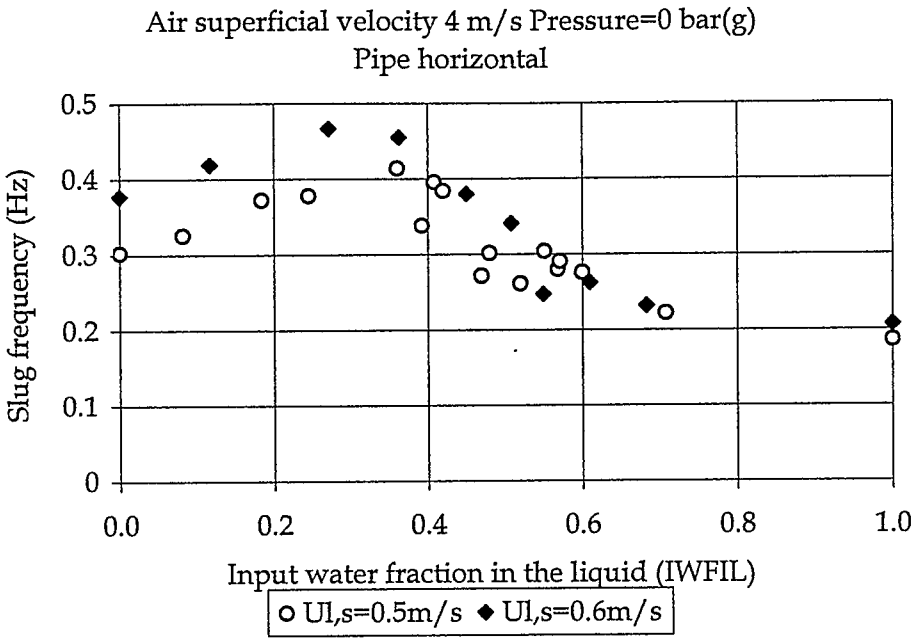


Figure 4.37: Measured slug frequency plotted against IWFIL at air superficial velocity 4m/s for two different total liquid superficial velocities 0.5 m/s and 0.6 m/s at 0 barg, horizontal pipe.

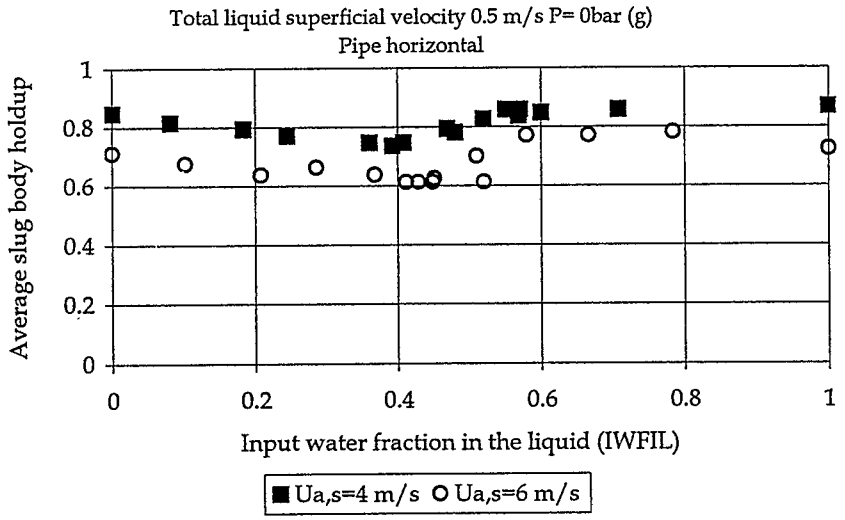


Figure 4.38: Measured slug body holdup plotted against IWFIL at total liquid superficial velocity 0.5 m/s for two different air superficial velocities at 0 barg, horizontal pipe

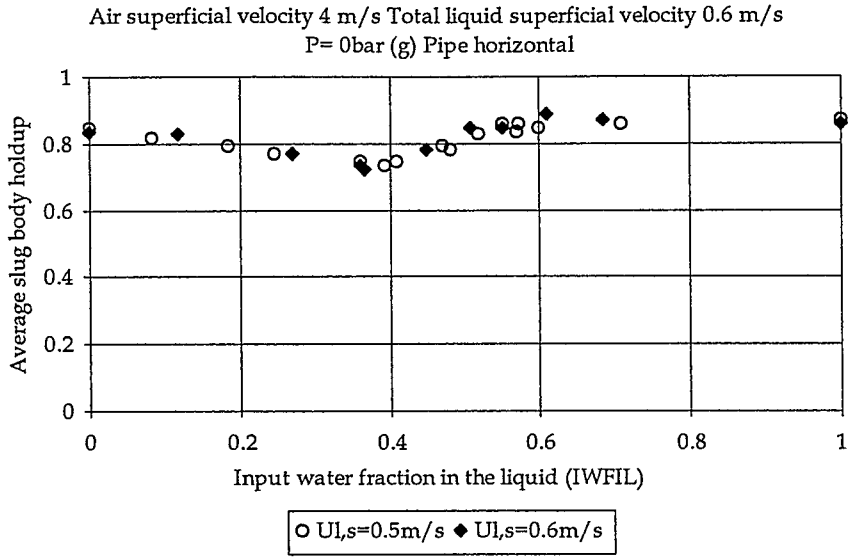


Figure 4.39: Measured average slug body holdup plotted against IWFIL at air superficial velocity 4m/s at two different liquid superficial velocities at 0 barg, horizontal pipe

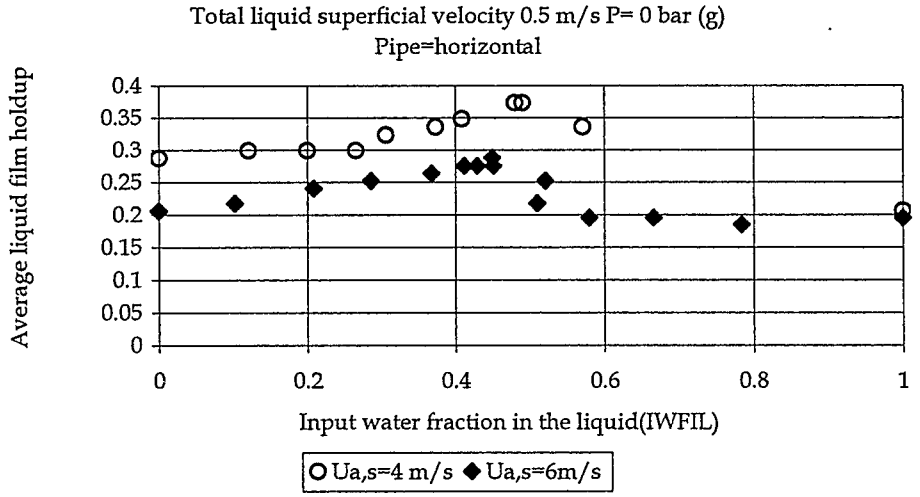


Figure 4.40: Measured average liquid film holdup plotted against IWFIL at total liquid superficial velocity 0.5 m/s at two different air superficial velocities 4 m/s and 6 m/s at 0 barg, horizontal pipe

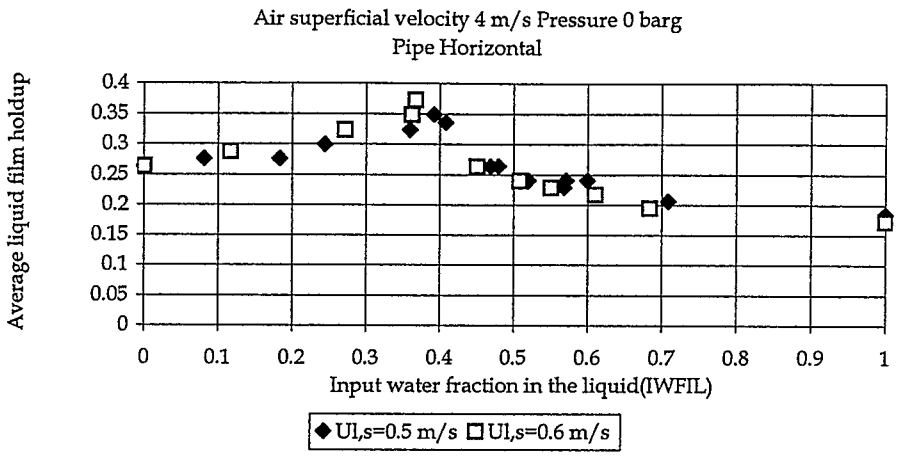


Figure 4.41: Measured average liquid film holdup plotted against IWFIL at air superficial velocity 4m/s, total liquid superficial velocity 0.6 m/s at 0 barg, horizontal pipe

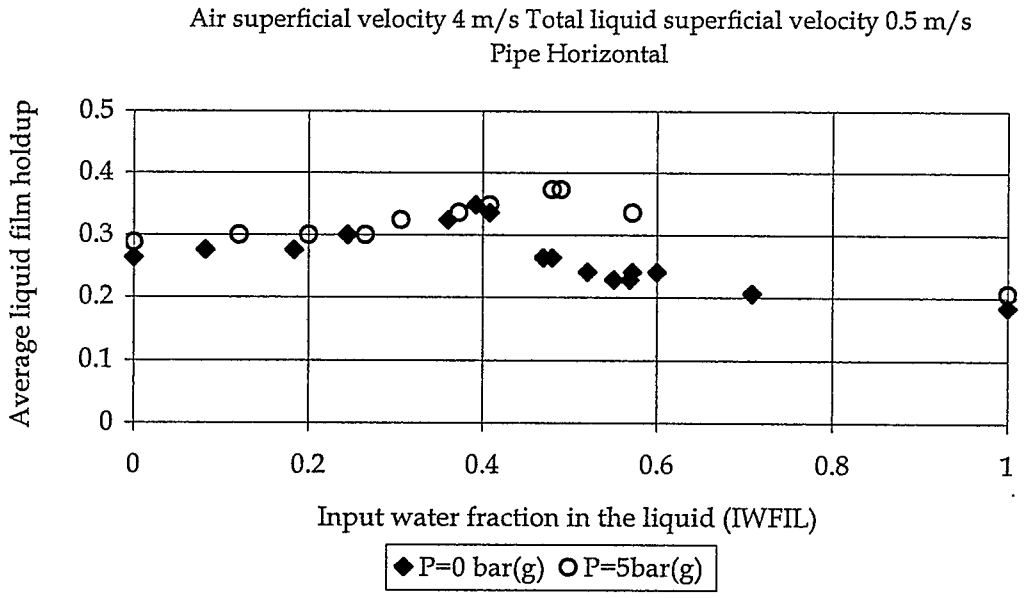


Figure 4.42: Measured average liquid film holdup plotted against IWFIL at air superficial velocity 4 m/s, total liquid superficial velocity 0.5 m/s at different system pressures 0 barg and 5 barg, horizontal pipe

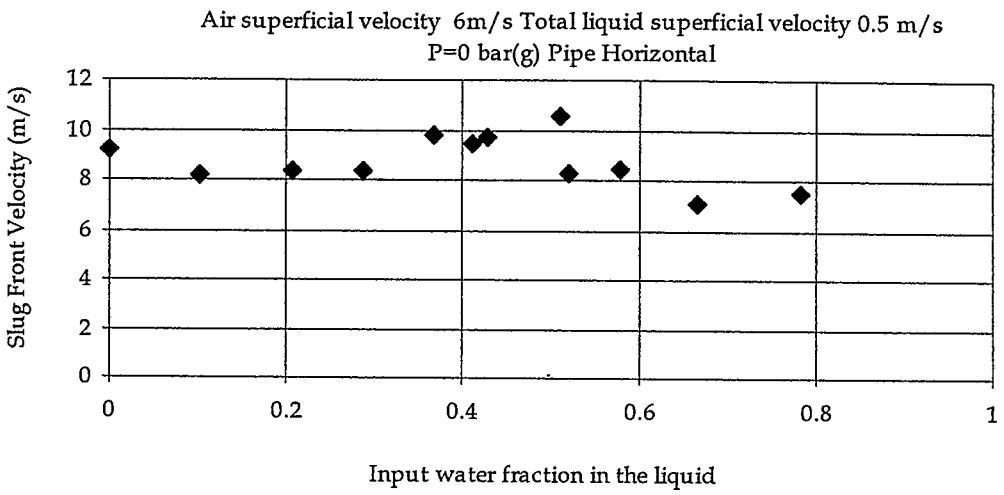


Figure 4.43: Measured slug front velocity plotted against IWFIL at air superficial velocity 6 m/s, total liquid superficial velocity 0.5 m/s at 0 barg, horizontal pipe

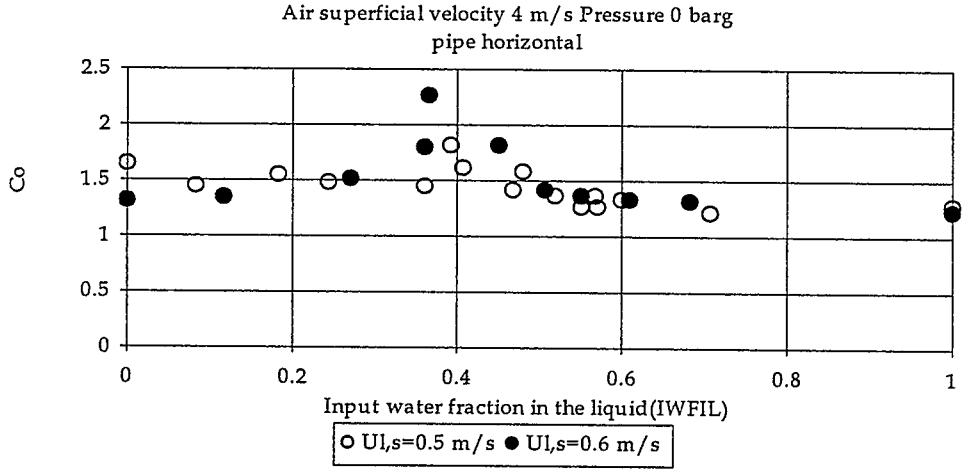


Figure 4.44: Measured Co ratios plotted against IWFIL at air superficial velocity 4 m/s for a range of total liquid superficial velocities at 0 barg, horizontal pipe

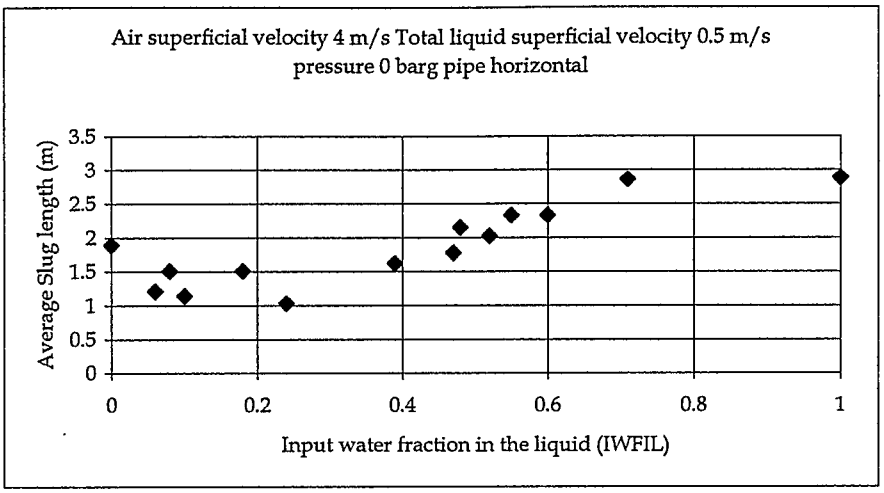


Figure 4.45: Measured average slug lengths plotted against IWFIL at air superficial velocity 4 m/s, at total liquid superficial velocity 0.5 m/s at 0 barg, horizontal pipe

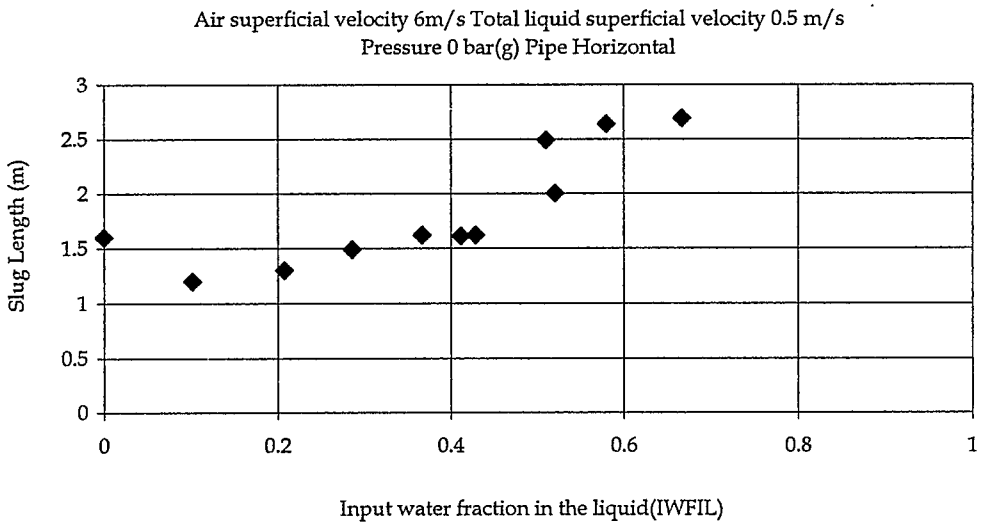


Figure 4.46: Measured average slug lengths plotted against IWFIL at air superficial velocity 6 m/s, at total liquid superficial velocity 0.5 m/s at 0 barg, horizontal pipe

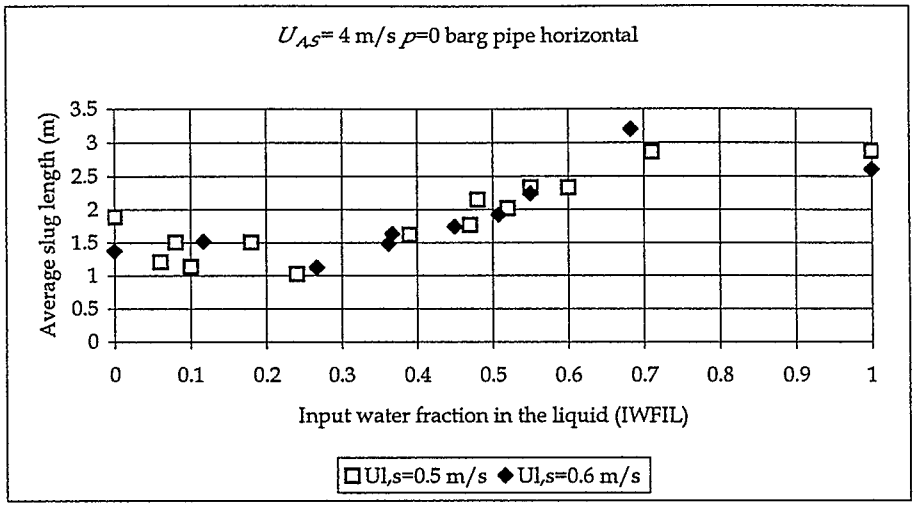


Figure 4.47: Measured average slug lengths plotted against IWFIL at air superficial velocity 4 m/s, at total liquid superficial velocities 0.5 m/s and 0.6 m/s at 0 barg for a horizontal pipe

Chapter 5

FLOW PATTERN AND FLOW PATTERN MAPS

In this Chapter, the flow pattern data obtained in this work, are presented in the form of flow pattern maps. These maps are subsequently discussed in terms of the effect of different parameters such as superficial velocities, system pressure and pipe inclination on the flow patterns observed as well as the effects on the transition from one flow pattern to another. Emphasis has been placed on the slug flow regime particularly on the transition between oil-continuous and water-continuous slug flows.

The flow pattern maps obtained in this work have also been compared with other three-phase gas-liquid-liquid flow pattern maps, namely those of Açikgoz *et al.* (1992) and Pan (1996).

5.1 FLOW REGIMES

5.1.1 Terminology

The flow regimes in two-phase gas-liquid flow are well established and can be divided into three main types: dispersed bubble, separated and intermittent flows. Annular and stratified flow are grouped under the separated flows and plug and slug flow regimes are grouped under intermittent flows.

However in three-phase gas-liquid-liquid flows, the presence of an extra liquid phase adds complexity to the flow pattern terminology. Due to the complexity in the flow pattern terminology, it is worth explaining the nomenclature used for describing the flow patterns.

In the course of the experiments carried out, nine different flow patterns were observed and the flow pattern notation of Pan (1996) has been adopted. In this notation, the three-phase flow pattern may be described in three parts as seen in Table 5.1:

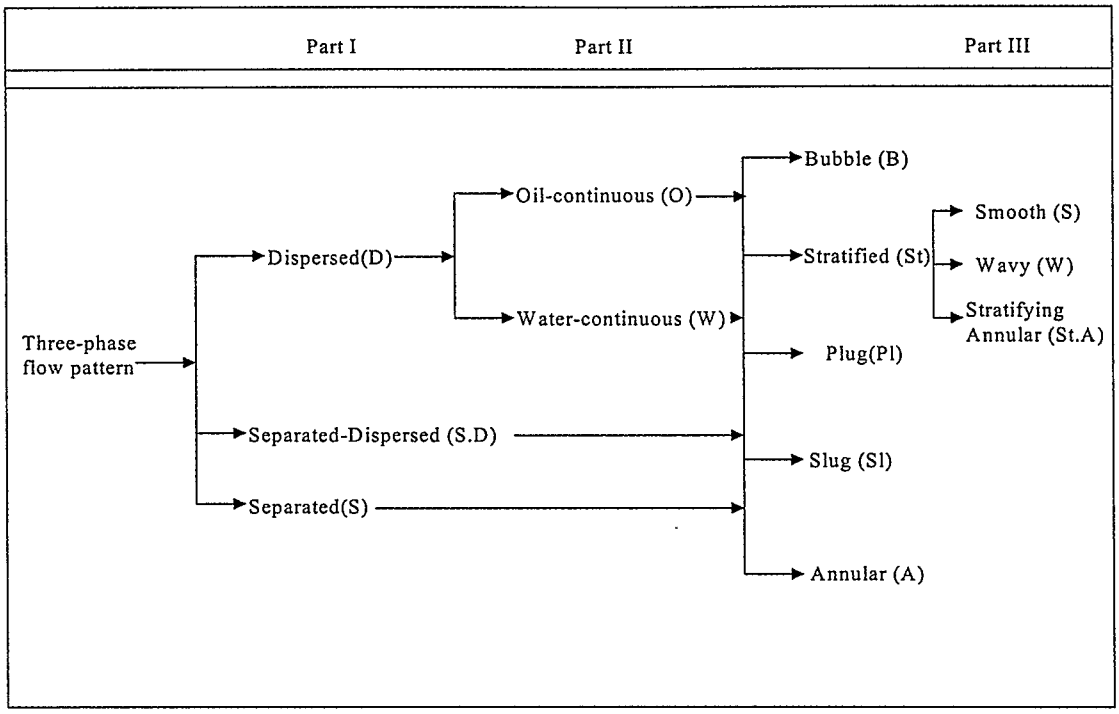


Table 5.1: The WASP Three-Phase Flow Pattern Classification

In part I, the terms *dispersed*, *separated* and *separated-dispersed* are used to describe the configuration relationship between the oil and water phases. When the oil and water are well mixed, the flow is said to be dispersed and when stratification in the liquid is present, the flow is said to be separated. In some cases, there may be the existence of both stratified and dispersed layers in the liquid phase, where this occurs, the terminology separated-dispersed is used to categorise the liquid phase. For instance in gas-liquid-liquid stratified flow, we could have four distinct layers namely: air, oil, an oil-water dispersion and a pure water layer beneath this.

In part II, the terms *oil-continuous* and *water-continuous,* are used to indicate which of the two liquid phases is the continuous phase and in contact with the pipe wall while the other liquid phase is dispersed in it. In Part III, bubble, stratified, plug, slug and annular are used to describe the configuration relationship between the total liquid phase and the gas phase and follow the same classifications as that used in two phase gas-liquid flow.

Additionally, the stratified flow regime, is divided into stratified-wavy, stratified-smooth and stratifying–annular. The main difference between the stratified-smooth and the stratified-wavy flow patterns is the presence of waves or ripples on the air-

liquid interface, whereas in the case of stratifying annular, some atomisation is present, whereby some of the top-most liquid layer is removed by the gas and entrained in the gas core. Some of the entrained droplets may deposit on the upper part of the tube forming a liquid film which may cover part or the whole of the upper surface of the pipe. When this layer covers the surface the flow is classified as being annular. Thus, the stratifying-annular flow regime is distinct from the annular flow regime because of the absence of a continuous liquid film flowing along the upper pipe wall.

5.1.2 Description

In the course of the experiments carried out, nine different flow patterns were observed. The flow pattern data presented here have been obtained from the analysis of high speed video footage taken of the transparent visualisation section of the pipeline, situated 35 m downstream of the inlet section.

1. Dispersed Stratified Smooth (D-St.S)

This flow pattern is characterised by a stratified layer of liquid at the bottom of the pipe with a smooth air/liquid interface. The liquid layer *appeared* to be well mixed for all the conditions covered. However, it was not possible to distinguish unequivocably between oil-continuous and water continuous flows purely on the basis of these visual observations.

2. Dispersed Stratified Wavy (D-St.W)

This flow pattern is entered from the D-St.S regime when the air superficial velocity is increased and ripples and waves begin to appear on the air-liquid interface. This is also accompanied by more intense mixing within the liquid layer.

3. Dispersed Water Continuous Slug Flow (D-W-Sl)

On further increasing the air superficial velocity, waves grow on the liquid interface leading to bridging the pipe establishing the slug flow regime. The fact that the continuous liquid phase is water can be verified by observing the liquid as it drains down from the top of the pipe soon after a slug has passed through the visualisation

section. In the case of dispersed water-continuous slug flow, the liquid drains quickly from the top of the pipe in a similar manner to water.

4. Dispersed Water-Continuous Stratifying Annular D-W-St.A

The dispersed water-continuous stratifying annular flow regime (D-W-St.A) is characterised by the rapid drainage of the atomised liquid layer from the pipe wall. This flow pattern occurs usually at relatively high gas superficial velocities and high liquid superficial velocities. This flow pattern can be distinguished from the dispersed water-continuous annular flow regime (D-W-A) because of the absence of a continuous liquid layer at the top of the pipe wall.

5. Dispersed Oil-Continuous Slug Flow (D-O-Sl)

This is similar to the dispersed water-continuous slug flow pattern (D-W-Sl) with the exception that the liquid drains slowly from the top of the pipe after the passage of a slug, suggesting a more viscous continuous liquid phase. Also present are wave structures in the film region separating the slugs; these structures stretch from the top of the pipe to the top of the liquid layer. Another difference between this flow pattern and the dispersed water-continuous slug flow pattern (D-W-Sl) is that, the slug frequency of the oil-continuous slugs is greater with occasional bouts of intense slugging.

6. Dispersed Oil Continuous Annular (D-O-A)

This flow pattern is characterised by the presence of complicated wave structures extending from the thin film at the top of the pipe to the relatively thicker film at the bottom of the pipe. These are similar to the structures observed in the film region in dispersed oil continuous slug flow (D-O-Sl).

7. Separated–Dispersed Oil-Continuous Slug Flow (S.D-O-Sl)

In this flow regime, the slug body appears to be well mixed whereas in the film region between the slugs, there is some stratification in the liquid layer. The drainage rate of the liquid from the top of the pipe after the passage of a slug indicates that the continuous liquid phase is oil. This flow regime is characterised by a relatively low slug frequency with sufficient time elapsing between successive slugs to allow for the

separation of the oil and water phases. The liquid film is also characterised by the presence of low amplitude roll waves on the air-liquid interface.

8. Separated-Dispersed Water Continuous Slug Flow (S.D-W-Sl)

This is similar to the separated-dispersed oil-continuous flow regime (S.D-O-Sl) with the exception that the continuous liquid phase is water as can be ascertained from the drainage rate of the liquid from the top of the pipe wall. Between the slugs, the liquid phases begin to separate in the film region There is also an absence of the roll waves, which characterise the film region in the S.D-O-Sl flow pattern.

9. Dispersed Oil-Continuous Stratifying Annular D-O-St.A

This flow regime is similar to the stratified wavy flow regime with the exception that there is atomisation of the liquid layer into the gas core. The atomised liquid deposits on the pipe wall forming a thin film which drains back into the liquid layer at the bottom of the pipe. The draining film covers only part of the pipe circumference.

In some cases, during an experimental run, the flow pattern appears unstable and there is a continuous switch from one flow pattern to another and back again. This occurs in the slug flow regime, particularly close to water-cuts of 50 %, where the flow pattern may switch from D-O-Sl to D-W-Sl and then back to D-O-Sl. These points have been labelled D-W-Sl/D-O-Sl.

5.2 FLOW PATTERN MAPS

Flow patterns obtained from the current series of experiments are presented in Figures 5.1-5.6, with the air superficial velocity on the X-axis and the water superficial velocity on the Y-axis.

5.2.1 Horizontal Flow Pattern Maps

For the horizontal flow pattern data presented in Figures 5.1-5.3, slug flow was found to be the predominant flow pattern. In Figure 5.1, which is obtained at a system pressure of 0 barg, with the pipe horizontal and at a constant oil superficial velocity of 0.5 m/s, two different flow patterns can be observed: dispersed oil continuous slug

flow (D-O-Sl) and dispersed water continuous slug flow (D-W-Sl). No separation between the oil and water phases was observed and this is attributed to the fact that the relatively high oil superficial velocity (0.5m/s) was sufficient to cause thorough mixing of the liquid phases. In contrast, Pan (1996) observed a significant region of separated slug flow; however his oil superficial velocity (0.1 m/s) was much lower than the value used in the present experiments. Pan's flow pattern map obtained under the same conditions, with the exception of the oil superficial velocity which was 0.1 m/s, revealed the presence of a significant amount of separated slug flow points

From Figure 5.1, it can be seen that the water superficial velocity at which the flow regime switches from dispersed oil-continuous slug flow (D-O-Sl) to the dispersed water continuous slug flow regime (D-W-Sl) is approximately 0.32 m/s which corresponds to a water-cut of 39 %. The water-cut λ_w is defined by the expression:

$$\lambda_W = \frac{U_{W,S}}{U_{W,S} + U_{O,S}} \tag{5.1}$$

where $U_{W,S}$ and $U_{O,S}$are the water superficial velocities and oil superficial velocities respectively. This again contrasts with the results of Pan (1996) where the water-cut at which this transition takes place occurs at water-cuts of approximately 55 % suggesting that the oil superficial velocity and thus the total liquid superficial velocity has a strong influence on the transition from dispersed oil-continuous slug flow regime (D-O-Sl) to dispersed water-continuous slug flow (D-W-Sl).

Figures 5.2 and 5.3 present the flow pattern data for the case of oil superficial velocity 0.2 m/s, for a horizontal pipe at system pressures of 0 barg and 5 barg respectively. In Figure 5.2, it can be seen that an increase in the air superficial velocity increases the value of the water-cut at which a transition from dispersed oil-continuous slug flow (D-O-Sl) to dispersed water-continuous slug flow (D-W-Sl) occurs. For example the switch from dispersed oil-continuous slug flow (D-O-Sl) to dispersed water-continuous slug flow (D-W-Sl) occurs at a water-cut of 50 % for an air superficial velocity of 4 m/s, whereas at an air superficial velocity of 12 m/s, this switch takes place at a water-cut of 60 %. When the results shown in Figures 5.2 and 5.3 are compared with those shown in Figure 5.1, it can be concluded that decreasing

the oil superficial velocity, increases, for a given air superficial velocity, the water-cut at which the transition from dispersed oil-continuous slug flow to dispersed water-continuous slug flow takes place.

In Figure 5.2, for the range of water-superficial velocities 0.05 – 0.2 m/s, at an air superficial velocity of 3 m/s, the flow pattern is dispersed oil-continuous slug flow. This flow pattern persists until an air superficial velocity of 14 m/s. At this air superficial velocity, we see the appearance of the dispersed oil-stratifying annular flow regime (D-O-St.A). Further increase in the air superficial velocity to 16 m/s leads to a transition from this regime to dispersed oil-continuous annular flow (D-O-A).

For water superficial velocities between 0.2 m/s and 0.3m/s and for air superficial velocities between 2 m/s and 6m/s, the flow pattern that predominates is unstable, fluctuating between dispersed oil-continuous slug flow (D-O-Sl) and dispersed water continuous slug flow (D-W-Sl). Increasing the air superficial velocity beyond 6 m/s leads to the establishment of the dispersed water continuous slug flow regime.

In Figure 5.3, the flow pattern map is shown for the same phase velocities as those in Figure 5.2, but with the system pressure increased from 0 barg to 5 barg. We can see the presence of two flow patterns not observed in Figure 5.2: separated-dispersed oil continuous slug flow (S.D-O-Sl) and separated-dispersed water continuous slug flow (S.D-W-Sl). These flow patterns occur at relatively low air superficial velocities, approximately 1 m/s and low water superficial velocities of approximately 0.1-0.2 m/s. In these flow patterns, the slug body appears to be well mixed while the low slug frequency allows the liquid film between successive slugs to separate into oil and water layers. On increasing the air superficial velocity beyond 2 m/s, the flow pattern changes to one of fully dispersed slug flow, where both the slug body and liquid film are well mixed. This flow pattern persists for air superficial velocities up to 4 m/s.
For air superficial velocities greater than 4 m/s there is a transition between dispersed oil-continuous slug flow (D-O-Sl) and the dispersed stratifying annular flow regime (D-O-St.A)

5.2.1.1 Effect Of System Pressure On Flow Pattern In Horizontal Flow

The effect of the system pressure on a horizontal flow pattern map can be observed by comparing Figures 5.2 and 5.3, which have been obtained under the same conditions with the exception of the system pressure which is 0 barg for the results shown in Figure 5.2 and 5 barg for those shown in Figure 5.3.

Increasing the system pressure has a significant effect on the slug/annular flow transition. In Figure 5.2, at a constant water superficial velocity of 0.05 m/s, the air superficial velocity at which the transition from slug flow to annular flow takes place is 14 m/s, whereas when the system pressure is increased to 5 barg in Figure 5.3, this transition takes place at an air superficial velocity of 4 m/s.

Thus the effect of increasing the system pressure is to decrease the air superficial velocity at which the transition from slug to annular flow takes place.

5.2.2 Inclined Flow Pattern Maps

The inclined flow pattern data has been plotted in Figures 5.4-5.6. Figure 5.4 shows the flow pattern map for oil superficial velocity 0.2 m/s, at atmospheric pressure at the outlet of the tube and with the pipe downwardly inclined at an angle of –1.5° to the horizontal.

The region of the flow pattern map occupied by the stratified flow regime is greater for this inclined downflow case than it was for horizontal flow. At low air superficial velocities between 1 and 5 m/s, only two flow patterns exist: dispersed stratified smooth (D-St.S) and dispersed stratified wavy (D-StW). Note that it was not possible, on the basis of these visual studies to determine which phase was continuous (oil or water). For air superficial velocities between 5m/s and 15 m/s, the flow pattern map can be divided into three distinct zones.

The first zone occurs at water superficial velocities between 0.05 and 0.10m/s; here at an air superficial velocity of 5 m/s, the flow pattern is dispersed stratified wavy (D-St.W) and increasing the air superficial velocity beyond 5 m/s leads to a transition to the dispersed oil-continuous stratifying annular flow regime (D-O-St.A).

The second distinct zone occurs for water superficial velocity greater than 0.10 m/s; here the predominant flow patterns are dispersed oil-continuous slug flow (D-O-Sl) and dispersed water continuous slug flow (D-W-Sl). The transition from dispersed oil continuous slug flow (D-O-Sl) to dispersed water-continuous slug flow (D-W-Sl) occurs at a water superficial velocity of 0.28 m/s, which corresponds to a water-cut of 58%.

The third distinct zone in the flow pattern map shown in Figure 5.4, occurs at air superficial velocities greater 15 m/s. For this set of conditions, the predominant flow patterns are dispersed oil-continuous annular flow (D-O-A) and dispersed oil-continuous stratifying annular flow (D-O-St.A).

In Figure 5.5, the flow pattern data have been plotted for the conditions of oil superficial velocity 0.2 m/s, system pressure of 5 barg; again, the pipe downwardly inclined at an angle of –1.5° to the horizontal. From this flow pattern map, six different flow patterns can be identified. For air superficial velocity between 1 and 4 m/s, the predominant flow pattern is stratified. When the air superficial velocity is increased beyond 4 m/s, there is a transition to the slug flow regime. Further increases in the air superficial velocity beyond 5 m/s, leads to a transition to the stratifying annular flow pattern.

The flow pattern data obtained at an oil superficial velocity of 0.2 m/s, system pressure 10 barg are shown in Figure 5.6. Three flow patterns are present here: Dispersed stratified wavy flow (D-St.W), dispersed water-continuous slug flow (D-W-Sl) and dispersed water-continuous stratifying–annular (D-W-St.A).

5.2.2.1 Effect Of System Pressure On The Flow Pattern In Downwardly Inclined Flow

Stratified smooth/stratified wavy transition

The effect of the system pressure on the flow pattern transitions for a downwardly inclined pipe can be observed by examining Figures 5.4 to 5.6. In Figure 5.4

(showing data for 0 barg outlet pressure), at water superficial velocity of 0.05 m/s, the transition between dispersed stratified smooth flow regime (D-St.S) and the dispersed stratified wavy flow regime (D-St.W) takes place at an air superficial velocity of 4 m/s.

On increasing the system pressure to 5 barg in Figure 5.5, the transition from dispersed stratified smooth (D-SS) to dispersed stratified wavy (D-St.W) at a water superficial velocity of 0.05 m/s takes place between 2 and 3 m/s. When the system pressure is increased further to 10 barg as shown in Figure 5.6, the transition between dispersed stratified smooth and dispersed stratified wavy for a water superficial velocity of 0.05 m/s, takes place at an air superficial velocity less than 1 m/s.

Thus on this basis, it can be concluded that for a downwardly inclined pipe of $-1.5°$ increasing the system pressure leads to a decrease in the air superficial velocity at which the transition between the dispersed stratified flow pattern (D-SS) and the dispersed stratified wavy flow (D-St.W), for a constant water superficial velocity takes place.

Stratified/Slug transition

The system pressure also has an effect on the stratified/slug transition. As shown in Figure 5.4, at a constant water superficial velocity of 0.3 m/s, the transition from the stratified flow regime to the slug flow regime occurs at an air superficial velocity of 6m/s. When the system pressure is increased to 5 barg in Figure 5.5, this transition, at a constant water superficial velocity of 0.3 m/s, takes place at an air superficial velocity of less than 5 m/s. At 10 barg (Figure 5.6), this transition takes place at an air superficial velocity less than 3m/s.

Therefore it can be seen that as in the stratified smooth/stratified wavy transition, increasing the system pressure in a downwardly inclined pipe leads to a decrease in the air superficial velocity at which the transition between the stratified flow and the slug flow regime takes place for a constant water superficial velocity.

Slug/Annular transition

The effect of the system pressure on the slug annular transition for a downwardly inclined pipe can be seen by examining Figures 5.4 to 5.6. At atmospheric outlet pressure (Figure 5.4), for a water superficial velocity of 0.2 m/s, the transition between the slug and annular flow regime occurs at an air superficial velocity between 15 and 20 m/s. When the system pressure is increased to 10 barg (Figure 5.6), at the same constant water superficial velocity of 0.2m/s, the transition between the slug flow and the annular flow regime takes place at an air superficial velocity of between 3 and 4 m/s.

Another example of the effect of the system pressure on the slug/annular transition can be seen by comparing Figures 5.4 and 5.5. At 0 barg (Figure 5.4) and at a water superficial velocity of 0.1 m/s, the transition between the slug flow and annular flow occurs at an air superficial velocity of between 15 and 17 m/s. When the system pressure is increased to 5 barg (Figure 5.5), this transition takes place at an air superficial velocity between 5 & 6 m/s.

5.2.3 Effect of Inclination Angle on Flow Pattern Transition

The effect of the inclination angle on the flow pattern transitions can be observed by comparing Figures 5.2 and 5.4. These Figures were obtained under the same conditions (atmospheric outlet pressure) with the exception that Figure 5.2 is for a horizontal pipe and Figure 5.4 is with the pipe downwardly inclined to the horizontal at an angle of –1.5°.

In Figure 5.2, for an horizontal pipe, there are no stratified flow data points and the predominant flow pattern is that of slug flow, whereas in Figure 5.4 obtained with the pipe downwardly inclined at an angle of –1.5°, the area of the flow pattern map occupied by the stratified flow is significant.

Thus, the effect of decreasing the angle of inclination below 0° is to increase the area of the flow pattern map occupied by the stratified flow regime at the expense of the slug flow regime.

The inclination angle has an effect on the slug/annular transition. From the results shown in Figure 5.2, obtained at horizontal conditions, it can be seen that at a water superficial velocity of 0.05 m/s, the transition between the slug flow regime and the annular regime takes place at an air superficial velocity of 15 m/s. When the pipe inclination angle is changed from 0° to –1.5°, the transition from slug to annular flow occurs at an air superficial velocity of 9m/s, for the same water superficial velocity. This is expected as the pipe inclination angle helps to reduce the liquid level in the pipe, thus hastening the transition from slug flow to annular flow.

Thus the effect of the inclining the pipe from 0° to –1.5°, is to reduce the air superficial velocity at which the transition from slug flow to annular flow, at constant water superficial velocity, takes place.

5.3 COMPARISON WITH OTHER FLOW PATTERN MAPS

Flow pattern data obtained from the present series of experiments have been compared with the horizontal flow pattern maps obtained by Açikgoz *et al.* (1992) and Pan (1996).

5.3.1 Comparison of Flow Pattern Data with Flow Pattern Map of Acikgoz *et al.* (1992)

In Figures 5.7-5.9, the flow pattern data obtained for different flow conditions have been plotted on the horizontal three-phase air-oil-water flow pattern map of Açikgoz *et al.* (1992) which was obtained at an oil superficial velocity of 0.095 m/s for a horizontal pipe at near atmospheric pressure and using an oil with a viscosity of 0.1164 Pas. The key to the numbered regions in Acikgoz et al's map is given in Table 5.2

Key	Flow Pattern
1	*D-O-Pl*
2	*D-O-Sl*
3	*D-O-St.W*
4	*S-O-St.W*
5	*S-O-A*
6	*S.D-O-A*
7	*D-W-Sl*
8	*D-W-St.W*
9	*S.D-W-A*
10	*D-W-A*

Table 5.2: Key for Acikgoz *et al's* Flow Pattern Map

5.3.1.1Horizontal Data

Two sets of horizontal data have been plotted on the horizontal flow pattern map of Acikgoz *et al.* (1992), namely data obtained at oil superficial velocity 0.2 m/s and oil superficial velocity 0.5 m/s. The data plotted were for atmospheric pressure outlet conditions.

(a) Oil superficial velocity 0.2 m/s

Figure 5.7, shows data from the present experiments carried out at an oil superficial velocity of 0.2 m/s, with the pipe in a horizontal configuration plotted on the horizontal flow pattern map of Acikgoz *et al.* The flow pattern map of Acikgoz *et al* has been obtained at an oil superficial velocity of 0.095 m/s. It can be seen from this Figure that none of the flow pattern data fall in the designated areas of the flow pattern map.

(b) Oil superficial velocity 0.5 m/s

In Figure 5.8, data obtained at an oil superficial velocity of 0.5 m/s, with the pipe horizontal have also been plotted on the flow pattern map of Acikgoz *et al.* As in the case of oil superficial velocity of 0.2 m/s (Figure 5.7), none of the flow patterns fall in the designated areas of Acikgoz et al's map.

It can be seen that for both cases, none of the flow pattern data fall in the designated area of the flow pattern map. This indicates a strong influence of both the pipe diameter, fluids and oil superficial velocity.

5.3.1.2 Inclined data

In Figure 5.9, data from experiments carried out an oil superficial velocity of 0.2 m/s, with the pipe downwardly inclined at an angle of $-1.5°$ have been plotted on the horizontal flow pattern map of Acikgoz *et al.*

It can be seen from this Figure that only the flow patterns dispersed stratified wavy (D-St.W) and the dispersed water-continuous annular flow (D-W-A) patterns fall in the designated areas.

Acikgoz et al's map fails to predict the position of the water and oil dispersed slug flow correctly and the reason for this is that the small downward inclined angle is sufficient to increase the stratified flow pattern area at the expense of the slug flow pattern area and also that for a downwardly inclined pipeline, the transition from stratified to slug flow takes place at much higher air superficial velocities than in the case of horizontal pipelines.

The conclusion from Figures 5.7-5.9 is that the map of Acikgoz *et al* (1992) is not comprehensive enough to account for data obtained from different pipes under different experimental conditions. Pan (1996) also arrived at the same conclusion when he compared his data with the Acikgoz *et al* map.

5.3.2 Pan (1996)

Pan (1996) also constructed flow pattern maps from his experiments in three-phase air-oil-water flow for oil superficial velocity 0.1 m/s, 0 barg outlet pressure and for a horizontal pipe. In Figures 5.10-5.12, data from the current experiments have been plotted on his flow pattern map. The numbered regions in Figures 5.10-5.12 are denoted by the flow patterns as described in table 5.3:

Map Key	Flow Pattern
1	*D-O-Sl*
2	*D-W-Sl*
3	*D-O-St*
4	*D-O-A*
5	*D-W-A*
6	*D-W-St*

Table 5.3: Flow Pattern Map Key for Pan's (1996) flow pattern map

5.3.2.1Horizontal Data

(a) Oil superficial velocity 0.2 m/s

In Figure 5.10, experimental data at oil superficial velocity of 0.2 m/s, 0 barg with the pipe horizontal have been plotted on the horizontal flow pattern map of Pan (1996) obtained at an oil superficial velocity of 0.1 m/s with the pipe horizontal.

From Figure 5.10, we can see there is good agreement with the experimental flow pattern data and the flow pattern map of Pan (1996). All the dispersed water-continuous slug flow points (D-W-Sl) fall in the designated area of the flow pattern map (region 2). In addition to this, the few dispersed oil-continuous annular flow points (D-O-A) also fall in the designated area of the flow pattern map (region 4).

The dispersed oil-continuous stratifying annular points (D-O-St.A) fall in the area of the flow pattern map designated as (D-O-A), this is due to the fact that Pan (1996) does not distinguish between the flow patterns dispersed oil-continuous annular (D-O-A) and the dispersed oil-continuous stratifying annular (D-O-St.A).

The only discrepancy observed is in the case of the dispersed oil-continuous slug (D-O-Sl) flow pattern. This flow pattern is spread over several designated areas. The reason for this is likely to be due to the higher oil superficial velocity at which the data from the experiments were obtained.

(b)Oil superficial velocity 0.5 m/s

In Figure 5.11, the horizontal flow pattern data obtained at an oil superficial velocity of 0.5 m/s, with the pipe horizontal have been plotted on the horizontal flow pattern map of Pan.

Figure 5.11 shows that the dispersed water-continuous slug flow pattern data (D-W-Sl) falls in the designated area of the flow pattern map (region 2), while this is not the case for the dispersed oil-continuous flow (D-O-Sl) pattern data. This discrepancy is likely to be due to the effect of increasing the oil superficial velocity from 0.1 m/s (Pan's flow pattern map) to 0.5 m/s (present flow pattern map) is to shift the transition line between D-O-Sl/D-W-Sl flow regimes towards higher water superficial velocities. This explains why some of the dispersed oil-continuous flow pattern data (D-O-Sl) are found in the area of the flow pattern map designated for dispersed water-continuous slug flow (D-W-Sl) (region 2).

In addition, increasing the oil superficial velocity also shifts the transition between dispersed oil-continuous slug flow (D-O-Sl) and dispersed oil-continuous annular

flow (D-O-A) towards higher air superficial velocities, explaining why some of the D-O-Sl points are found in the D-O-A (region 4).

5.3.2.2 Inclined Data

A total of 25 air-oil-water data points obtained for a 1.5° downwardly inclined pipe at an oil superficial velocity of 0.1 m/s were plotted on the horizontal flow pattern map of Pan (1996) and this is shown in Figure 5.12. From this Figure, it can be seen that all the dispersed water-continuous slug flow patterns (D-W-Sl) fall into the designated area of the flow pattern map (region 2).

Also observed is that the data for dispersed oil-stratifying–annular (D-O-St.A) flow pattern falls into the areas designated as dispersed oil-annular (region 4) and oil dispersed slug flow (region 1). There are two factors here; firstly Pan did not distinguish separately the D-O-St.A region and secondly, the downwardly inclination of the pipe reduces the propensity for slug flow.

5.4 SUMMARY

Flow patterns have been presented from three-phase air-oil-water experiments carried out under various flow conditions, system pressures and pipeline inclinations.

Results showed that the increasing system pressure decreased the air superficial velocity at which the stratified/slug and slug/ annular transitions took place for both horizontal and inclined flows.

The pipe inclination also was shown to have a profound influence on the flow pattern map. When the pipeline inclination was changed from 0° (horizontal) to –1.5°, the area of the flow pattern map occupied by the slug flow regime reduced drastically.

A comparison of the horizontal flow pattern data from this work with the horizontal flow pattern map of Acikgoz *et al.* (1992) revealed that this map was not applicable. The reason for this was attributed to the fact that the map of *Acikgoz et al.* was derived from a different pipe diameter, utilising an oil of a different viscosity.

On the other hand, when the data were compared with the horizontal flow pattern map of Pan (1996), there was a much better performance with a few discrepancies. The reason for the improved performance was because the same facilities and fluids were used in both cases. Differences between the present data and that of Pan (1996) could be ascribed to the wider range of oil superficial velocities used here and (for the inclined pipe data) to the significant effect of pipe inclination on flow pattern.

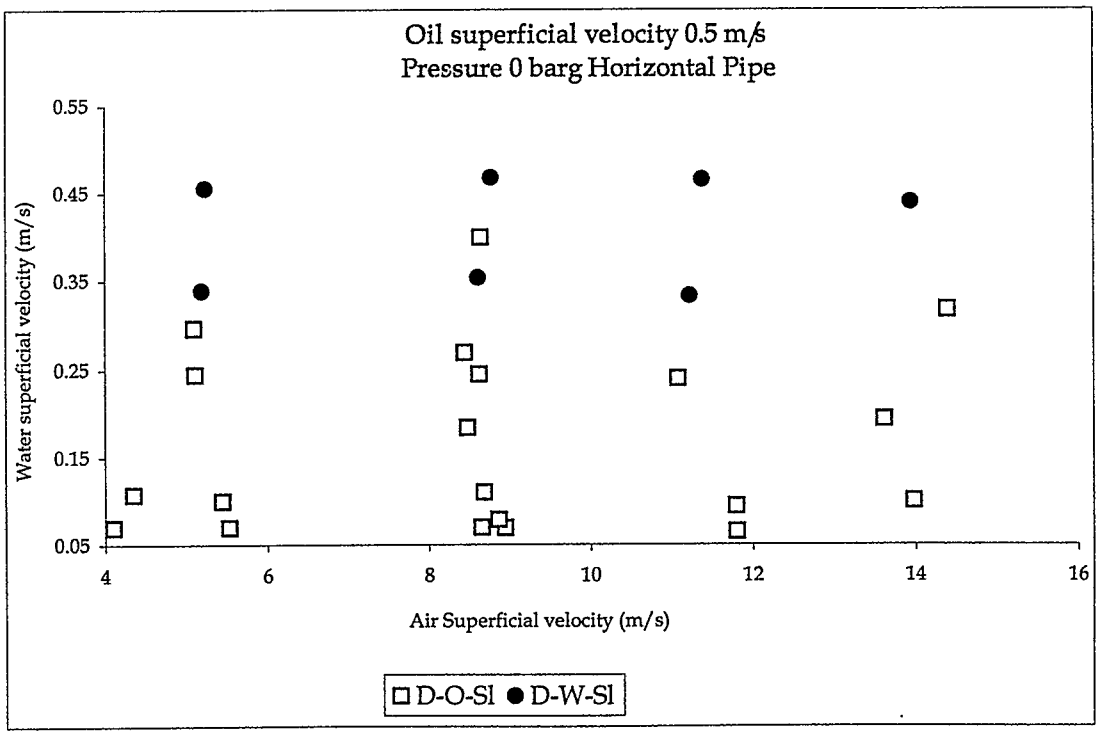


Figure 5.1: WASP Flow Pattern Map for Horizontal Pipe at Atmospheric Pressure at Oil Superficial velocity 0.5 m/s

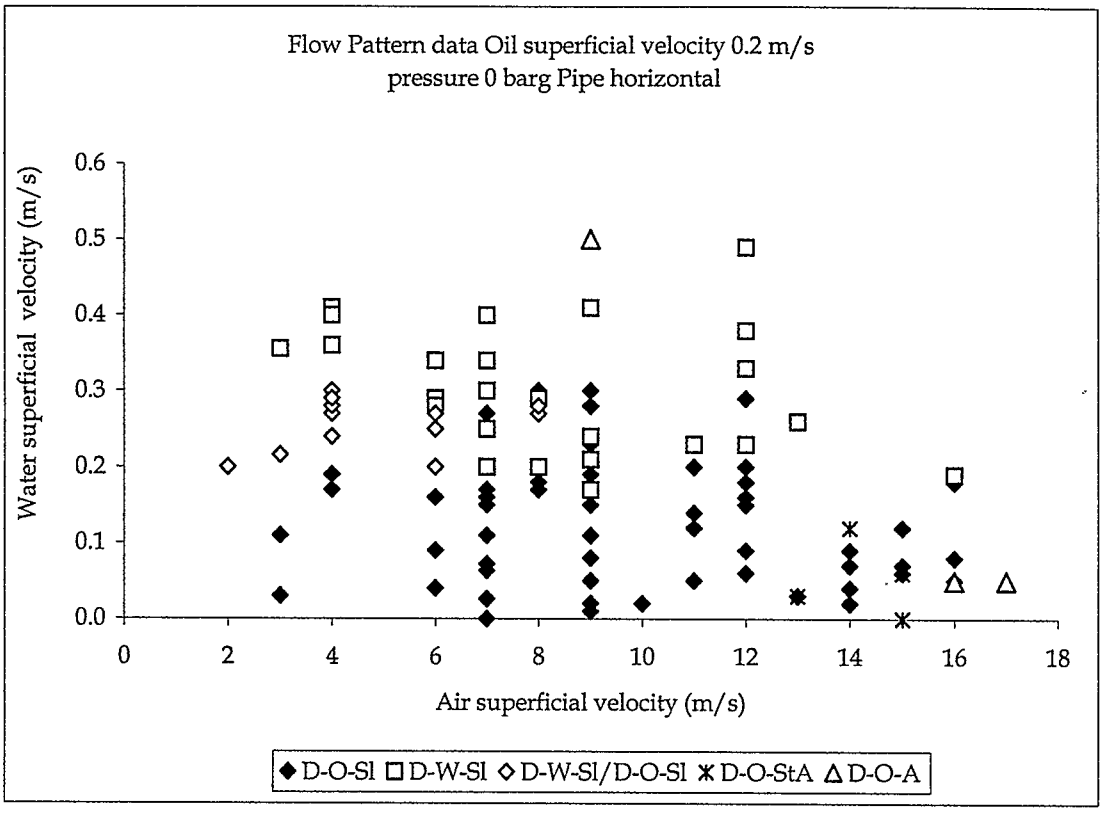


Figure 5.2: WASP Flow Pattern Map for Horizontal Pipe at Atmospheric Pressure at Oil Superficial velocity 0.2 m/s

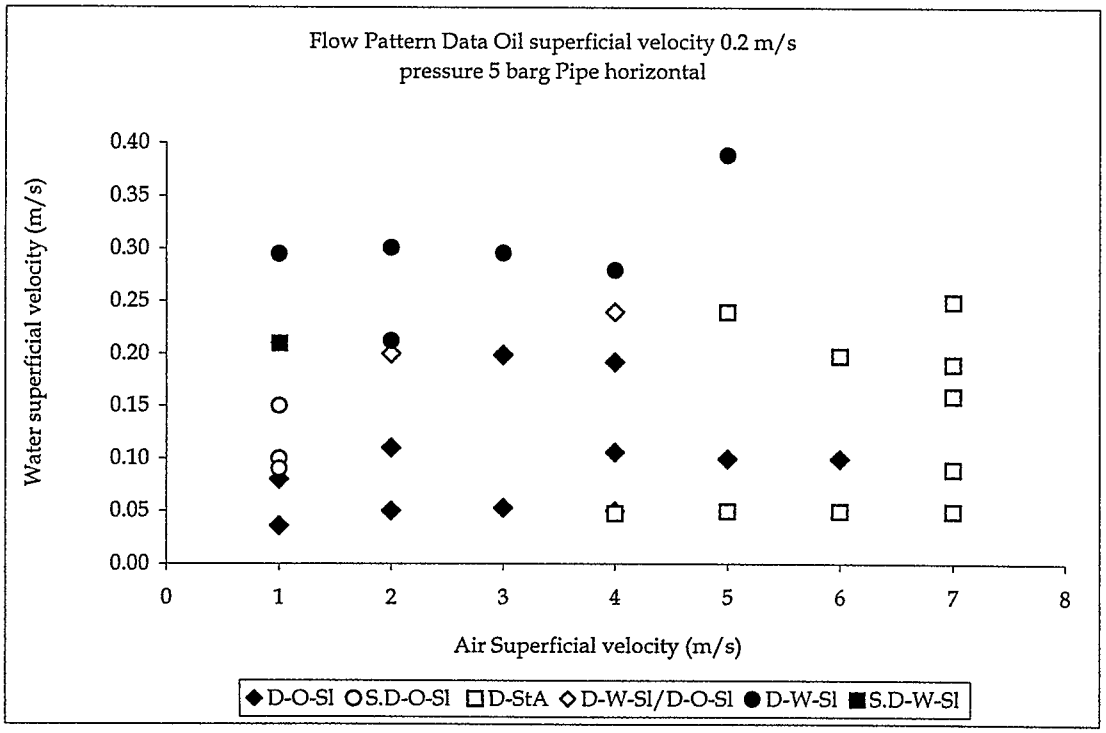


Figure 5.3: WASP Flow Pattern Map for Horizontal Pipe at 5 barg at Oil Superficial velocity 0.2 m/s

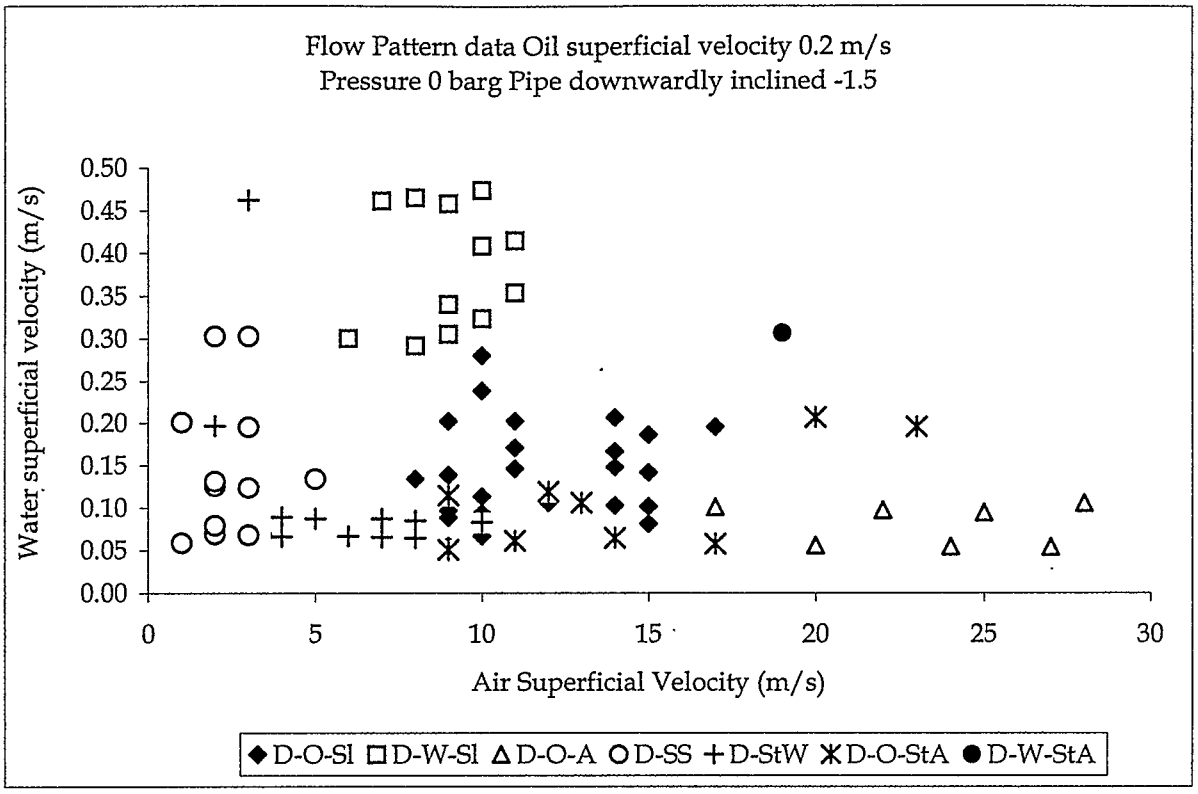


Figure 5.4: WASP Flow Pattern Map at 0 barg at Oil Superficial velocity 0.2 m/s for a pipe downwardly inclined 1.5° to the horizontal

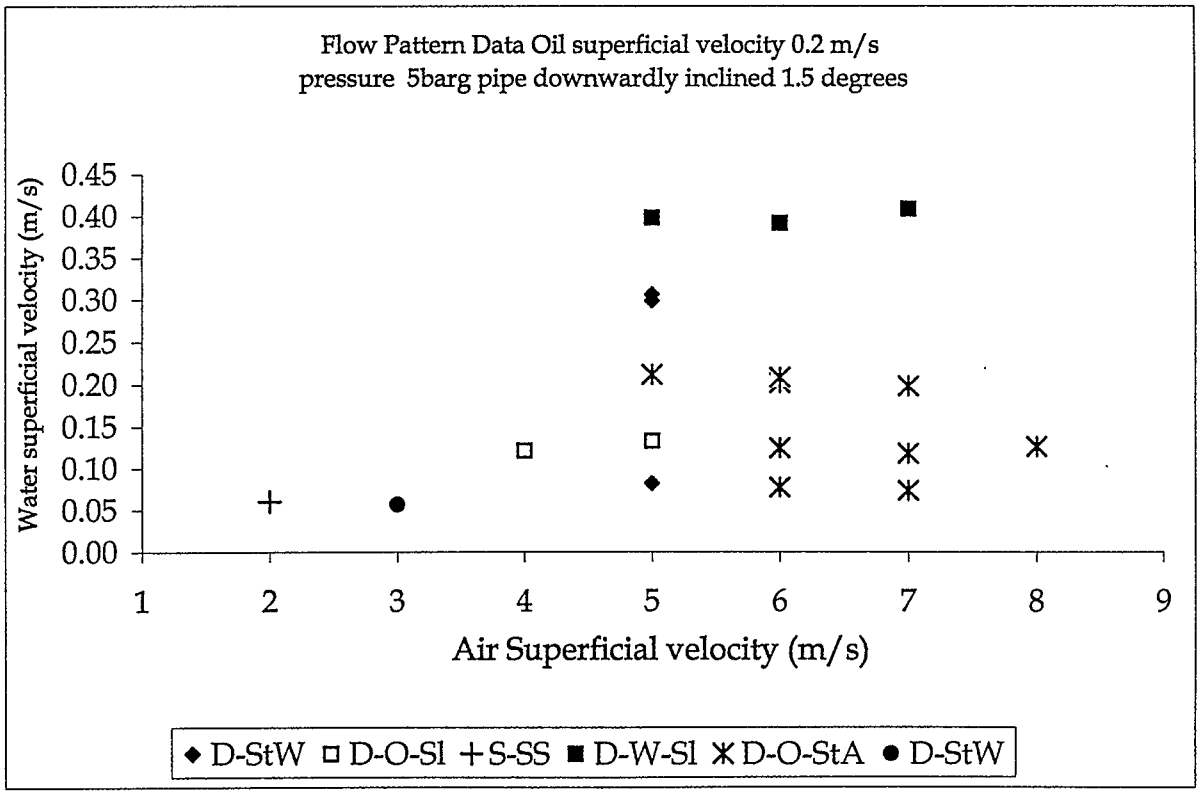


Figure 5.5: WASP Flow Pattern Map at 5 barg at Oil Superficial velocity 0.2 m/s for a pipe downwardly inclined 1.5° to the horizontal

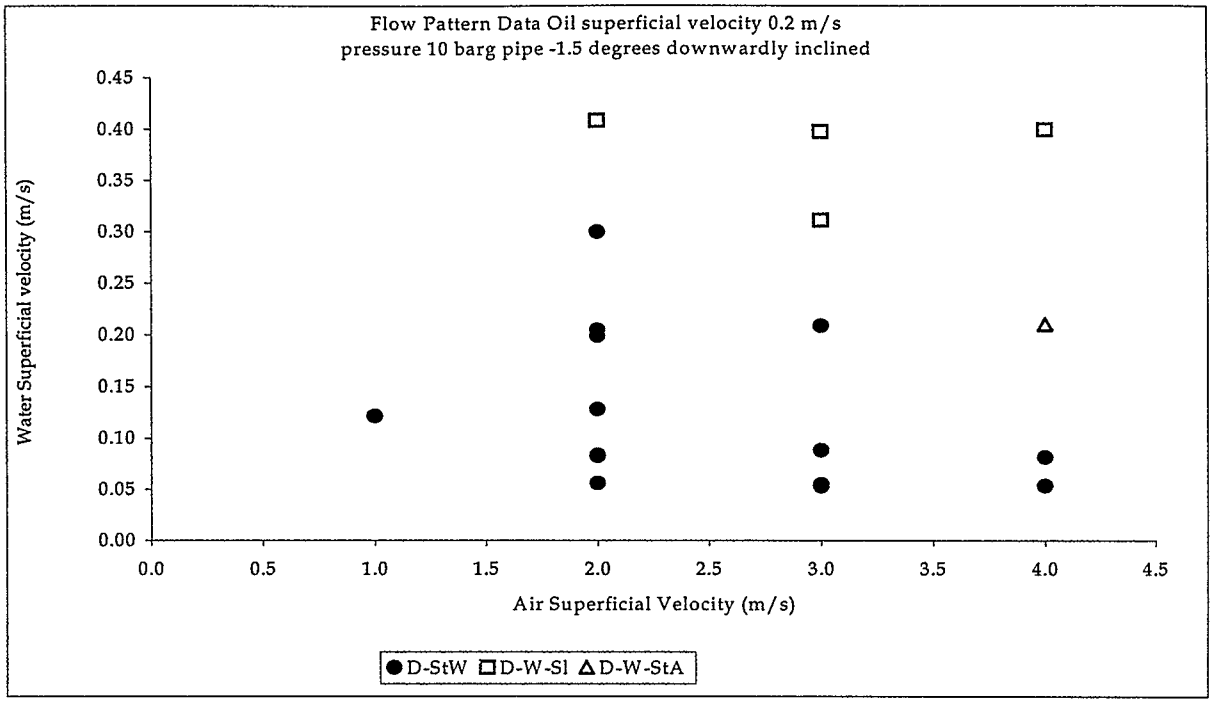


Figure 5.6: WASP Flow Pattern Map at 10 barg at Oil Superficial velocity 0.2 m/s for a pipe downwardly inclined 1.5° to the horizontal

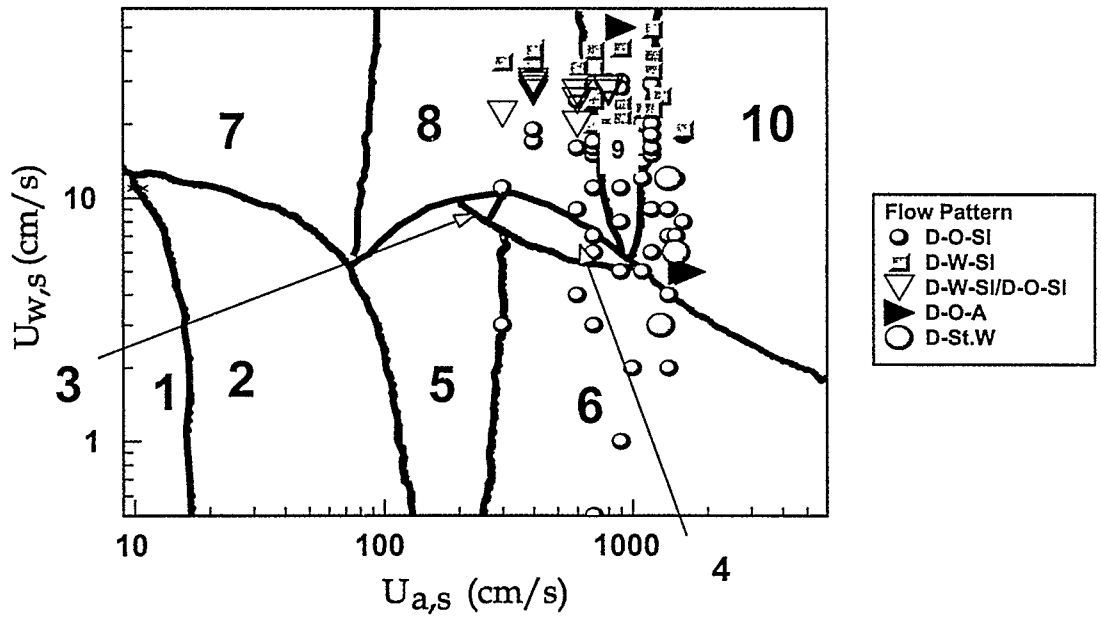


Figure 5.7: WASP horizontal flow pattern data obtained at oil superficial velocity 0.2 m/s plotted on the horizontal flow pattern map of Açikgoz et al.

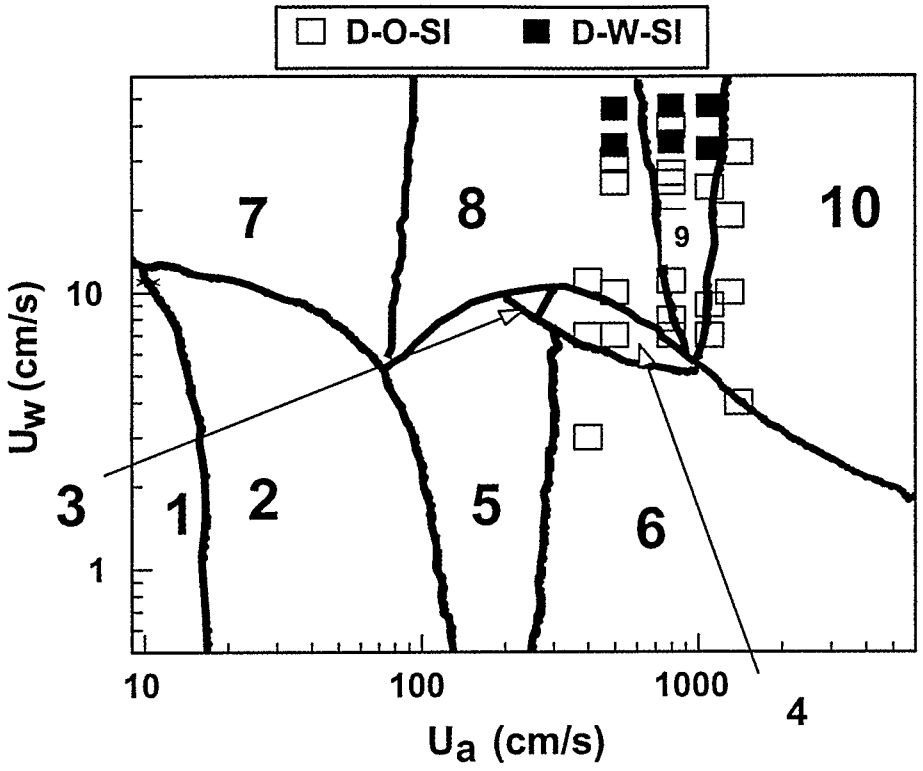


Figure 5.8: WASP horizontal flow pattern data obtained at oil superficial velocity 0.5 m/s plotted on the horizontal flow pattern map of Açikgoz et al.

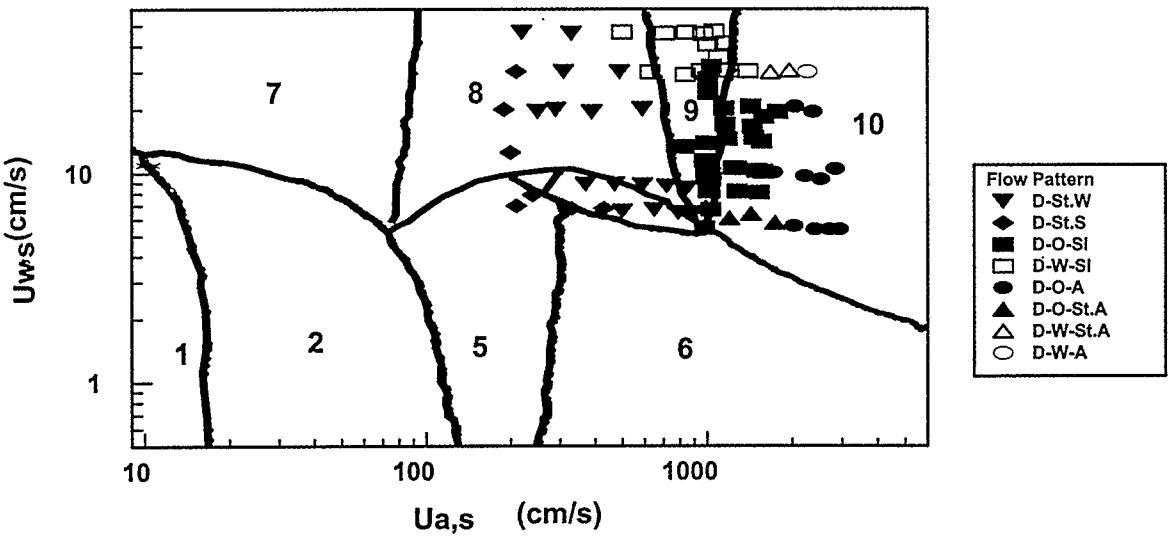


Figure 5.9: WASP flow pattern data obtained at an oil superficial velocity of 0.2 m/s with the pipe downwardly inclined at an angle of –1.5° to the horizontal plotted on Acikgoz et al's Horizontal Flow Pattern Map (1992)

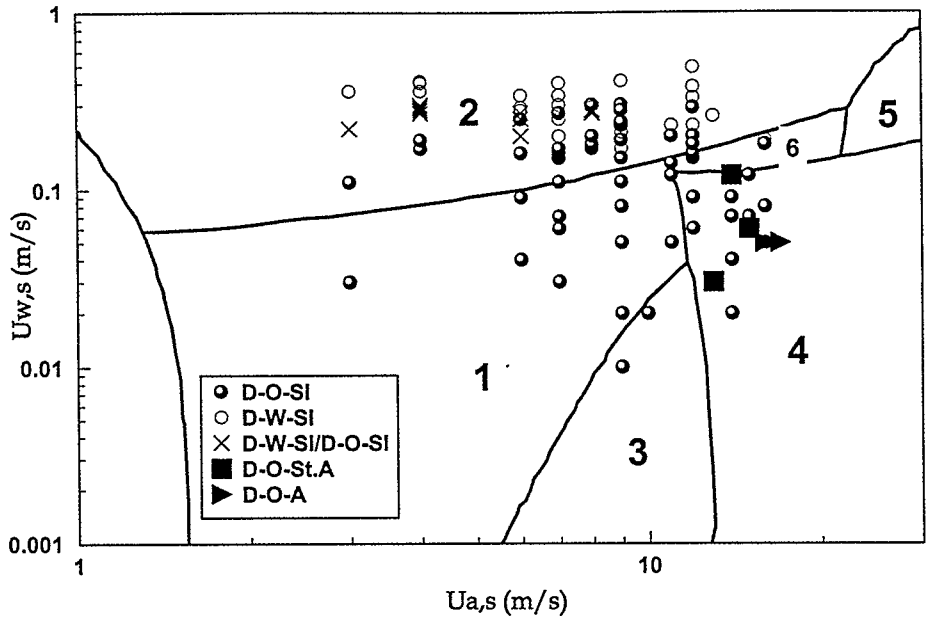


Figure 5.10: WASP horizontal flow pattern data obtained at an oil superficial velocity of 0.2 m/s plotted on Pan's Horizontal Flow Pattern Map (1996)

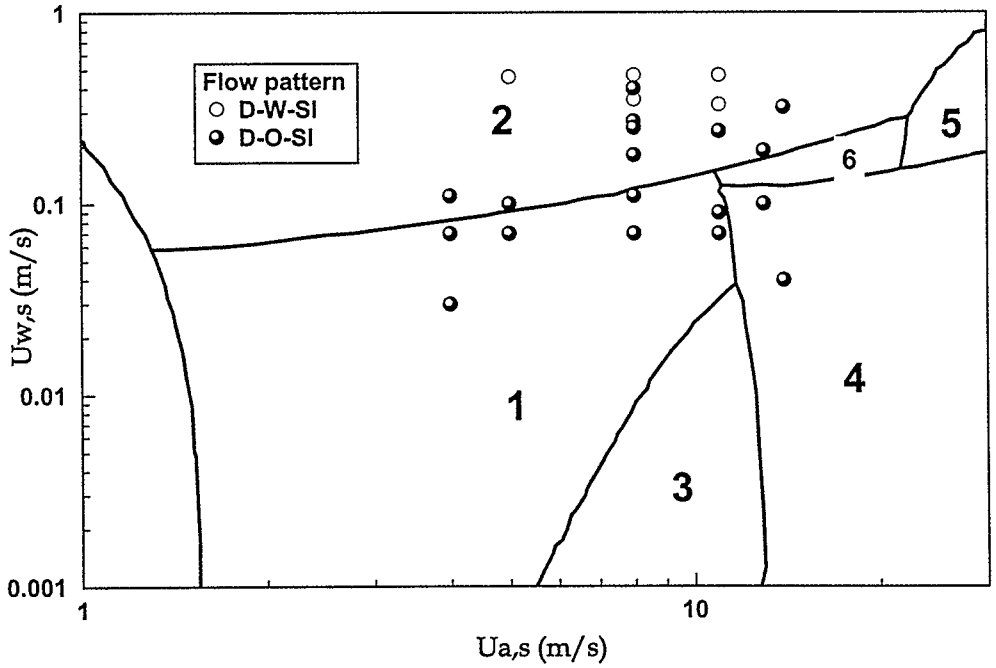


Figure 5.11: WASP horizontal flow pattern data obtained at an oil superficial velocity of 0.5 m/s plotted on Pan's Horizontal Flow Pattern Map (1996)

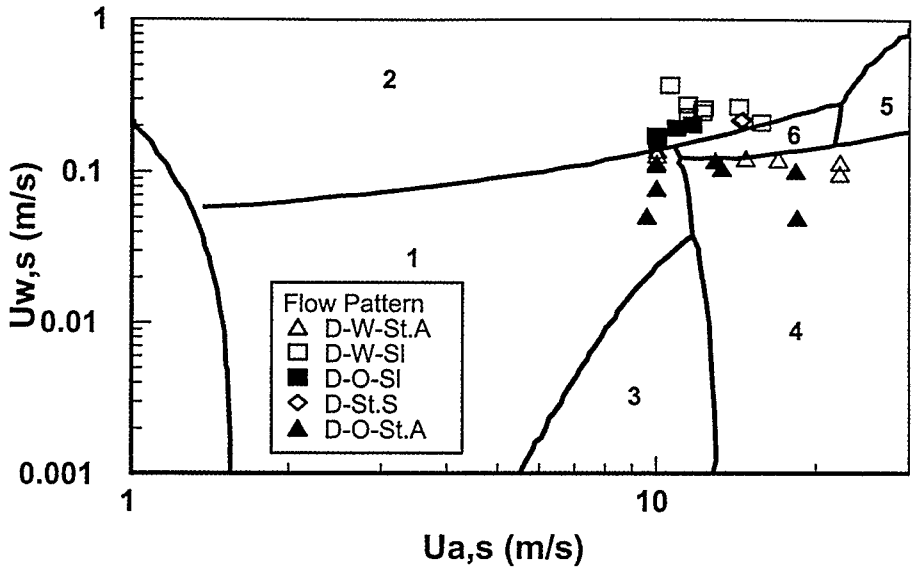


Figure 5.12: WASP flow pattern data obtained at an oil superficial velocity of 0.1 m/s with the pipe downwardly inclined at an angle of –1.5° to the horizontal plotted on Pan 's Horizontal Flow Pattern Map (1996)

Chapter 6

COMPARISON OF DATA WITH PREDICTIVE METHODS

As will have been seen from the literature survey in Chapter 2, there is a dearth of predictive models for three-phase flows. The common approach is to use an adaptation of models for two-phase flows. Such models themselves fall into three main categories namely:

(1)Purely empirical correlations based on reduction of experimental data. These models also fall into two main groups namely those which are based on the assumption of a *homogeneous flow* which can be calculated in the same manner as single phase flows by ascribing suitably averaged viscosity and density. These models are exemplified by the Dukler *et al.* (1964) correlation. The other main group of empirical models is the *separated flow models*. Here, it is recognized that the two phases flow at different velocities and the pressure drop is calculated by means of empirically correlated *multipliers* (see Chapter 2), which multiply the pressure gradients for single phase flows of the phases to obtain the two-phase pressure drop. This group of correlations is typified by the classical Lockhart and Martinelli (1949) correlation. In the separated flow models, correlations for *phase fraction* are also required to calculate total pressure gradient in non-horizontal flows. Some models are essentially hybrids between these two groups; thus the widely used Beggs and Brill (1973) correlation uses a homogeneous friction factor but relates this to the (non-homogeneous phase fractions).

(2) One-dimensional two-fluid models. Here, the two phases are assumed to flow in separate fields, the interactions between these fields and the wall and between the fields, being represented by appropriate closure laws. Recent studies of such models for stratified flow are reported, for instance, by Shaha (1999). As commonly applied in commercial codes, the two-fluid model is not very suitable for prediction of hydrodynamic slug flows, though one of the notable successes of these codes is in predicting "severe" or "terrain-induced" slugging where the mechanisms are rather different. However, if a large number of grid nodes are used (i.e. orders of magnitudes more than are

commonly used in applications of the commercial codes) then many of the features of two-phase hydrodynamic slug flow can be captured (Issa, 1998).

(3) Phenomenological models which take account of complexities of real flows such as the behaviour of slugs in slug flow and droplet entrainment and deposition in annular flow. Typical of such models are those of Taitel and Barnea (1990) for slug flow, Hewitt and Govan (1990) for annular flow and Badie (2000) for stratifying annular flow.

The predominant regime in the present study was slug flow, accounting for around 75% of the data. A decision was made, therefore, to focus the comparisons reported in this Chapter on the *slug flow data only*. An extensive data set (and associated analysis) on three-phase stratified flows was presented by Khor (1998), who concluded that the multi-fluid model (with optimized choices for closure laws) gave the best predictions for this case. It was felt, therefore, that the present exercise should concentrate on the (more complex) case of slug flows.

The complexity of the interactions between the liquid phases in three-phase slug flow, coupled with the gas-liquid interactions (which exist in both two-phase and three-phase slug flow) make prediction of slug flows a formidable challenge. The approach taken here is to evaluate the application of the empirical models for two-phase flow to the whole range of present data for pressure drop and liquid holdup and to evaluate the applicability of two-phase phenomenological models for slug flow to the three-phase slug flow pressure drop and holdup data. No attempt has been made to use the one-dimensional two-phase two-fluid model approach directly (though the model is implicit in one of the phenomenological models studied, i.e. that of Taitel and Barnea, 1990).

In the use of two-phase flow prediction methods for predicting three-phase flows the assumption is made here that the two liquid phases can be represented as a single fluid flowing at a superficial velocity equal to the sum of the superficial velocities of the water and oil. This single fluid has a density ρ_L given by the homogeneous model:

$$\rho_L = \rho_W \lambda_W + \rho_O (1 - \lambda_W) \tag{6.1}$$

Where ρ_W and ρ_O are the water and oil densities respectively and λ_W is the water-cut (i.e. volume fraction of water in the total liquid volume flow). Calculation of the viscosity of the single combined liquid presents particular difficulties and was a major focus of the analytical work performed as part of the present study. The viscosity model developed is described in detail in Section 6.1. In addition to the data for pressure drop and holdup, data were also obtained for slug characteristics (slug velocity, slug frequency, slug length and slug body total liquid holdup). These data have also been compared with various two-phase flow correlations.

A particularly interesting feature of the detailed data obtained on slug characteristics was the observation that there was a peak in translational velocity of the slugs at the phase inversion point. In order to investigate this further, calculations were carried out using a computational fluid dynamic code (CFX 4.2). These calculations are described in Section 6.8.

In what follows, Section 6.1 describes the new viscosity model and Section 6.2 and 6.3 describe the comparisons of the pressure gradient data with empirical correlations and (for slug flow) with phenomenological models for two-phase flow respectively. Section 6.4 describes comparisons of the total holdup data with two-phase flow correlations for holdup and Sections 6.5 to 6.8 deal with the detailed slug parameters (slug frequency, slug body holdup, slug length and slug velocity respectively). Finally, Section 6.9 summarises the main findings and gives an overview of the situation regarding predictions of three-phase flows.

6.1 A MODEL FOR MEAN LIQUID VISCOSITY IN THREE-PHASE FLOW

The available methods for estimating the effective viscosity of the combined liquid phases in three-phase flow were described in Chapter 2. The present model has as its starting point the equation of Pan (1996), which is as follows:

$$\mu_L = (1 - C_M)\mu_{LIN} + C_M \mu_{NONLIN} \tag{6.2}$$

Where μ_{LIN} is a viscosity linearly interpolated between the oil and water viscosities in terms of water cut λ_W,

$$\mu_L = (1 - \lambda_W)\mu_O + \lambda_W \mu_W \tag{6.3}$$

and μ_{NONLIN} is a viscosity estimated from an equation which represents the anomalous viscosity around the inversion point. Pan (1996) used the equations of Brinkman (1952) as follows:

$$\mu_{NONLIN} = \frac{\mu_{cont}}{(1-\lambda_{dis})^{k_1}} \tag{6.4}$$

Where μ_{cont} is the viscosity of the continuous phase, λ_{dis} the concentration of the dispersed phase and k_1 is a constant with a recommended value of 2.5. In Equation 6.2, C_M is a *mixing degree coefficient* which Pan (1996) correlated by the following equation:

$$C_M = 1 - exp\left(\frac{-Re_{3p}}{K}\right) \tag{6.5}$$

Where Re_{3p} is a nominal three-phase Reynolds number given by:

$$Re_{3p} = \frac{\dot{m}DU_M}{(U_{G,S}\mu_G + U_{O,S}\mu_O + U_{W,S}\mu_W)} \tag{6.6}$$

Pan suggested a value of 15,000 for the constant K in Equation 6.5.

It should be noted that μ_{NONLIN} shows a discontinuity at the phase inversion point. Pan (1996) assumed an arbitrary value of λ_W=0.55 for the inversion point in analyzing his data. However, assuming that the peaks in pressure drop described in Chapter 4 are associated with phase inversion, it will be seen that the value of water-cut for phase inversion ($\lambda_{w,i}$) varies with flow conditions, particularly the air and liquid superficial velocities. Hence, without some sort of predictive technique for calculating $\lambda_{w,i}$, it is difficult to know the water-cut at which the phase inversion occurs.

Previous studies carried out in three-phase air-oil-water flow by Pan (1996) and Donnelly (1997) also showed that the phase inversion point, where the continuous liquid phase changes from oil to water or vice versa is influenced by superficial velocity.

The present data for horizontal flow, together with the data of Pan (1996) (representing a databank of over 1500 data points) were examined to establish the

conditions for phase inversion (i.e. the position of the peak in the pressure gradient versus water-cut curve).

From Figure 6.1, where the phase inversion water-cut has been plotted against the air superficial velocity at three different total liquid superficial velocities, it can be seen that the air superficial velocity exerts a stronger influence on the phase inversion water-cut than the total liquid superficial velocity for the range of conditions covered.

For a constant total liquid superficial velocity of 0.2 m/s, increasing the air superficial velocity from 2 m/s to 5 m/s leads to an increase in the phase inversion water-cut from approximately 40% to 46%. Increasing the air superficial velocity further from 5 m/s to 8 m/s leads to an increase in the phase inversion water-cut from 46% to 53%. The results for higher liquid superficial velocity were similar. For the two outlet pressures considered (near atmospheric and 5 barg), there was no discernible effect of pressure on the phase inversion point.

As a result of this, it was decided to focus on producing a correlation for the phase inversion water-cut as a function of only the gas superficial velocity. Although some data were obtained for slug flow beyond an air superficial velocity of 10 m/s, due to the fact that the nature of the slug flow for these velocities changed radically, due to the proximity to the slug/annular flow transition, it was decided not to include data points obtained under these conditions in the formulation of the empirical correlation.

A curve was fitted to the atmospheric pressure data presented in Figure 6.1 and is represented by the expression:

$$\lambda_{wi} = 0.3372 U_{G,S}^{\ 0.2219} \tag{6.7}$$

Although the present data at elevated pressure were limited, no significant trend in the phase inversion with pressure at given phase velocities could be discerned.

Extensive comparisons were made between two-phase empirical pressure drop and holdup correlations and data obtained for three-phase slug flow both in the present work and by Pan (1996). It was assumed that the liquid phase could be represented as

a single mixed liquid with a viscosity given by Equation 6.2. The following conclusions were reached from these comparisons:

(1) For the slug flow data, the value of C_M calculated from Equation 6.5 was generally close to unity since the liquid phase was well mixed. Thus the results were relatively insensitive to the parameter K in Equation 6.5; the value 15 000 suggested by Pan (1996) was therefore retained to allow the model for effective viscosity to be used also for stratified flows where C_M is low.

(2) On balance, the non-linear viscosity model of Hatschek (1928) performed slightly better than that of Brinkman (1952) which was recommended by Pan (1996).

To summarize, therefore the liquid viscosity model used in all the comparisons reported in this Chapter is as follows:

$$\mu_L = C_M \mu_{LIN} + (1 - C_M)\mu_{Ha} \tag{6.8}$$

Where μ_{Ha} is the viscosity given by the Hatschek (1928) equation as follows:

$$\mu_{Ha} = \frac{\mu_{cont}}{\left(1 - \lambda_{dis}^{\ k_2}\right)} \tag{6.9}$$

The continuous phase is oil for $\lambda_W < \lambda_{W,i}$ and is water for $\lambda_W > \lambda_{W,i}$ where $\lambda_{W,i}$ is the water cut for phase inversion obtained from the correlation given by Equation 6.7.

6.2 Comparison Of Data With Two-Phase Gas-Liquid Pressure Drop Correlations

A total of five empirical two-phase gas-liquid pressure drop correlations were selected for comparison with the three-phase pressure drop experimental data. A total of 186 data points were used in the comparisons; all were for the slug flow regime. In the comparisons of the three phase flow data with the two-phase flow correlations, the two liquid phases were treated as a single liquid phase with a mixed mean density ρ_L given by:

$$\rho_L = \rho_W \lambda_W + \rho_o(1 - \lambda_W) \tag{6.10}$$

Where ρ_W and ρ_O are the water and oil densities respectively and λ_W is the water-cut (fraction of input liquid volume flow which is water). The viscosity of the mixed liquid phase was calculated from the viscosity model described in Section 6.1. The following correlations were compared with the data:

Dukler *et al.* (1964) (Case 1) (Section 6.2.1)

Chisholm (1967) (Section 6.2.2)

Beggs and Brill (1973) (Section 6.2.3)

Lockhart and Martinelli (1949) (Section 6.2.4)

Schlichting (1970) (Section 6.2.5)

Details of these correlations are given in Chapter 2 (Section 2.1.2.1). In what follows, Section 6.2.1-6.2.5 report graphical comparisons. Section 6.2.6 then gives statistical data on the comparisons.

6.2.1 Dukler *et al.* (1964)

In Figures 6.2-6.4, the results obtained from a comparison between the homogeneous model correlation of Dukler *et al.* (1964) and the experimentally measured pressure gradient are presented.

In Figure 6.2, where the comparison has been made for a case of an air superficial velocity 4 m/s, total liquid superficial velocity 0.5 m/s and system pressure 0 barg, it can be seen that the Dukler *et al.* pressure gradient prediction agrees well with the experimental measurements. For oil-continuous flows, i.e. water-cuts between 0% and 50%, the correlation slightly under-predicts the measurements, with the greatest discrepancy occurring at a water-cut of 40%. However, for water-continuous flows, there is much better agreement between the correlation and the data.

In Figure 6.3, the experimental data and predictions are plotted for an air superficial velocity of 4 m/s, total liquid superficial velocity of 0.5 m/s and system pressure of 5 barg. The results of the comparison show larger discrepancies than those observed in Figure 6.2; for oil continuous flows, the Dukler *et al.* correlation under-predicts the data, with the maximum discrepancy occurring at a water-cut of 40%.

In Figure 6.4, showing experimental and calculated results for an air superficial velocity of 6 m/s, total liquid superficial velocity of 0.5 m/s and system pressure of 0 barg, good agreement is observed between the predictions and the experimental data for both oil and water-continuous flows.

In Figure 6.5, the predictions of the Dukler *et al.* correlation have been plotted against the experimentally measured pressure gradient for the entire data set. In general there is good agreement, with a tendency for the correlation to under-predict the measurements.

6.2.2 Chisholm (1967)

In Figures 6.6-6.8, the predictions of the pressure drop obtained using the correlation of Chisholm (1967) are presented. In Figure 6.6, for the case of an air superficial velocity of 4 m/s, total liquid superficial velocity 0.5 m/s and system pressure of 0 barg, it can be seen that although the correlation of Chisholm (1967) correctly predicts the trend in the pressure gradient data in the oil continuous region (the increase in pressure gradient with increasing water-cut), the correlation over predicts the measurements by a factor of 5 in this region.

For water-continuous flows, however, there is good agreement between the correlation and the measurements. The same type of performance is observed in Figures 6.7-6.8 for other experimental conditions. In Figure 6.9, where the comparisons between the Chisholm (1967) correlation and the entire data set has been made, it can be seen that there is poor agreement, with the correlation over-predicting the majority of the data.

6.2.3 Beggs and Brill (1973)

This correlation takes into account the effect of the nature of the flow pattern on the pressure drop through the liquid holdup. This occurs in the form of flow regime dependent correlations for the liquid holdup.

However, due to the fact that the flow pattern prediction criteria proposed by Beggs and Brill do not account for the effects of the liquid viscosity, use has been made of the various holdup correlations for the flow patterns observed in the actual experiments rather than those suggested by Beggs and Brill criteria. Using these latter criteria, larger discrepancies are observed.

In Figure 6.10, on comparing the Beggs and Brill (1973) pressure gradient correlation with the experimental measurements, it can be seen that the Beggs and Brill correlation predicts the trend in the pressure drop, although with a tendency to over-predict the pressure drop in both oil and water based flows. This trend is again observed in Figures 6.11 and 6.12, obtained for different sets of flow conditions and system pressure. Another common feature in Figures 6.10-6.12, is that the discrepancy between the prediction and the measurements is greater for oil-continuous flows than it is for water-continuous flows.

In Figure 6.13, where the predictions of the Beggs and Brill correlation are compared with the entire experimental data set, it can be seen there is a tendency (on average) for the correlation to over-predict the experimental data.

6.2.4 Lockhart and Martinelli (1949)

In Figures 6.14-6.16, the comparisons of the experimental data with the prediction of the Lockhart and Martinelli pressure gradient correlation are depicted. An illustration of the overall performance of the Lockhart and Martinelli correlation is shown in Figure 6.17, where the predictions of the correlation are compared with all the experimental data. It can be seen that the performance of Lockhart and Martinelli correlation is variable, with under prediction in some regions and over prediction in others.

6.2.5 Schlichting (1970)

The correlation of Schlichting (1970) was selected on the basis of the fact that that it had been modified for gas-oil-water three-phase flows. This correlation is similar to that utilized by Lockhart and Martinelli (1949) with the two-phase multiplier ϕ_L modified to account for oil viscosities ranging from 10 to 6000 mPas.

In Figures 6.18 and 6.19, comparisons between the prediction of the pressure gradient using the correlation of Schlichting (1970) and the experimental results are presented. It can be seen from Figures 6.18 and 6.19, that reasonable agreement is obtained between the correlation and the measured data for both oil and water continuous flows

though there is an overall tendency for the correlation to under predict the data. This tendency is confirmed in the plot shown in figure 6.20 where the prediction of the Schlichting correlation has been compared with the entire experimental data set.

6.2.6 Statistical Comparisons

It is of interest to compare the correlations in terms of statistically averaged parameters. The definitions of the parameters used in the data analysis on this basis are given in Appendix B. The results are shown in Table 6.1.

Correlation	Average Relative Error % (ARE)	Average Relative Absolute Error % (ARAE)	SD1 %	Average Error (Pa/m) (AE)	Average Absolute Error (Pa/m) (AAE)	SD2 (Pa/m)
Dukler *et al.* (1964)	**-11**	**29**	**37**	**-94**	**164**	**199**
Schlichting (1970)	**-16**	**35**	**42**	**-120**	**190**	**204**
Lockhart and Martinelli (1949)	**15**	**38**	**44**	**46**	**184**	**243**
Beggs and Brill (1973)	**30**	**42**	**52**	**142**	**214**	**257**
Chisholm (1967)	**190**	**196**	**286**	**937**	**972**	**1016**

Table 6.1: Summary of statistical errors for pressure drop correlations when compared to WASP data

Based on all of the statistical parameters, it will be seen that the correlation which performs best was in fact, the simplest, namely the Dukler *et al.* (1964) Case 1 (homogeneous) model! The Chisholm (1967) correlation performed notably badly whereas the other three correlations (Schlichting 1970, Begg and Brill 1973 and Lockhart and Martinelli 1949) performed only slightly worse than the Dukler *et al.* (1964) correlation. It will be noted that even the best correlation has a standard deviation of the order of 40% and it is clear that improved models are needed.

When the results shown in Table 6.1, are compared with the results obtained by Pan (1996), who also tested his three-phase air-oil-water WASP data with the predictions of a number of empirical pressure drop correlations, a number of similarities are observed. Pan (1996) also observed that the homogeneous model of Dukler *et al* (1964) was best for predicting his data set, which concurs with the results of Table 6.1. However the present data set is much more extensive than that of Pan.

Further analysis of the data reveals that, using the correlation of Dukler *et al.* (1964) the errors (Average Relative Absolute Error) in the water-continuous data and oil-continuous data are similar as shown in Table 6.2 (though the standard deviation for the water continuous data are higher). Similarly the error (Average Relative Absolute Error) for the near atmospheric pressure data are similar to that for the elevated pressure data as shown in Table 6.3, 2 (though the standard deviation for the near atmospheric data are higher).

	Average Relative Error % (ARE)	Average Relative Absolute Error % (ARAE)	SD1 %	Average Error (Pa/m) (AE)	Absolute Average Error (Pa/m) (AAE)	SD2 (Pa/m)
Oil-continuous	**-18**	**30**	**34**	**-139**	**189**	**192**
Water-continuous	**-6**	**32**	**45**	**2**	**143**	**216**

Table 6.2: Performance of Dukler *et al.* (1964) correlation when applied to oil-continuous and water-continuous data separately.

	Average Relative Error % (ARE)	Average Relative Absolute Error % (ARAE)	SD1 %	Average Error (Pa/m) (AE)	Absolute Average Error (Pa/m) (AAE)	SD2 (Pa/m)
Atmospheric data	**-3**	**28**	**41**	**-41**	**135**	**184**
Pressure data	**26**	**32**	**25**	**-187**	**215**	**188**

Table 6.4. Performance of Dukler *et al.* (1964) correlation when applied to atmospheric and pressure data points separately.

6.3 *Pressure Drop Phenomenological Models*

There is an increasing tendency to prefer phenomenological models for specific flow regimes to the use of the traditional empirical-type correlation. Though such models may not always predict given sets of data more accurately than the empirical correlations, it is often argued that they offer a more secure route for extrapolations.

Phenomenological models for two-phase, gas-liquid slug flow are reviewed in Chapter 2 (Section 2.1.3.1) and the methods selected for comparison with the present data (those of Bonnecaze *et al.*, 1971 and Taitel and Barnea, 1990) are described in detail.

In comparing the present data with the selected slug flow phenomenological models, it has been assumed that the liquids can be treated as a combined phase with a density given by Equation 6.10 and a viscosity given by the viscosity model described in Section 6.1.

6.3.1 Bonnecaze *et al.* (1971)

In Figures 6.21 and 6.22, the experimentally measured pressure gradient has been compared against the predictions of the slug model of Bonnecaze *et al.* (1971). It can be seen from the comparisons that the Bonnecaze *et al.* (1971) model over-predicts the measurements significantly in the oil-continuous region. However, for water continuous flows, the model tends to under-predict the data slightly. It should be remembered that the model is a simplistic one and that its assumption were selected on the basis of comparisons with air-water data thus the results obtained here are not too surprising.

6.3.2 Taitel and Barnea (1990)

In the present work, a modified version of the Taitel and Barnea model (1990) was applied in the prediction of pressure drop and holdup in three-phase flow. The main modification was to represent the two liquid phases as a combined liquid phase with a density calculated from Equation (6.10) and with a viscosity calculated from the model described in Section 6.1. A detailed description of this model can be found in section 2.1.3.1.2 of Chapter 2.

The closure laws used for the model were as follows:

(1) The empirical correlation of Gregory *et al.* (1978) was used to calculate the slug body holdup (see Chapter 2).

(2) The slug translational velocity was calculated using the expression:

$$U_t = C_o U_M + 0.542\sqrt{gD} \tag{6.11}$$

Where a value of 1.2 was utilised for C_o

(3) The relationship l_s=30D was used to calculate the slug length.

These closure laws were within the range recommended by Taitel and Barnea (see Chapter 2)

The predictions of the average pressure gradient obtained from the Taitel and Barnea (1990) slug flow model have been compared with the experimental data and the results are illustrated in Figures 6.23-6.24. The Taitel and Barnea model is in much better agreement with the present data than is the Bonnecaze *et al.* (1971) model. There is a tendency for the model to overpredict the data. This tendency is strongest when the pressure is highest (Figure 6.24) and when the gas superficial velocity is lowest. The following observations may be made about these comparisons:

(1) The closure laws used (selected from those recommended by Taitel and Barnea) are probably not adequate for the present (three-phase flow) case. Thus:

   (a) The slug body holdup predicted by the Gregory *et al.* (1978) correlation is somewhat lower than that observed experimentally (see Figures 6.61-6.62)

   (b) The slug translational velocity may be higher than that predicted by Equation (6.11) (i.e. the relationship proposed by Bendiksen, 1984) (see Section 6.8 below)

   (c) The observed slug lengths are considerably shorter than the 30D assumed in the model.

   These factors may combine to increase the actual pressure drop compared to that predicted. Thus, a higher slug body holdup would increase the pressure gradient in the slug body. A higher slug velocity and a lower slug length would tend to increase the effect of entrance conditions (increasing friction) at the slug front.

(2) Both the experimental data and the predictions show a pressure gradient which is insensitive to change of pressure (compare Figures 6.23 and 6.24). This finding is consistent with the two-phase air-water data of Manolis (1995) which showed that, for given superficial velocities the pressure gradient in slug flow did not vary significantly with pressure over a range of a factor of 25 in pressure (and hence density). This contrasts, however with the predictions of some of the empirical correlations where

strong variations of pressure gradient are observed with change of pressure (see Section 6.2 and Figures 6.2 to 6.20).

It is interesting to compare the performance of the Taitel and Barnea (1990) model with that of the best-fitting of the empirical equations, namely that of (1964). Such a comparison is given in Table 6.4. As will be seen, the performance of the Dukler *et al.* correlation and the Taitel and Barnea model are similar; however, the phenomenological model shows a more realistic prediction of the fact that the effect of pressure is small and one could conclude that such phenomenological models are a more reliable basis for extrapolation outside the range of experimental data.

	Average Relative Error % (ARE)	Average Relative Absolute Error % (ARAE)	SD1 %	Average Error (Pa/m) (AE)	Absolute Average Error (Pa/m) (AAE)	SD2 (Pa/m)
Dukler *et al.*(1942)	**-11**	**29**	**37**	**-94**	**164**	**199**
Modified Taitel and Barnea (1990)	**-18**	**35**	**41**	**-133**	**195**	**213**

Table 6.4: Statistical errors obtained on comparing the modified Taitel and Barnea model and the correlation of Dukler *et al* (1964) with the experimental data.

6.4 Mean Liquid Holdup Correlations

Measurements of the holdups of the individual liquid phases were made (see Chapter 4), their sum being the total liquid holdup. Only the latter can be compared with predictions from two-phase holdup correlations. The total holdup data was compared with predictions from various liquid holdup correlations, using a liquid phase density calculated from Equation (6.1) and a liquid phase viscosity determined from the viscosity model described in Section 6.1

The liquid hold up correlations of Lockhart-Martinelli (1949), Guzhov *et al.* (1967), Beggs and Brill (1973) and Minami and Brill (1987) were compared against the experimental measurements. A description of these empirical correlations is given in Chapter 2.

6.4.1Lockhart and Martinelli (1949)

In Figures 6.25-6.27, the experimentally measured total liquid holdup ε_L, measured using the dual-energy gamma densitometer, is compared with the predictions of the holdup correlation of Lockhart and Martinelli.

In Figure 6.25, it can be seen that the Lockhart and Martinelli holdup correlation correctly predicts the increase in total liquid with increasing water-cut, for water-cuts between 0% and 40%, as well as the subsequent decrease in the total liquid holdup for water-cuts greater than 40%. The reason why the Lockhart and Martinelli correlation correctly predicts the trend in the total liquid holdup is because it accounts for the influence of the liquid viscosity.

However, though the Lockhart and Martinelli correlation predicts the correct trends (Figure 6.25), the correlation over-predicts the measured total liquid holdup for oil and water-continuous flows at the lower (near atmospheric) pressure. As the system pressure is increased from 0 barg to 5 barg, the correlation (see Figure 6.26) over-predicts the measured holdup, for oil-continuous flows and under-predicts the holdup for water-continuous flows. A common trend in Figures 6.25 and 6.26 is that the discrepancy between the measurements and the correlation is lower for water continuous flows than for oil-continuous flows. This probably reflects the data on which the correlation is based.

At an air superficial velocity of 6 m/s, total liquid superficial velocity 0.5 m/s at 0 barg (see Figure 6.27), the result obtained is similar to that observed in Figure 6.25.

A comparison has been made between the predictions of the holdup correlation of Lockhart and Martinelli and the experimental data in Figure 6.28; there is a general tendency for the correlation to over-predict the data.

6.4.2Guzhov *et al.* (1967)

In Figures 6.29 to 6.31, the experimental data are compared with the correlation of Guzhov *et al.* (1967). All the figures, show that the correlation fails to predict the trend in the total liquid holdup with water-cut correctly. In fact, the correlation

predicts a constant liquid holdup for water-cuts ranging from 0% to 100%. The reason for this is because the holdup expression, (Equation 2.41) does not to include the liquid viscosity.

As in the case of the Lockhart and Martinelli (1949) correlation, the discrepancy between the Guzhov *et al.* (1967) correlation and the measurements is more pronounced for oil-continuous flows. Figure 6.32, shows the tendency for the Guzhov *et al.* correlation to under-predict the data set.

6.4.3 Beggs and Brill (1973)

The Beggs and Brill (1973) correlation was based on liquid holdup measurements carried out using quick closing valves, with air and water as the test fluids. The correlation was developed to be applicable to a wide range of flow patterns as well as pipe inclinations (-90° to +90°).

Comparison between the Beggs and Brill liquid holdup correlation and the present WASP horizontal three-phase flow experimental data is illustrated in Figures 6.33-6.35. From the comparisons, it can be seen that the Beggs and Brill correlation does not take adequate account of the effect of the liquid viscosity on the total liquid holdup.

Figures 6.33-6.35 show that the Beggs and Brill correlation under-predicts the total liquid holdup for water-continuous and oil–continuous flows, although the discrepancy in the water-continuous flows is less pronounced, probably due to the fact that the correlation is based on data obtained from an air-water two-phase system.

The Beggs and Brill correlation is compared with the entire data set in Figure 6.36. As can be seen the correlation under-predicts the data over the full range.

6.4.4 Minami and Brill (1987)

Figures 6.37 to 6.39 show comparisons between the experimental data and the holdup correlation of Minami and Brill (1987). In Figure 6.37 which has been plotted for a case of air superficial velocity 4 m/s, total liquid superficial velocity of 0.5 m/s, and system pressure 0 barg, it can be seen that the correlation of Minami and Brill (1987) correctly predicts the trend of the variation in the total liquid holdup with water-cut, although the predicted variation is quite small compared to that observed experimentally.

However, the Minami and Brill correlation over-predicts the results obtained from the experiments for both oil-continuous and water-continuous flows. The same result is obtained is shown in Figures 6.38 and 6.39. The Minami and Brill correlation over-predicts nearly all of the data set as can be seen from Figure 6.40.

6.4.5 Statistical Comparisons

The statistical errors obtained in comparing the mean liquid holdup correlations with the experimentally measured mean liquid hold up are shown in Table 6.5:

Correlation	Average Relative Error % (ARE)	Average Relative Absolute Error % (ARAE)	SD1 %	Average Error (Pa/m) (AE)	Absolute Average Error (AAE)	SD2
Guzhov (1967)	**-17**	**20**	**16**	**-0.068**	**0.075**	**0.06**
Lockhart and Martinelli (1949)	**26**	**30**	**26**	**0.0730**	**0.093**	**0.081**
Beggs and Brill (1973)	**-32**	**32**	**16**	**-0.11**	**0.11**	**0.06**
Minami and Brill (1987)	**62**	**62**	**31**	**0.196**	**0.20**	**0.07**

Table 6.5: Summary of statistical errors for empirical liquid holdup correlations when compared to WASP mean liquid hold-up data

It can be seen from Table 6.5 the lowest errors are observed with the correlation of Guzhov *et al.* However, this correlation fails to account for the effect of the liquid viscosity on the total liquid holdup, a trend clearly seen in the data. The Lockhart and Martinelli correlation most clearly predicts this trend but is in relatively poor agreement with the data.

6.5 SLUG FREQUENCY

The two-phase gas-liquid slug frequency correlations of Gregory and Scott (1969), Heywood and Richardson (1979), Tronconi (1990), Hill and Wood (1990) and Manolis (1995) were compared with the experimental data. To adapt these correlations for the three-phase air-oil-water data, the liquids were treated as a single combined phase having a density given by Equation 6.1 and a viscosity given by the viscosity model described in Section 6.1.

6.5.1 Gregory and Scott(1969)

This correlation was selected because of its simplicity and its wide use. Details of the correlation are given in Chapter 2 (see Equation 2.119)

In Figures 6.41-6.43, the prediction from the correlation of Gregory and Scott has been compared with the experimentally measured slug frequency. It can be seen from the Figures that the correlation of Gregory and Scott fails to predict the trend in the slug frequency. In the oil continuous region, the correlation under-predicts the experimental data, and fails to predict the rise in slug frequency with increasing water-cut for water-cuts between 0% and 40%. The reason for this can be attributed to the fact that the correlation does not account for the effect of the liquid viscosity on the slug frequency. In fact, the correlation assumes that the slug frequency is a function of only the gas and liquid superficial velocities and the pipe diameter.

In Figure 6.44, the predictions of the Gregory and Scott correlation have been compared with the entire data set. The greatest discrepancy occurs for the higher slug frequencies (slug frequency > 0.4 Hz). Overall there is a tendency for the correlation to under-predict the data.

6.5.2 Heywood and Richardson (1979)

This correlation was developed based on γ-ray measurements of the liquid holdup in a 1.65-inch internal diameter pipeline. By determining the power spectral density functions (PSD) and the probability density function (PDF), Heywood and Richardson were able to estimate the slug frequency. Details of the correlation are given in Chapter 2.

The predictions of this correlation have been compared with the experimental measurements and the results are shown in Figures 6.45-6.47 for different sets of conditions of air and liquid flowrates and system pressures.

From the comparisons in Figures 6.45 and 6.47, it can be seen that the correlation of Heywood and Richardson does not account for the influence of the water-cut on the slug frequency. For oil-continuous flows, the correlation under-predicts the data, while for water continuous flows, the correlation predicts higher values than those observed experimentally. The discrepancies between the predictions of the correlation and the measurements appear greater for oil-continuous flows, reflecting, once again, the source of the correlations.

The predictions of the Heywood and Richardson correlation are compared with all the experimentally measured values in Figure 6.48. As with the Gregory and Scott correlation, the greatest discrepancy occurs for higher slug frequencies.

6.5.3 Tronconi (1990)

The expression for the slug frequency using the semi-empirical approach of Tronconi is given in Equation (2.123). The values of U_G, the actual gas velocity and h_g, the gas height have been calculated by using the Taitel and Dukler (1976) model for equilibrium stratified two-phase flow. This model was adapted for the three-phase flow case by treating the oil and water as a single fluid with the mixture density calculated using Equation 6.1 and the mixture viscosity using the model described in Section 6.1. Because of the turbulent nature of the flow a value of 15 was assumed for the ratio f_i/f_g. Since all the variables in Equation (2.123) depend only on the dimensionless liquid height, the equation can be solved for the liquid film thickness. Results of the comparison between the correlation of Tronconi (1990) and the experimental data are illustrated in Figures 6.49-6.51. From the figures, it can be seen that the correlation accounts for the influence of the water-cut on the slug frequency. This is achieved through the effect of the dimensionless liquid height

However, for the higher pressure data shown in Figure 6.50, there is significant discrepancy between the prediction and the data and this is probably due to the fact

that the correlation attributes a more significant effect of the system pressure (i.e. gas density) on the slug frequency than is observed in the experimental data.

The relatively poor performance of the Tronconi correlation in predicting the entire data set is shown in Figure 6.52.

6.5.4 Hill and Wood (1990)

The Hill and Wood (1990) correlation is described in Chapter 2 (see Section 2.1.3.2.4). This correlation also uses the stratified flow liquid height and therefore accounts for the effect of the liquid viscosity on the slug frequency through the calculated liquid height.

In Figures 6.53-6.55, the correlation is compared with the experimental data. The Hill and Wood (1990) correlation, predicts the increase in slug frequency with increasing water-cut for oil-continuous flows. However, the correlation significantly under-predicts the data for water-cuts between 0 % and 40%. At the phase inversion point there is a closer match with the data. However for water-continuous flows, the correlation under-predicts the data.

Figure 6.56 summarises the comparison between the Hill and Wood correlation and the experimental data. There is a general trend towards under prediction.

6.5.5 Manolis (1995)

Because of the inadequacy of existing slug frequency correlations in predicting his data, Manolis, developed a new slug frequency correlation based on seven non-dimensional numbers. The correlation is described in Chapter 2.

It can be seen from Figures 6.57–6.59, where the predictions of the correlation and the measured slug frequencies have been plotted, that the Manolis (1995) correlation accounts for the effect of the liquid viscosity on the slug frequency.

In Figures 6.57-6.59, it can be seen that water-cuts between 0% and 20%, there is good agreement between the correlation and the measurements. In the phase inversion region, the correlation over-predicts the data in the oil continuous region

and under-predicts the data for water-continuous flows. However, there is good agreement between the correlation and the measurements for water-continuous flows. The comparison between the correlation and the complete data set is shown in Figure 6.60. Considerable scatter is demonstrated.

6.5.6 Statistical Comparisons

The error analysis relating to the comparisons between the above-mentioned slug frequency correlations and the data is summarized in Table 6.6:

Correlation	Average Relative Error % (ARE)	Average Relative Absolute Error % (ARAE)	SD1 %	Average Error (Pa/m) (AE)	Absolute Average Error Hz (AAE)	SD2 Hz
Heywood and Richardson (1979)	-5	31	42	-0.04	0.084	0.09
Gregory and Scott (1969)	-32	40	31	-0.11	0.12	0.09
Hill and Wood (1990)	-19	49	58	-0.085	0.154	0.177
Manolis (1995)	42	70	114	0.13	0.21	0.33
Tronconi (1990)	262	280	600	0.95	1.01	2.63

Table 6.6:Table listing the statistical errors for various correlations' performance against slug frequency data

From Table 6.6 it can be seen that the lowest error for all the data is given by the Gregory and Scott (1969) and the Heywood and Richardson (1979) correlations. However, these correlations do not adequately represent the effects of water-cut (and hence mean viscosity).

6.6 SLUG BODY HOLDUP

The experimentally measured slug body holdup obtained using the dual-energy gamma densitometer has been compared against four slug body holdup correlations: Gregory *et al.* (1978), Ferschneider (1983), Malnes (1983) and Gomez *et al.*. (2000).

6.6.1 Gregory *et al.* (1978)

In Figures 6.61-6.63, the comparisons between the prediction of the slug body holdup correlation of Gregory *et al.* (1978) and the experimentally measured values are shown. In Figures 6.61-6.63, it can be seen that the Gregory *et al.* (1978) correlation predicts a constant slug body holdup with increasing water-cut, whereas the experimental data show that the water-cut has an influence on the average slug body

holdup. The correlation under-predicts the data for both oil and water-continuous flows (Figures 6.61-6.63).

6.6.2 Ferschneider (1983)

In Figures 6.64 and 6.65, the predictions of the slug body holdup correlation of Fershneider (1983) have been plotted together with the experimental data. Again, in contrast to the data, the Ferschneider correlation does not predict any influence of the water-cut on the slug body holdup. For an air superficial velocity of 4 m/s total liquid superficial velocity of 0.5 m/s and at a pressure of 0 barg (Figure 6.64), it can be seen that the Ferschneider correlation over-predicts the data in the oil-continuous region, whereas in the water continuous region there is a closer match with the data. On increasing the system pressure from 0 barg to 5 barg, the results (Figure 6.65), show that the Ferschneider correlation over-predicts the data in both water and oil continuous flows.

6.63 Malnes(1983)

In Figures 6.66 and 6.67, the results obtained from Malnes' (1983) slug body holdup correlation have been compared with the experimental data. The Malnes correlation does not account for the effect of the water-cut on the average slug body holdup, as there is no viscosity term in the correlation.

In Figure 6.66, where the average slug body holdup has been plotted against water-cut for an air superficial velocity of 4 m/s and total liquid superficial velocity 0.5 m/s for a system pressure of 0 barg, it can be seen that the Malnes correlation, under-predicts the data for both water and oil continuous flows, although the discrepancy between the predictions and the water-continuous data is more pronounced.

On increasing the system pressure from 0 barg to 5 barg, the experimental average slug body holdup results and the predictions are closer, although there is a tendency for the correlation to under-predict the data for water-continuous flows and over-predict the data for oil-continuous flows.

6.6.4 Gomez *et al.* (2000)

From an experimental database containing the slug body holdup data of Schmidt (1977), Kouba (1986), Rothe *et al.* (1986), Kokal (1987), Brandt and Fuchs (1989) and Felizola (1992), Gomez *et al.* (2000) were able to develop a correlation for the slug body holdup as a function of the slug Reynolds number and the inclination angle of the pipe. The correlation is described in Chapter 2.

The predictions using the correlation of Gomez *et al.* (2000) were compared with the experimental results and the results of these comparisons can be seen in Figures 6.68 and 6.69, where the average slug body holdup has been plotted against the water-cut. In Figure 6.68, plotted for the case of air superficial velocity 4 m/s, total liquid superficial velocity 0.5 m/s, atmospheric pressure for a horizontal pipe, it can be seen that the correlation of Gomez *et al.* (2000) over-predicts the data for oil-continuous flows, while for water-continuous flows, the correlation under-predicts the measurements.

In Figure 6.69, plotted for the same conditions as those in Figure 6.68, with the exception of the system pressure which has been increased from 0 barg to 5 barg, the same results are obtained on comparing the correlation of Gomez *et al.* (2000) to the data. For water-cuts between 0 % and 30%, there is agreement in the trend of the slug body holdup between the Gomez *et al.* correlation and the experimental data, as both show a slight increase in the slug body holdup with increasing water-cut for this range of water-cuts. However, as in the case of the low pressure data (Figure 6.68), the correlation of Gomez *et al.* (2000) over-predicts the data for oil-continuous flows and under-predicts the data for water-continuous flows.

6.7 SLUG LENGTH

Through calculating the slug velocity by cross-correlating the holdup signals of the two gamma densitometers, it was also possible to calculate the length of the slugs in three-phase air-oil-water slug flow. The results obtained have been compared with expressions and correlations postulated in the literature.

The correlations evaluated were those of Brill *et al.* (1979), Norris (1982) and Scott *et al.* (1986). These correlations are detailed in Chapter 2.

In Figures 6.70 and 6.71, the experimentally measured average slug lengths have been compared with these correlations. From the comparisons, it can be seen that all the correlations significantly over-predict the data. A possible reason for this is that the data on which the correlations are based were obtained from much larger diameter pipelines than that of the WASP facility.

Another important point to note is that most of the existing correlations assume the slug length to be a function of the pipe diameter alone, whereas the data show that the liquid viscosity clearly affects the slug length. However, other researchers have proposed values for the slug length, which are much closer to that observed in the experiments.

Dukler and Hubbard (1975) observed a stable slug length to be about 12-30 diameters for horizontal slugs. This would translate to slug lengths of 0.9-2.3 m in the case of the WASP diameter of 0.0779 m. This range of slug lengths is much more commensurate with the present data.

6.8 SLUG VELOCITY

The present experimental data for slug velocity have been compared with two kinds of predictions, namely those from Equation 6.11 (from Bendiksen *et al.* 1984 and those obtained from a computational fluid dynamics (CFD) model. The comparisons are made in terms of the ratio of the translational velocity to the mixture velocity.

6.8.1 Comparisons with Bendiksen (1984) Equation

Bendiksen suggested the use of Equation 6.11 for Fr<3.5 and the second term on the right hand side be omitted for higher Froude numbers. Comparison of this approach and the data are shown in Figure 6.72 with the parameter C_o being assigned values of 1.2 and 1.3 respectively. As will be seen the equation under-predicts the data (even with C_o=1.3) and does not predict the observed peak in translational velocity near the phase inversion point.

6.8.2 CFD Predictions of Translational Velocity

It is clear from Figure 6.72 that there is an additional effect not predicted by Equation 6.11. It seems likely that this is related to the change of effective liquid viscosity as the phase inversion point is approached. The influence of liquid viscosity in two-phase vertical slug flow has been investigated by Frechou (1986) who showed that the translational velocity of the slugs increased when the Reynolds number in the slug became low, probably due to laminar rather than turbulent flow occurring in the slug. It was decided, therefore to investigate this effect using CFD modelling. Again the liquids were assumed to be represented by a combined liquid phase having a density given by Equation 6.1 and a viscosity given by the model described in Section 6.1. In what follows, previous work on CFD simulation of slug flow is first summarised (Section 6.8.2.1) and then the basic elements of the commercial code used (CFX 4.2) are briefly explained (Section 6.8.2.2). Section 6.8.2.3 describes the basic set-up and Section 6.8.2.4 presents the results.

6.8.2.1 Previous Work On CFD Prediction Of Slug Translational Velocity

Hope (1990), using the PHOENICS code, showed that it was possible to simulate a single slug tail in horizontal flow by utilising a moving frame coordinate system thereby trapping the slug within the computational domain. However, no quantitative results were shown.

Pan (1996), expanding on the method developed by Hope, investigated the motion of Taylor bubbles in horizontal, vertical upward and flows of different inclinations using the CFD Code CFDS FLOW 3D (now renamed CFX). His results for the translational velocity of the bubble were compared with the experimental data obtained by Bendiksen (1985) and Manolis (1995) with good agreement obtained. Pan also showed that translational velocity could increase with liquid viscosity at high liquid viscosity.

Shaha *et al.* (1996) used CFX4.1 (an earlier version of the CFX code) to simulate the rise of a Taylor bubble in a vertical pipe using both a moving frame model and a stationary frame model. He compared his results with those from the literature and obtained good agreement.

6.8.2.2 Description of the CFX software

The CFX software is supplied by AEA Technology and consists of three main types of modules:

- Pre-processing modules and Front-end module (CFX-SETUP) (CFX-MESHBUILD, CFX-BUILD)
- Flow solver module (CFX-F3D)
- Post processor module (CFX-VIEW, CFX-LINEGRAPH, CFX-VISUALISE)

Pre-processor

The pre-processor enables the user to input the necessary information needed to solve the flow problem. This is done via a user-friendly interface. The following are examples of the information needed to be specified by the user:

(a) Geometry Definition: The nature of the problem usually dictates the type of geometry to be employed.

(b) Grid Generation: this involves subdividing the computational domain into a grid of cells

(c) Chemical and Physical models: this involves choosing the type of models to be employed in the course of the simulation. An example involves the choice between laminar and turbulent flows.

(d) Numerical algorithm: this enables the user to select a scheme for discretising the relevant partial differential equations.

(e) Fluid properties: The physical properties of the fluids such as density, viscosity, can be specified. In addition, there is a built-in database, which contains the physical and chemical properties of a wide range of compounds.

(f) Boundary and Initial conditions: The user may set boundary and initial conditions which are necessary for the solution of the flow problem.

(g) Termination criteria: there are three possible options for terminating a simulation i.e. specifying a number of iterations, specifying the total simulation time or through the use of a simulation accuracy.

The shape of the computational domain dictates the type of grid to be employed in the simulation. For simple, regular shapes, a rectangular grid or a cylindrical grid may be used. However for more complex geometries, a body-fitted grid is suitable.

Flow solver

The flow solver carries out the simulation by first transforming the partial differential equations, and then discretizing the transformed equations before solving these equations.

If a rectangular or cylindrical grid is used, there is no need to transform the partial differential equations. However in reality most domain shapes are irregular and require the use of a body-fitted grid. However, the body fitted grid requires a transformation step. This step involves transforming the continuity Equation (6.12) and momentum equations Equations (6.13-6.15) from a Cartesian coordinate system into another coordinate system such as cylindrical depending on the geometry of the problem.

$$\frac{\partial u}{\partial x}+\frac{\partial v}{\partial y}+\frac{\partial w}{\partial z}=0 \tag{6.12}$$

$$\rho\left[\frac{\partial u}{\partial t}+u\frac{\partial u}{\partial x}+v\frac{\partial u}{\partial y}+w\frac{\partial u}{\partial z}\right]=-\frac{\partial P}{\partial x}+\mu\left[\frac{\partial^2 u}{\partial x^2}+\frac{\partial^2 u}{\partial y^2}+\frac{\partial^2 u}{\partial z^2}\right]+F_x \tag{6.13}$$

$$\rho\left[\frac{\partial v}{\partial t}+u\frac{\partial v}{\partial x}+v\frac{\partial v}{\partial y}+w\frac{\partial v}{\partial z}\right]=-\frac{\partial P}{\partial y}+\mu\left[\frac{\partial^2 v}{\partial x^2}+\frac{\partial^2 v}{\partial y^2}+\frac{\partial^2 v}{\partial z^2}\right]+F_y \tag{6.14}$$

$$\rho\left[\frac{\partial w}{\partial t}+u\frac{\partial w}{\partial x}+v\frac{\partial w}{\partial y}+w\frac{\partial w}{\partial z}\right]=-\frac{\partial P}{\partial z}+\mu\left[\frac{\partial^2 w}{\partial x^2}+\frac{\partial^2 w}{\partial y^2}+\frac{\partial^2 w}{\partial z^2}\right]+F_z \tag{6.15}$$

Where F_x, F_y and F_z are the x, y and z components of body forces.

Once the equations have been transformed they need to be converted into a form which the computer can handle, this is done by a procedure called *discretization*. Discretization converts the non-linear partial differential equations into a set of linear algebraic equations. The solver then solves the linear equations through a wide range of iterative techniques.

For the CFX code, the discretization is carried out using Taylor series expansion. A choice of several differencing schemes are offered to the user namely, central differencing schemes, downwind differencing scheme, etc. Detailed description of

the differencing schemes available within the solver can be found in the software manual (AEA Technology, 1997)

Post-processor

The processor consists of several graphic packages which convert information in the dump file into forms such as graphs, shaded contour plots, surfaces, etc for assessment by the user.

6.8.2.3 Simulation Set-Up

The simulation was set-up to calculate the slug translational velocity of a Taylor slug. The method used was the dam break model developed by Hope (1990) and adapted by Pan (1996) for the simulation of slug motion in two-phase flow.

The modelling of the slug tail is carried out by concentrating on the rear of the liquid slug body and the front of the elongated gas bubble behind it. This is the region between the dashed lines depicted in Figure 6.73. The slug translational velocity is U_t and the mean velocity of the liquid in the slug is U_L. In the present calculations, it is assumed that the slug body holdup is unity (i.e. no gas in the slug). This allows the effect of combined liquid phase viscosity to be investigated and is consistent with the fact that holdup is, indeed, relatively high for the conditions studied here. Making this assumption, it follows that U_L=U_M.

In the computational domain moving with the slug at the translational velocity U_T, liquid moves through the domain (from left to right in Figure 6.74) at a superficial velocity $U_L^{'}$, due to liquid being picked up at the slug front and discharged at the slug tail. It follows that:

$$U_L^{'} = U_T - U_L \tag{6.16}$$

To set up the initial condition for the simulation as shown in Figure 6.75, the left-hand side of the cylindrical pipe is filled with a uniform oil-water mixture. The right hand side of the cylindrical pipe (diameter 0.07792 m, length 1.2m) is filled with air and both halves of the pipe are separated by an imaginary dam at the start of the simulation.

The pipe wall is set to move at a velocity U_T so as to keep the slug tail within the computational domain and oil-water mixture with the same composition as that in the pipe is fed in with a velocity of $U_L^{'}$ to simulate the liquid pick up process which takes place at the front of the slug.

The simulation is initiated by specifying a value for U_T and then by a trial and error procedure, several values of $U_L^{'}$ are tried until steady state is reached. By steady state, one means that between successive simulation runs, there is no perceptible change with time in the volume fractions of both the gaseous and the liquid phases over the computational domain.

Figure 6.76, illustrates the geometry of the computational domain used in the simulation. A close view of the pipe inlet is also shown in Figure 6.77, where the mesh used to subdivide the inlet can be seen. The computational grid essentially consists of 20×10×10 cells.

6.8.2.4 Results

In Figures 6.78-6.80, typical graphic output files obtained from the CFX simulations of slug tails are shown for the case of mixture superficial velocity 4 m/s, and water-cut 40 %. These outputs are shown at 1, 2 and 3 seconds into the calculation from the "dam break" initial condition. The calculations show that a stable condition is achieved after 3s (there is little discernible difference between the results at 2 and 3s) and results at 2 or 3 seconds were used in further analysis. The liquid slug can be seen to the left of the diagrams, while the elongated bubble is on the right hand side of the figures.

The effect of the viscosity of the combined liquid phases on the bubble nose shape can be discerned more clearly from Figures 6.81-6.86, where the steady state results for the cases of water-cut 0%, 20%, 40%, 55%, 70 %, and 100% are plotted for a mixture velocity 4 m/s after 3 seconds of simulation time has elapsed.

For zero water cut, the bubble nose is near the top of the pipe but, as the water-cut (and hence effective viscosity) is increased up to the phase inversion point, the position of the nose moves towards the pipe axis. Beyond the phase inversion point, the bubble nose again moves towards the top of the pipe.

The changes in interface geometry shown in Figure 6.81-6.86 are also reflected in systematic changes in translational velocity. The translational velocity calculated is simply the sum of the mixture velocity U_M and the value of the superficial liquid velocity U_L' which is required to maintain the interface stationary in the computational frame (see Equation 6.16).

In Figure 6.87 the results obtained from the CFX code for the ratio of translational velocity to mixture velocity have been compared with the experimentally measured ratios. In Figure 6.87, it can be seen that the CFX code correctly predicts an increase in the ratio of the slug translational velocity to the total mixture superficial velocity with increasing water-cut for water-cuts ranging from 0% to 40%. The predicted and experimental values both fall at the phase inversion point. However for oil-continuous flows, the CFX code slightly under-predicts the data, though for water-continuous flows there is good agreement between the code and the experimental data. A possible reason for the significant under-prediction of the oil-continuous flow data could be due to the fact that the viscosity model used (Section 6.1) refers to average conditions in the flow whereas the local effective viscosity may vary along the slug unit. Nevertheless the trends are correctly predicted.

6.9 SUMMARY AND OVERVIEW

In this Chapter, a new model is presented for the prediction of the mixed liquid phase viscosity in three-phase flow is presented. A key component of the model is a correlation for phase inversion water-cut.

Using this viscosity model, the experimental data collected were tested against existing two-phase flow correlations for a number of parameters.

For pressure drop prediction, it was found that the correlations of Dukler *et al.* (1964) and Schlichting (1970) showed the closest match with the experimental data.

The total liquid holdup as measured by the dual-energy gamma densitometer was compared with the correlations of Lockhart and Martinelli (1949), Guzhov *et al.* (1967), Beggs and Brill (1973) and Minami and Brill (1987). Comparisons showed that the correlations of Beggs and Brill (1973) and Guzhov *et al.* failed to predict the influence of the water-cut on the total liquid holdup. Although the correlations of Lockhart and Martinelli and Minami and Brill accounted for the influence of the viscosity on the total liquid holdup, there was a tendency for these correlations to over-predict the experimental data.

In addition, the experimental data were compared with two phenomenological slug models by Bonnecaze *et al.* (1971) and Taitel and Barnea (1990). The models were modified and adapted to three-phase flow by assuming the two liquid phases could be represented as a combined liquid phase with the density calculated using a linear volume weighted expression and the viscosity calculated from the new viscosity model. Comparisons of these phenomenological models with the experimental data showed that the Bonnecaze *et al.* model significantly over-predicts the data, while the modified Taitel and Barnea model gives a good prediction of the data

In the present work, a wide range of new data were obtained for the characteristics of three-phase gas-liquid–liquid slug flows. These characteristics included slug frequency, slug body holdup, slug length and slug velocity. These results were compared with a variety of relationships for these parameters in gas-liquid slug flow, treating the liquid phases as a single fluid with a viscosity given by the new viscosity model.

It was shown that all the two-phase slug frequency correlations performed poorly against the data. The correlations of Gregory and Scott (1969) and Heywood and Richardson (1979) failed to account for the influence of the liquid viscosity on the slug frequency. Of the correlations which account for the influence of the liquid viscosity on the slug frequency, the correlation of Hill and Wood (1990) came closest in predicting the trend in the slug frequency with water-cut though the discrepancies were still large.

Likewise, in the case of the slug body hold-up prediction, none of the existing correlations (Gregory *et al,*.1978, Ferschneider, 1983 and Malnes, 1983) account for the observed influence of the liquid viscosity on the slug body holdup with the exception of Gomez *et al* (2000). All the correlations, predict a constant slug body holdup with increasing water-cut contrary to the experimental data. The results obtained in the present work are consistent with the results of Manolis (1995) and Nadler and Mewes (1995), which showed the significant effects of the liquid viscosity on the slug body hold-up even in gas-liquid flows.

None of the existing relationships in the literature predicted the trends in the slug lengths obtained The slug velocities were clearly influenced by water cut (and hence viscosity) and this is not predicted by currently used relationships (e.g. that of Bendiksen, 1984). The viscosity (i.e. water-cut) effect was investigated using CFD modeling in which the slug tail velocity and shape were predicted. The trend in slug velocity with water cut was correctly predicted and reasonable quantitative agreement obtained with the predicted values.

Though the application of two-phase flow models (through the use of a combined liquid phase) has proved reasonably successful and interesting, there is, of course, a need for more detailed models of three-phase flow. A number of programmes at Imperial College and elsewhere are pursuing this goal. For stratified flows, a three fluid model can be applied and the choice of closure relationship for such a model is discussed by (Khor, 1998). Models which aim to model mixing processes in liquid-liquid and liquid-liquid-gas flows are being pursued by Valle (2000) who is developing prediction schemes involving these models. The extension of the two-fluid dynamic models for slug flow (Issa and Woodburn 1998) to the three-phase flow case is also being pursued at Imperial College. Though these advanced models are not yet producing results which are significantly better than those obtained by adapting two-phase flow models, there is clearly much development potential for the future.

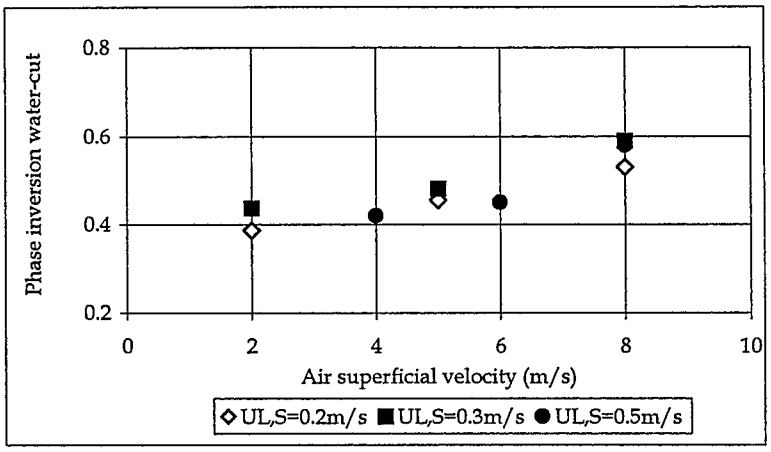


Figure 6.1: Graph showing influence of air and total liquid superficial velocity on the phase inversion water-cut

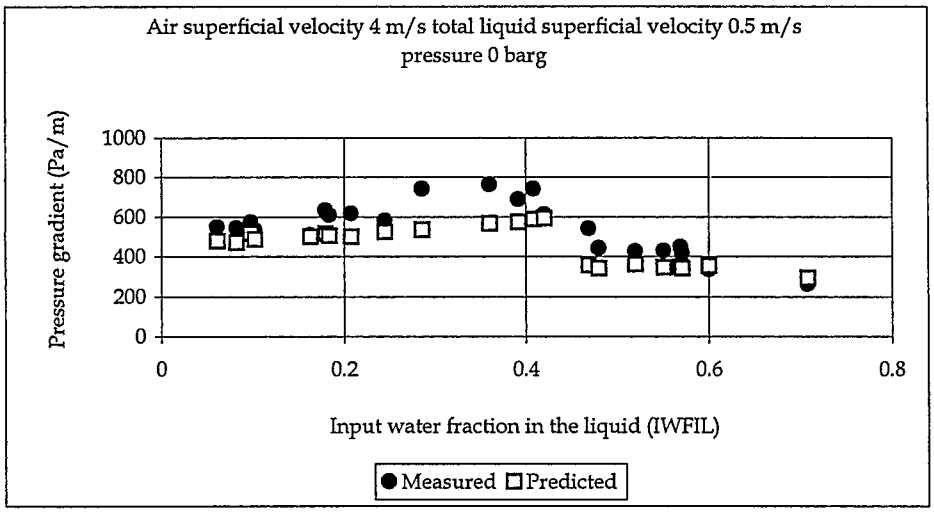


Figure 6.2: Comparison of WASP three-phase pressure drop experimental data with predictions by the correlation of Dukler *et al.* (1964) ($U_{A,S}$ = 4 m/s, $U_{L,S}$= 0.5 m/s, p= 0 barg pipe = horizontal)

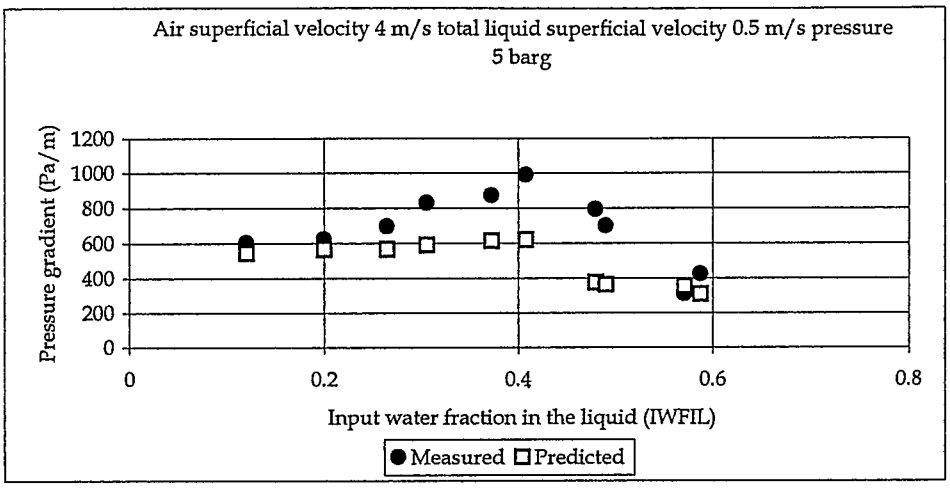


Figure 6.3: Comparison of WASP three-phase pressure gradient experimental data with predictions by the correlation of Dukler *et al.* (1964) ($U_{A,S}$ = 4 m/s, $U_{L,S}$= 0.5 m/s, p= 5 barg pipe = horizontal)

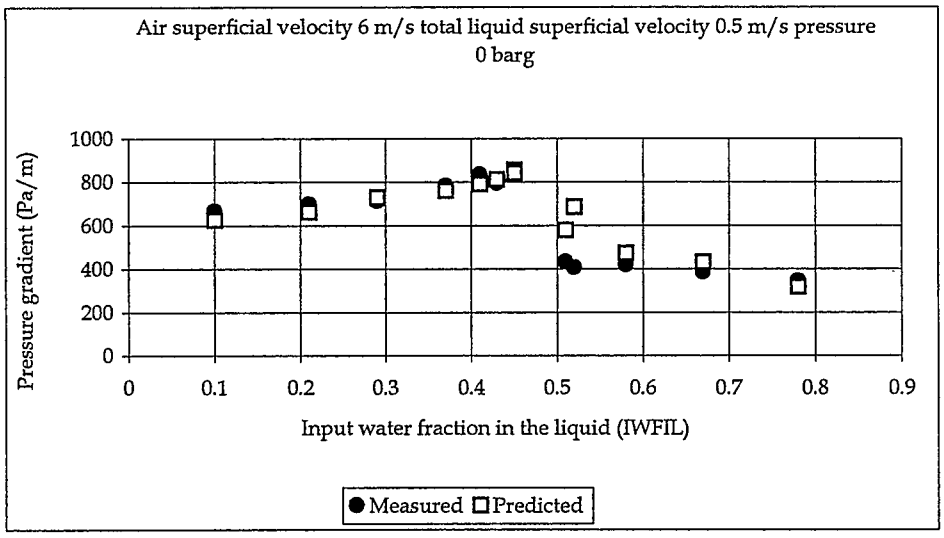


Figure 6.4: Comparison of WASP three-phase pressure gradient experimental data with predictions by the correlation of Dukler *et al.* (1964) ($U_{A,S}$ = 6 m/s, $U_{L,S}$= 0.5 m/s, p= 0 barg pipe = horizontal)

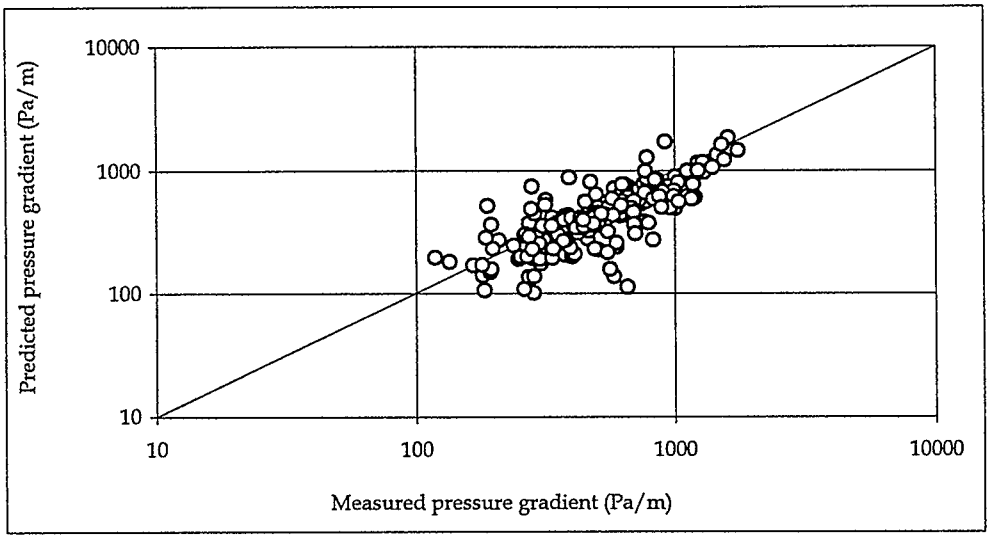


Figure 6.5: Comparison of WASP three-phase pressure gradient experimental data with predictions by the correlation of Dukler *et al.* (1964)

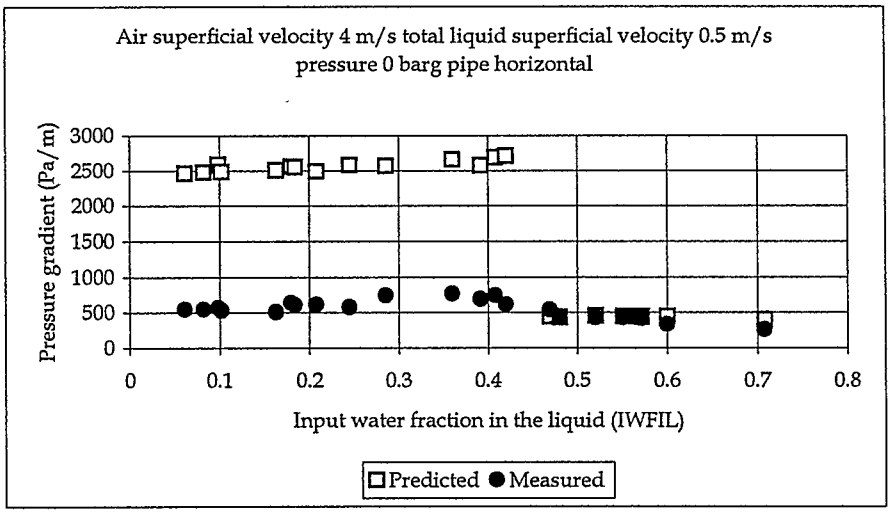


Figure 6.6: Comparison of WASP three-phase pressure gradient experimental data with predictions by the correlation of Chisholm (1967) ($U_{A,S}$ = 4 m/s, $U_{L,S}$= 0.5 m/s, p= 0 barg, pipe = horizontal)

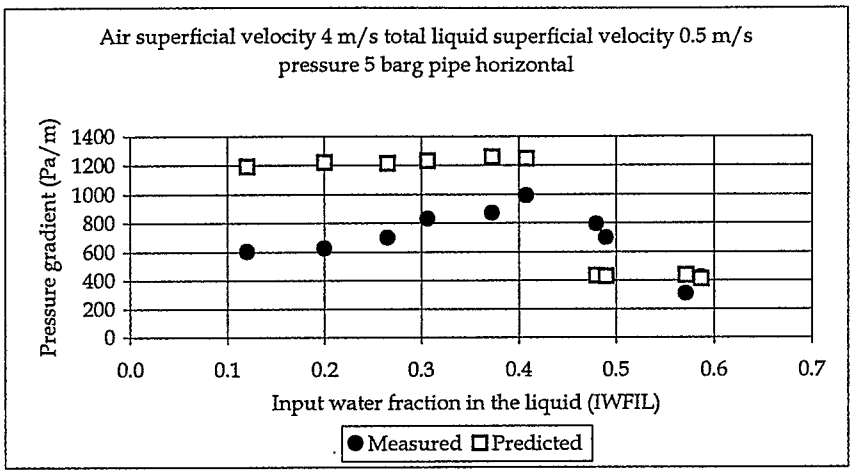


Figure 6.7: Comparison of WASP three-phase pressure gradient experimental data with predictions by the correlation of Chisholm (1967) ($U_{A,S}$ = 4 m/s, $U_{L,S}$= 0.5 m/s, p= 5 barg, pipe = horizontal)

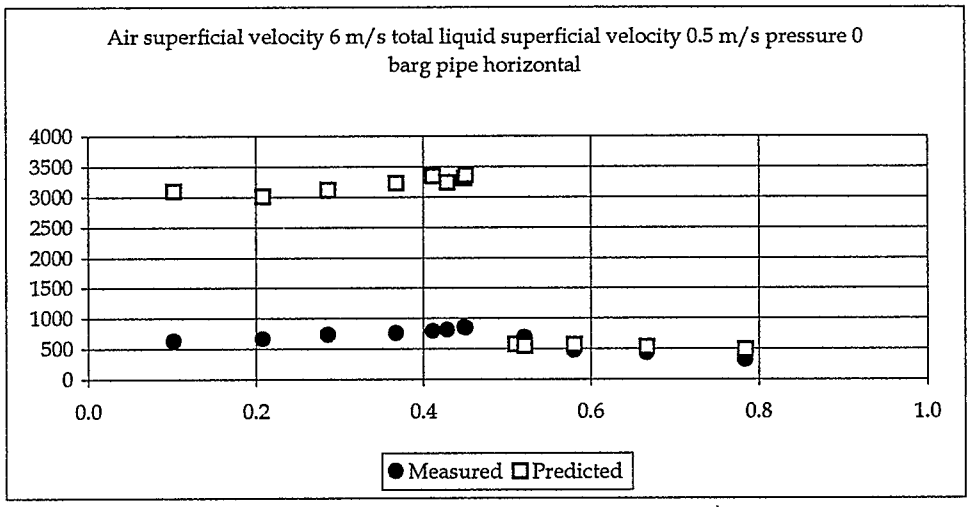


Figure 6.8: Comparison of WASP three-phase pressure gradient data with predictions by the correlation of Chisholm (1967) ($U_{A,S}$ = 6 m/s, $U_{L,S}$= 0.5 m/s, p= 0 barg, pipe = horizontal)

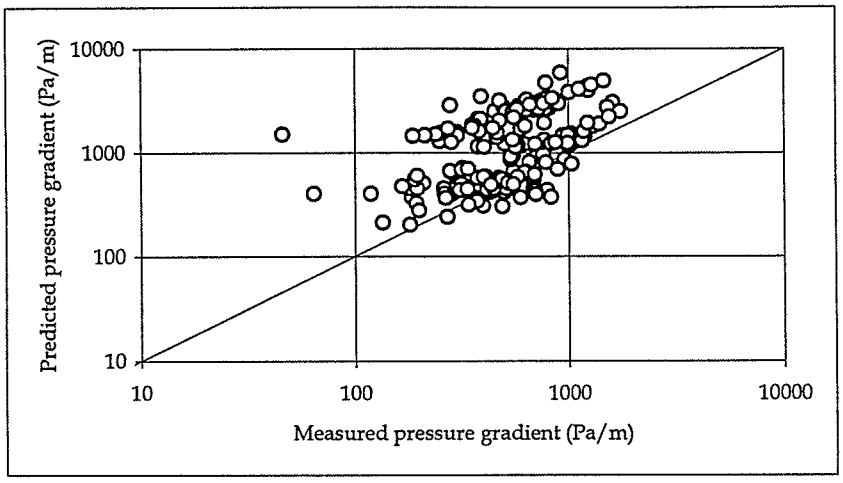


Figure 6.9: Comparison of WASP three-phase pressure gradient data with predictions by the correlation of Chisholm (1966)

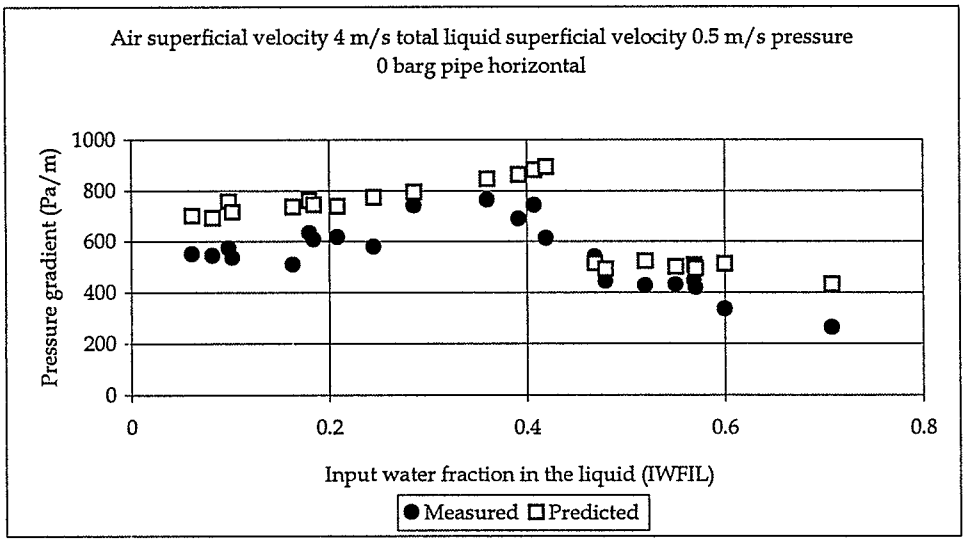


Figure 6.10: Comparison of WASP three-phase pressure gradient experimental data with predictions by the correlation of Beggs and Brill (1973) ($U_{A,S}$ = 4 m/s, $U_{L,S}$= 0.5 m/s, p= 0 barg pipe = horizontal)

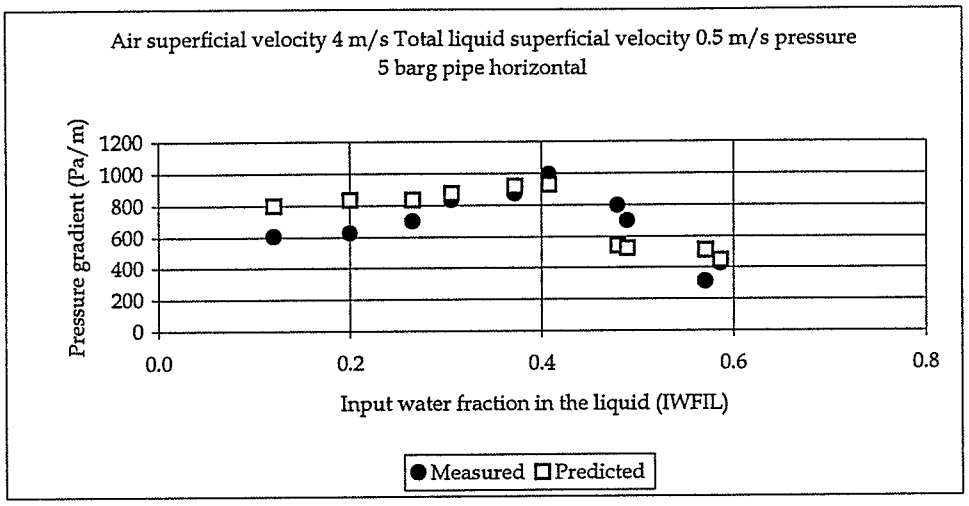


Figure 6.11: Comparison of WASP three-phase pressure gradient experimental data with predictions by the correlation of Beggs and Brill (1973) ($U_{A,S}$ = 4 m/s, $U_{L,S}$= 0.5 m/s, p= 5 barg pipe = horizontal)

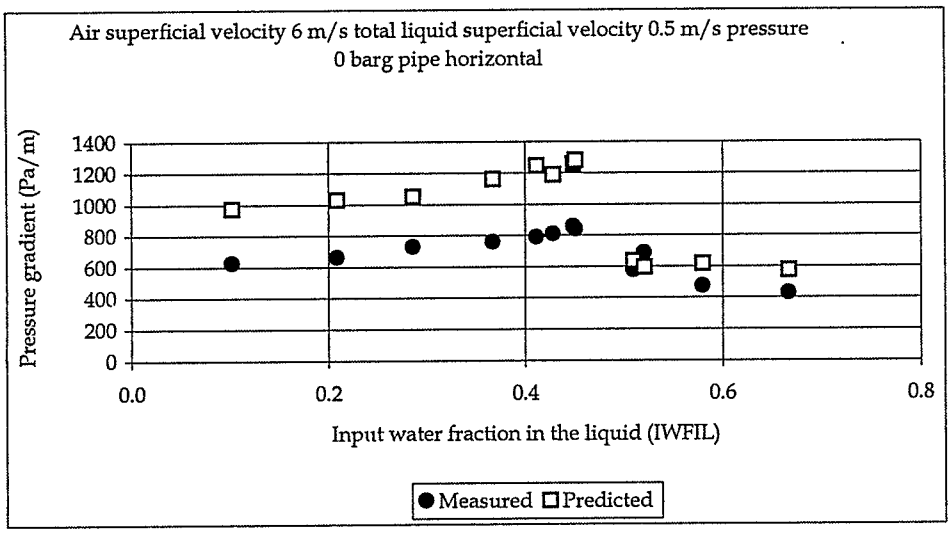


Figure 6.12: Comparison of WASP three-phase pressure gradient experimental data with the predictions by the correlation of Beggs and Brill (1973) ($U_{A,S}$ = 6 m/s, $U_{L,S}$= 0.5 m/s, p= 0 barg pipe = horizontal)

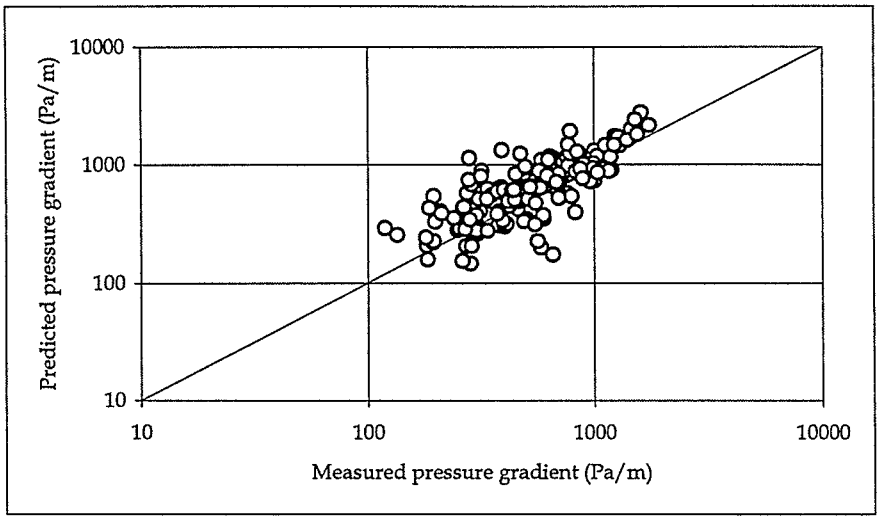


Figure 6.13: Comparison of WASP three-phase pressure gradient experimental data with predictions by the correlation of Beggs and Brill (1973)

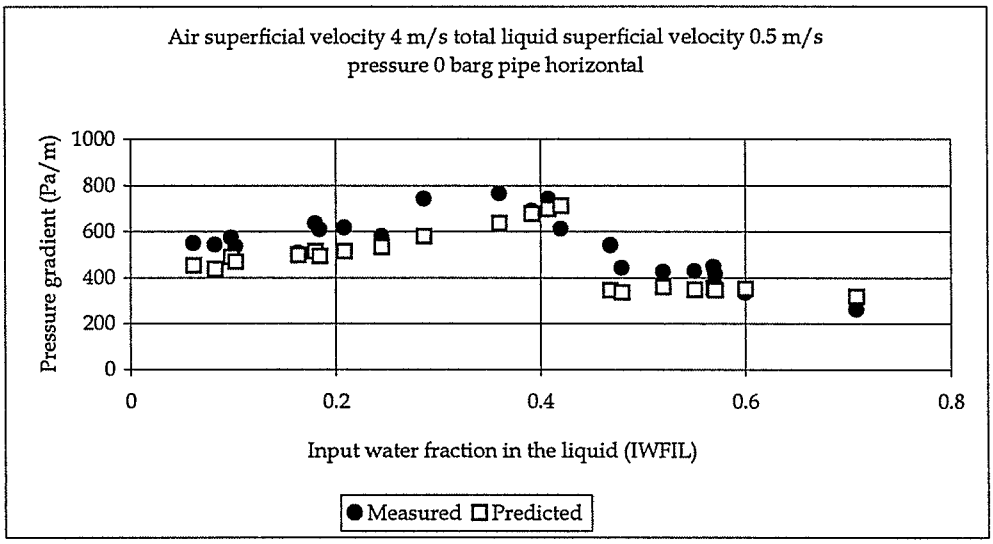


Figure 6.14 Comparison of WASP three-phase pressure gradient experimental data with predictions by the correlation of Lockhart and Martinelli (1949) ($U_{A,S}$ = 4 m/s, $U_{L,S}$= 0.5 m/s, p= 0 barg, pipe = horizontal)

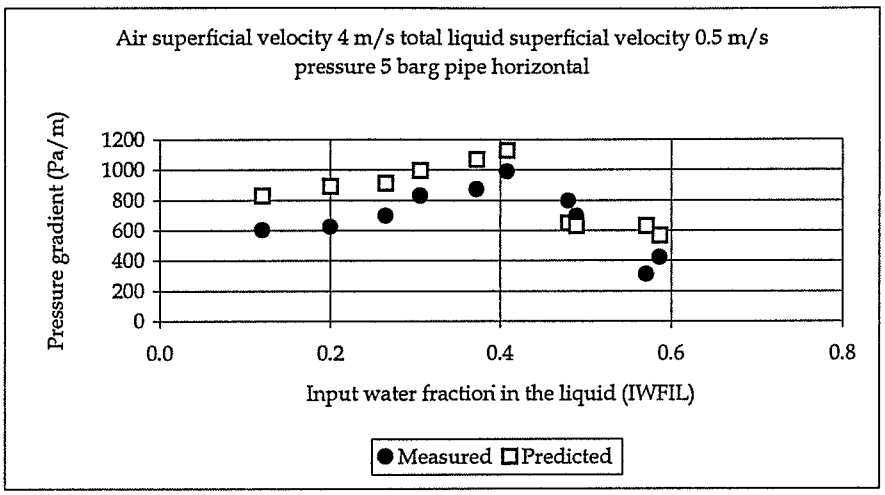


Figure 6.15 Comparison of WASP three-phase pressure gradient experimental data with predictions by the correlation of Lockhart and Martinelli (1949) ($U_{A,S}$ = 4 m/s, $U_{L,S}$ = 0.5 m/s, p= 5 barg pipe = horizontal)

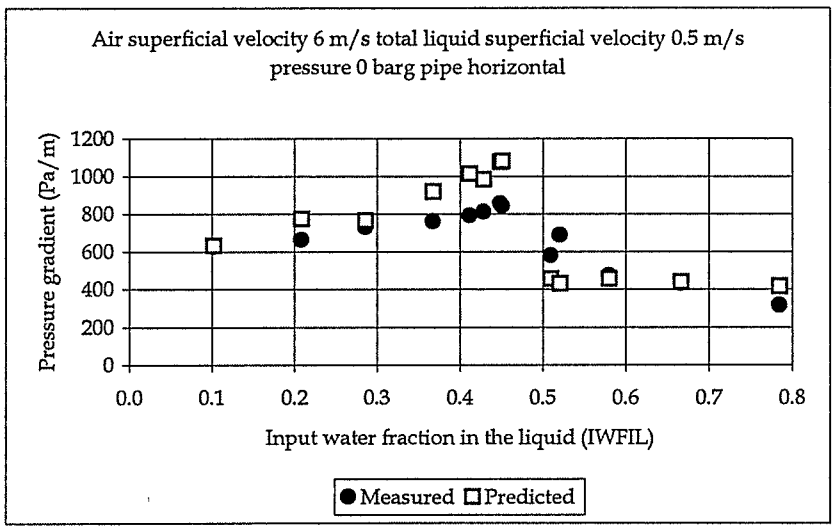


Figure 6.16: Comparison of WASP three-phase pressure gradient experimental data with predictions by the correlation of Lockhart and Martinelli (1949) ($U_{A,S}$ = 6 m/s, $U_{L,S}$ = 0.5 m/s, p= 0 barg, pipe = horizontal)

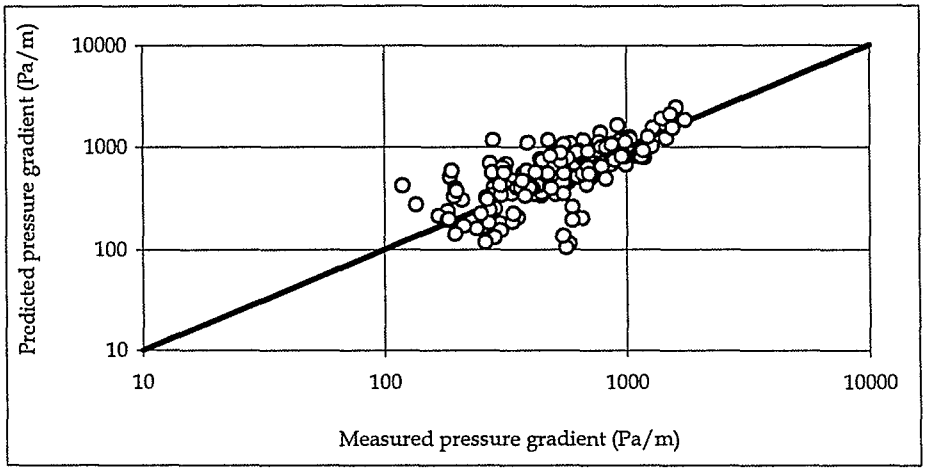


Figure 6.17: Comparison of WASP three-phase pressure gradient experimental data with predictions by the correlation of Lockhart and Martinelli (1949)

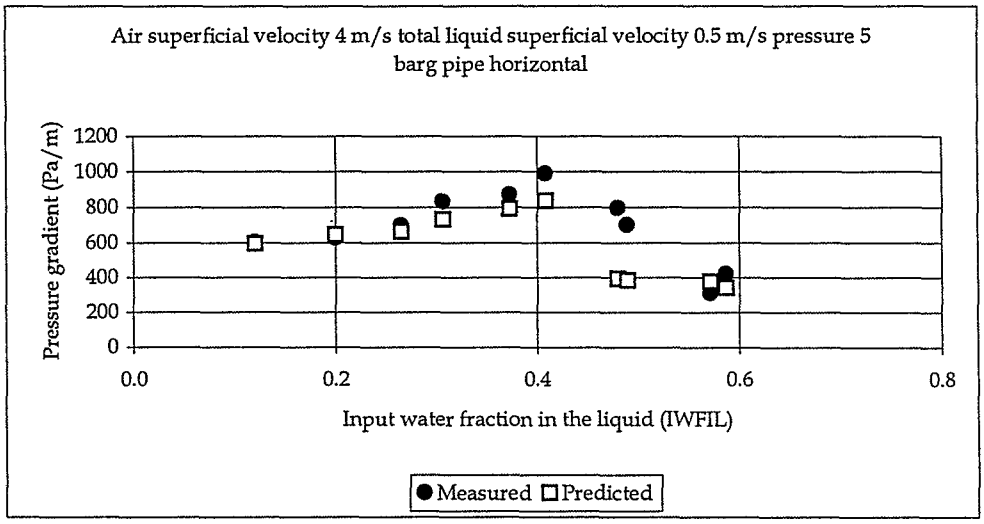


Figure 6.18: Comparison of WASP three-phase pressure gradient experimental data with predictions by the correlation of Schlichting (1970) ($U_{A,S}$ = 4 m/s, $U_{L,S}$= 0.5 m/s, p= 5 barg pipe, = horizontal)

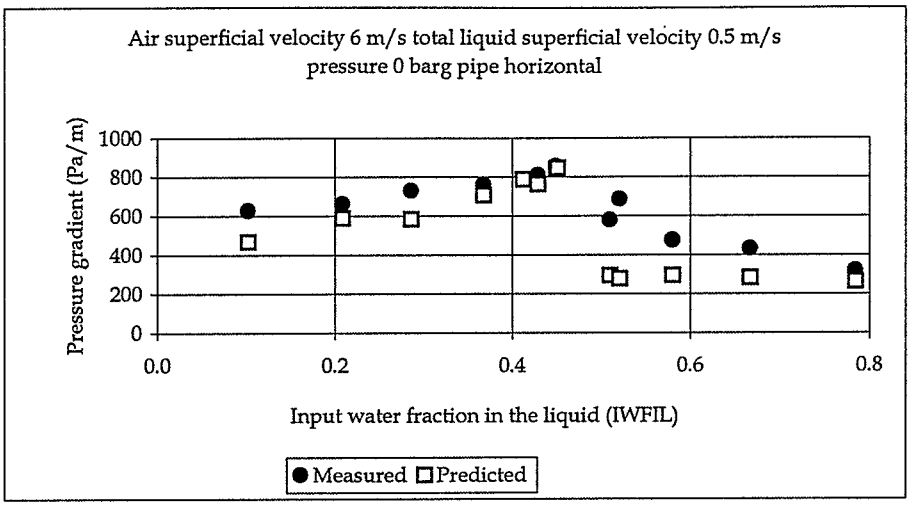


Figure 6.19: Comparison of WASP three-phase pressure gradient experimental data with predictions by the correlation of Schlichting (1970) ($U_{A,S}$ = 6 m/s, $U_{L,S}$= 0.5 m/s, p= 0 barg pipe = horizontal)

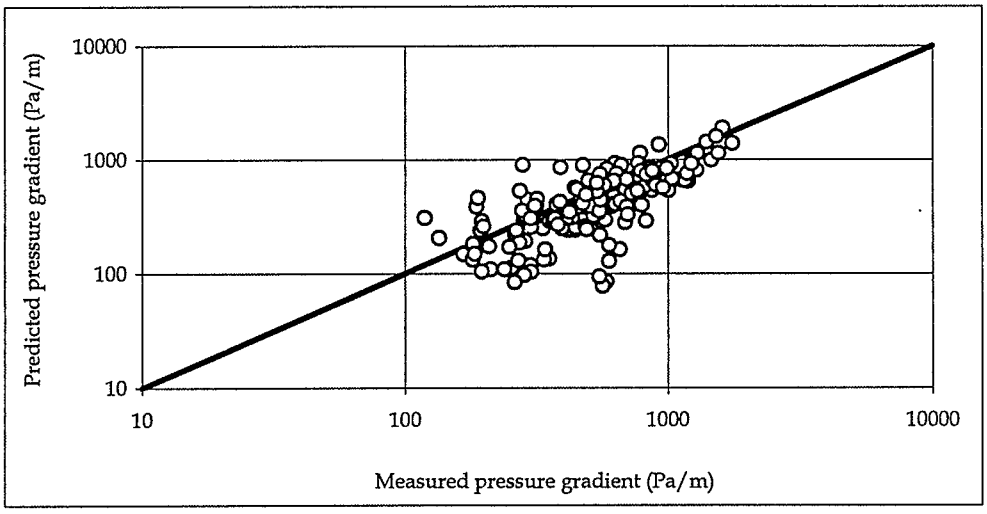


Figure 6.20: Comparison of WASP three-phase pressure gradient experimental data with predictions by the correlation of Schlichting (1970)

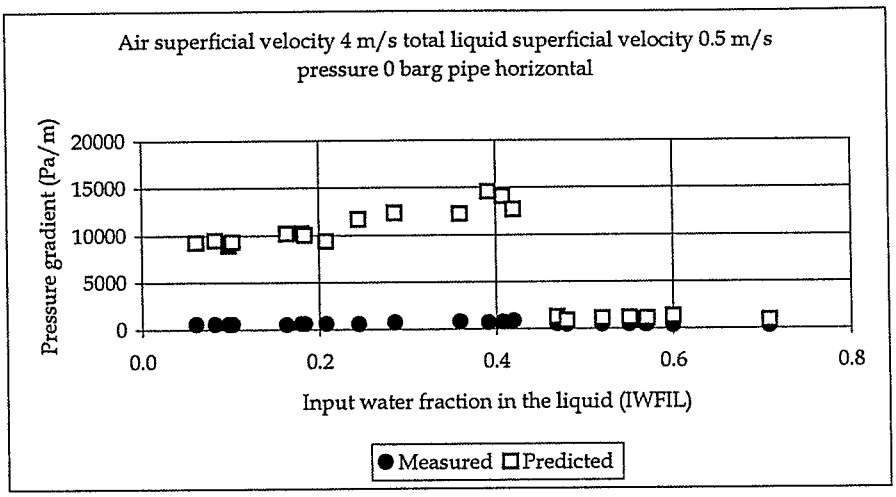


Figure 6.21: Comparison of WASP three-phase pressure gradient experimental data with the predictions of the slug model of Bonnecaze *et al.* ($U_{A,S}$ = 4 m/s, $U_{L,S}$ = 0.5 m/s, p= 0 barg pipe = horizontal)

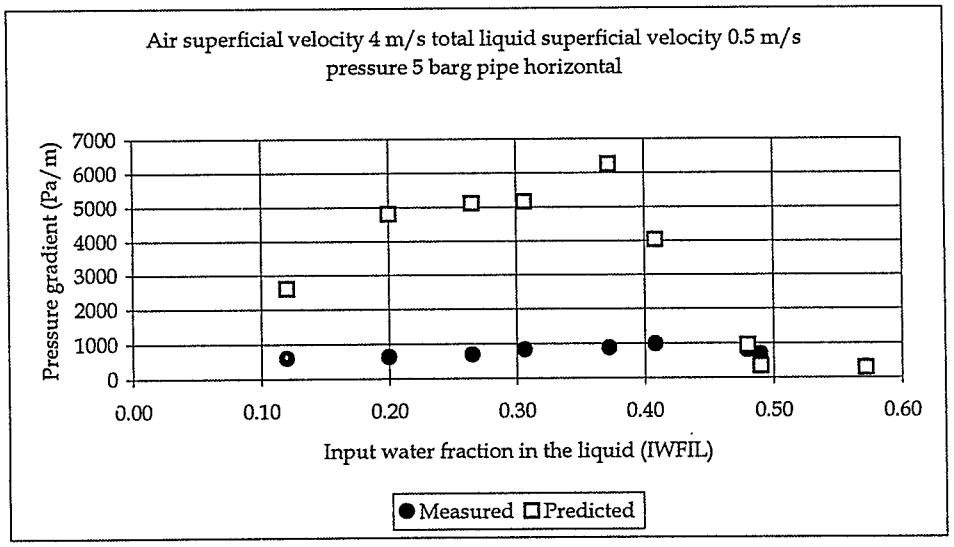


Figure 6.22: Comparison of WASP three-phase pressure gradient experimental data with the predictions of the slug model of Bonnecaze *et al.* ($U_{A,S}$ = 4 m/s, $U_{L,S}$ = 0.5 m/s, p= 5 barg pipe = horizontal)

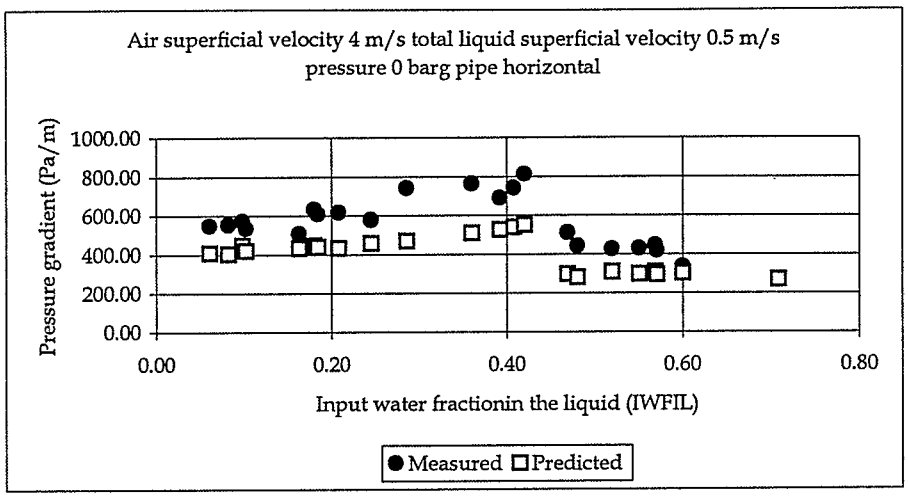


Figure 6.23: Comparison of WASP pressure gradient experimental data with the predictions by the slug model of Taitel and Barnea (1990) ($U_{A,S}$ = 4 m/s, $U_{L,S}$= 0.5 m/s, p= 0 barg, pipe = horizontal)

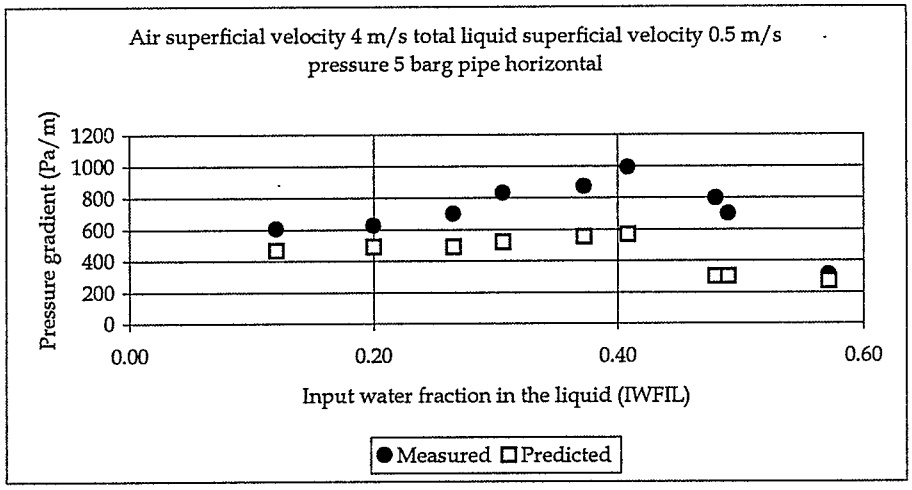


Figure 6.24: Comparison of WASP pressure gradient experimental data with the predictions by the slug model of Taitel and Barnea (1990) ($U_{A,S}$ = 4 m/s, $U_{L,S}$ = 0.5 m/s, p= 5 barg pipe = horizontal)

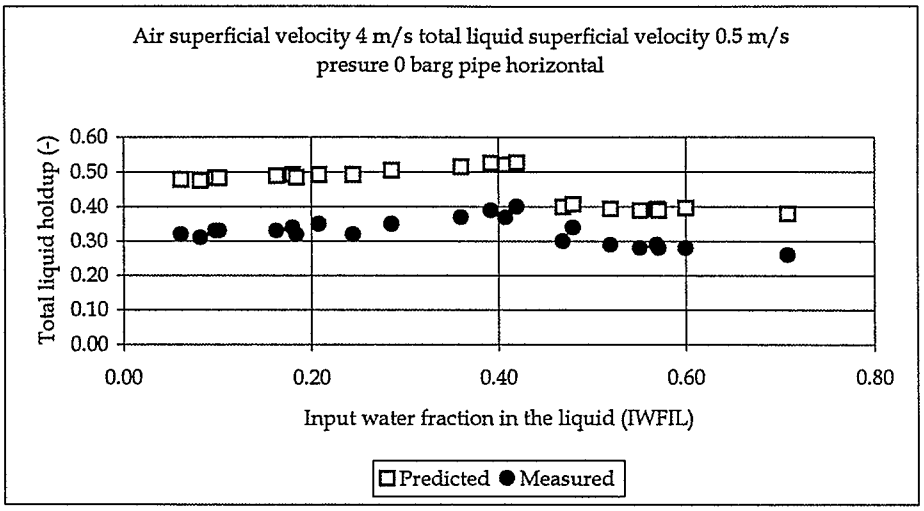


Figure 6.25: Comparison of WASP three-phase total liquid holdup experimental data with predictions by the correlation of Lockhart and Martinelli (1949) ($U_{A,S}$ = 4 m/s, $U_{L,S}$= 0.5 m/s, p= 0 barg pipe = horizontal)

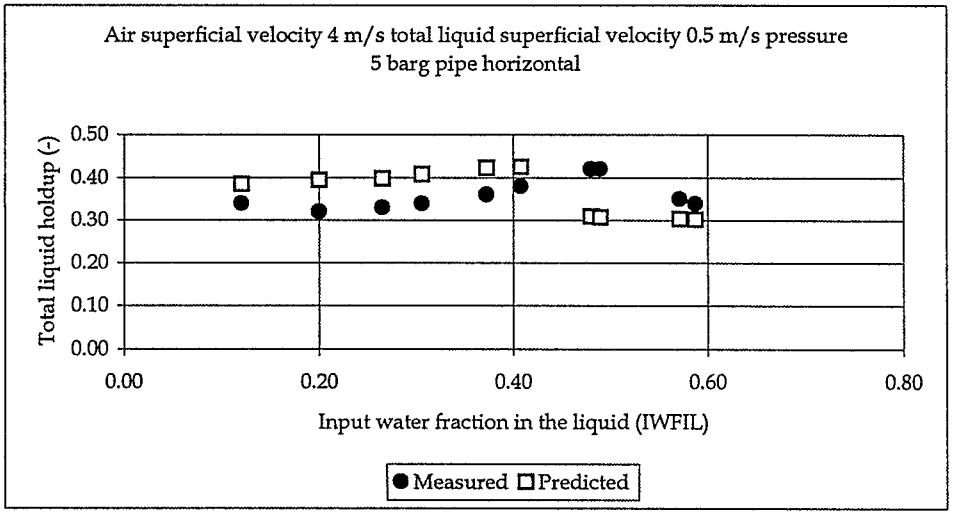


Figure 6.26: Comparison of WASP three-phase total liquid holdup experimental data with predictions by the correlation of Lockhart and Martinelli (1949) ($U_{A,S}$ = 4 m/s, $U_{L,S}$= 0.5 m/s, p= 5 barg, pipe = horizontal)

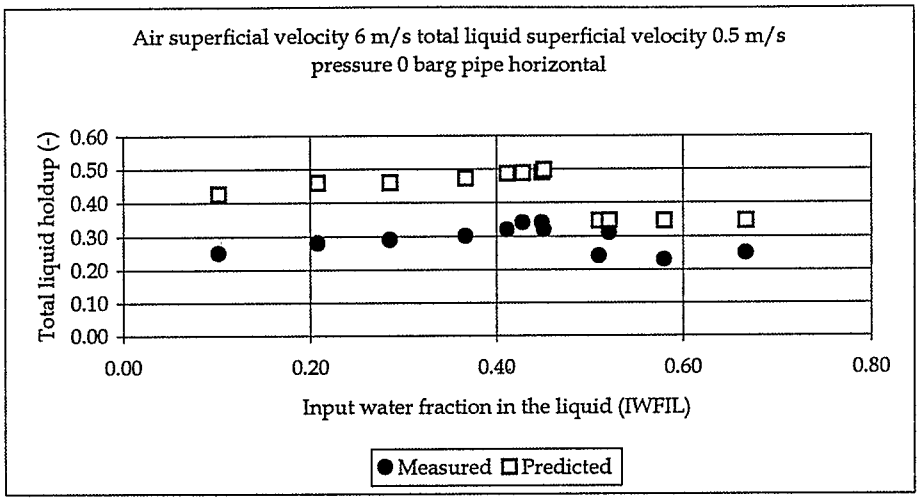


Figure 6.27: Comparison of WASP three-phase total liquid holdup experimental data with predictions by the correlation of Lockhart and Martinelli (1949) ($U_{A,S}$ = 6 m/s, $U_{L,S}$ = 0.5 m/s, P= 5 barg pipe = horizontal)

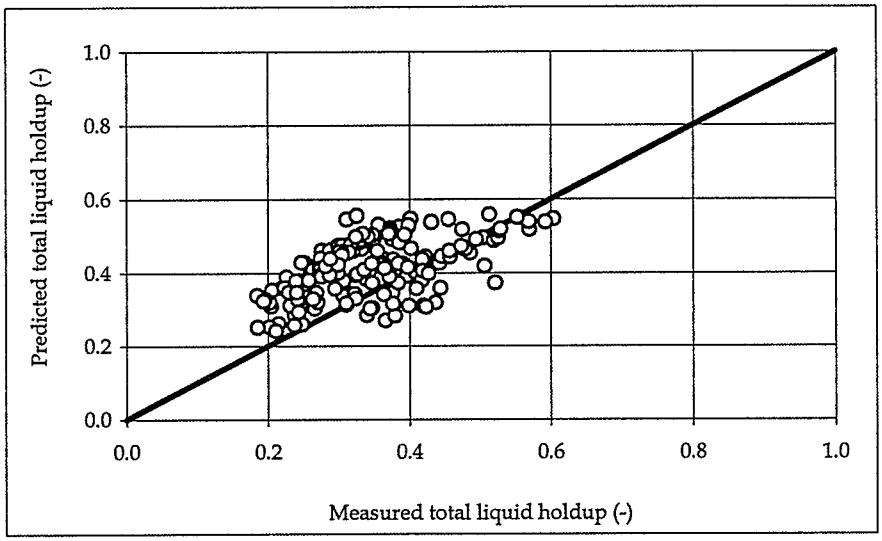


Figure 6.28: Comparison of WASP three-phase total liquid holdup experimental data with predictions by the correlation of Lockhart and Martinelli (1949)

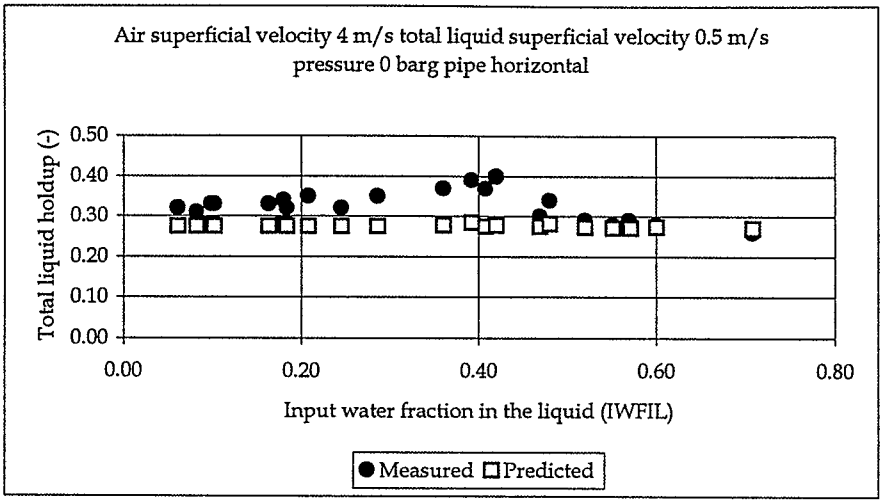


Figure 6.29: Comparison of WASP three-phase total liquid holdup experimental data with predictions by the correlation of Guzhov *et al.* (1967) ($U_{A,S}$ = 4 m/s, $U_{L,S}$ = 0.5 m/s, P= 0 barg pipe = horizontal)

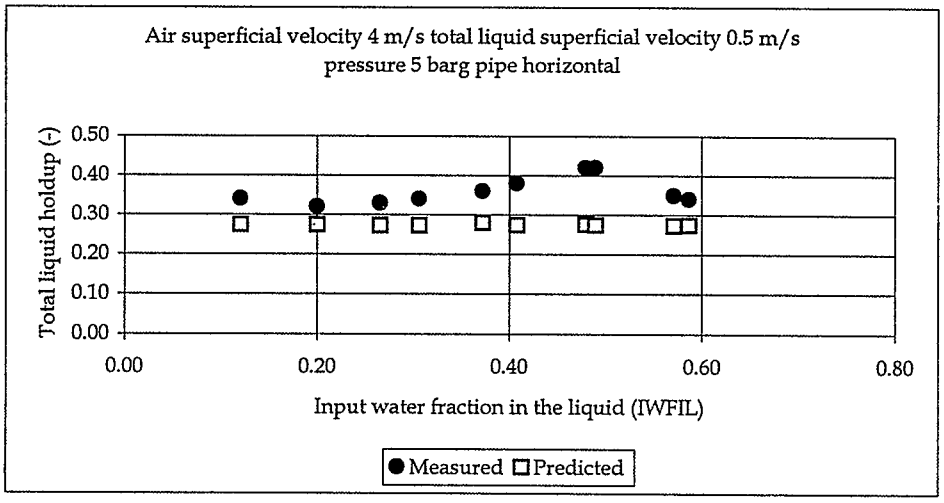


Figure 6.30: Comparison of WASP three-phase total liquid holdup experimental data with predictions by the correlation of Guzhov *et al.* (1967) ($U_{A,S}$ = 4 m/s, $U_{L,S}$ = 0.5 m/s, p= 5 barg pipe = horizontal)

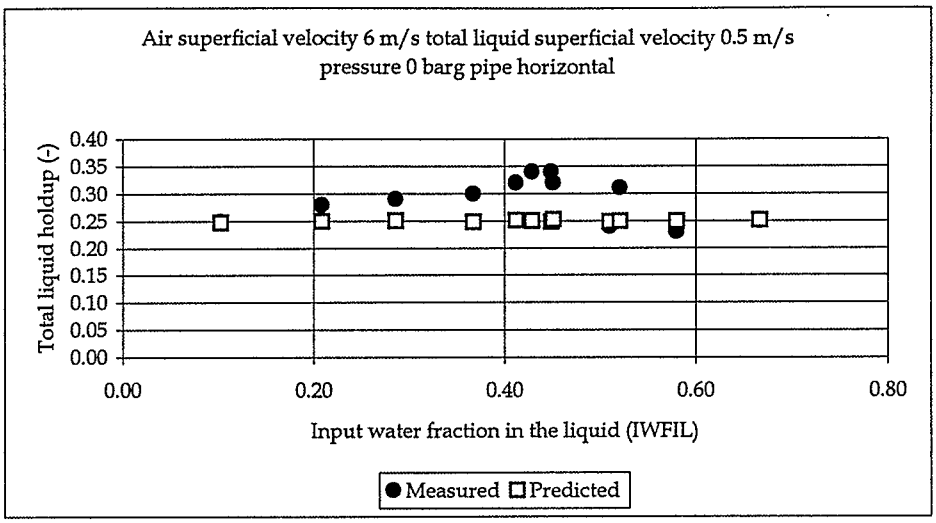


Figure 6.31: Comparison of WASP three-phase total liquid holdup experimental data with predictions by the correlation of Guzhov *et al.* (1967) ($U_{A,S}$ = 6 m/s, $U_{L,S}$ = 0.5 m/s, p = 0 barg, pipe = horizontal)

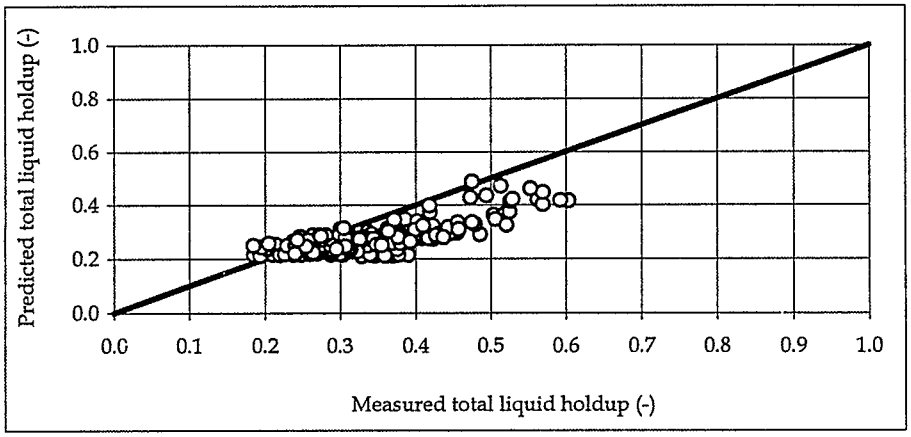


Figure 6.32: Comparison of WASP three-phase total liquid holdup experimental data with predictions by the correlation of Guzhov *et al.* (1967)

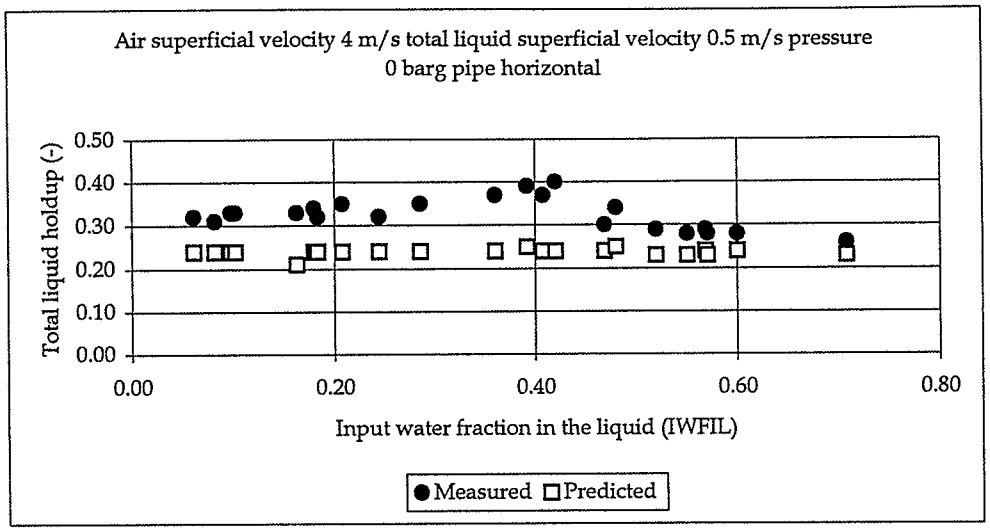


Figure 6.33: Comparison of WASP three-phase total liquid holdup experimental data with predictions by the correlation of Beggs and Brill (1973) ($U_{A,S}$ = 4 m/s, $U_{L,S}$ = 0.5 m/s, p= 0 barg pipe = horizontal)

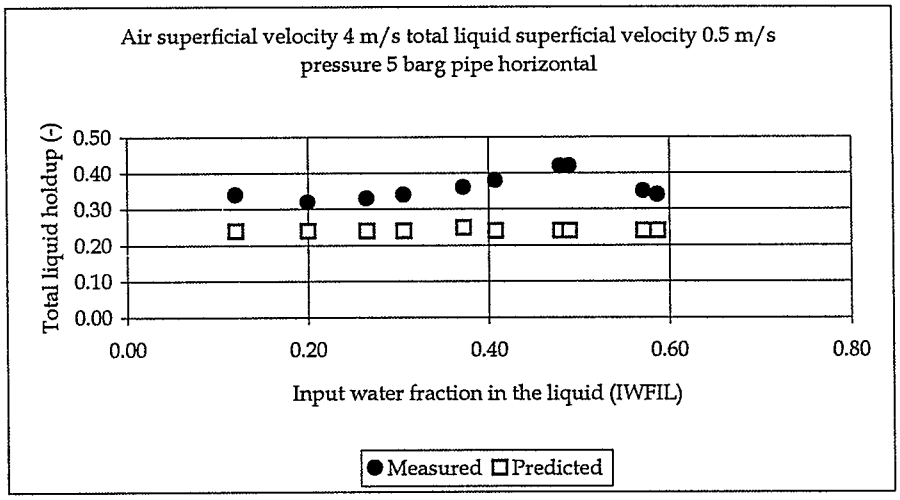


Figure 6.34: Comparison of WASP three-phase total liquid holdup experimental data with predictions by the correlation of Beggs and Brill (1973) ($U_{A,S}$ = 4 m/s, $U_{L,S}$= 0.5 m/s, p= 5 barg, pipe = horizontal)

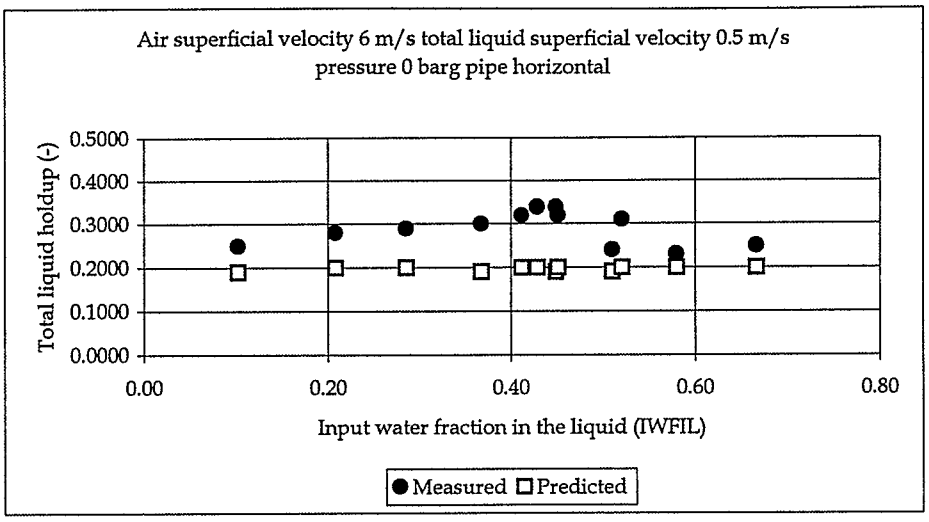


Figure 6.35: Comparison of WASP three-phase total liquid holdup experimental data with predictions by the correlation of Beggs and Brill (1973) ($U_{A,S}$ = 6 m/s, $U_{L,S}$ = 0.5 m/s, P= 0 barg pipe = horizontal)

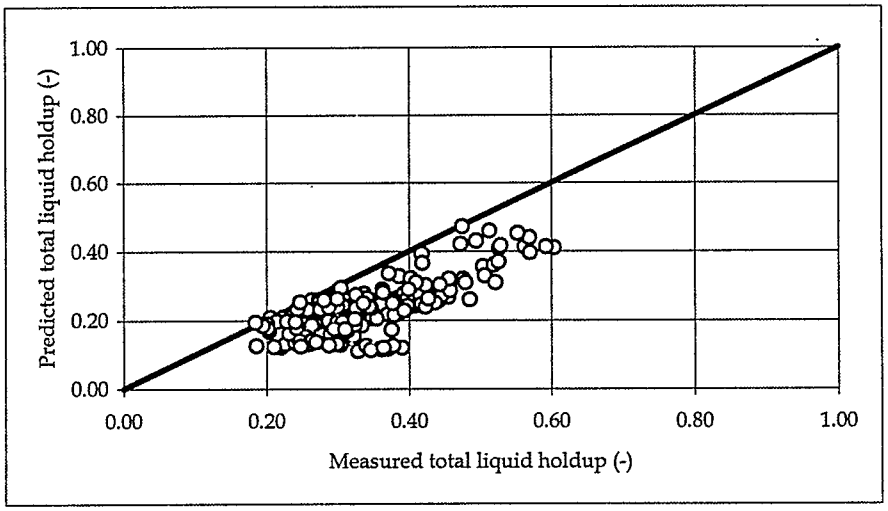


Figure 6.36: Comparison of WASP three-phase total liquid holdup experimental data with predictions by the correlation of Beggs and Brill (1973)

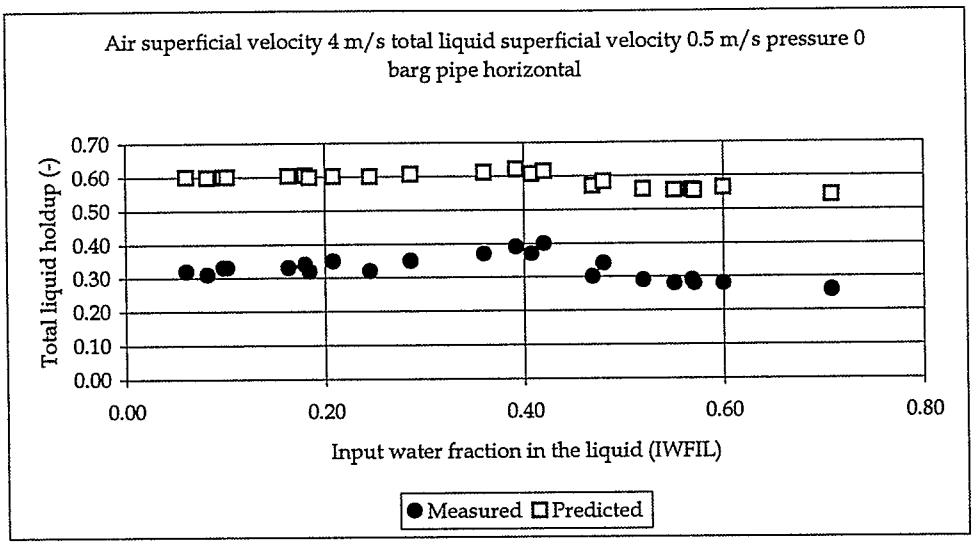


Figure 6.37: Comparison of WASP three-phase total liquid holdup experimental data with predictions by the correlation of Minami and Brill (1987) ($U_{A,S}$ = 4 m/s, $U_{L,S}$ = 0.5 m/s, p= 0 barg pipe = horizontal)

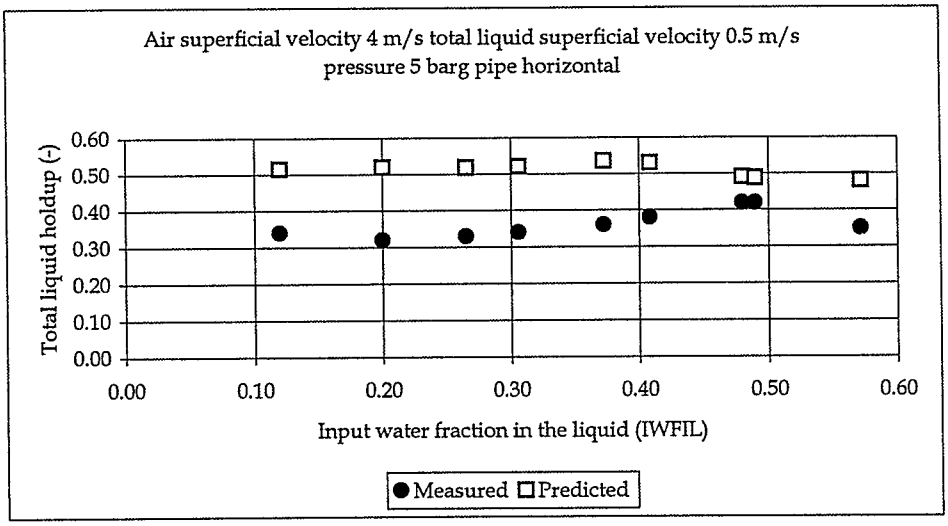


Figure 6.38: Comparison of WASP three-phase total liquid holdup experimental data with predictions by the correlation of Minami and Brill (1987) ($U_{A,S}$ = 4 m/s, $U_{L,S}$ = 0.5 m/s, P= 5 barg, pipe = horizontal)

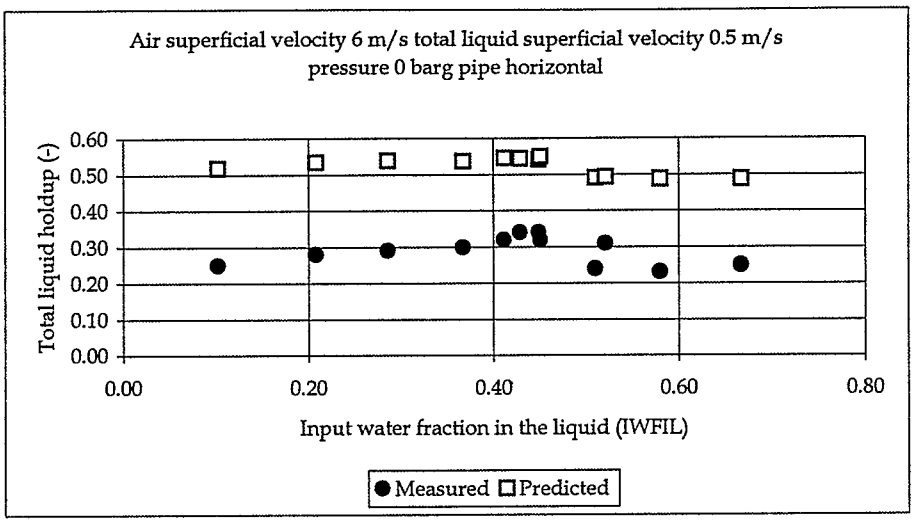


Figure 6.39: Comparison of WASP three-phase total liquid holdup experimental data with predictions by the correlation of Minami and Brill (1987) ($U_{A,S}$ = 6 m/s, $U_{L,S}$ = 0.5 m/s, P= 0 barg, pipe = horizontal)

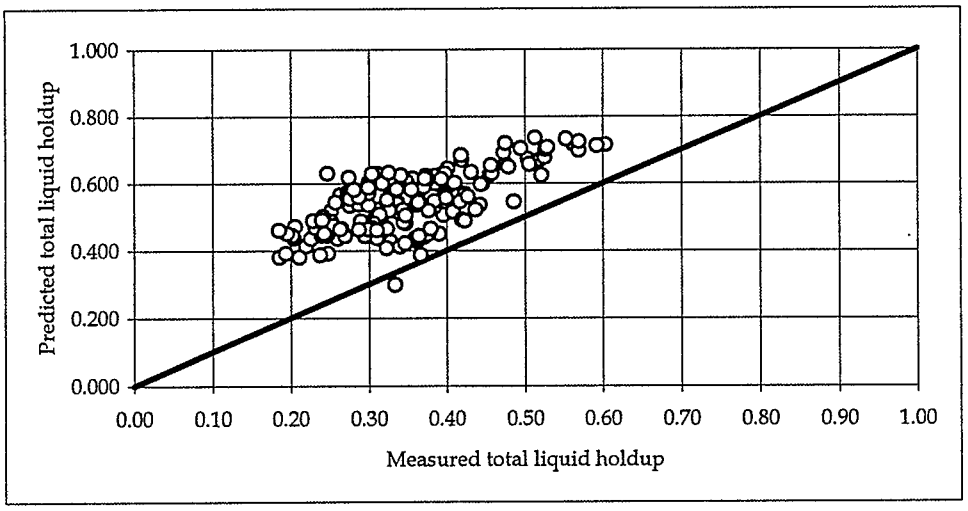


Figure 6.40: Comparison of WASP three-phase total liquid holdup experimental data with predictions by the correlation of Minami and Brill (1987)

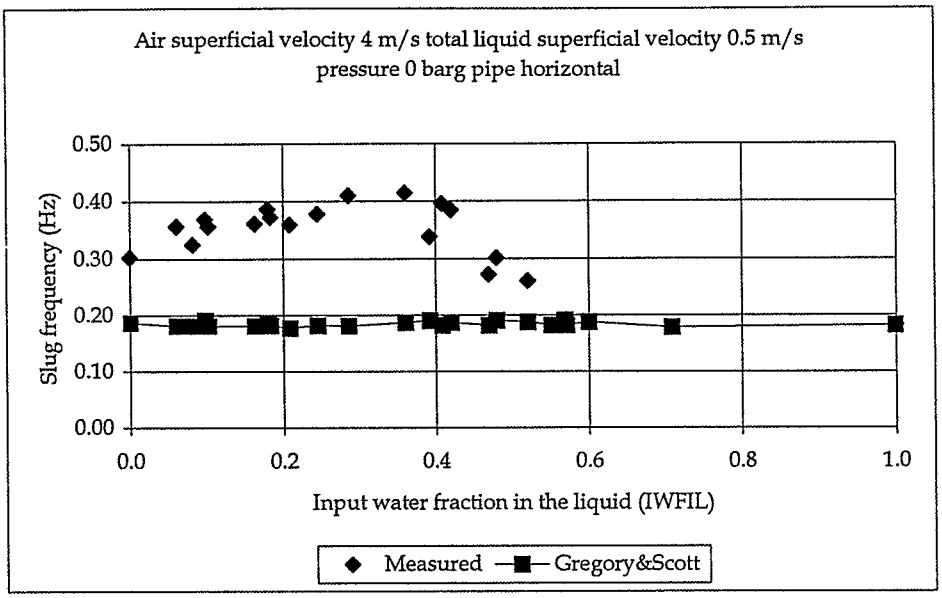


Figure 6.41: Comparison of WASP three-phase slug frequency experimental data with predictions by the correlation of Gregory and Scott (1969) ($U_{A,S}$ = 4 m/s, $U_{L,S}$ = 0.5 m/s, p= 0 barg pipe = horizontal)

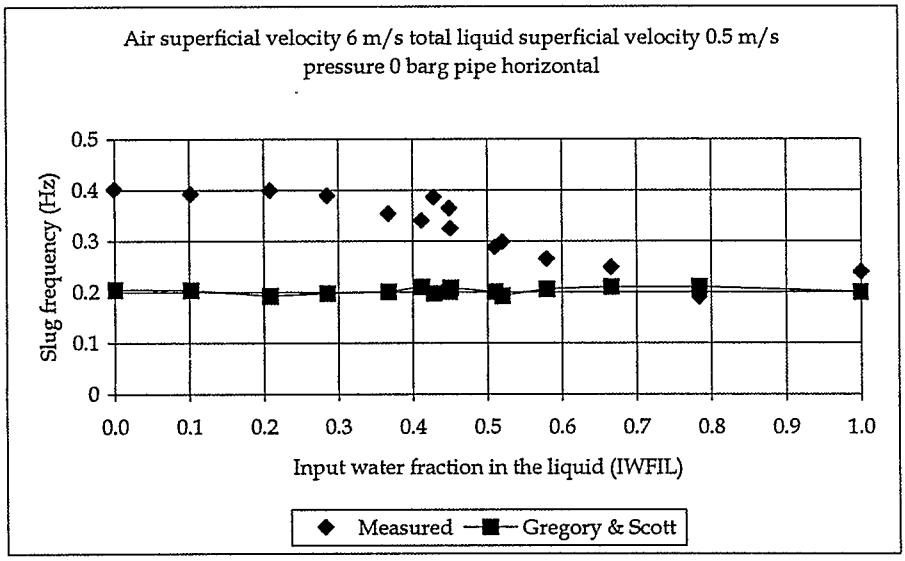


Figure 6.42: Comparison of WASP three-phase slug frequency experimental data with predictions by the correlation of Gregory and Scott (1969) ($U_{A,S}$ = 6 m/s, $U_{L,S}$ = 0.5 m/s, p= 0 barg pipe = horizontal)

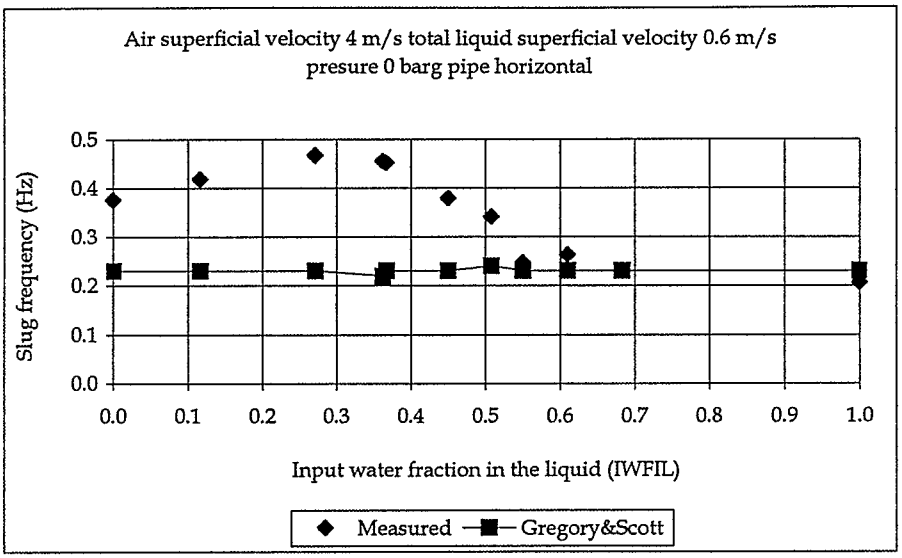


Figure 6.43: Comparison of WASP three-phase slug frequency experimental data with predictions by the correlation of Gregory and Scott (1969) ($U_{A,S}$ = 4 m/s, $U_{L,S}$ = 0.6 m/s, p= 0 barg pipe = horizontal)

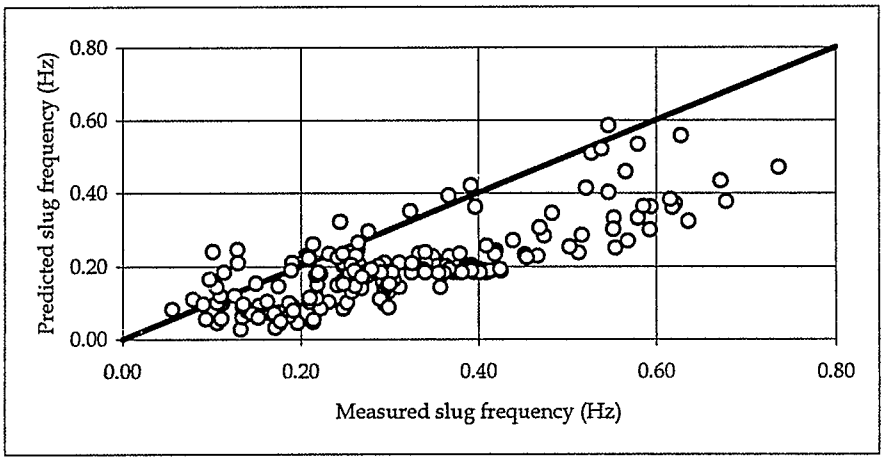


Figure 6.44:Comparison of WASP three-phase slug frequency experimental data with predictions by the correlation of Gregory and Scott (1969)

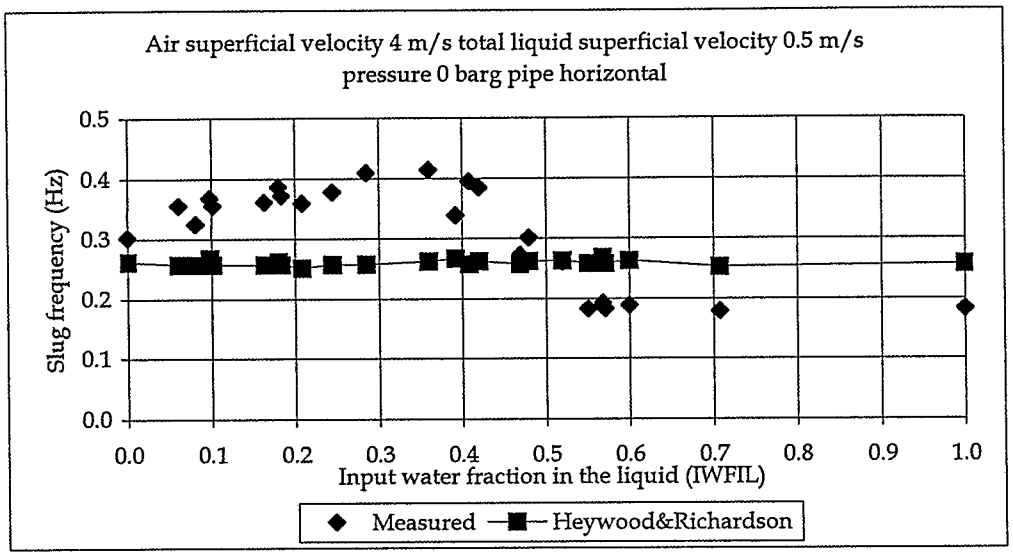


Figure 6.45:Comparison of WASP three-phase slug frequency experimental data with predictions by the correlation of Heywood and Richardson (1979) ($U_{A,S}$ = 4 m/s, $U_{L,S}$ = 0.5 m/s, p= 0 barg pipe = horizontal)

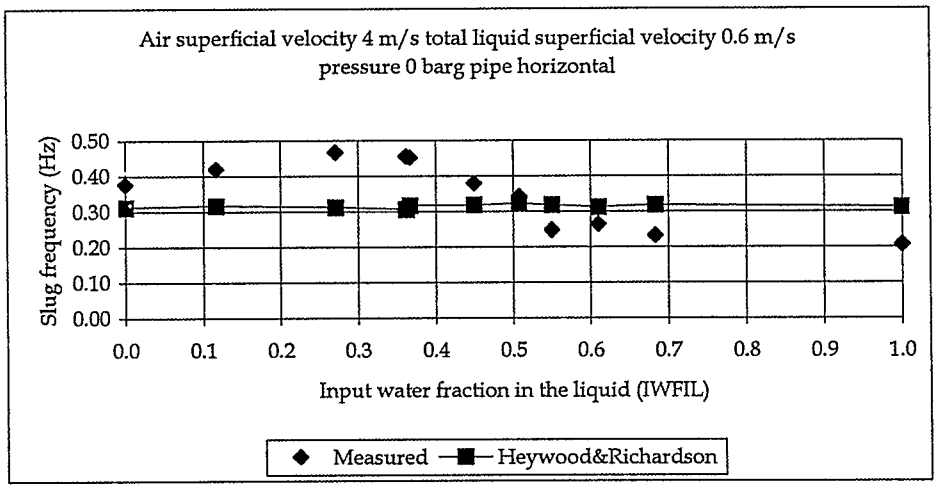


Figure 6.46:Comparison of WASP three-phase slug frequency experimental data with predictions by the correlation of Heywood and Richardson (1979) ($U_{A,S}$ = 4 m/s, $U_{L,S}$ = 0.6m/s, P= 0 barg pipe = horizontal)

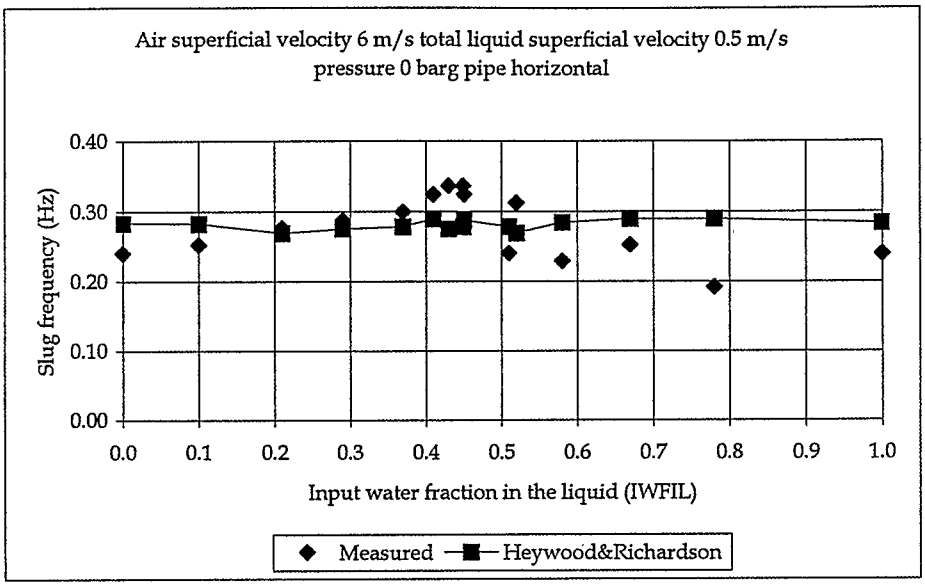


Figure: 6.47:Comparison of WASP three-phase slug frequency experimental data with predictions by the correlation of Heywood and Richardson (1979) ($U_{A,S}$ = 6 m/s, $U_{L,S}$ = 0.5 m/s, p= 0 barg pipe = horizontal)

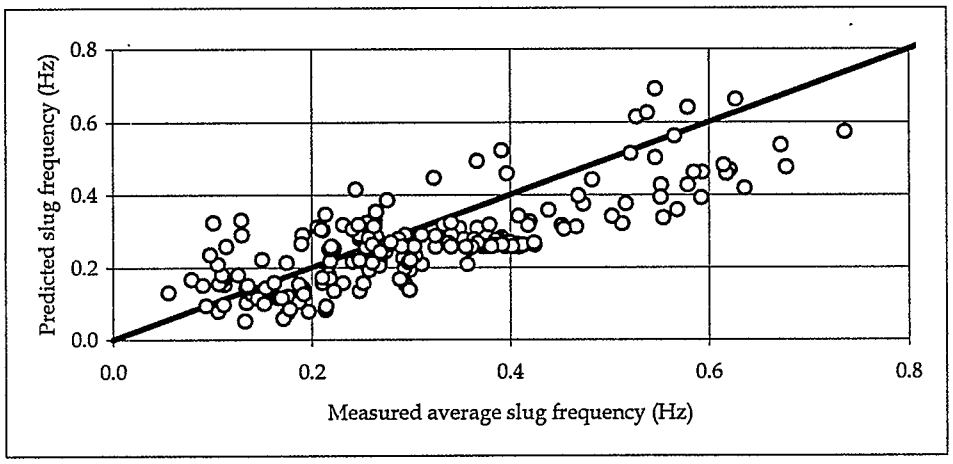


Figure 6.48:Comparison of WASP three-phase slug frequency WASP experimental data with predictions by the correlation of Heywood and Richardson (1979)

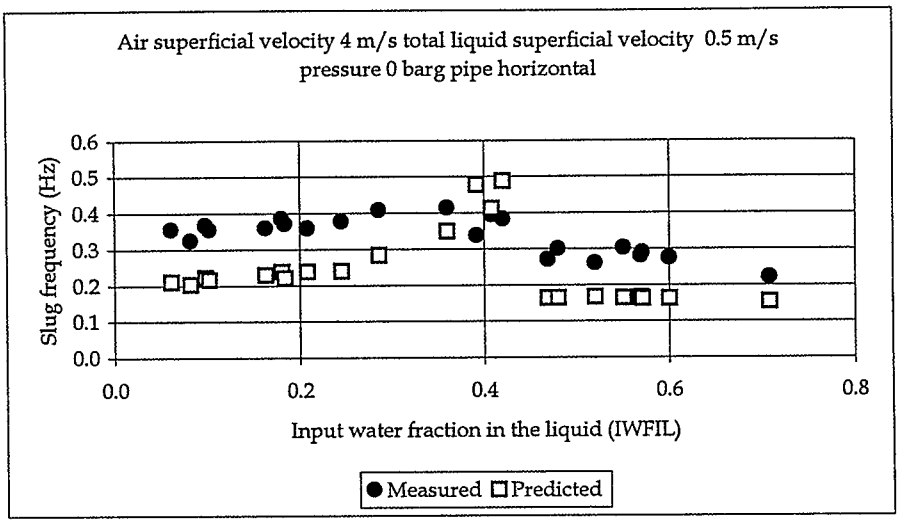


Figure 6.49:Comparison of WASP three-phase slug frequency experimental data with predictions by the correlation of Tronconi (1990) ($U_{A,S}$ = 4 m/s, $U_{L,S}$ = 0.5 m/s, P= 0 barg, pipe = horizontal)

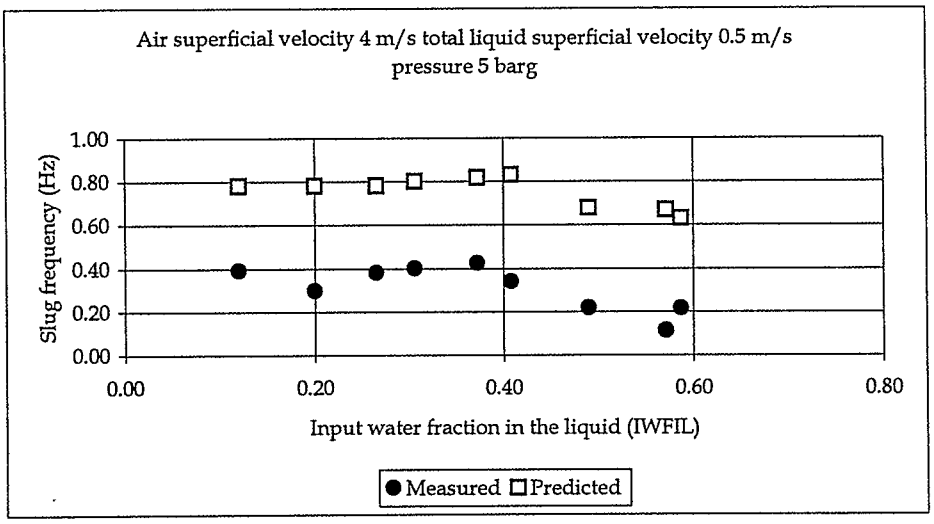


Figure 6.50:Comparison of WASP three-phase slug frequency experimental data with predictions by the correlation of Tronconi (1990) ($U_{A,S}$ = 4 m/s, $U_{L,S}$ = 0.5 m/s, p= 5 barg, pipe = horizontal)

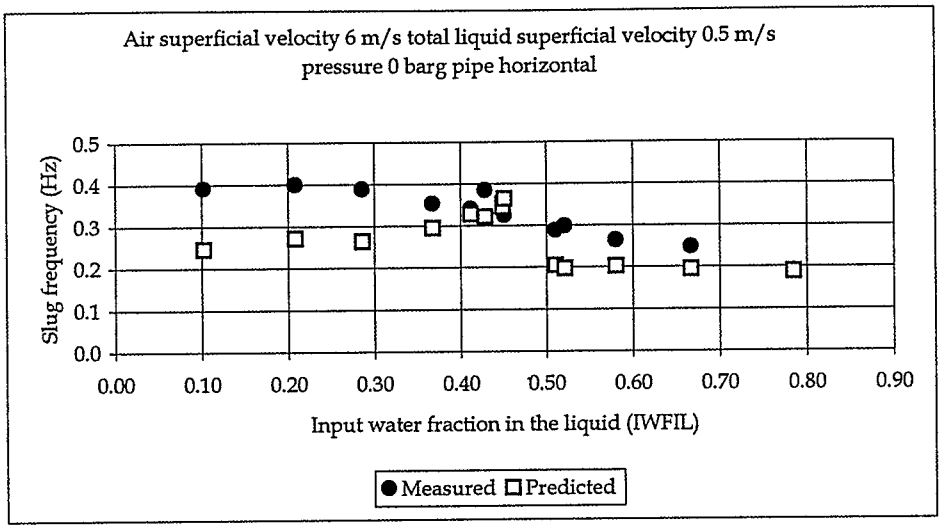


Figure 6.51: Comparison of WASP three-phase slug frequency experimental data with predictions by the correlation of Tronconi (1990) ($U_{A,S}$ = 6 m/s, $U_{L,S}$ = 0.5 m/s, p= 0 barg pipe = horizontal)

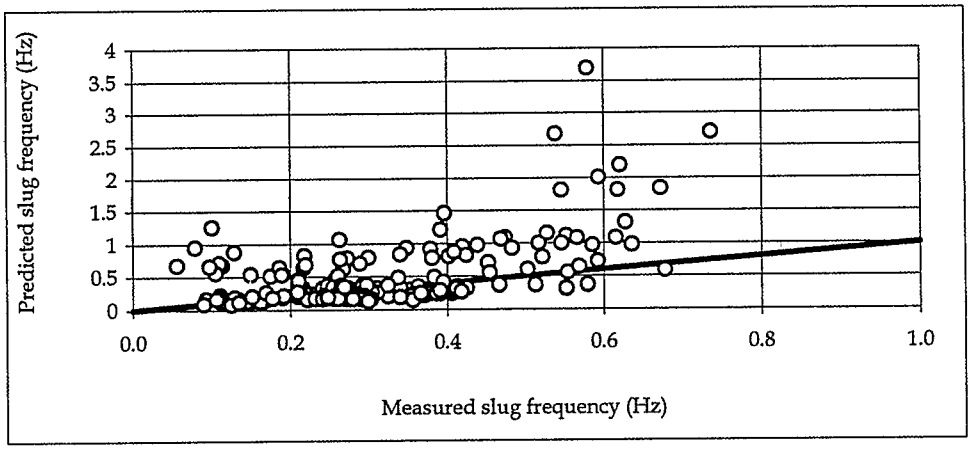


Figure 6.52:Comparison of WASP three-phase slug frequency experimental data with predictions by the correlation of Tronconi (1990

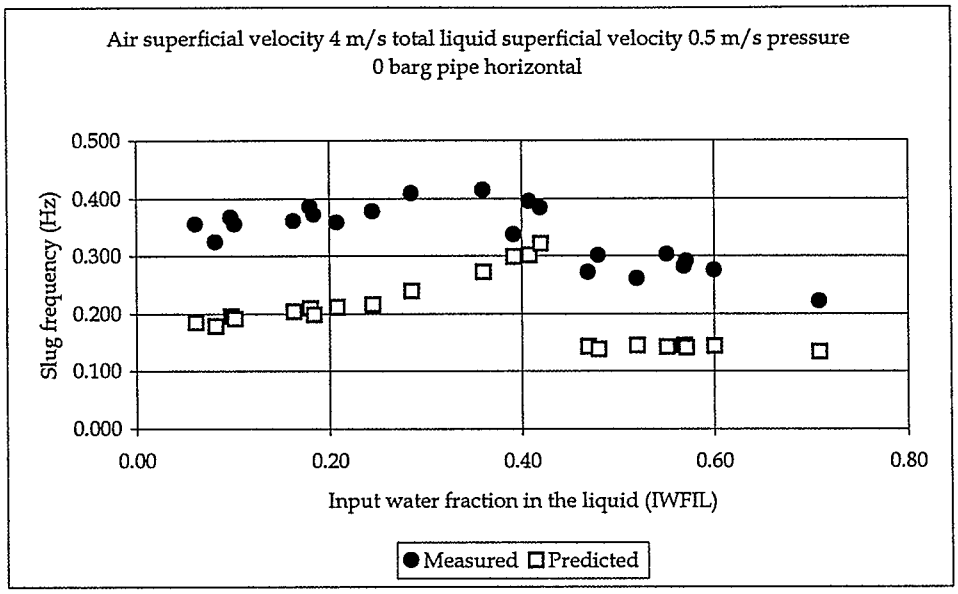


Figure 6.53:Comparison of WASP three-phase slug frequency experimental data with predictions by the correlation of Hill andWood (1990) ($U_{A,S}$ = 4 m/s, $U_{L,S}$ = 0.5 m/s, p= 0 barg pipe = horizontal)

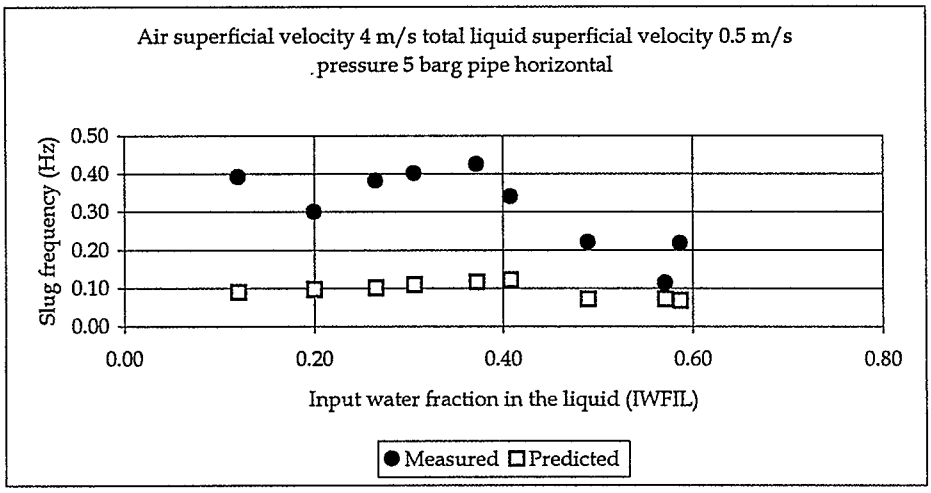


Figure 6.54:Comparison of WASP three-phase slug frequency experimental data with predictions by the correlation of Hill and Wood (1990) ($U_{A,S}$ = 4 m/s, $U_{L,S}$ = 0.5 m/s, p= 5 barg, pipe = horizontal)

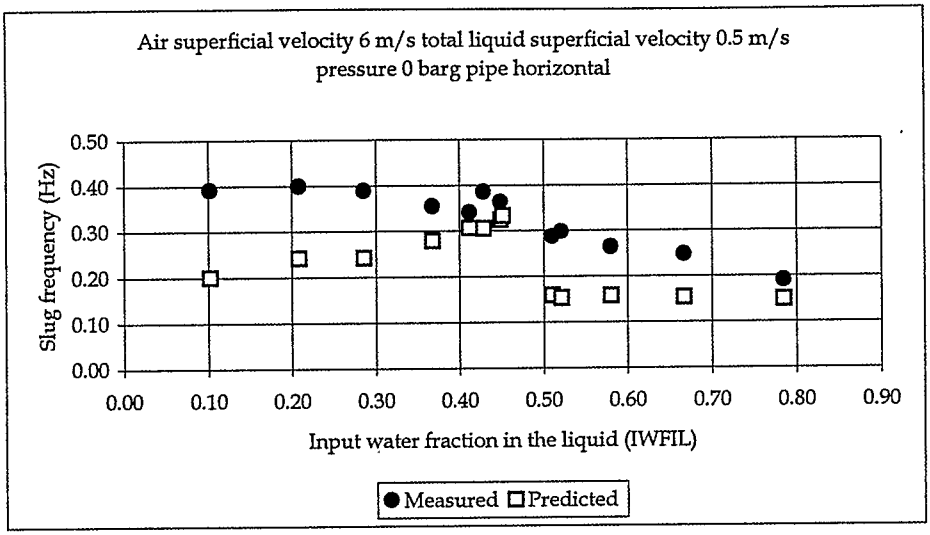


Figure 6.55:Comparison of WASP three-phase slug frequency experimental data with the predictions by the correlation of Hill and Wood (1990) ($U_{A,S}$ = 6 m/s, $U_{L,S}$ = 0.5 m/s, p= 0 barg, pipe = horizontal)

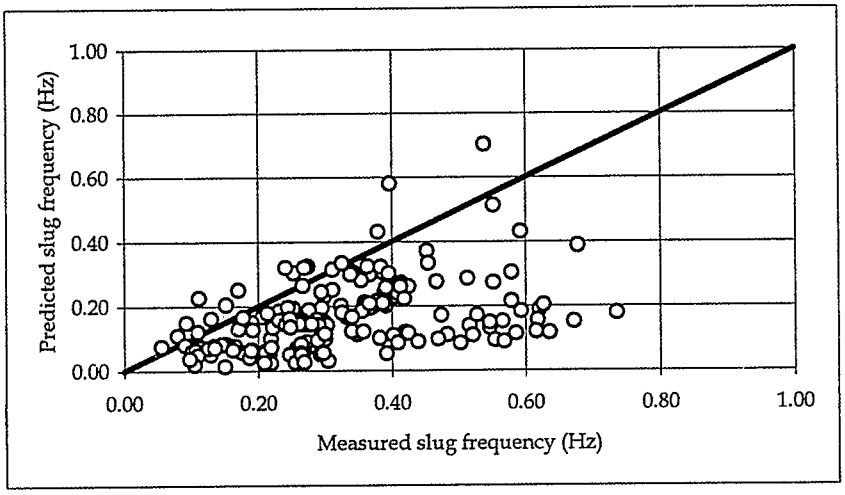


Figure 6.56:Comparison of WASP three-phase slug frequency experimental data with predictions by the correlation of Hill and Wood (1990)

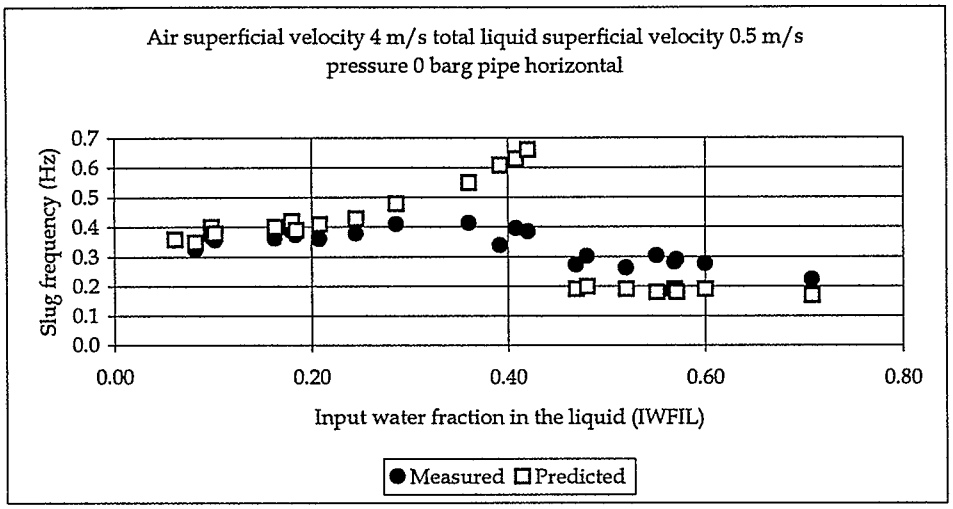


Figure 6.57:Comparison of WASP three-phase slug frequency data with predictions by the correlation of Manolis (1995) ($U_{A,S}$ = 4 m/s, $U_{L,S}$ = 0.5 m/s, p= 0 barg pipe = horizontal)

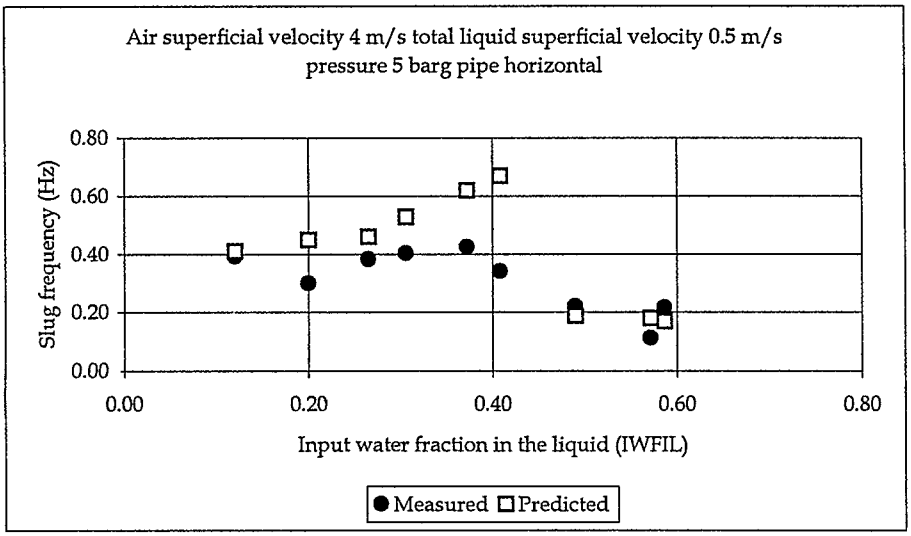


Figure 6.58: Comparison of WASP three-phase slug frequency experimental data with the correlation of Manolis (1995) ($U_{A,S}$ = 4 m/s, $U_{L,S}$ = 0.5 m/s, p= 5 barg pipe = horizontal)

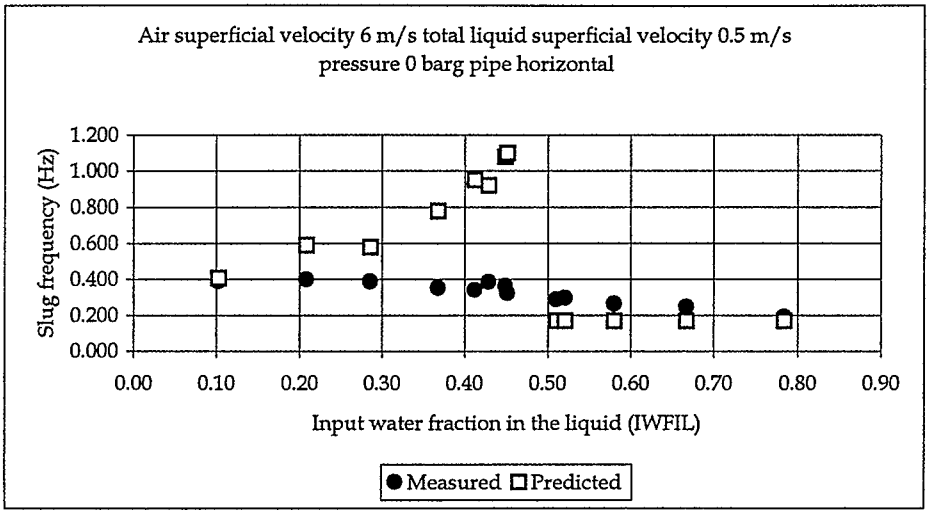


Figure 6.59: Comparison of WASP three-phase slug frequency experimental data with predictions by the correlation of Manolis (1995) ($U_{A,S}$ = 6 m/s, $U_{L,S}$ = 0.5 m/s, p= 0 barg, pipe = horizontal)

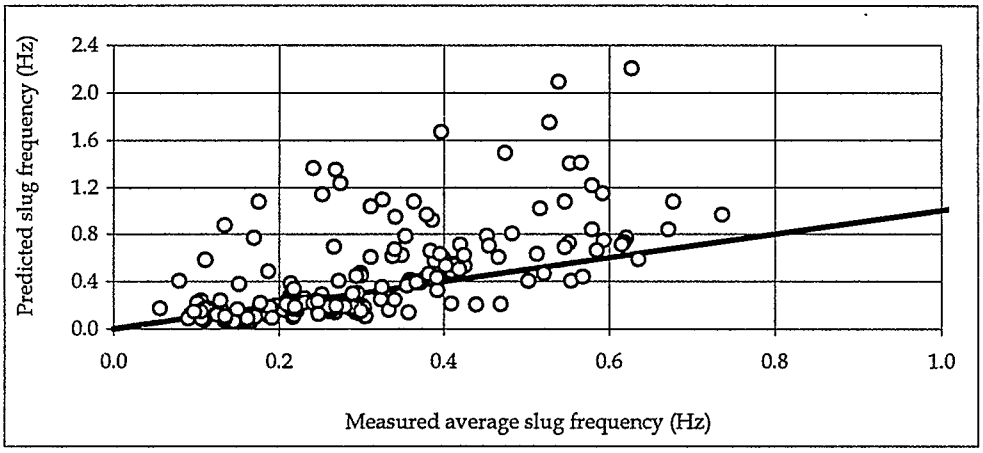


Figure 6.60: Comparison of WASP three-phase slug frequency experimental data with Manolis' correlation (1995)

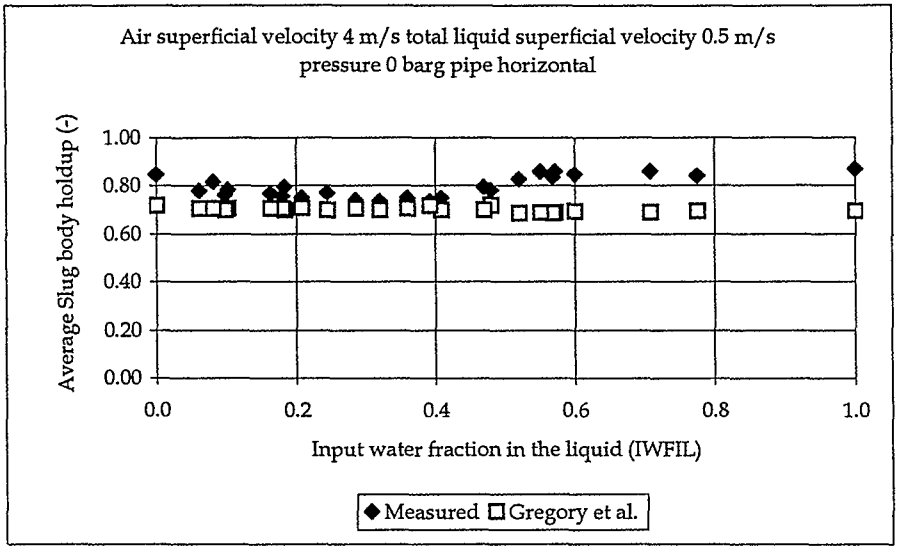


Figure 6.61: Comparison of WASP three-phase slug body holdup experimental data with the predictions by the correlation of Gregory *et al.* (1978) ($U_{A,S}$ = 4 m/s, $U_{L,S}$ = 0.5 m/s, P= 0 barg pipe = horizontal)

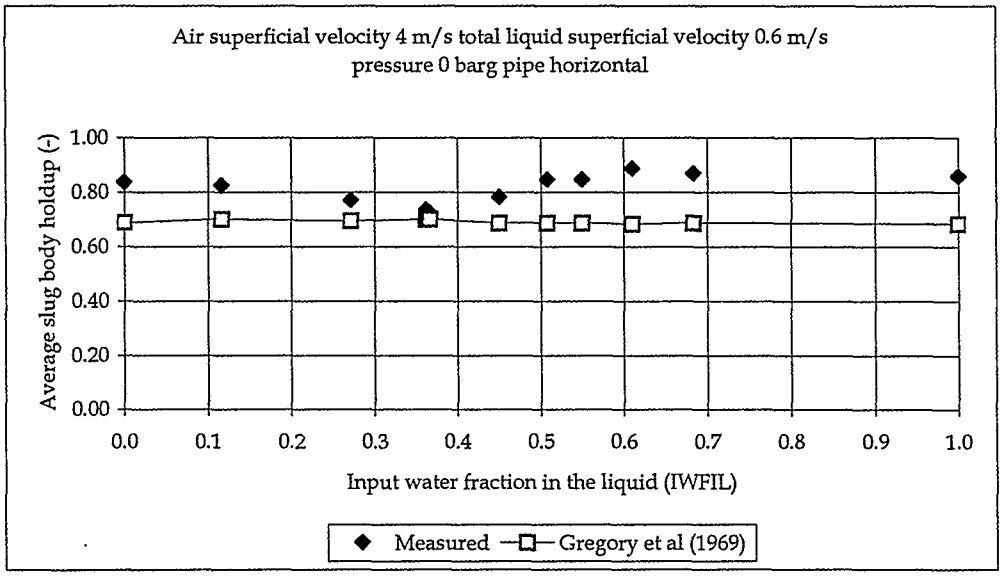


Figure 6.62: Comparison of WASP three-phase slug body holdup experimental data with the predictions by the correlation of Gregory *et al.* (1978) ($U_{A,S}$ = 4 m/s, $U_{L,S}$ = 0.5 m/s, p= 5 barg pipe = horizontal)

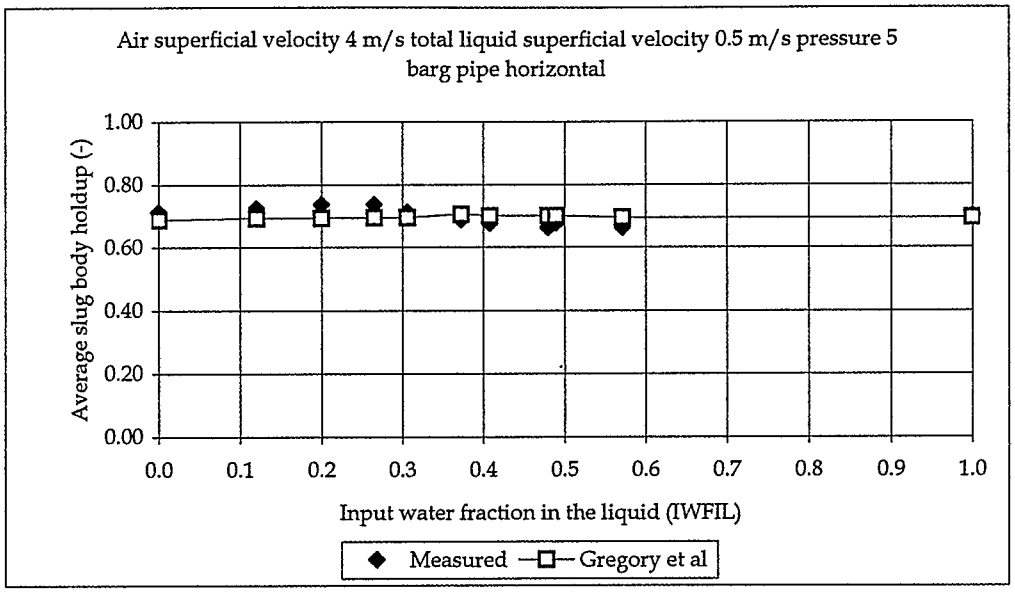


Figure 6.63: Comparison of WASP three-phase slug body holdup experimental data with the predictions by the correlation of Gregory *et al.* (1978) ($U_{A,S}$ = 4 m/s, $U_{L,S}$ = 0.5 m/s, p= 5 barg pipe = horizontal)

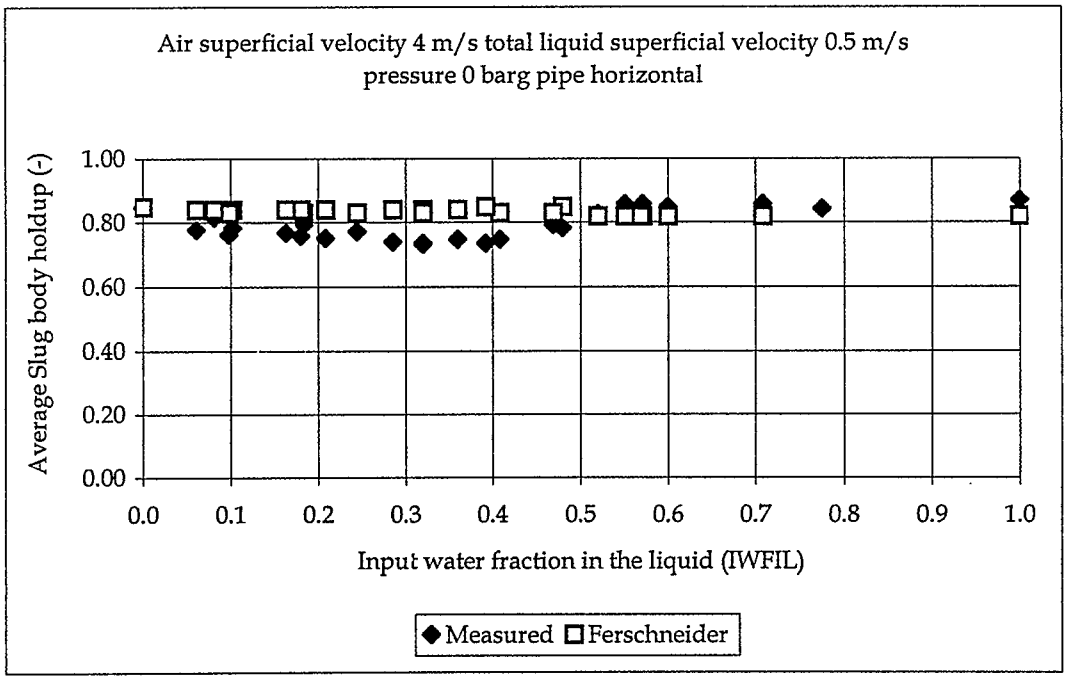


Figure 6.64: Comparison of WASP three-phase slug body holdup experimental data with the predictions by the correlation of Ferschneider (1983) ($U_{A,S}$ = 4 m/s, $U_{L,S}$ = 0.5 m/s, p= 0 barg, pipe = horizontal)

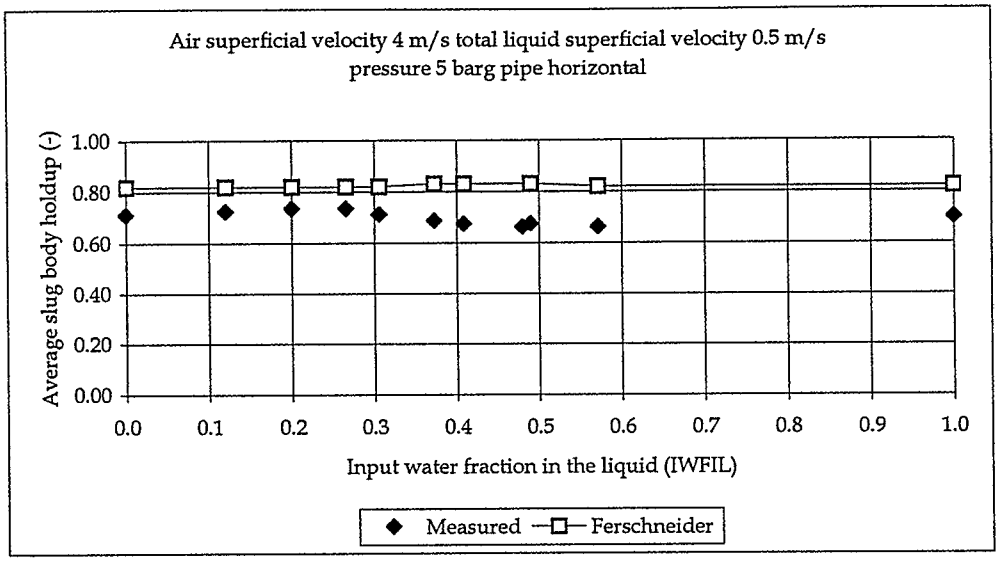


Figure 6.65: Comparison of WASP three-phase slug body holdup experimental data with the predictions by the correlation of Ferschneider (1983) ($U_{A,S}$ = 4 m/s, $U_{L,S}$ = 0.5 m/s, p= 5 barg, pipe = horizontal)

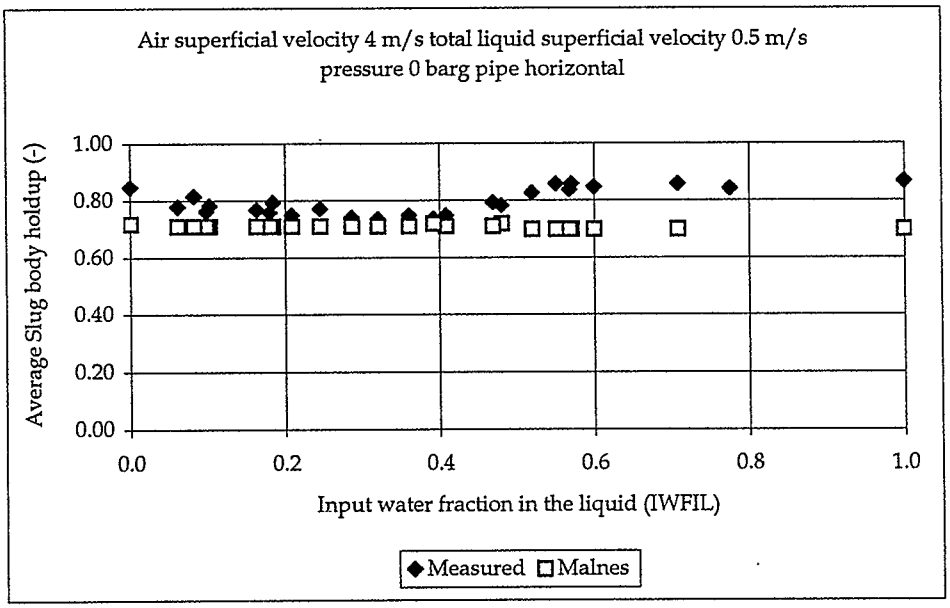


Figure 6.66: Comparison of WASP three-phase slug body holdup experimental data with the predictions by the correlation of Malnes (1983) ($U_{A,S}$ = 4 m/s, $U_{L,S}$ = 0.5 m/s, p= 0 barg, pipe = horizontal)

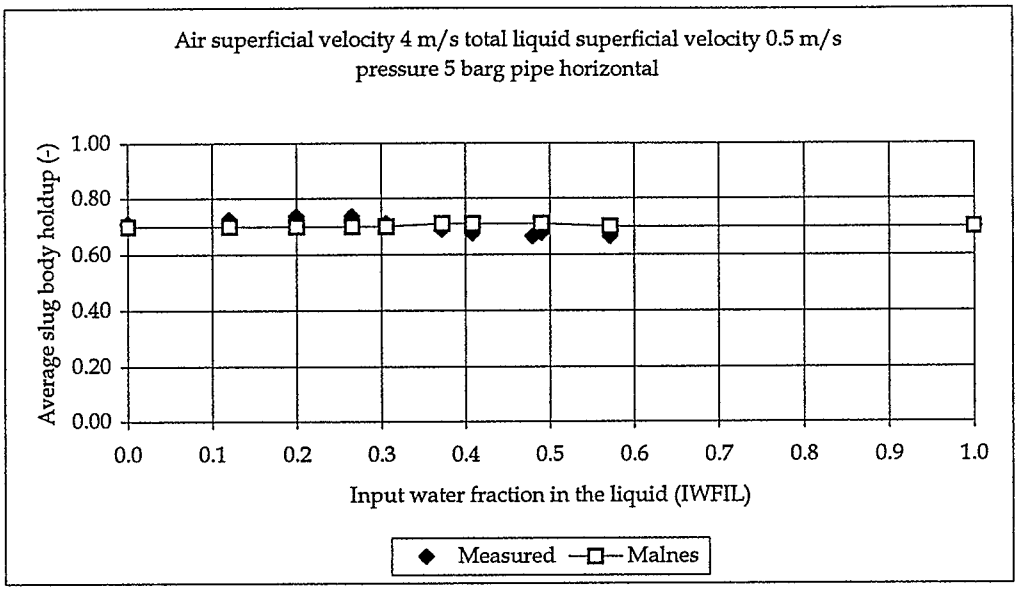


Figure 6.67: Comparison of WASP three-phase slug body holdup experimental data with the predictions by the correlation of Malnes (1983) ($U_{A,S}$ = 4 m/s, $U_{L,S}$ = 0.5 m/s, p= 5 barg, pipe = horizontal)

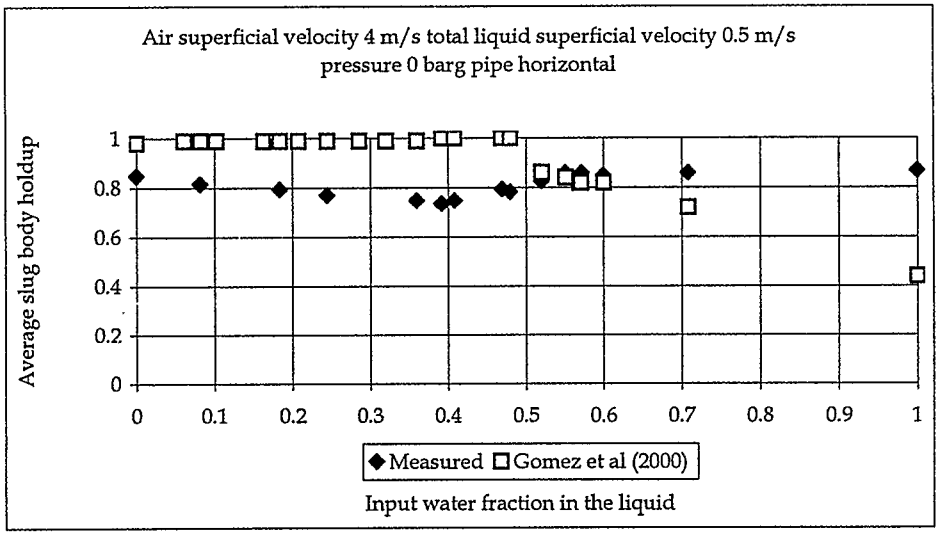


Figure 6.68: Comparison of WASP three-phase slug body holdup experimental data with the predictions by the correlation of Gomez *et al.* (2000) ($U_{A,S}$ = 4 m/s, $U_{L,S}$ = 0.5 m/s, p= 0 barg pipe = horizontal)

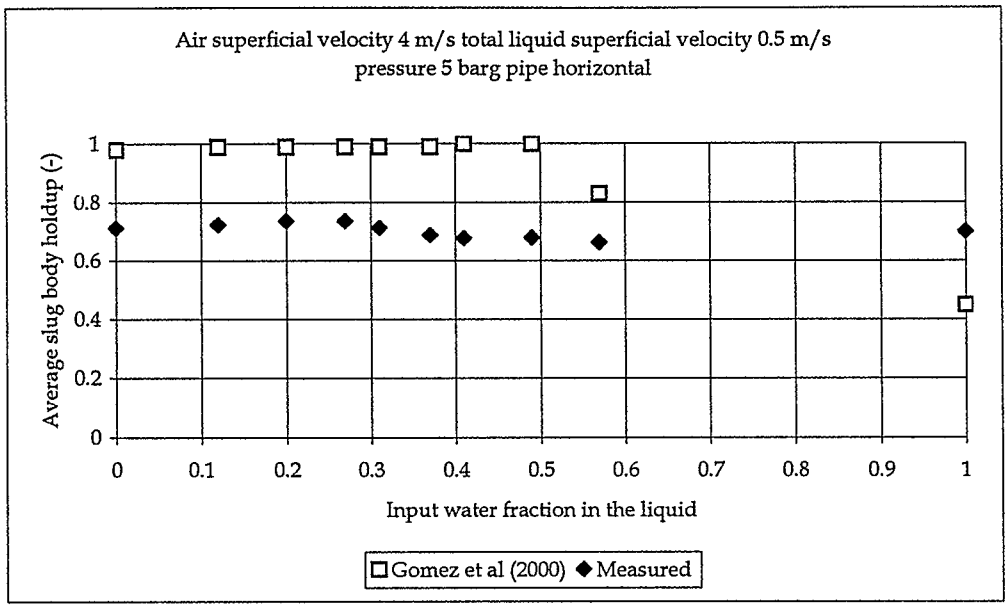


Figure 6.69: Comparison of WASP three-phase slug body holdup experimental data with the predictions by the correlation of Gomez *et al.* (2000) ($U_{A,S}$ = 4 m/s, $U_{L,S}$ = 0.5 m/s, p= 5 barg, pipe = horizontal)

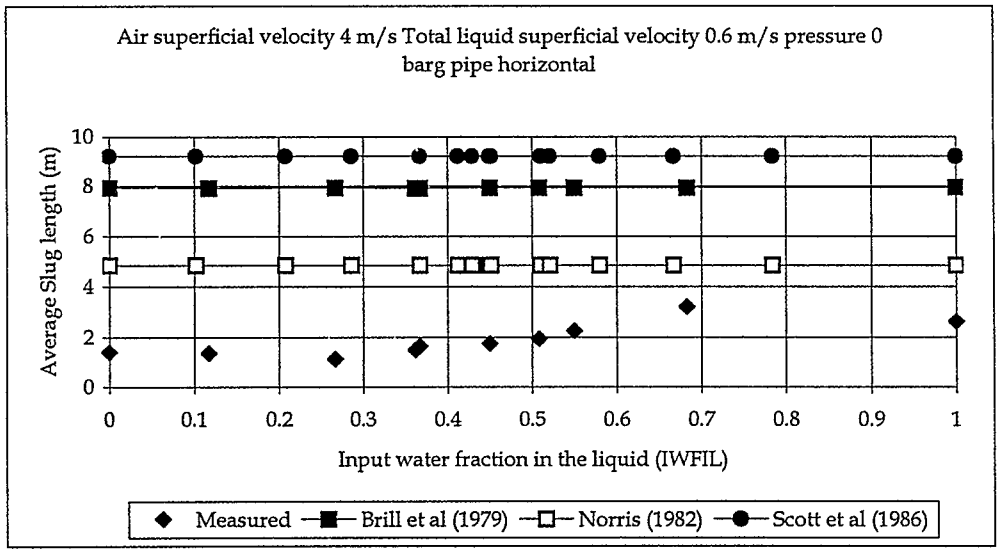


Figure 6.70: Comparison of WASP three-phase average slug length data with the predictions from the correlations of Brill *et al.* (1979), Norris (1982) and Scott *et al.* (1986) ($U_{A,S}$ = 4 m/s, $U_{L,S}$ = 0.6 m/s, p= 0 barg pipe = horizontal)

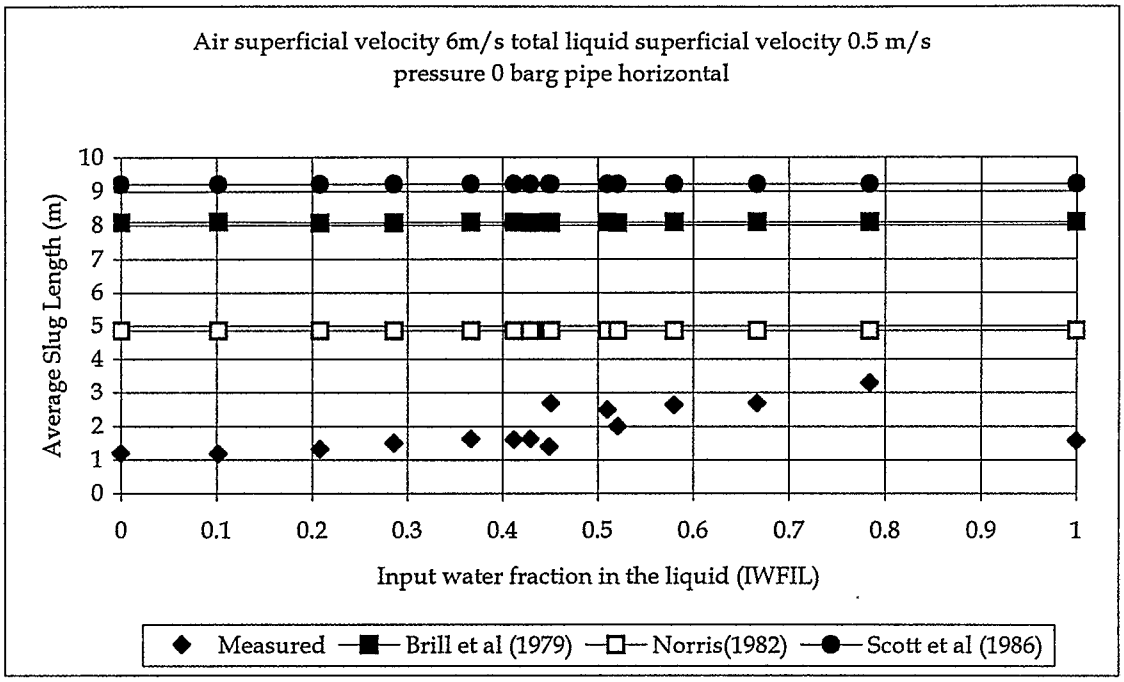


Figure 6.71: Comparison of WASP three-phase average slug length data with the predictions from the correlations of Brill *et al.* (1979), Norris (1982) and Scott *et al.* (1986) ($U_{A,S}$ = 6 m/s, $U_{L,S}$ = 0.5 m/s, p= 0 barg pipe = horizontal)

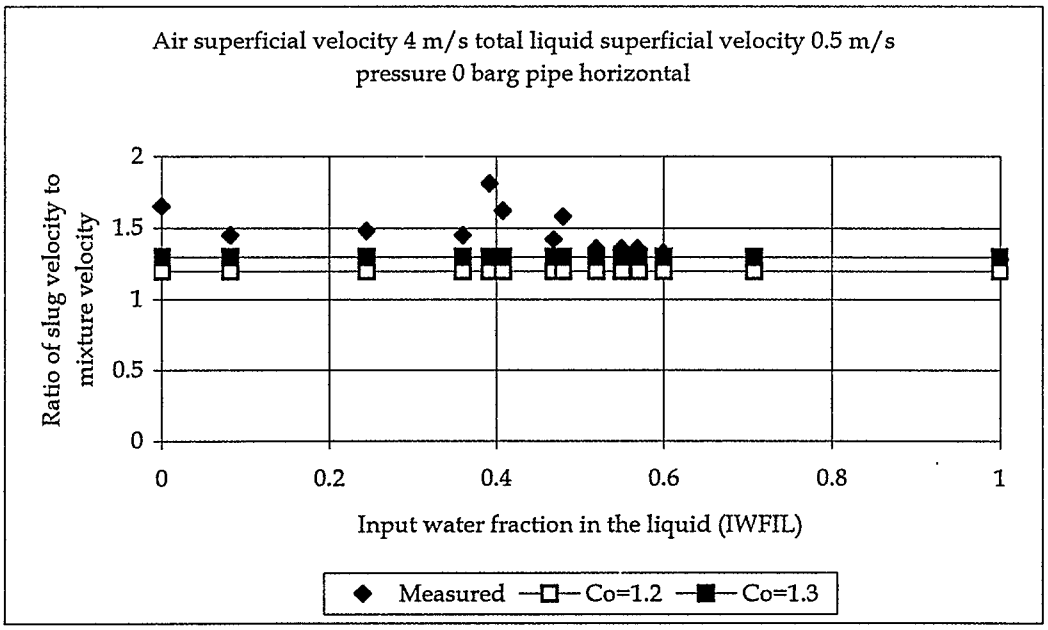


Figure 6.72: Comparison of WASP three-phase Co ratio experimental data with the predictions by the expression of Bendiksen (1984) ($U_{A,S}$ = 4 m/s, $U_{L,S}$= 0.5 m/s, p= 0 barg pipe = horizontal)

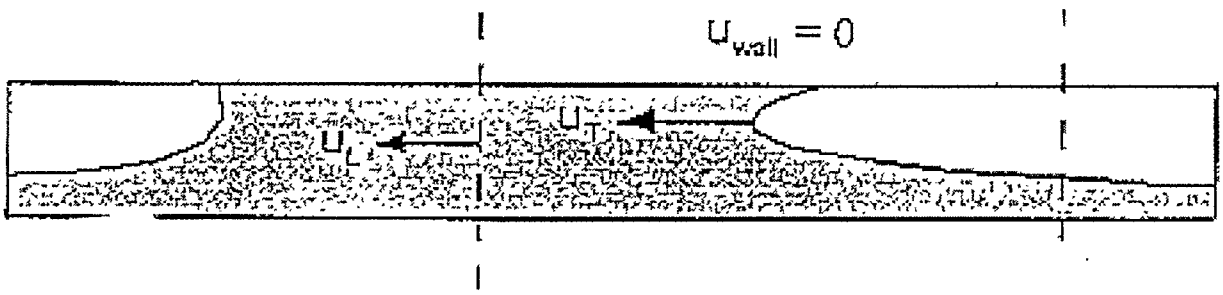


Figure 6.73: Slug flow in a fixed coordinate system

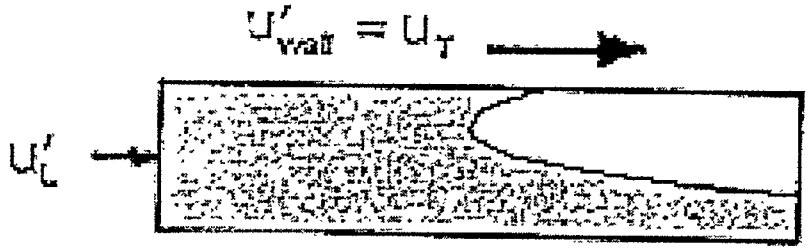


Figure 6.74: Slug flow in a moving coordinate system

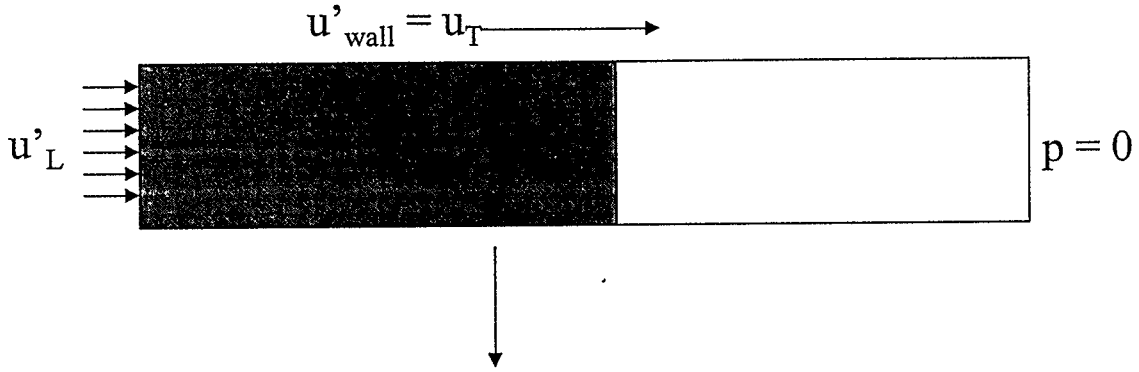


Figure 6.75: Initial conditions for slug tail simulation

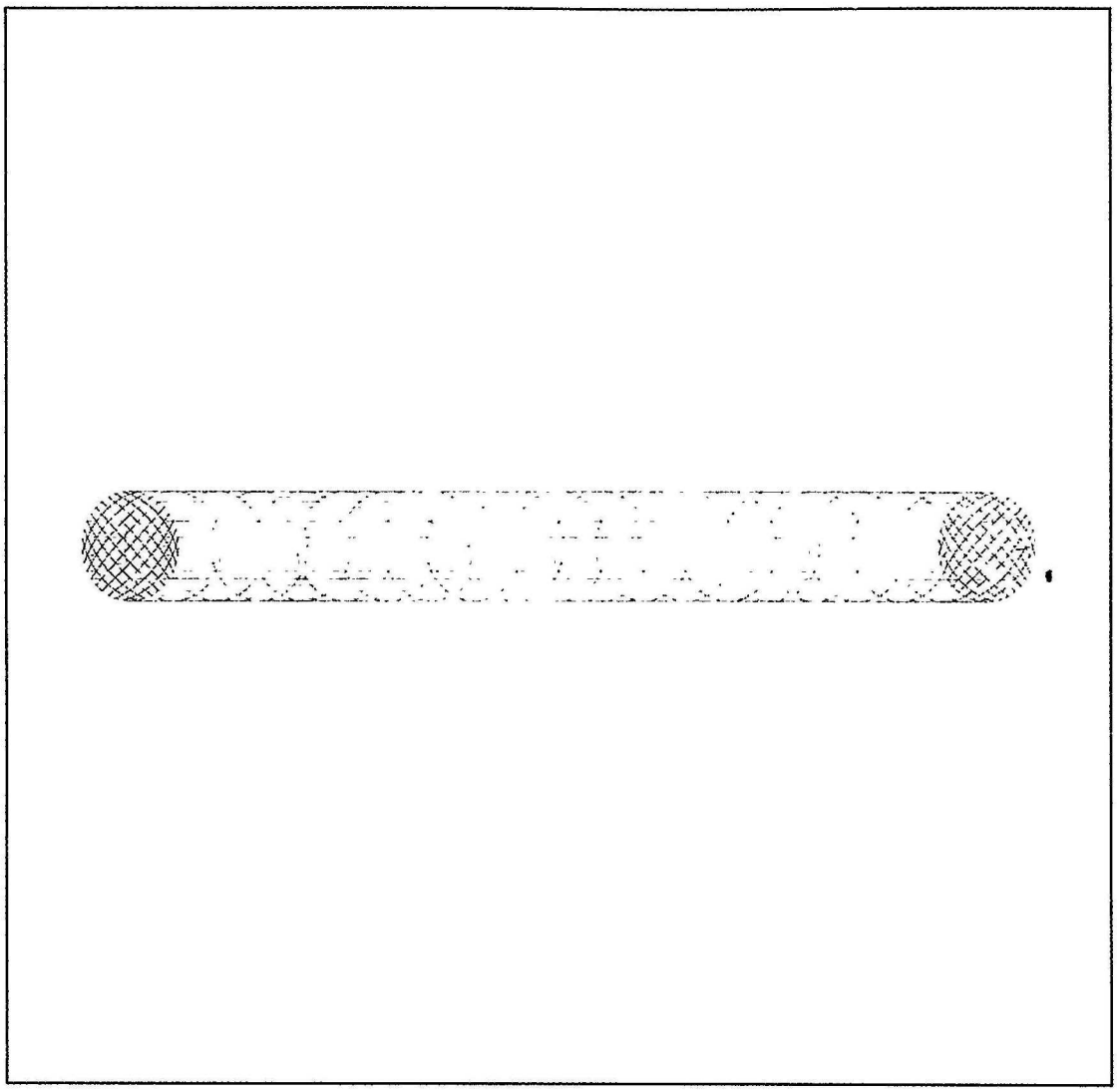


Figure 6.76:The Geometry of the Computational Domain

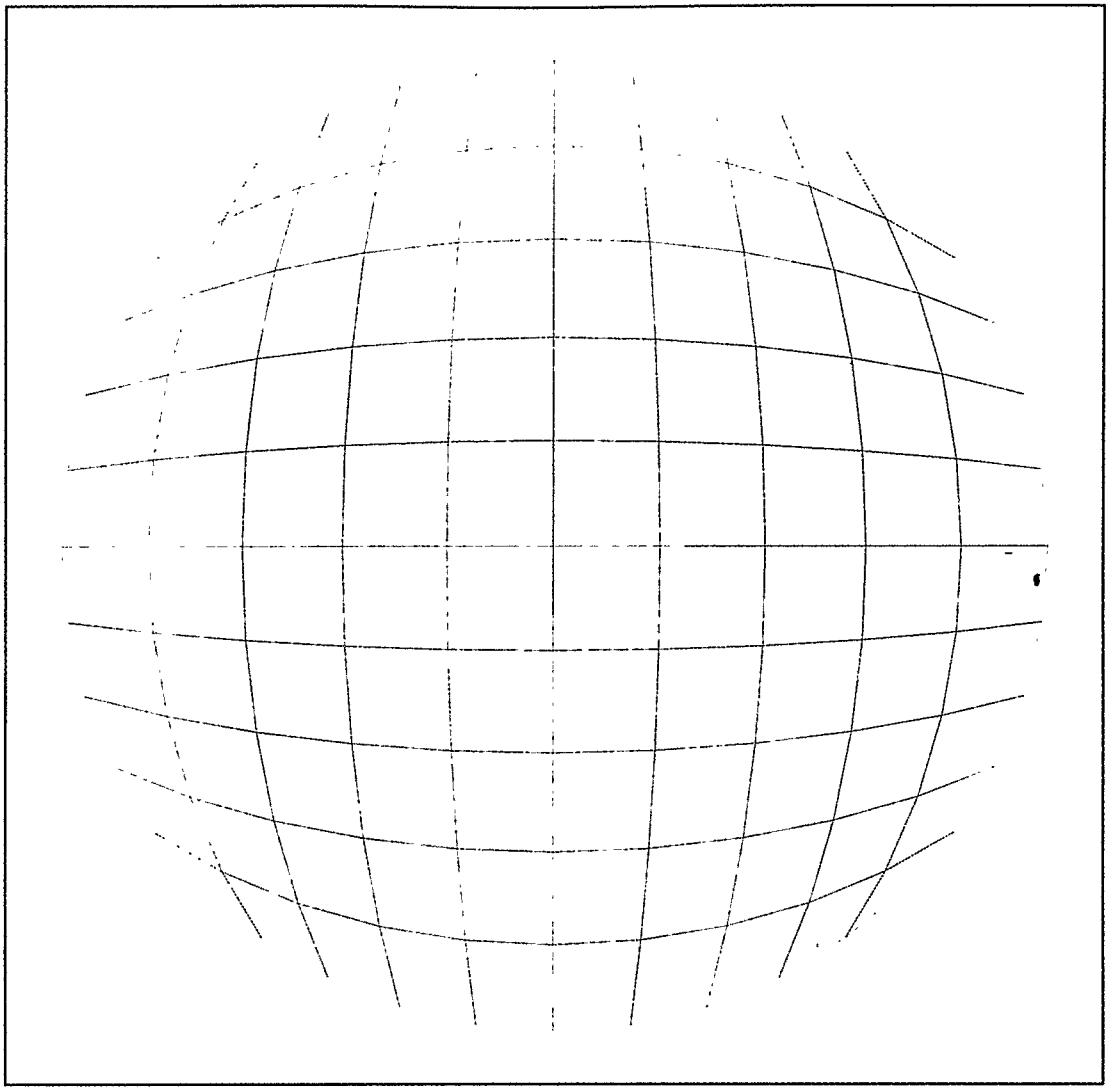


Figure 6.77: The Mesh of the Computational Domain

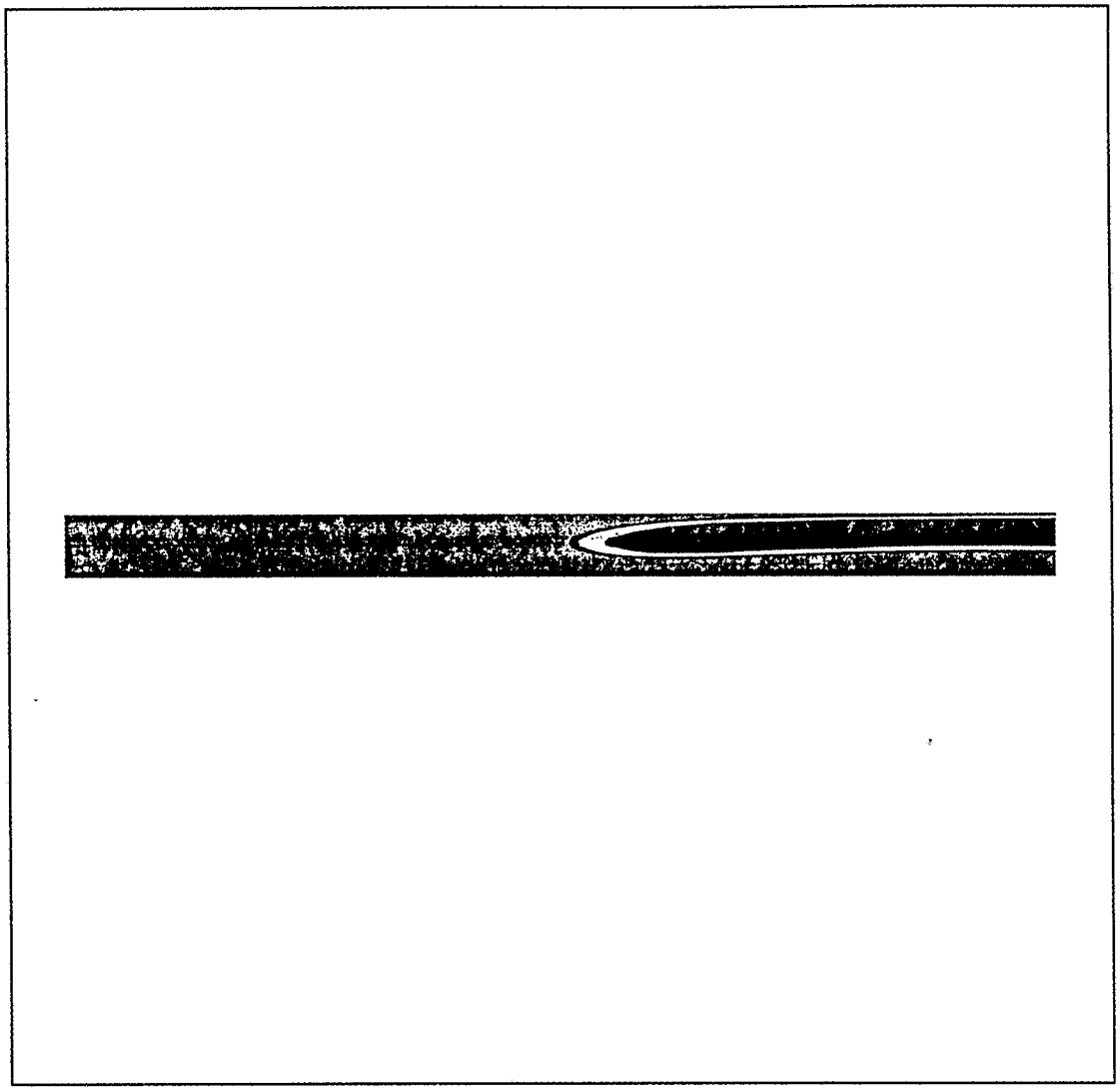


Figure 6.78: Gas-Liquid Phase Distribution for Horizontal Air-Oil-Water Slug Flow (Mixture Velocity 4.0 m/s Time: 1.0 s Water cut 40 %)

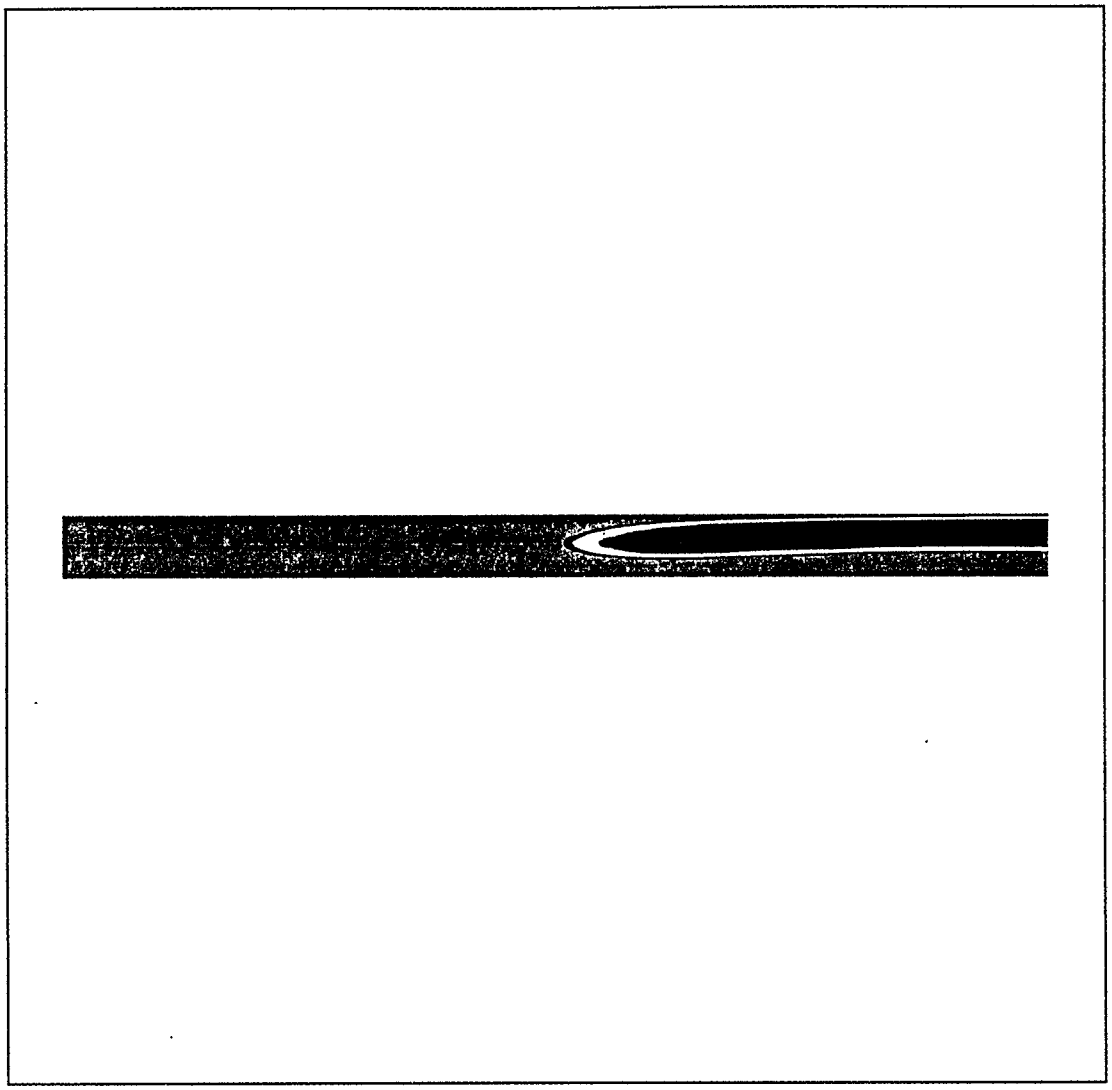


Figure 6.79: Gas Phase Distribution for Horizontal Air-Oil-Water Slug Flow (Mixture Velocity 4.0 m/s Time: 2.0 s Water-cut 40%)

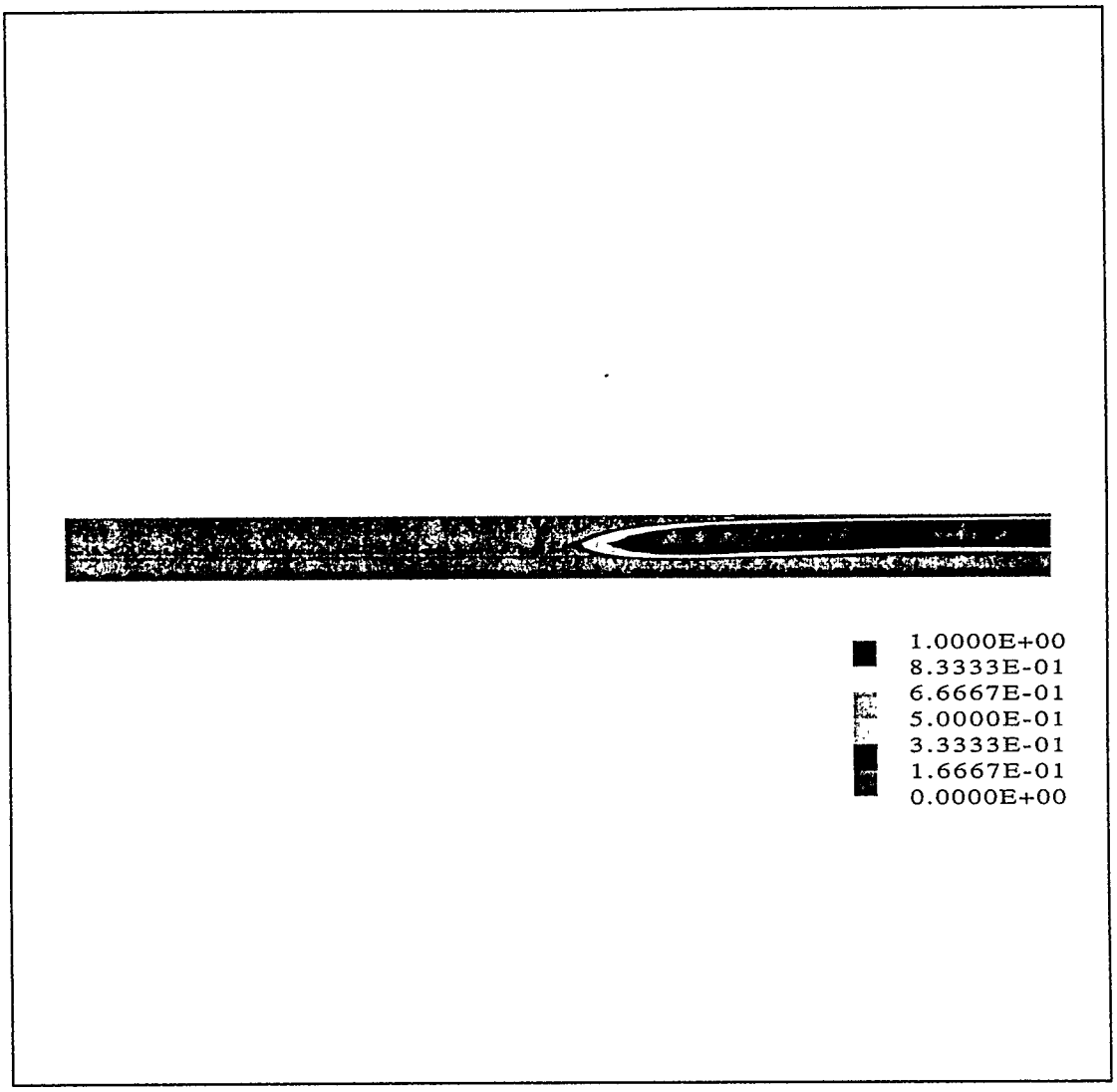


Figure 6.80: Gas Phase Distribution for Horizontal Air-Oil-Water Slug Flow (Mixture Velocity 4.0 m/s Time: 3.0 s. Water-cut 40 %)

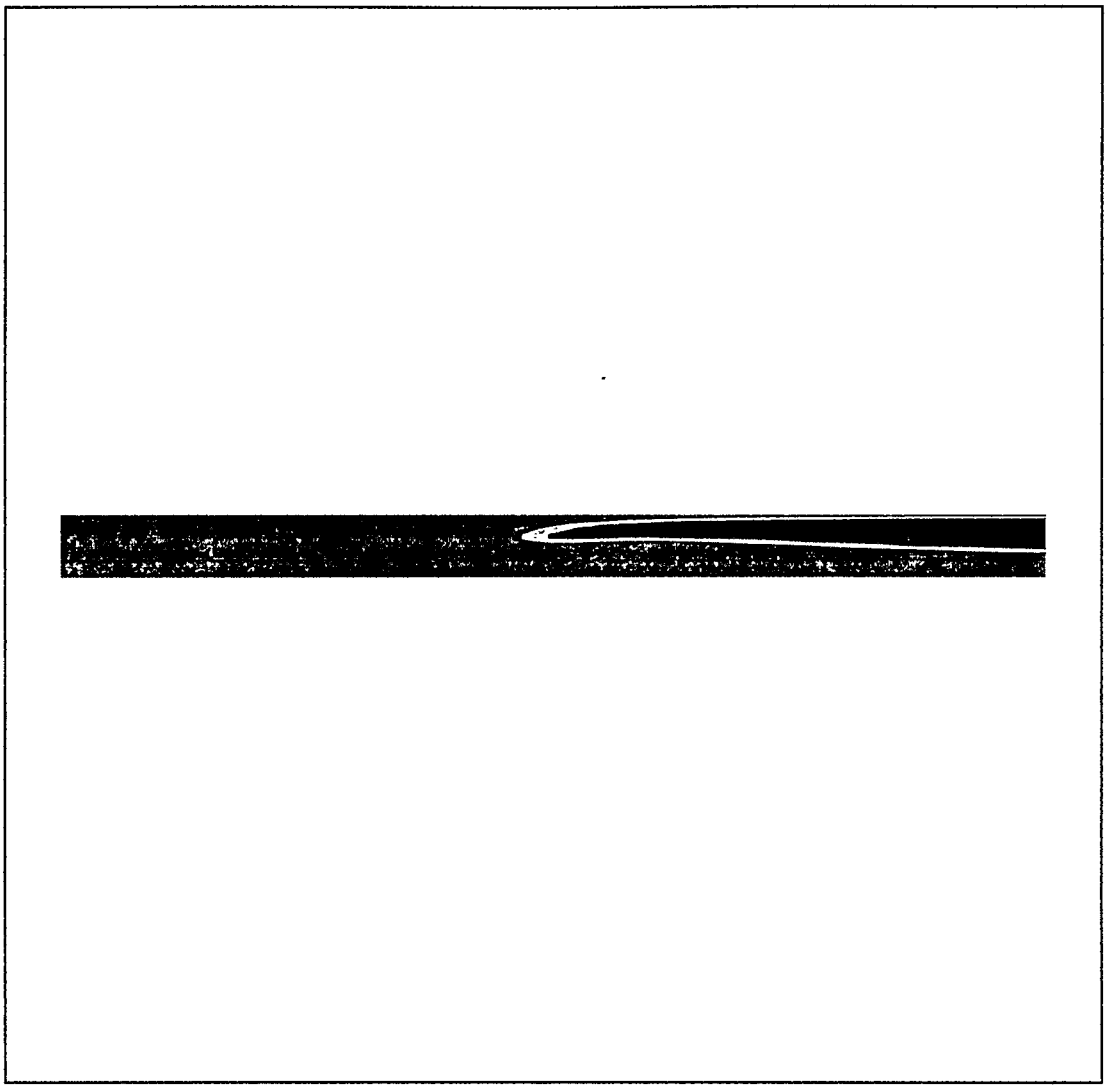


Figure 6.81: Gas-Liquid Phase Distribution for Horizontal Air-Oil-Water Slug Flow (Mixture Velocity 4.0 m/s Time: 3.0 s Water-Cut 0%)

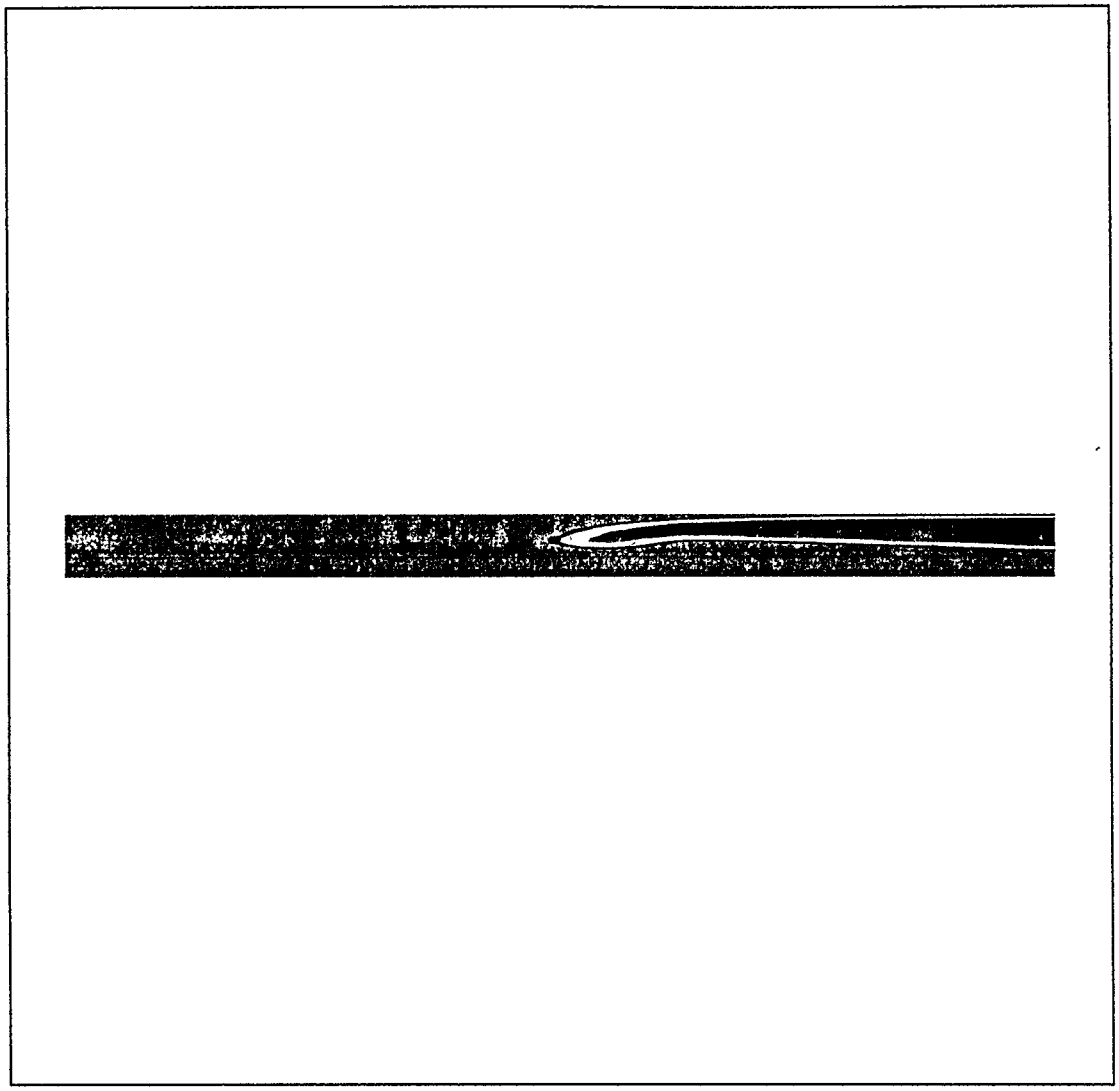


Figure 6.82: Gas-Liquid Phase Distribution for Horizontal Air-Oil-Water Slug Flow (Mixture Velocity 4.0 m/s Time: 3.0 s Water-Cut 20%)

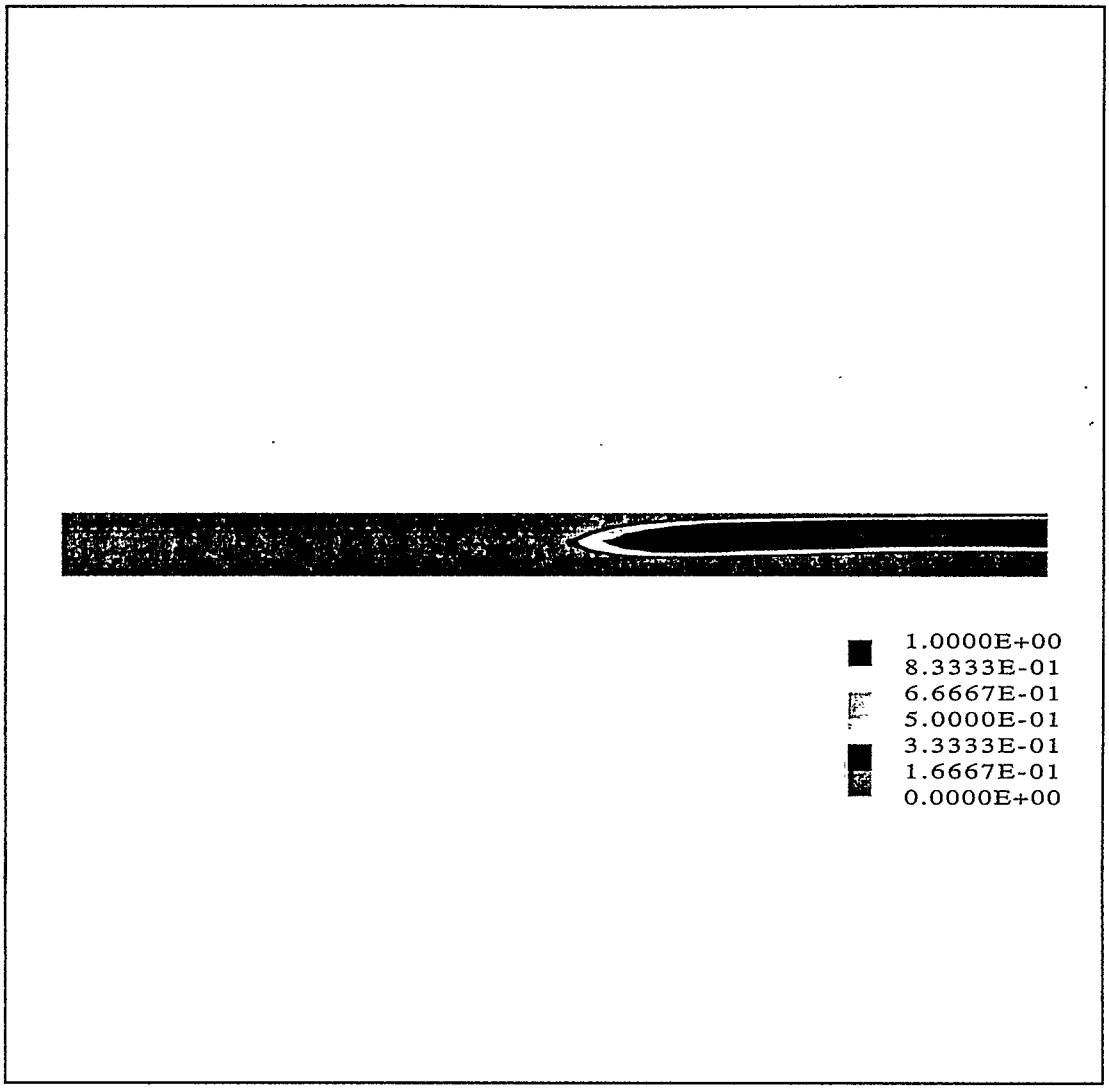


Figure 6.83: Gas-Liquid Phase Distribution for Horizontal Air-Oil-Water Slug Flow (Mixture Velocity 4.0 m/s Time: 3.0 s Water-Cut 40%)

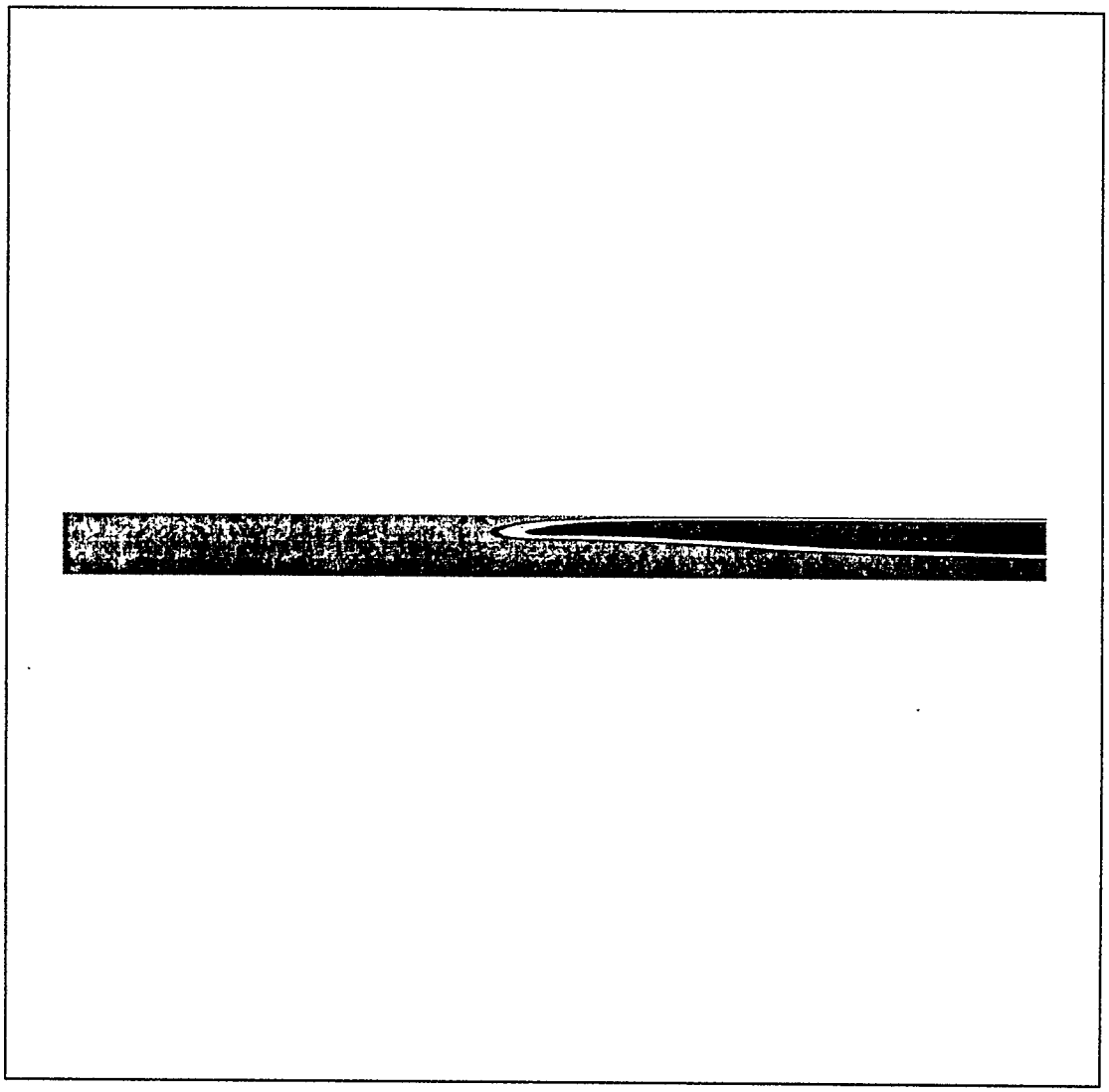


Figure 6.84: Gas-Liquid Phase Distribution for Horizontal Air-Oil-Water Slug Flow (Mixture Velocity 4.0 m/s Time: 3.0 s Water-Cut 55%)

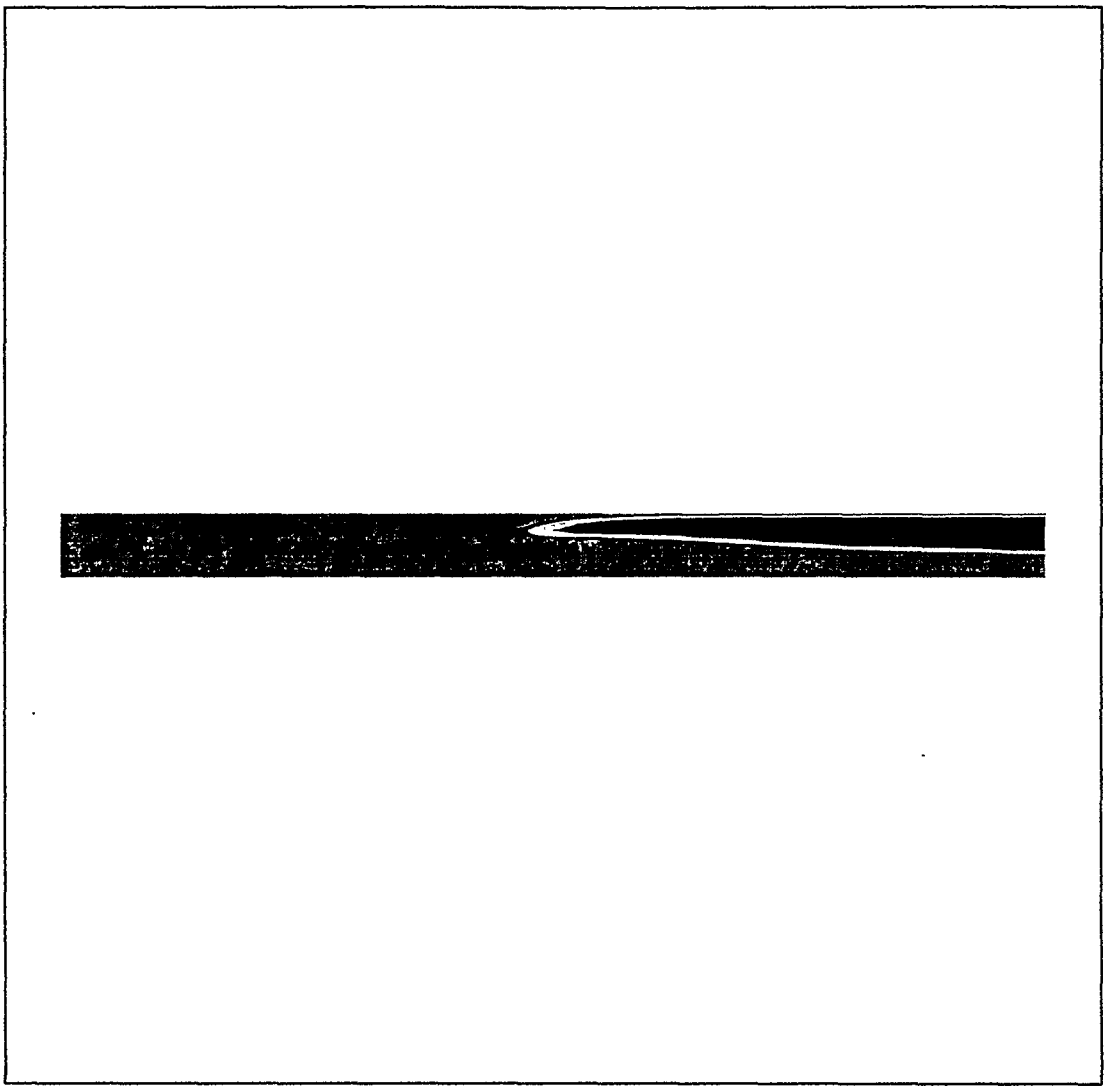


Figure 6.85: Gas-Liquid Phase Distribution for Horizontal Air-Oil-Water Slug Flow (Mixture Velocity 4.0 m/s Time: 3.0 s Water-Cut 70%)

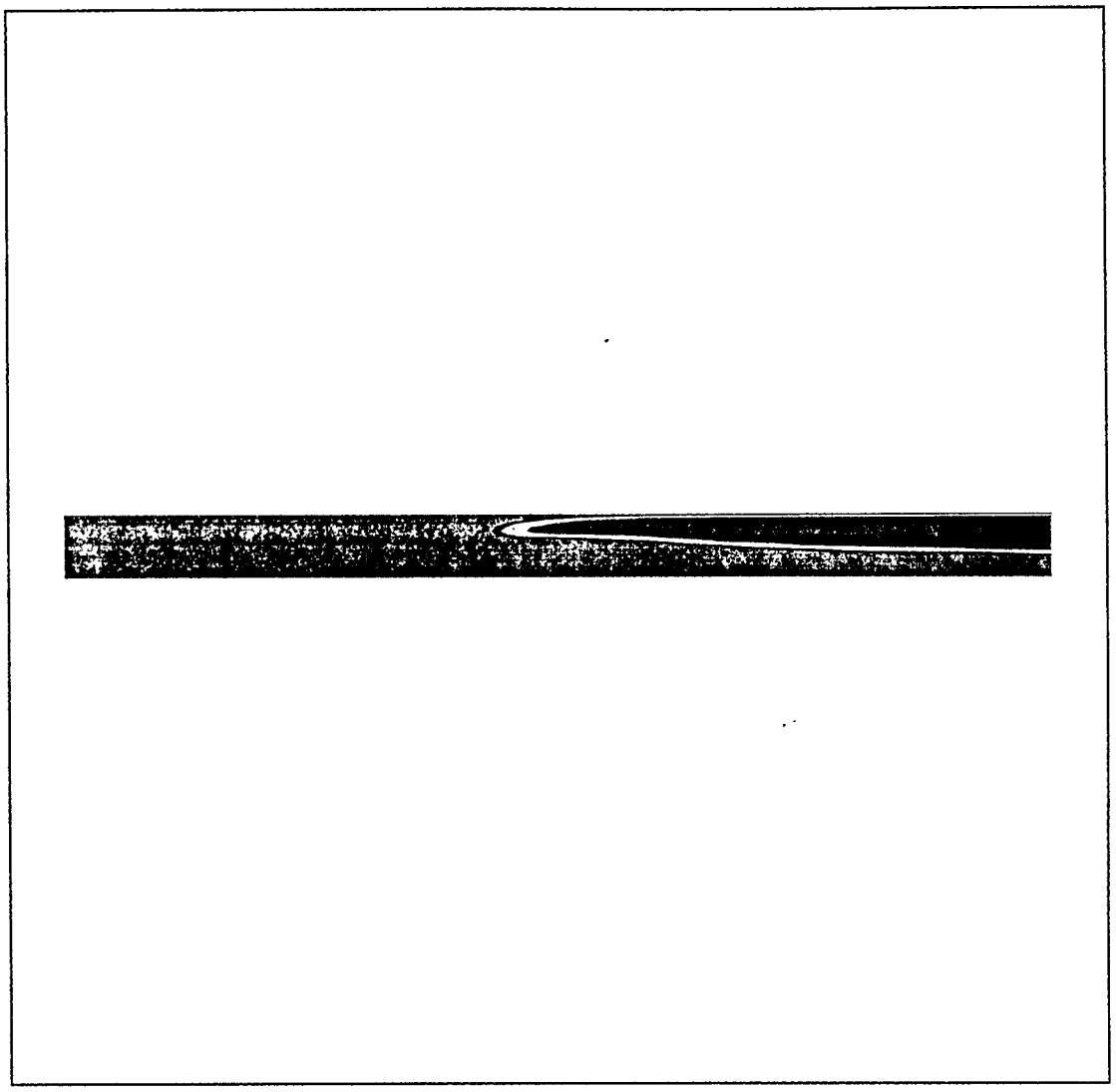


Figure 6.86: Gas-Liquid Phase Distribution for Horizontal Air-Oil-Water Slug Flow (Mixture Velocity 4.0 m/s Time: 3.0 s Water-Cut 100%)

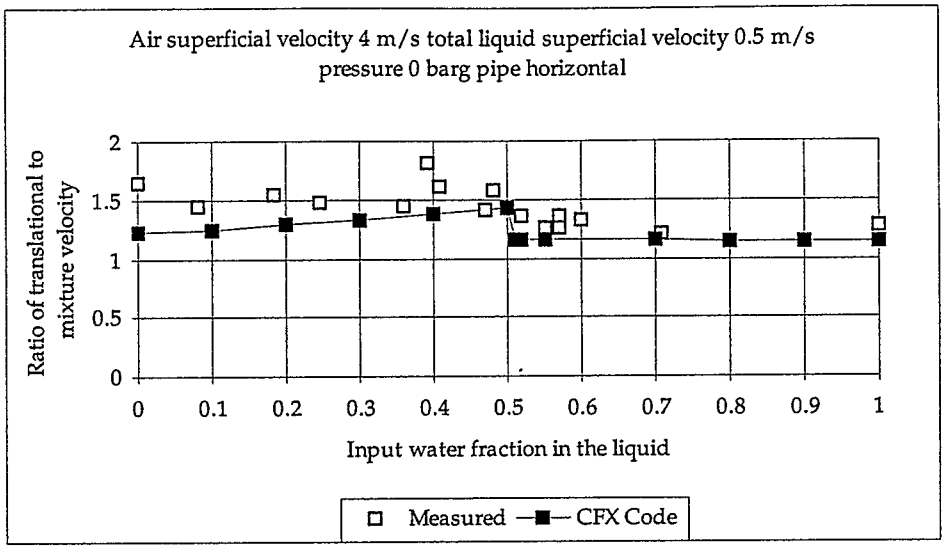


Figure 6.87: Comparison of WASP ratio of translational velocity to mixture velocity with the predictions by the CFX code ($U_{A,S}$= 4 m/s, $U_{L,S}$= 0.5 m/s, p= 0 barg, pipe = horizontal)

Chapter 7

CONCLUSIONS AND RECOMMENDATIONS FOR FUTURE WORK

The work that was carried out in the course of this thesis is summarised and conclusions made. In addition to this, recommendations for future work are put forward.

7.1 CONCLUSIONS

7.1.1 Steady state results

Three-phase air-oil-water flow data were obtained on pressure gradient and hold-up for a wide range of flow conditions, pipe configurations and system pressures. The effect of the air superficial velocity and the liquid superficial velocity on the position of the peak on the pressure gradient versus water-cut plot was investigated.

The experimental results showed that the air superficial velocity had a significant effect on the position of the pressure gradient peak. Increasing the air superficial velocity (holding all other factors constant) leads to a decrease in the water-cut at which the peak in the measured pressure gradient occurs.

Peaks were observed in both the measured pressure gradient and the total liquid holdup, when these parameters were plotted against the water-cut. The data are in good agreement with those of Pan (1996) for the range of conditions he covered. However, the present data greatly extend this range, particularly in the case of oil superficial velocity.

New data on three-phase air-oil water slug flow characteristics were obtained. The data showed the significant effect the water-cut and thus the apparent liquid viscosity had on these characteristics.

Experimental data on slug frequency revealed that the slug frequency for oil-continuous flows exceeded those measured in water-continuous flows for the same set

of conditions. Under some sets of conditions, the slug frequency exhibited the same trends as observed in the pressure gradient (a peak in the phase inversion region)

Unique data on the slug body holdup in three-phase air-oil-water flow were presented and these showed that the water-cut has a significant effect on the slug body holdup, particularly for water-cuts in the phase inversion region. The results of the average liquid film holdup showed significant increases in the phase inversion region.

By cross-correlating the signals from two dual-energy gamma densitometers, it was possible to obtain data on slug translational velocities in three-phase air-oil-water slug flow. Experimental data on the ratio of the slug velocity to the mixture velocity showed that its value was a strong function of the water-cut, with maximum values of as high as 2 observed in the phase inversion region.

The cross-correlation procedure also revealed slug lengths for three-phase air-oil-water flow. The slug lengths in water-continuous flows were found to be greater than those for oil-continuous flows for the same set of conditions.

7.1.2 Flow Patterns and Flow Pattern Maps

Flow pattern data obtained from three-phase air-oil-water experiments carried out under various flow conditions, system pressures and pipeline inclinations were presented.

The data revealed that the system pressure had strong effects on the transition lines between various flow regimes. It was observed that increasing the system pressure decreased the air superficial velocity at which the stratified/slug and slug/ annular transitions took place for both horizontal and inclined flows.

The pipe inclination was shown to have a profound influence on the flow pattern map. When the pipeline inclination was changed from 0° (horizontal) to –1.5°, the area of the flow pattern map occupied by the stratified flow regime increased drastically at the expense of the slug flow regime.

A comparison of the horizontal flow pattern data from this work with the horizontal flow pattern map of Acikgoz *et al.* (1992) revealed that this map was not applicable. The reason for this was attributed to the fact that the map of Acikgoz *et al* was derived from a different pipe diameter, utilising an oil of a different viscosity.

When the flow pattern data from this work was compared with the horizontal flow pattern map of Pan (1996), there was good agreement as most of the flow patterns fell in the designated area of Pan's flow pattern map. The reason for the improved performance was because the same facilities and fluids were used in both cases. However, the map could be extended to the higher oil superficial velocity used in the current work.

7.1.3 Comparisons with empirical correlations

The experimental data on pressure gradient, liquid holdup and slug parameters obtained for horizontal flows was tested against existing two-phase gas-liquid correlations. A new viscosity model was derived for the combined liquid phase.

For pressure drop prediction, it was found that the correlations of Dukler *et al.* (1964) and Schlichting (1970) showed the closest match with the experimental data while the correlation of Chisholm (1967) showed the largest errors.

The measured total liquid holdup was compared with the empirical correlations of Lockhart and Martinelli (1949), Guzhov *et al.* (1967), Beggs and Brill (1973) and Minami and Brill (1987). Comparisons showed that the correlations of Beggs and Brill (1973) and Guzhov *et al.* (1967) failed to predict the influence of the water-cut on the total liquid holdup. Although the correlations of Lockhart and Martinelli (1949) and Minami and Brill (1987) accounted for the influence of the viscosity on the total liquid holdup, there was a tendency for these correlations to over-predict the experimental data.

The slug frequency data were compared against a number of existing gas-liquid slug frequency correlations. The correlations of Gregory and Scott (1969) and Heywood and Richardson (1979) failed to account for the influence of the liquid viscosity on the

slug frequency. Although the correlations of Hill and Wood (1990), Tronconi (1990) and Manolis (1995) account for the influence of the liquid viscosity on the slug frequency, the correlations significantly over-predicted the slug frequency in the phase inversion region. The correlation of Hill and Wood (1990) came closest in predicting the trend in the slug frequency with water-cut.

Likewise, in the case of the slug body hold-up prediction, none of the existing gas-liquid correlations (Gregory *et al.*, 1978, Ferschneider, 1983, and Malnes, 1983) with the exception of Gomez *et al.* (2000) account for the influence of the liquid viscosity on the slug body holdup. All the correlations, predict a constant slug body holdup with increasing water-cut contrary to the experimental data and contrary to the results of Manolis (1995) and Nadler and Mewes (1995) for gas-liquid flow, which showed the significant effects of the liquid viscosity on the slug body hold-up.

7.1.4 Comparisons with Phenomenological models

The experimental data was compared with two phenomenological slug models Bonnecaze *et al* (1971) and a modified version of the Taitel and Barnea (1990). The comparisons showed that the Bonnecaze model significantly over-predicts the data, whereas the modified Taitel and Barnea model gives a more reasonable prediction of the data.

7.1.5 Comparisons with CFD code

Using the dam break model developed by Hope (1990) and following up on the work of Pan (1990), slug tails in three-phase air-oil-water flow were modelled. The work focused on investigating the effect of the water-cut on the ratio of slug to mixture velocity. Results from the CFD simulations using CFX 4.2, a commercially available code, were presented and compared with the experimental data. The CFX code predicted a significant increase in the velocity ratio near the phase inversion, in agreement with the experimental data.

7.2 FUTURE WORK

In the light of the work that has been carried out, there is room for future work to be carried out along the areas outlined

7.2.1 Steady state flows

(1) The phase inversion water-cut was correlated here with the air superficial velocity. The effects of liquid velocity and pressure appeared to be small. However, it is recommended that the data be extended to obtain a correlation for the effects of these and other parameters.

(2) Although data on slug parameters such as slug velocity and slug length were obtained in three-phase air-oil-water slug flow, the acquisition frequency of the gamma densitometer (25 Hz) limited the mixture velocities that could be used. It is recommended that a higher frequency gamma densitometer be employed for tracking the slugs to obtain slug characteristics over a wider range of flow conditions.

(3) The Taitel and Barnea model was modified and compared to the experimental data with good results. However, the model makes use of closure laws, which have been found to be inadequate for three-phase flow. It is recommended that improved closure laws be developed and used.

(4) It is recommended that further experiments be carried out to develop three-phase air-oil-water correlations for slug body holdup and slug length.

7.2.2 CFD Study

Slug tails for three-phase air-oil-water flows have been successfully modelled using CFD. These simulations however, were carried out for fully dispersed slug flow, which is a reasonable assumption, for the data presented in this thesis. It is

recommended that the model be extended to those flow conditions where separation takes place within the liquid layer.

REFERENCES

Açikgoz, M., Lahey, Jr., R. T. and França, F. (1992), "An Experimental Study Of Three-Phase Flow Regimes," *Int. J. Multiphase Flow,* Vol. 18, No. 3, p.341.

Andreussi, P. and Bendiksen K. (1989) " An Investigation Of Void Fraction In Liquid Slugs For Horizontal And Inclined Gas-Liquid Pipe Flow" *Int. J. Multiphase Flow* Vol. 15, p 937.

Angeli P. (1996) "Liquid-Liquid Dispersed Flows In Horizontal Pipes" Ph.D. dissertation, Chem. Eng. Dept., Imperial College, University of London.

Aziz, K., Nicholson M. K and Gregory, G. A. (1978) "Intermittent Two-Phase Flow In Horizontal Pipes- Predictive Models," *Can J Chem. Eng.* Vol. 56, No. 12, p. 653

Badie, S. B. (2000) "Horizontal Stratifying /Annular Gas-Liquid Flow" Ph.D. dissertation, Chem. Eng. Dept., Imperial College, University of London.

Barnea, D and Brauner, N (1985) "Holdup of the Liquid Slug in two-phase intermittent Flow" *Int. J. Multiphase Flow*, Vol. 11, No 1, p. 43.

Baroczy, C. J. (1966), " A systematic correlation for two-phase pressure drop," *CEP Symp. Ser.*, Vol. 62, No. 44, p. 232.

Beggs, H. D. and Brill J. P., (1973),"A Study Of Two-Phase Flow In Inclined Pipes," *Trans. J. of Petroleum Technology, Transactions* Vol. 255, p.607.

Benjamin, T. B. (1968) "Gravity Currents And Related Phenomena" *J. Fluid Mech.* Vol. 31, 209-248.

Bhongale S. (1995) "Effect Of Pressure, Temperature And Froude Number On Corrosion Under Horizontal Multiphase Flow" M. S. Thesis Ohio University, Athens, Ohio

Bonnecaze, R. H., Erskine, W. Jr. And Greskovich, E. J. (1971) "Holdup And Pressure Drop For Two Phase Slug Flow In Inclined Pipes" *AIChE Journal*, Vol. 17, No. 5, p. 1109.

Brandt I., and Fuches P. (1989) "Liquid Holdup In Slugs: Some Experimental Results From The SINTEF Two-Phase Flow Laboratory" *Proceedings of the BHRG 4th International Conference on Multiphase Flow*, Nice, France.

Brill, J. P., Schmidt, Z., Coberly, W. A, Herring, G. D. and Moore D. W (1981) "Analysis Of Two-Phase Tests In Large Diameter Flow Lines In Prudhoe Bay Field". *Soc. Pet Eng. Journal* Vol. 271, p. 363.

Brinkman, H. C. (1952)," The Viscosity of Concentrated Suspensions and Solutions, " *J. of Chemical Physics,* Vol. 20, No. 3, p 571.

Cai J., Chen T. and Luo Y. (1998) "The Experimental Investigations on the Pressure Drop of The three-Phase Flow of Gas-Water-Oil Emulsions in Horizontal Pipes" *3rd International Conference on Multiphase Flow*, ICMF'98, Lyon, France, June 8-12, 1998.

Chen X., Guo, L., Li G. and. Yu L. (1997) "Flow Patterns, Pressure Drop And Phase Separation In Air-Oil-Water Three-Phase Flow Through Pipelines" *ISMF 1997 Beijing October 7-11 1997*

Chisholm, D. (1967), "A theoretical basis for the Lockhart-and Martinelli correlation for two-phase flow" *Int. J. Heat Mass Transfer*, Vol. 10, p. 1767.

Crawley C. J. Richard S. C, Wallis G.B and Mehta D.C (1984) "Slug Flow in Large Diameter pipes I Effect of Fluid properties" *AIChE Annual Meeting* Nov. 25-30 San Francisco, California.

Davies, R. M. and Taylor, G. I. (1949), "The Mechanics Of Large Bubbles Rising Through Extended Liquids And Through Liquid Flowing In A Tube," *Proc. R. Soc.*, v. 200A, p. 375.

Davies, S. R. (1992) "Studies Of Two-Phase Intermittent Flow In Pipelines" Ph.D. thesis, Imperial College University of London, UK

Donnelly, G. F. (1997) "An Analytical Evaluation of Horizontal Multiphase Flow" Ph.D. Thesis, Queen's University of Belfast.

Dukler, A. E., Moye Wicks, III and Cleveland, R. G (1964) "Frictional Pressure Drop In Two-Phase Flow: A Comparison Of Existing Correlations For Pressure Loss And Holdup,"AIChE J. Vol. 10, No. 1, p. 38

Dukler, A. E. and Hubbard, M. G. (1975), "A Model For Gas-Liquid Slug Flow In Horizontal And Near Horizontal Tubes," *Ind. Eng. Chem., Fundam.*, Vol. 14, No. 4, p. 337.

Dumitrescu, D. T. (1943), "Stromung an einer Luftblase in senkrecten Rohr," *Z. Angew. Math. Mech.*, Vol. 23, p. 139.

Eilers H., (1941) Kolloid Z Vol. 97, p. 313

Einstein A. (1906) " A New Definition of Molecular Dimensions" Annlen der Physik (4) Vol. 19. P. 289 (in German)

Felizola H., (1992) " Slug Flow In Extended Reach Directional Wells" M.S. Thesis, The University of Tulsa.

Ferschneider, G. (1983) "Écoulements Diphasiques à Pouches en Conduite Horizontale" *Rev Inst. Fr Petr.*, Vol. 34, p. 113

Friedel L (1970) "Improved Friction Pressure Drop Correlations For Horizontal and Vertical Two-Phase Pipe Flow" European Two-phase Flow Group Meeting No. E2 Ispra Italy, June 1979

Gomez L. E., Shoham O. and Taitel Y. (2000) "Prediction Of Slug Liquid Holdup: Horizontal To Upward Vertical Flow" *Int. J. Multiphase Flow.* Vol. 26, p. 517.

Goncalves M. A. L., Silva C. B. C., and Pedras M. H. J. (1996) "Slug Measurements in Gas-Oil Pipeline" Petrobras Research Centre Internal Report.

Gregory, G. A. and Scott, D. S. (1969), "Correlation of liquid slug velocity and frequency in horizontal cocurrent gas-liquid slug flow," *AIChE J.*, Vol. 15, No. 6, p. 933.

Gregory, G. A., Nicholson, M. K and Aziz, K. (1978), "Correlation Of The Liquid Volume Fraction In The Slug For Horizontal Gas-Liquid Slug Flow," *Int. J. Multiphase Flow*, Vol. 4, No. 1, p. 33.

Greskovich, E.J, and Shrier A.L (1972) "Slug Frequency In Horizontal Gas-Liquid Flow" *Ind Eng., Proc. Des Develop.* Vol. 11 No. 2, p.317

Griffith P. and Wallis G. B. (1961) " Two Phase Slug Flow " *Journal of Heat Transfer*, Vol. 83, p. 307.

Guzhov, A. I., Mamayev, V. A. and Odishariya, G. E. (1967), "A Study Of Transportation In Gas-Liquid Systems," *Proc. 10th Int. Gas Union Conference*, June 6-10, Hamburg, Germany

Hall, A. R. W. (1992), "Multiphase flow of oil-water-gas in Horizontal pipes," Ph.D. dissertation, Chem. Eng. Dept., Imperial College, University of London.

Hall A. R. W. (1997) "Flow Patterns In Three Phase Flows of Oil-Water and Gas"

Hardin S. (1995) "The Viscosity of Stable and Unstable Oil/Water Emulsions and The Comparison of the UK National Multiphase Flow Database with Oil/Water/Gas Flow Models of Pipelines". Link Project Report, Imperial College London

Hatschek, E. (1928), *The Viscosity of Liquids*, Bell and Sons Ltd., London.

Herm Stapelberg, H. and D. Mewes (1994) " The Pressure Loss and Slug Frequency of Liquid-Liquid-Gas Slug Flow in Horizontal Pipes" *Int. J. Multiphase Flow* Vol. 20, No. 2 p. 285.

Hewitt, G. F (1982) Chapter Two "Gas-Liquid Flows" Handbook of Multiphase Flows. Ed. G. Hetsroni, Hemisphere Publishing Corporation, Washington McGraw-Hill

Hewitt G. F. & Govan A. H., (1990) "Phenomena and Prediction in Annular Two-Phase Flow." Int. Symposium on Advances in Gas-Liquids. *Proc. ASME Winter Annual Meeting* ASME New York, Vol. FED 99, HTD 155, 40

Heywood, N. I. and Richardson J. F. (1979) "Slug Flow of Air-Water Mixtures in a Horizontal Pipe: Determination of Liquid Holdup by γ-Ray Absorption" *Chemical Engineering Science* Vol. 34, p. 17

Hill T. J and Wood D. G (1990) "A New Approach to the Prediction of Slug Frequency". *65th Annual Technical Conference of the Society of Petroleum Engineers* New Orleans, LA, September 23-26

Hill T. J and Wood D. G (1994) "Slug Flow: Occurrence, Consequences And Prediction" SPE 27960 paper presented at the University of Tulsa Centennial Petroleum Engineering Symposium Tulsa OK, USA 29-31 August 53-62.

Hope C. B. (1990) "The Development Of A Water Soluble Photo-chronic Dye Tracing Technique And Its Application To Horizontal Two Phase Flow" Ph.D. dissertation, Chem. Eng. Dept. Imperial College, University of London

Hubbard, M .G (1965)" An analysis of horizontal gas-liquid slug flow" Ph.D. Thesis, University of Houston.

Issa R. I., and Woodburn P. J. (1998) "Numerical Prediction of Instabilities and Slug Formation in horizontal Two-Phase Flows." 3rd International Conference on Multiphase Flow, ICMF'98, Lyon, France, June 8-12, 1998

Jepson, W.P and Taylor, R. E (1988) "Slug Flow and its transitions in large diameter horizontal pipes." *Report AERE-R 12992* Thermal hydraulics division Harwell UK 1-26

Kago, T., Saruwatari, S., Ohno , S., Morooka, S. and Kato , Y. (1987) "Axial Mixing of liquid in Horizontal Two-Phase Slug flow" *J Chem. Eng. Japan*, Vol. 20 , p. 252

Khor S. H. K. (1998) "Three-Phase Liquid-Liquid-Gas Stratified Flow in Pipelines" Ph.D. dissertation, Chem. Eng. Dept. Imperial College, University of London

Kokal, S.L and Stanislav, J.F (1989) "An Experimental Study Of Two-Phase Flow In Slightly Inclined Pipes-I Flow Patterns" *Chem. Eng. Sci.*, Vol. 44, No 3, p. 665

Kouba G.E (1986) "Horizontal Slug Flow Modelling and Metering" Ph.D. thesis University of Tulsa, Tulsa U.S.A.

Knervold, O., Vindoy, V., Sontvedt T., Saasen A., and Selmer-Olsen S. (1984) "Velocity Distribution in Horizontal Slug Flow" *Int. J Multiphase Flow*, Vol. 10, p.441.

Lahey R. T., Acikgoz A and Franca F (1992) "Global Volumetric Phase Fractions In Horizontal Three-Phase Flows" *AIChE. J.*, Vol. 38, No. 7, p 1049.

Laflin G. C. and Oglesby K. D. (1976), "An Experimental Study On The Effects Of Flow Rate, Water Fraction And Gas-Liquid Ratio On Air-Oil-Water Flow In Horizontal Pipes," B. S. Thesis, University of Tulsa

Lee A-H, Sun J-Y and Jepson W. P. (1993) " Study of Flow Regime transitions of Oil-Water-Gas mixtures in Horizontal pipes" *Third International Offshore and Polar Engineering Conference, Singapore*

Lee A-H (1993) " A study of Flow Regime transitions for Oil-Water-Gas Mixtures in Large Diameter Horizontal Pipelines" M.S Thesis, College of Engineering and Technology, University of Ohio

Lockart R W and Martinelli RC (1949) "Proposed Correlation Of Data For Isothermal Two-Phase, Two Component Flow In Pipes," *Chem. Eng. Prog.*, Vol. 45, No. 1, p.39.

Lunde K., S. Nuland and M. Lingelem (1993) "Aspects Of Three-Phase Flows In Gas Condensate Pipelines" *Sixth International Conference on Multiphase Production, Cannes, France 16-18 June*

Malhotra A, (1998) "Study of Two and Three-Phase Flows in Large Diameter Horizontal Pipelines" M.S Thesis, Russ College of Engineering and Technology, University of Ohio.

Malinowsky, M. (1975) "An Experimental Study of Oil-Water and Air-Oil-Water Flowing Mixtures in Horizontal Pipes" M. S. Thesis,. The University of Tulsa

Malnes, D. (1983) "Slug Flow in Vertical, Horizontal and Inclined Pipes" *Institt Energy Technol. Report IFE / KR / E-83 / 002, Norway*

Mandhane J. M., G. A. Gregory and K. Aziz (1974) "A Flow Pattern Map For Gas-Liquid Flow in Horizontal Pipes" *Int. J. Multiphase Flow* Vol. 1, p. 537-553

Manolis, I. G. (1995) "High Pressure Gas-Liquid Slug Flow" Ph.D. dissertation Imperial College, University of London

Mantripragada V. (1998) "Effect of Inclination on Flow Regime Transitions, Slug Flow Characteristics and Corrosion Rates in Multiphase Flow Pipelines at Low Pressure" M.S Thesis, Russ College of Engineering and Technology, Ohio University

Marcano R., Chen X. T.,Sarica C. and Brill, J.P (1998) "A Study Of Slug Characteristics For Two-Phase Horizontal Flow" SPE 39856 1998 International Petroleum Conference and Exhibition Villahermosa , Mexico 3-5 March 1998

Minami, K. and Brill, J. P. (1987), "Liquid holdup in wet-gas pipelines," *SPE Production Eng.* (Feb. 1987).

Mkpadi, M.C and Igho J.T (1990) "The Viscosity Of Salt-Free Oilfield Liquid Mixtures" *J. of the Institute of Energy,* p 9

Nadler M and D. Mewes (1992) "Characteristics of Gas-Liquid and Gas-Liquid-Liquid Slug Flow in Horizontal Pipes" *Multiphase Flow in Wells and Pipelines* FED Vol. 144, ASME 1992

Nadler M and D. Mewes (1995) "Effects of the liquid Viscosity on the Phase distributions in Horizontal Gas-Liquid Slug Flow" *Int. J. Multiphase Flow* Vol. 21, No. 2 p. 253.

Nicholson, M. K., Aziz, K. and Gregory, G. A. (1978), "Intermittent two-phase flow in horizontal pipes: predictive models," Can. *J. Chem. Eng.*, Vol. 56, p. 653.

Nicklin, D. J., Wilkes, J. O. and Davidson, J. F. (1962), "Two-phase flow in vertical tubes," *Trans. Int. Chem. Eng.*, Vol. 40, p. 61.

Norris, L. (1982) "Correlation of Prudhoe Bay Liquid Slug lengths and holdups including 1981 large diameter flowline tests" Exxon Internal Report

Nydal, O. J. (1991) " An Experimental Investigation of Slug Flow" Ph.D. thesis, University of Oslo, Norway

Odozi U. A., M. A. Mendes-Tatsis and G. F. Hewitt (1998) "Pressure Drop and liquid Holdup in Three-Phase Slug Flow" *Multiphase Flow Systems Programme, Report WASP/38 MPS/102,* Imperial College

Oliemans R. V. A. (1987) "Modelling Of Gas Condensate Flow In Horizontal And Inclined Pipes" *ASME Pipeline Eng. Symposium ECTE*, Dallas, Texas. p. 73

Pan, L. (1996) " High Pressure Three-phase (Gas/Liquid/Liquid Flow)" Ph.D. thesis Imperial College, University of London

Perry R.H. and Green D.W (1997) "Perry's Chemical Engineers' Handbook" Seventh Edition. McGraw-Hill

Richardson, E.G. (1950) "The Formation and Flow of Emulsion" *Journal of Colloid Science,* Vol. 5, p. 404.

Rothe P.H., Crowley C. J. and Sam, R. G., (1986)"Investigation of two-phase flow in horizontal pipes at large pipe size and high gas density. AGA Pipe Research Committee Project, PR-172-507.

Roumazeilles, P. M. (1994) "An Experimental Study on Downward Slug Flow in Inclined Pipes" M. S. Thesis, The university of Tulsa

Russel T. W. F. Charles, M. E. (1959) "The Effect Of The Less Viscous Liquid In The Laminar Flow Of Two Immiscible Liquids" *Can J Chem. Eng.* Vol. 37 p.18.

Russel T. W. F., Hodgson G. W. and Govier G. W. (1959) "Horizontal Pipeline Flow Of Equal Density Oil-Water Mixtures" *Can J Chem. Eng.* Vol. 39 p.27.

Schlichting, P (1970) "The transport of oil-water-gas mixtures in oil field gathering systems," *Erdol-Erdgas-Zeitschrift,* Vol. 86, p. 235 (in German)

Schmidt Z. (1977) "Experimental study of two-phase slug flow in a pipeline-riser system" Ph.D. dissertation, The University of Tulsa.

Scott, S. L., Shoham, O. and Brill, J. P. (1986) "Prediction of Slug lengths in horizontal large diameter pipes" *Paper presented at the SPE 56th Annual California Regional meeting, Oakland, California April*

Shaha J., Pan L. and Hewitt, G. F. (1996) "Computational Modelling of a Slug Tail in Horizontal and Inclined Tubes." Diploma Thesis, Imperial College, University of London

Sobocinski, D.P. (1955) "Horizontal Concurrent Flow of Air, Gas-Oil, and Water in a Horizontal Pipe" M. S. Thesis University of Oklahoma

Soleimani A. (1999) "Phase Distribution And Associated Phenomena In Oil-Water Flows In Horizontal Tubes" Ph.D. thesis Imperial College, University of London

Stapelberg, H.H and Mewes D (1994) "The Pressure Loss And Slug Frequency Of Liquid-Liquid -Gas Flow In Horizontal Pipes" *Int. J Multiphase Flow* Vol. 20 p. 285

Taitel Y and Dukler A. E. (1976) "A Model For Predicting Flow Regime Transitions in Horizontal and Near Horizontal Gas-Liquid Flow" *AIChE J* Vol. 22, p. 47.

Taitel Y and Dukler A. E (1977) "A Model For Predicting Slug Frequency in Horizontal and Near Horizontal Gas-Liquid Flow" *Int. J. Multiphase Flow,* Vol. 3, p. 585.

Taitel Y. and Barnea, D. (1990), "Two-Phase Slug Flow," *Advances in Heat Transfer*, Vol. 20, p.83.

Trallero J. L. (1995)"Oil-Water Flow Patterns in Horizontal Pipes" Ph.D. dissertation, University of Tulsa.

Tronconi, E. (1990) "Prediction of Slug Frequency in Horizontal Two-phase Slug Flow" *AIChE Journal.* Vol. 36, p. 701.

Urdahl, O., Fredheim, A. O., and Loken Karl-Petter (1997) "Viscosity Measurements Of Water-In-Crude-Oil Emulsions Under Flowing Conditions: A Theoretical and practical Approach" *Colloids and Surfaces A: Physicochemical and Engineering Aspects* 123-124 p. 623.

Valle A. (1999) "Multiphase Pipeline Flows In Hydrocarbon Recovery" *Multiphase Science And Technology* Vol. 10, p. 1.

Van Wingen, N. (1950) "Secondary Recovery of Oil in the United States " American Petroleum Institute p.127.

Vand V. (1948) "Journal Of Physical And Colloidal Chemistry" Vol. 52, p.277.

Vermeulen, L. R and Ryan J. T (1971) " Two-Phase Flow In Horizontal And Inclined Tubes" *The Can J of Chem. Eng.* Vol. 49, 195.

Wilkens and Jepson W. P. (1996) "Studies of Multiphase Flow in High Pressure Horizontal And +5 Degree Inclined Pipelines" *Proc. of the 6th International Offshore and Polar Engineering Conference Los-Angeles USA.*

Yang, J., Sarica, C., Chen X. and Brill J. (1996) "A Study of Intermittent Flow In Downward Inclined Pipelines" HTD-Vol. 334, *Proceedings of the ASME Heat Transfer Division,* ASME 1996, Vol. 3, p. 115.

Zukoski, E. E. (1966), "Influence Of Viscosity, Surface Tension And Inclination Angle On Motion of Long Bubbles in Closed Tubes," *J. Fluid Mech.*, Vol. 25, part 4, p. 821.

Table A1: WASP Experimental Data of air-oil-water flow in horizontal pipe (Campaign #1)

File Name	T (°C)	p (bar)	$U_{A,S}$ (m/s)	$U_{O,S}$ (m/s)	$U_{W,S}$ (m/s)	$\frac{dp}{dz}$ (Pa/m)	ε_O	ε_W	ε_L	Flow Pattern	Mean Slug frequency (Hz)
utaow13	10	1.04	2.34	0.10	0.06	656	0.13	0.20	0.33	S.D-O-Sl	0.093
utaow14	10	1.04	2.37	0.11	0.14	584	0.08	0.19	0.27	S.D-O-Sl	0.090
utaow15	10	1.04	2.40	0.10	0.20	564	0.03	0.22	0.25	S.D-W-Sl	0.126
utaow16	10	1.04	4.50	0.10	0.19	550	0.03	0.21	0.24	S.D-W-Sl	0.135
utaow17	10	1.05	5.26	0.11	0.04	378	0.20	0.17	0.37	D-O-Sl	0.196
utaow18	10	1.06	5.27	0.10	0.06	505	0.19	0.20	0.39	D-O-Sl	0.214
utaow19	10	1.05	5.35	0.10	0.09	293	0.11	0.19	0.30	D-W-Sl	0.111
utaow20	10	1.05	5.32	0.10	0.10	283	0.12	0.15	0.27	D-W-Sl	0.151
utaow21	10	1.04	5.34	0.10	0.12	255	0.09	0.16	0.25	D-W-Sl	0.145
utaow22	10	1.04	5.35	0.11	0.18	240	0.06	0.18	0.23	D-W-Sl	0.112
utaow23	10	1.06	8.26	0.10	0.03	347	0.23	0.06	0.28	D-O-Sl	0.112
utaow25	10	1.06	7.24	0.11	0.09	444	0.18	0.17	0.35	S.D-O-Sl	0.170
utaow26	10	1.06	7.24	0.10	0.10	616	0.19	0.17	0.36	D-O-Sl	0.176
utaow27	10	1.06	7.22	0.10	0.11	598	0.16	0.21	0.37	D-O-Sl	0.140
utaow28	10	1.04	7.34	0.10	0.14	301	0.08	0.17	0.25	D-W-Sl	0.134
utaow29	10	1.05	8.00	0.11	0.16	355	0.09	0.15	0.24	D-W-Sl	0.135
utaow30	10	1.04	8.03	0.11	0.19	317	0.11	0.13	0.24	D-W-Sl	0.149
utaow31	13	1.05	5.53	0.10	0.04	403	0.24	0.09	0.33	D-O-Sl	0.176
utaow33	13	1.05	5.46	0.11	0.05	283	0.26	0.10	0.36	S.D-O-Sl	0.178
utaow35	13	1.04	5.51	0.11	0.08	187	0.16	0.12	0.29	S.D-O-Sl	0.152
utaow36	13	1.06	5.95	0.10	0.07	462	0.20	0.09	0.29	S.D-O-Sl	0.214
utaow37	13	1.06	5.94	0.11	0.09	466	0.08	0.09	0.17	D-W-Sl	0.187
utaow38	13	1.05	6.01	0.10	0.10	302	0.18	0.07	0.25	D-StW	-
utaow39	13	1.05	6.03	0.11	0.10	275	0.06	0.11	0.17	D-W-Sl	-
utaow40	13	1.06	8.18	0.10	0.05	352	0.07	0.05	0.12	D-O-Sl	-
utaow41	13	1.06	8.14	0.11	0.05	340	0.04	0.12	0.16	D-W-Sl	-
utaow42	13	1.07	8.42	0.10	0.09	535	0.19	0.10	0.29	D-W-Sl	-
utaow43	13	1.07	7.86	0.09	0.10	627	0.11	0.14	0.25	D-StW	-
utaow44	13	1.07	8.06	0.11	0.11	627	0.04	0.13	0.15	D-W-Sl	0.153
utaow45	13	1.06	8.07	0.11	0.14	410	0.16	0.14	0.30	D-O-Sl	0.174

File Name	T (°C)	p (bar)	$U_{A,S}$ (m/s)	$U_{O,S}$ (m/s)	$U_{W,S}$ (m/s)	$\frac{dp}{dz}$ (Pa/m)	ε_O	ε_W	ε_L	Flow Pattern	Mean Slug frequency (Hz)
utaow46	13	1.05	7.81	0.10	0.15	213	0.15	0.16	0.31	D-O-Sl	0.106
utaow47	13	1.05	7.95	0.10	0.17	209	0.06	0.12	0.19	D-W-Sl	0.110
utaow48	13	1.05	5.68	0.11	0.23	228	0.08	0.15	0.23	D-StW	-
utaow49	13	1.05	12.70	0.10	0.03	202	0.11	0.08	0.19	D-StW	-
utaow50	13	1.06	12.39	0.10	0.17	313	0.07	0.09	0.16	S.D-W-Sl	0.179
utaow51	13	1.07	12.05	0.11	0.04	517	0.20	0.09	0.29	S.D-O-Sl	0.053
utaow52	13	1.06	11.78	0.10	0.18	284	0.08	0.09	0.17	D-W-Sl	0.133
utaow53	13	1.08	11.56	0.11	0.05	438	0.18	0.07	0.25	D-StW	-
utaow54	13	1.07	11.45	0.11	0.24	402	0.06	0.11	0.17	D-W-Sl	0.307
utaow55	13	1.00	11.20	0.10	0.07	325	0.07	0.05	0.12	-	0.421
utaow56	12	1.06	11.90	0.10	0.21	347	0.04	0.12	0.16	D-W-Sl	0.270
utaow57	12	1.08	11.27	0.10	0.07	548	0.19	0.10	0.29	D-W-Sl	0.098
utaow58	12	1.05	11.69	0.11	0.14	228	0.11	0.14	0.25	D-StW	-
utaow59	12	1.07	11.95	0.10	0.28	416	0.04	0.13	0.15	D-W-Sl	0.338
utaow60	12	1.09	11.39	0.11	0.09	658	0.16	0.14	0.30	D-O-Sl	0.141
utaow61	12	1.10	11.36	0.10	0.12	764	0.15	0.16	0.31	D-O-Sl	0.124
utaow62	12	1.09	11.37	0.11	0.10	667	0.14	0.15	0.29	D-O-Sl	0.153
utaow63	12	1.08	11.38	0.10	0.07	507	0.15	0.12	0.27	D-O-Sl	0.124
utaow64	12	1.05	12.19	0.10	0.13	433	0.05	0.11	0.16	D-W-Sl	0.150
utaow65	12	1.08	11.61	0.10	0.08	606	0.17	0.13	0.30	D-O-Sl	0.096
utaow66	12	1.06	11.78	0.11	0.18	726	0.07	0.10	0.18	D-W-Sl	0.167
utaow67	12	1.07	12.03	0.10	0.06	1124	0.18	0.10	0.28	D-O-Sl	0.076
utaow68	12	1.07	11.95	0.11	0.24	188	0.04	0.13	0.17	D-W-Sl	0.289
utaow69	12	1.07	11.90	0.10	0.03	350	0.19	0.05	0.24	D-O-Sl	0.086
utaow70	12	1.10	11.36	0.11	0.13	464	0.15	0.17	0.32	D-O-Sl	0.141
utaow71	13	1.06	5.44	0.43	0.06	753	0.29	0.04	0.33	D-O-Sl	0.406
utaow72	13	1.06	4.35	0.50	0.11	870	0.31	0.07	0.38	D-O-Sl	0.513
utaow73	13	1.06	5.24	0.48	0.46	784	0.15	0.15	0.30	D-W-Sl	0.392
utaow74	13	1.07	5.20	0.49	0.34	784	0.16	0.16	0.33	D-W-Sl	0.397
utaow75	13	1.08	5.10	0.48	0.30	1231	0.28	0.18	0.46	D-O-Sl	0.552
utaow76	13	1.08	5.11	0.47	0.25	1235	0.22	0.14	0.36	D-O-Sl	0.593
utaow78	12	1.09	8.77	0.47	0.47	1037	0.11	0.13	0.24	D-W-Sl	0.528
utaow79	12	1.10	8.61	0.48	0.35	992	0.14	0.13	0.27	D-W-Sl	0.358
utaow80	12	1.11	8.44	0.49	0.27	1443	0.26	0.14	0.40	D-O-Sl	0.522

File Name	T (°C)	p (bar)	$U_{A,S}$ (m/s)	$U_{O,S}$ (m/s)	$U_{W,S}$ (m/s)	$\frac{dp}{dz}$ (Pa/m)	ε_O	ε_W	ε_L	Flow Pattern	Mean Slug frequency (Hz)
utaow81	11	1.09	8.48	0.46	0.18	1180	0.25	0.07	0.33	D-O-Sl	0.529
utaow82	11	1.09	8.86	0.44	0.08	936	0.20	0.02	0.22	D-W-Sl	-
utaow83	11	1.11	11.38	0.50	0.47	1291	0.09	0.13	0.22	D-W-Sl	0.573
utaow84	16	1.12	11.22	0.49	0.33	1106	0.13	0.11	0.24	D-W-Sl	0.337
utaow85	16	1.12	11.08	0.46	0.24	1533	0.21	0.10	0.30	D-O-Sl	0.536
utaow86	13	1.13	13.94	0.47	0.44	1419	0.09	0.11	0.20	D-W-Sl	0.560
utaow87	13	1.15	14.38	0.45	0.32	1794	0.20	0.14	0.34	D-O-Sl	0.426
utaow88	13	1.11	11.80	0.50	0.07	1243	0.22	0.02	0.25	D-O-Sl	0.454
utaow89	12	1.09	8.94	0.47	0.07	1016	0.25	0.03	0.27	D-O-Sl	0.462
utaow90	12	1.12	14.51	0.44	0.04	972	0.14	0.05	0.20	D-O-Sl	0.239
utaow91	14	1.11	8.62	0.49	0.25	1549	0.25	0.14	0.38	D-O-Sl	0.500
utaow92	14	1.14	13.98	0.50	0.10	1540	0.21	0.05	0.26	D-O-Sl	0.532
utaow93	14	1.11	11.80	0.49	0.09	1360	0.22	0.04	0.26	D-O-Sl	0.519
utaow94	14	1.14	13.61	0.48	0.19	1580	0.20	0.07	0.26	D-O-Sl	0.514
utaow95	14	1.07	5.22	0.66	0.06	1005	0.32	0.05	0.38	D-O-Sl	0.552
utaow96	14	1.07	5.21	0.67	0.10	1120	0.33	0.05	0.38	D-O-Sl	0.579
utaow97	14	1.08	5.21	0.67	0.19	1282	0.31	0.08	0.39	D-O-Sl	0.678
utaow99	14	1.07	5.06	0.66	0.29	1459	0.25	0.15	0.40	D-O-Sl	-
utaow100	14	1.10	8.56	0.67	0.10	1466	0.26	0.05	0.31	D-O-Sl	0.670
utaow101	14	1.11	8.48	0.61	0.20	1451	0.26	0.06	0.32	D-O-Sl	0.667
utaow102	16	1.07	5.03	0.65	0.46	922	-	-	-	D-W-Sl	0.538
utaow104	16	1.15	9.94	0.68	0.38	1795	-	-	-	D-O-Sl	-
utaow106	16	1.12	8.36	0.69	0.36	1603	0.25	0.16	0.41	D-O-Sl	0.549
utaow107	16	1.13	11.81	0.71	0.10	1578	0.24	0.04	0.28	D-O-Sl	0.652
utaow108	16	1.14	13.85	0.67	0.10	1526	0.21	0.04	0.21	D-O-Sl	0.615
utaow109	16	1.14	14.25	0.66	0.05	1356	0.21	0.08	0.22	D-O-Sl	0.453
utaow110	16	4.93	2.06	0.46	0.10	716	0.41	0.09	0.50	D-O-Sl	0.555
utaow111	16	4.96	2.03	0.50	0.31	1121	0.44	0.12	0.56	D-O-Sl	0.621
utaow112	16	4.93	2.04	0.49	0.30	1194	0.41	0.19	0.60	D-O-Sl	0.594
utaow113	16	4.91	2.03	0.50	0.39	683	0.30	0.20	0.49	D-W-Sl	0.521
utaow114	15	5.92	1.99	0.49	0.07	710	0.44	0.08	0.52	D-O-Sl	0.503
utaow115	15	5.90	1.98	0.49	0.10	762	0.42	0.10	0.53	D-O-Sl	0.568
utaow116	15	5.91	1.97	0.49	0.20	1003	0.39	0.18	0.57	D-O-Sl	0.636
utaow117	15	5.90	1.97	0.48	0.29	1162	0.37	0.22	0.59	D-O-Sl	0.618

File Name	T (°C)	p (bar)	$U_{A,S}$ (m/s)	$U_{O,S}$ (m/s)	$U_{W,S}$ (m/s)	$\frac{dp}{dz}$ (Pa/m)	ε_O	ε_W	ε_L	Flow Pattern	Mean Slug frequency (Hz)
utaow118	15	5.83	2.00	0.43	0.39	502	0.25	0.23	0.47	D-W-Sl	-
utaow119	12	6.02	5.03	0.50	0.07	944	0.39	0.08	0.40	D-O-Sl	0.349
utaow120	12	6.00	4.98	0.50	0.11	1031	0.39	0.02	0.41	D-O-Sl	0.420
utaow121	12	5.98	4.92	0.49	0.20	1295	0.37	0.07	0.44	D-O-Sl	0.517
utaow122	12	5.96	4.85	0.39	0.30	1400	0.36	0.13	0.49	D-O-Sl	0.474
utaow123	12	5.80	5.00	0.50	0.40	693	0.34	0.16	0.50	D-StW	-
utaow124	14	5.82	2.06	0.72	0.08	759	0.43	0.10	0.53	D-O-Sl	0.585
utaow125	14	5.81	2.06	0.72	0.11	773	0.43	0.10	0.53	D-O-Sl	0.615
utaow126	14	5.82	1.99	0.71	0.21	992	0.43	0.14	0.57	D-O-Sl	0.672
utaow127	14	5.91	1.98	0.70	0.29	1182	0.33	0.22	0.55	D-O-Sl	0.736
utaow128	17	5.83	2.15	0.73	0.52	630	0.22	0.25	0.47	D-W-Sl	0.546
utaow129	17	5.82	2.15	0.73	0.42	771	0.26	0.25	0.51	D-W-Sl	0.579
utaow130	17	5.88	4.92	0.68	0.50	1609	0.16	0.23	0.39	D-O-Sl	0.627
utaow131	17	5.91	4.85	0.70	0.40	1521	0.15	0.26	0.40	D-O-Sl	0.528
utaow132	17	5.90	5.11	0.70	0.30	1751	0.22	0.21	0.42	D-O-Sl	0.566
utaow133	17	5.87	5.05	0.70	0.21	1552	0.23	0.13	0.36	D-O-Sl	0.546
utaow134	17	5.90	4.95	0.70	0.10	1230	0.27	0.07	0.34	D-O-Sl	0.483

Table A2: WASP Experimental Data of air-oil-water flow in downwardly inclined pipe -1.5° (Campaign #2)

File Name	T (°C)	p (bar)	$U_{A,S}$ (m/s)	$U_{O,S}$ (m/s)	$U_{W,S}$ (m/s)	$\frac{dp}{dz}$ (Pa/m)	ε_O	ε_W	ε_L	Flow Pattern	Mean Slug frequency (Hz)
utaow135	28	1.04	2.14	0.20	0.07	26	0.45	0.12	0.57	D-StS	-
utaow136	28	1.04	3.27	0.19	0.07	37	0.42	0.08	0.50	D-StS	-
utaow137	28	1.04	4.26	0.21	0.07	58	0.39	0.06	0.46	D-StS	-
utaow138	28	1.04	4.98	0.19	0.07	101	0.35	0.08	0.42	D-St.W	-
utaow139	28	1.04	6.46	0.21	0.07	138	0.35	0.07	0.41	D-St.W	-
utaow140	28	1.06	7.85	0.20	0.07	157	0.31	0.07	0.37	D-St.W	-
utaow141	28	1.07	8.88	0.19	0.06	177	0.29	0.06	0.35	D-St.W	-
utaow143	28	1.04	2.41	0.20	0.08	33	0.38	0.23	0.61	D-St.S	-
utaow144	28	1.04	3.70	0.20	0.09	73	0.30	0.12	0.42	D-StS/D-St.W	-
utaow145	28	1.04	4.67	0.21	0.09	260	0.27	0.07	0.35	D-St.W	-
utaow146	28	1.06	5.89	0.20	0.09	195	0.31	0.08	0.39	D-St.W	-
utaow147	28	1.04	7.24	0.21	0.09	223	0.29	0.09	0.37	D-St.W	-
utaow148	28	1.05	8.48	0.20	0.09	230	0.26	0.08	0.34	D-St.W	-
utaow149	28	1.05	10.03	0.20	0.08	229	0.26	0.06	0.32	D-St.W	-
utaow150	28	1.04	2.04	0.19	0.13	60	0.20	0.18	0.38	D-St.S	-
utaow151	27	1.00	2.28	0.21	0.13	16	0.20	0.14	0.34	D-St.S	-
utaow152	27	1.04	3.52	0.19	0.12	31	0.19	0.13	0.32	D-St.S	-
utaow153	27	1.04	5.33	0.21	0.13	68	0.21	0.12	0.33	D-St.S	-
utaow154	27	1.05	6.65	0.20	0.13	149	0.21	0.13	0.34	D-StW	-
utaow155	27	1.08	8.32	0.21	0.13	478	0.19	0.08	0.27	D-O-Sl	0.279
utaow158	22	1.04	1.90	0.19	0.20	26	0.17	0.21	0.38	D-StS	-
utaow159	24	1.04	2.88	0.21	0.20	37	0.17	0.21	0.38	D-StW	-
utaow160	24	1.04	3.87	0.20	0.20	49	0.18	0.19	0.37	D-StW	-
utaow161	24	1.04	5.86	0.21	0.20	149	0.18	0.20	0.38	D-StW	-
utaow162	24	1.07	7.01	0.20	0.18	788	0.17	0.18	0.36	D-StW	-
utaow163	24	1.09	9.26	0.19	0.20	1002				D-O-Sl	0.336
utaow164	20	1.03	2.13	0.20	0.30	24	0.12	0.32	0.44	D-St.S	-
utaow165	20	1.04	3.15	0.22	0.30	42	0.14	0.30	0.44	D-St.S	-

File Name	T (°C)	p (bar)	$U_{A,S}$ (m/s)	$U_{O,S}$ (m/s)	$U_{W,S}$ (m/s)	$\frac{dp}{dz}$ (Pa/m)	ε_O	ε_W	ε_L	Flow Pattern	Mean Slug frequency (Hz)
utaow167	20	1.05	6.34	0.20	0.30	402	0.07	0.20	0.27	D-W-Sl	0.130
utaow168	20	1.05	8.45	0.21	0.29	270	0.12	0.20	0.32	D-W-Sl	0.042
utaow169	20	1.08	9.63	0.20	0.31	579	0.09	0.17	0.26	D-W-Sl	0.110
utaow170	24	1.03	2.18	0.21	0.47	21	0.08	0.44	0.52	D-StW	-
utaow171	24	1.03	3.26	0.22	0.46	44	0.11	0.41	0.52	D-StW	-
utaow172	24	1.05	5.00	0.20	0.47	461	0.05	0.21	0.27	D-W-Sl/D-StW	-
utaow173	24	1.06	7.11	0.22	0.46	623	0.03	0.19	0.22	D-W-Sl	0.245
utaow174	24	1.07	8.48	0.21	0.46	779	0.03	0.18	0.21	D-W-Sl	0.298
utaow175	24	1.09	9.66	0.20	0.46	901	0.03	0.17	0.20	D-W-Sl	0.341
utaow176	24	1.05	9.94	0.15	0.07	246	0.17	0.05	0.22	D-O-StW	-
utaow177	15	1.06	10.00	0.12	0.08	464	0.17	0.12	0.29	D-O-StW	-
utaow178	15	1.07	9.99	0.11	0.11	611	0.14	0.14	0.28	D-O-St.A	-
utaow179	15	1.06	9.98	0.08	0.11	317	0.09	0.18	0.27	D-W-St.A	-
utaow180	15	1.05	10.00	0.08	0.13	203	0.08	0.15	0.23	D-W-St.A	-
utaow181	15	1.05	10.02	0.07	0.14	173	0.06	0.15	0.21	D-W-St.A	-
utaow182	15	1.11	9.89	0.32	0.07	1385	0.21	0.03	0.24	D-O-Sl	0.420
utaow183	15	1.00	9.52	0.32	0.10	1429	-	-	-	D-O-Sl	
utaow184	22	1.06	11.96	0.21	0.06	384	0.24	0.07	0.31	D-O-St.A	-
utaow185	21	1.07	14.33	0.20	0.06	594	0.20	0.07	0.28	D-O-St.A	-
utaow186	21	1.08	17.42	0.18	0.06	681	0.17	0.06	0.24	D-O-St.A	-
utaow187	19	1.09	20.34	0.20	0.06	853	0.16	0.06	0.21	D-O-A	-
utaow188	19	1.11	24.09	0.20	0.05	1072	0.14	0.04	0.19	D-O-A	-
utaow189	19	1.13	27.13	0.21	0.05	1251	0.14	0.03	0.17	D-O-A	-
utaow190	21	1.09	29.26	0.21	0.05	1465	0.12	0.03	0.15	D-O-Sl	0.251
utaow191	16	1.09	13.70	0.19	0.11	1182	0.14	0.10	0.24	D-O-StA)	
utaow192	16	1.10	17.25	0.21	0.10	1288	0.15	0.09	0.23	D-O-A	
utaow193	16	1.12	22.18	0.20	0.10	1408	0.13	0.09	0.22	D-O-A	
utaow194	16	1.13	25.25	0.21	0.09	1584	0.12	0.08	0.20	D-O-A	
utaow195	16	1.16	28.40	0.21	0.11	1966	0.11	0.06	0.17	D-O-A	
utaow196	16	1.08	12.89	0.08	0.12	684	0.10	0.19	0.29	D-O-StA)	
utaow197	16	1.09	14.72	0.08	0.12	948	0.14	0.21	0.35	D-W-Sl/D-O-Sl	
utaow198	16	1.11	11.52	0.21	0.20	1084	0.14	0.15	0.29	D-O-Sl	0.322
utaow199	16	1.13	14.30	0.22	0.21	1136	0.15	0.14	0.28	D-O-Sl	0.258
utaow200	16	1.14	17.83	0.21	0.20	1184	0.13	0.13	0.27	D-O-Sl	0.088

File Name	T (°C)	p (bar)	$U_{A,S}$ (m/s)	$U_{O,S}$ (m/s)	$U_{W,S}$ (m/s)	$\frac{dp}{dz}$ (Pa/m)	ε_O	ε_W	ε_L	Flow Pattern	Mean Slug frequency (Hz)
utaow201	16	1.15	20.55	0.20	0.21	1352	0.10	0.16	0.26	D-O-StA	-
utaow202	16	1.20	23.65	0.21	0.20	1934	0.09	0.12	0.21	D-O-StA	-
utaow203	16	1.05	13.87	0.05	0.15	227	0.05	0.13	0.18	D-O-StA	-
utaow204	16	1.07	13.27	0.11	0.11	667	0.15	0.13	0.28	D-O-Sl	
utaow205	16	1.09	18.30	0.10	0.10	800	0.12	0.12	0.24	D-O-StA	
utaow207	23	1.07	11.97	0.21	0.31	583	0.05	0.15	0.20	D-W-Sl(with sep film)	0.181
utaow208	23	1.09	14.04	0.21	0.30	681	0.08	0.12	0.20	S.D-W-Sl	0.166
utaow209	23	1.10	16.77	0.20	0.30	583	0.06	0.15	0.21	D-W-Sl/D-O-Sl	0.094
utaow210	23	1.11	19.63	0.22	0.31	1127	0.08	0.16	0.24	D-W-StA	-
utaow211	23	1.16	22.69	0.20	0.30	1871	0.05	0.15	0.20	D-W-A	-
utaow212	23	1.21	16.96	0.08	0.12	950	0.10	0.16	0.26	D-W-St.A	-
utaow213	23	1.10	22.20	0.07	0.12	1349	0.09	0.12	0.22	D-W-St.A	-
utaow214	23	1.13	22.16	0.12	0.10	1014	0.10	0.10	0.20	D-W-St.A	-
utaow215	24	1.11	1.90	0.20	0.06	16	0.26	0.08	0.35	D-SS	-
utaow216	24	11.05	2.90	0.21	0.06	119	0.29	0.10	0.39	D-StW	-
utaow217	24	10.85	3.42	0.20	0.05	222	0.31	0.09	0.41	D-St.W	-
utaow218	24	10.85	3.89	0.20	0.05	242	0.29	0.09	0.38	D-St.W	-
utaow219	24	10.91	4.76	0.20	0.05	333	0.27	0.07	0.34	D-St.W	-
utaow220	22	10.73	2.02	0.20	0.08	10	0.22	0.11	0.34	D-St.W	-
utaow221	22	11.69	2.94	0.20	0.08	222	0.26	0.14	0.40	D-St.W	-
utaow222	22	11.55	3.88	0.21	0.09	463	0.23	0.13	0.36	D-St.W	-
utaow223	22	11.69	4.33	0.20	0.08	510	0.24	0.11	0.34	D-St.W	-
utaow224	22	11.24	1.94	0.20	0.12	78	0.23	0.13	0.36	D-St.W	-
utaow225	22	11.63	2.93	0.20	0.13	159	0.23	0.16	0.39	D-St.W	-
utaow226	22	6.36	5.07	0.21	0.08	436	0.25	0.11	0.35	D-St.W	-
utaow227	22	6.15	6.33	0.21	0.08	452	0.23	0.09	0.32	D-St.W	-
utaow228	22	6.21	6.95	0.20	0.08	506	0.22	0.08	0.30	D-O-St.A	-
utaow229	22	6.35	7.95	0.20	0.07	588	0.19	0.08	0.26	D-O-St.A	-
utaow230	22	6.28	5.00	0.20	0.12	523	-	-	0.00	D-O-SL/ D-O-St.A	-
utaow231	22	6.28	5.95	0.21	0.13	680	0.20	0.14	0.34	D-O-SL/ D-O-St.A	-
utaow232	22	6.31	6.88	0.20	0.12	716	0.19	0.13	0.32	D-O-St.A	-
utaow233	22	6.41	7.70	0.20	0.12	733	0.18	0.12	0.30	D-O-St.A	-
utaow234	22	6.20	8.70	0.20	0.13	965	0.16	0.12	0.28	D-O-St.A	-

File Name	T (°C)	p (bar)	$U_{A,S}$ (m/s)	$U_{O,S}$ (m/s)	$U_{W,S}$ (m/s)	$\frac{dp}{dz}$ (Pa/m)	ε_O	ε_W	ε_L	Flow Pattern	Mean Slug frequency (Hz)
utaow235	22	1.12	13.44	0.08	0.13	869	0.12	0.18	0.30	D-O-St.A	-
utaow236	22	1.15	18.13	0.08	0.12	1257	-	-	-	-	-
utaow237	19	6.04	5.03	0.20	0.21	839	0.18	0.22	0.40	D-O-St.A	-
utaow238	19	6.09	6.17	0.21	0.20	990	0.16	0.19	0.35	D-O-St.A	-
utaow239	19	6.16	6.99	0.20	0.21	1097	0.15	0.20	0.34	D-O-St.A	-
utaow240	19	6.10	7.81	0.21	0.20	1133	0.15	0.17	0.32	D-O-St.A	-
utaow241	19	6.12	5.10	0.20	0.31	259	0.09	0.20	0.29	D-St.W	-
utaow242	19	6.18	5.99	0.20	0.30	335	0.06	0.20	0.26	D-St.W	-
utaow243	19	6.22	6.87	0.21	0.30	499	0.06	0.19	0.24	D-St.W/D-W-Sl	-
utaow244	21	5.98	5.07	0.21	0.40	500	0.06	0.21	0.27	D-W-Sl	0.264
utaow245	20	6.12	5.86	0.21	0.40	694	0.05	0.19	0.24	D-W-Sl	0.409
utaow246	20	6.13	6.97	0.20	0.39	892	0.05	0.17	0.21	D-W-Sl	0.439
utaow247	21	6.07	7.85	0.21	0.41	1036	0.04	0.16	0.20	D-W-Sl	0.469
utaow248	20	6.09	7.94	0.21	0.31	819	0.09	0.15	0.24	D-St.W	-
utaow249	20	1.09	9.59	0.15	0.05	248	0.24	0.08	0.32	D.St.W/D-O-St.A	-
utaow250	20	1.11	18.42	0.14	0.05	551	0.16	0.06	0.21	D-O-St.A	-
utaow251	21	10.98	2.01	0.19	0.20	99	0.17	0.22	0.40	D-StW	-
utaow252	21	10.99	2.92	0.19	0.20	281	0.16	0.24	0.39	D-StW	-
utaow253	21	11.06	3.89	0.20	0.21	526	0.19	0.23	0.42	D-StW	-
utaow254	21	11.02	4.92	0.20	0.21	882	0.17	0.21	0.38	D-W-St.A	-
utaow255	21	10.94	2.08	0.20	0.30	245	0.13	0.33	0.46	D-StW	-
utaow256	21	10.93	2.90	0.21	0.30	294	0.10	0.28	0.38	D-StW /D-W-Sl	-
utaow267	21	1.10	9.77	0.24	0.06	377	0.31	0.03	0.34	D-O-Sl	0.063
utaow268	21	1.11	10.26	0.22	0.09	837	0.21	0.04	0.25	D-O-Sl	0.231
utaow269	21	1.11	10.22	0.18	0.11	747	0.19	0.07	0.25	D-O-Sl	0.235
utaow270	21	1.12	10.04	0.14	0.16	1020	0.17	0.12	0.28	D-O-Sl	0.236
utaow271	21	1.09	10.41	0.11	0.19	222	0.10	0.18	0.28	D-StW	-
utaow272	21	1.10	11.84	0.08		419	0.04	0.12	0.16	D-W-Sl	0.166
utaow273	21	1.11	11.69	0.04	0.26	454	0.00	0.15	0.15	D-W-Sl	0.170
utaow274	21	1.11	11.43	0.07	0.28	480	0.03	0.13	0.16	D-W-Sl	0.188
utaow275	21	1.10	11.46	0.13	0.23	469	0.10	0.12	0.23	D-W-Sl	0.098

File Name	T (°C)	p (bar)	$U_{A,S}$ (m/s)	$U_{O,S}$ (m/s)	$U_{W,S}$ (m/s)	$\frac{dp}{dz}$ (Pa/m)	ε_O	ε_W	ε_L	Flow Pattern	Mean Slug frequency (Hz)
utaow276	21	1.14	10.88	0.15	0.19	1244	0.15	0.14	0.29	D-O-Sl	0.239
utaow278	21	1.13	9.98	0.16	0.17	1154	0.17	0.12	0.29	D-O-Sl	0.311
utaow279	21	1.13	9.95	0.22	0.14	1044	0.19	0.07	0.27	D-O-Sl	0.290
utaow280	21	1.12	9.92	0.24	0.11	956	0.20	0.05	0.25	D-O-Sl	0.314
utaow281	21	1.12	9.96	0.26	0.09	860	0.21	0.03	0.24	D-O-Sl	0.183
utaow282	21	1.11	12.24	0.07	0.26	545	0.04	0.11	0.16	D-W-Sl	0.242
utaow283	21	1.11	12.19	0.11	0.25	560	0.05	0.11	0.16	D-W-Sl	0.154
utaow284	21	1.14	11.67	0.15	0.20	1346	0.17	0.15	0.32	D-O-Sl	0.272
utaow285	21	1.14	11.63	0.18	0.17	1195	0.17	0.11	0.28	D-O-Sl	0.227
utaow286	21	1.13	11.81	0.20	0.15	1163	0.19	0.07	0.26	D-O-Sl	0.293
utaow287	21	1.11	12.45	0.24	0.11	757	0.19	0.04	0.23	D-O-Sl	0.245
utaow288	21	1.10	12.77	0.26	0.08	841	0.20	0.02	0.23	D-O-Sl	0.219
utaow289	21	1.10	15.34	0.25	0.08	706	0.23	0.03	0.26	D-O-Sl	0.088
utaow290	21	1.11	14.96	0.24	0.10	1010	0.18	0.03	0.22	D-O-Sl	0.229
utaow291	21	1.12	14.74	0.20	0.15	1172	0.16	0.09	0.25	D-O-Sl	0.196
utaow292	21	1.12	14.54	0.16	0.17	1262	0.17	0.11	0.28	D-O-Sl	0.170
utaow293	21	1.11	14.55	0.14	0.22	833	0.17	0.17	0.34	D-StW	-
utaow294	19	1.07	14.28	0.09	0.27	597	0.06	0.10	0.16	D-W-Sl	0.100
utaow295	19	1.06	14.37	0.12	0.22	452	0.08	0.14	0.22	D-StW	-
utaow296	19	1.08	16.29	0.29	0.06	586	0.28	0.02	0.30	D-StW	-
utaow297	19	1.10	15.85	0.24	0.10	980	0.21	0.03	0.24	D-O-Sl	-
utaow298	19	1.11	15.62	0.20	0.14	1106	0.18	0.07	0.25	D-O-Sl	0.132
utaow299	19	1.12	15.95	0.17	0.19	1354	0.16	0.12	0.29	D-O-Sl	-
utaow300	19	1.13	15.73	0.14	0.21	1564	0.16	0.14	0.30	D-O-Sl	-
utaow301	20	1.10	10.14	0.22	0.41	982	0.07	0.11	0.19	D-W-Sl	0.264
utaow302	20	1.09	11.55	0.21	0.41	1026	0.08	0.10	0.17	D-W-Sl	0.227
utaow303	20	1.14	15.24	0.21	0.42	1165	0.10	0.13	0.22	D-O-Sl	-
utaow304	20	1.15	17.69	0.21	0.40	1338	0.08	0.17	0.26	D-W-A	-
utaow305	20	1.17	19.48	0.20	0.41	1248	0.05	0.14	0.20	D-W-A	-
utaow306	20	1.08	11.03	0.22	0.35	809	0.09	0.15	0.23	D-W-Sl	0.157
utaow307	20	1.04	10.34	0.22	0.00	189	-	-	-	O-StW flow	-

File Name	T (°C)	p (bar)	$U_{A,S}$ (m/s)	$U_{O,S}$ (m/s)	$U_{W,S}$ (m/s)	$\frac{dp}{dz}$ (Pa/m)	ε_O	ε_W	ε_L	Flow Pattern	Mean Slug frequency (Hz)
utaow308	20	1.05	10.22	0.00	0.31	255	0.00	0.18	0.18	W StW/W-Sl	-
utaow309	20	1.04	10.40	0.30	0.00	217	0.36	0.00	0.36	O-StW	-
utaow310	20	1.04	10.37	0.26	0.04	247	0.36	0.01	0.37	D-O-St.A	-
utaow311	20	1.06	10.26	0.23	0.07	622	0.25	0.01	0.26	D-O-Sl	0.186
utaow312	20	1.06	10.10	0.22	0.08	674	0.23	0.03	0.26	D-O-Sl	0.213
utaow313	20	1.08	9.87	0.20	0.10	685	0.21	0.04	0.24	D-O-Sl	0.235
utaow314	20	1.09	9.85	0.19	0.11	764	0.18	0.06	0.24	D-O-Sl	-
utaow315	20	1.05	10.68	0.00	0.34	351	0.00	0.19	0.19	W-Sl	0.144
utaow316	20	1.06	12.98	0.00	0.34	466	0.00	0.16	0.16	D-W-Sl	0.210
utaow317	20	1.09	11.68	0.36	0.00	820	0.19	0.00	0.19	O-Sl	0.198
utaow319	20	1.08	12.41	0.30	0.04	539	0.26	0.01	0.27	D-O-Sl/D-O-StW	-
utaow320	20	1.07	12.40	0.28	0.05	509	0.26	0.02	0.28	D-O-Sl/D-O-StW	-
utaow321	20	1.06	10.43	0.00	0.50	592	0.00	0.19	0.20	W-Sl	0.318
utaow322	20	1.08	12.32	0.00	0.50	762	0.00	0.00	0.17	W-Sl	0.335
utaow323	20	1.11	14.86	0.00	0.51	1118	0.00	0.15	0.15	W-Sl	0.425
utaow324	21	1.08	10.57	0.12	0.37	834	0.08	0.10	0.19	D-W-Sl	0.266
utaow325	20	1.09	10.38	0.17	0.32	989	0.15	0.17	0.32	D-W-Sl	0.141
utaow326	20	1.12	10.08	0.20	0.28	1525	0.18	0.15	0.32	D-O-Sl	0.347
utaow327	20	1.11	10.10	0.23	0.24	1398	0.18	0.11	0.29	D-O-Sl	0.393
utaow328	20	1.11	10.09	0.26	0.23	1476	0.19	0.09	0.28	D-O-Sl	0.451
utaow329	20	1.10	10.16	0.32	0.17	1223	0.20	0.06	0.26	D-O-Sl	0.353
utaow330	20	1.07	10.00	0.15	0.34	661	0.10	0.11	0.20	D-W-Sl	0.281
utaow331	20	1.07	9.84	0.51	0.00	1013	0.29	0.05	0.23	O-Sl	0.375
utaow332	20	1.08	9.71	0.41	0.08	971	0.24	0.01	0.24	D-O-Sl	0.306
utaow333	20	1.09	9.54	0.34	0.14	1158	0.21	0.04	0.25	D-O-Sl	0.400
utaow334	20	1.08	9.70	0.00	0.68	932	0.00	0.19	0.19	W-Sl	0.330
utaow335	18	1.11	10.64	0.20	0.47	1079	0.05	0.13	0.18	D-W-Sl	0.406
utaow336	18	1.11	10.58	0.28	0.40	1070	0.10	0.11	0.21	D-W-Sl	0.275
utaow337	18	1.14	10.26	0.35	0.34	1834	0.18	0.15	0.32	D-O-Sl	0.480
utaow338	18	1.13	10.87	0.41	0.26	1645	0.20	0.09	0.28	D-O-Sl	0.449
utaow339	18	1.12	9.74	0.47	0.22	1509	0.22	0.05	0.28	D-O-Sl	0.500

File Name	T (°C)	p (bar)	$U_{A,S}$ (m/s)	$U_{O,S}$ (m/s)	$U_{W,S}$ (m/s)	$\frac{dp}{dz}$ (Pa/m)	ε_O	ε_W	ε_L	Flow Pattern	Mean Slug frequency (Hz)
utaow340	21	1.09	9.85	0.70	0.00	1354	0.24	0.00	0.24	O-Sl	0.585
utaow341	21	1.12	9.61	0.56	0.15	1462	0.26	0.02	0.27	D-O-Sl	0.468
utaow342	21	1.11	9.55	0.32	0.37	1345	0.20	0.19	0.39	D-O-Sl	0.240
utaow343	21	1.12	9.44	0.39	0.31	1578	0.35	0.12	0.47	D-O-Sl	0.424
utaow344	20	1.09	10.45	0.29	0.09	1052	0.20	0.04	0.24	D-O-Sl	0.239
utaow345	20	1.10	10.24	0.49	0.09	1306	0.22	0.02	0.24	D-O-Sl	0.394
utaow346	20	1.12	11.34	0.50	0.16	1476	0.20	0.03	0.23	D-O-Sl	0.451
utaow347	20	1.14	11.08	0.50	0.27	1753	0.21	0.06	0.27	D-O-Sl	0.541
utaow348	20	1.05	10.54	0.00	0.30	270	0.00	0.18	0.18	W-Sl	0.199
utaow349	20	1.13	9.86	0.51	0.69	1682	0.10	0.12	0.22	D-W-Sl	0.615
utaow350	20	1.13	9.91	0.49	0.60	1640	0.10	0.11	0.22	D-W-Sl	0.563
utaow351	20	1.13	9.85	0.50	0.50	1546	0.13	0.11	0.24	D-O-Sl/D-W-Sl	0.468
utaow352	20	1.15	9.61	0.51	0.40	1869	0.21	0.11	0.32	D-O-Sl	0.500

Table A3: WASP Experimental Data of air-oil-water flow in horizontal pipe (Campaign #3)

File Name	T (°C)	p (bar)	$U_{A,S}$ (m/s)	$U_{O,S}$ (m/s)	$U_{W,S}$ (m/s)	$\frac{dp}{dz}$ (Pa/m)	ε_L	Flow Pattern	Mean Slug frequency (Hz)
utaow391	20	1.11	7.57	0.21	0.00	275	0.19	O-Sl	0.192
utaow392	20	1.11	7.30	0.20	0.03	355	0.22	D-O-Sl	0.248
utaow393	20	1.11	7.26	0.20	0.06	377	0.23	D-O-Sl	0.231
utaow394	20	1.11	7.27	0.19	0.07	389	0.26	D-O-Sl	0.252
utaow395	20	1.11	7.32	0.21	0.11	452	0.29	D-O-Sl	0.299
utaow396	20	1.11	7.00	0.21	0.15	499	0.29	D-O-Sl	0.267
utaow397	20	1.11	7.52	0.20	0.20	475	0.29	D-O-Sl	0.275
utaow398	20	1.11	7.62	0.20	0.25	338	0.20	D-W-Sl	0.248
utaow399	20	1.11	7.62	0.20	0.30	288	0.20	D-W-Sl	0.206
utaow400	20	1.11	7.71	0.21	0.34	280	0.20	D-W-Sl	0.214
utaow401	20	1.11	7.68	0.21	0.40	317	0.18	D-W-Sl	0.276
utaow402	20	1.11	7.65	0.20	0.50	319	0.21	D-O-Sl	0.324
utaow403	16	1.11	9.78	0.20	0.30	280	0.19	D-O-Sl	0.186
utaow404	20	1.11	9.76	0.20	0.05	332	0.21	D-O-Sl	0.197
utaow405	20	1.11	9.63	0.20	0.08	337	0.22	D-O-Sl	0.216
utaow406	20	1.11	9.37	0.20	0.11	427	0.22	D-O-Sl	0.297
utaow407	20	1.11	9.36	0.19	0.15	475	0.24	D-O-Sl	0.316
utaow408	20	1.11	9.27	0.18	0.21	584	0.28	D-O-Sl	0.320
utaow409	20	1.11	9.42	0.21	0.28	329	0.17	D-W-Sl	0.300
utaow410	20	1.11	9.36	0.21	0.24	578	-	D-O-Sl	0.328
utaow411	20	1.11	9.76	0.21	0.02	348	0.16	D-O-Sl	0.210
utaow412	20	1.11	10.19	0.20	0.34	453	0.16	D-W-Sl	0.269
utaow413	20	1.11	9.76	0.20	0.00	294	0.16	O-Sl	0.150
utaow414	20	1.11	9.66	0.20	0.00	285	0.16	O-Sl	0.148
utaow415	20	1.10	9.10	0.21	0.17	620	0.25	-	0.333
utaow416	21	1.11	9.30	0.20	0.41	387	0.18	D-W-Sl	0.321

File Name	T (°C)	p (bar)	$U_{A,S}$ (m/s)	$U_{O,S}$ (m/s)	$U_{W,S}$ (m/s)	$\frac{dp}{dz}$ (Pa/m)	ε_L	Flow Pattern	Mean Slug frequency (Hz)
utaow418	19	1.11	9.33	0.20	0.50	417	0.18	D-W-Sl	0.299
utaow419	19	1.11	14.10	0.19	0.02	287	0.23	D-O-A	
utaow420	20	1.11	10.90	0.21	0.02	354	0.17	D-O-Sl	0.226
utaow421	15	1.11	7.56	0.19	0.16	586	0.31	D-O-Sl	0.253
utaow422	15	1.11	7.70	0.18	0.17	281	0.32	D-O-Sl	0.241
utaow423	15	1.11	7.63	0.18	0.17	666	0.32	D-O-Sl	0.269
utaow424	15	1.11	9.45	0.21	0.19	741	0.29	D-O-Sl	0.333
utaow425	20	1.11	9.39	0.20	0.19	730	0.27	D-O-Sl	0.379
utaow427	17	1.11	11.20	0.18	0.05	449	0.21	D-O-Sl	0.198
utaow428	17	1.11	11.20	0.19	0.09	378	0.22	D-O-Sl	0.212
utaow429	17	1.11	11.16	0.21	0.12	690	0.24	D-O-Sl	0.289
utaow430	17	1.10	11.98	0.21	0.14	744	0.25	D-O-Sl	0.365
utaow431	17	1.11	11.70	0.20	0.20	873	0.29	D-O-Sl	0.320
utaow432	16	1.11	8.81	0.21	0.17	769	0.29	D-O-Sl	0.343
utaow433	16	1.11	8.17	0.21	0.18	700	0.30	D-O-Sl	0.330
utaow434	16	1.11	8.69	0.20	0.20	780	0.33	D-O-Sl	0.281
utaow435	16	1.11	8.62	0.19	0.20	675	0.29	D-O-Sl	0.300
utaow436	16	1.11	9.78	0.19	0.24	439	0.19	D-W-Sl	0.273
utaow437	16	1.11	9.71	0.18	0.23	429	0.19	D-W-Sl	0.272
utaow438	16	1.11	9.70	0.18	0.01	321	0.19	D-O-Sl	0.208
utaow439	20	1.11	13.37	0.20	0.03	367	0.20	D-O-Sl	0.152
utaow440	20	1.11	13.83	0.19	0.03	363	0.21	D-O-Sl	-
utaow441	20	1.11	14.49	0.18	0.07	548	0.26	D-O-StA	-
utaow443	20	1.11	15.22	0.21	0.06	526	0.20	D-O-Sl	0.168
utaow444	20	1.11	15.22	0.21	0.07	598	0.20	D-O-Sl	0.265
utaow445	17	1.11	13.08	0.21	0.03	282	0.20	D-O-Sl	0.248
utaow446	17	1.11	12.84	0.20	0.06	408	0.21	D-O-Sl	0.228
utaow447	17	1.11	12.71	0.19	0.09	585	0.22	D-O-Sl	0.213
utaow448	17	1.11	12.31	0.21	0.15	720	0.25	D-O-Sl	0.315
utaow449	17	1.11	12.12	0.21	0.20	775	0.27	D-O-Sl	0.353
utaow450	17	1.11	11.99	0.20	0.23	805	0.30	D-O-Sl	0.260

Table A4: WASP Experimental Data of air-oil-water flow in horizontal pipe (Campaign #4)

File Name	T (°C)	P (bar)	$U_{a,s}$ (m/s)	$U_{o,s}$ (m/s)	$U_{w,s}$ (m/s)	Dp/dz (Pa/m)	ε_o	ε_w	ε_L	Flow Pattern	Mean Slug frequency (Hz)	Mean Slug Body Holdup	Mean Slug length (m)	Mean Slug velocity
uaow480	18	1.14	8.50	0.48	0.00	605	-	-	-	O-Sl	0.404	-	-	-
uaow481	18	1.14	8.70	0.45	0.05	540	-	-	-	D-O-Sl	0.364	-	-	-
uaow482	18	1.15	8.60	0.40	0.11	518	-	-	-	D-O-Sl	0.368	-	-	-
uaow483	18	1.15	8.60	0.36	0.15	518	-	-	-	D-O-Sl	0.411	-	-	-
uaow484	20	1.15	8.50	0.29	0.20	591	-	-	-	D-O-Sl	0.379	-	-	-
uaow485	20	1.16	8.40	0.27	0.25	637	-	-	-	D-O-Sl	0.358	-	-	-
uaow486	20	1.16	8.50	0.19	0.30	458	-	-	-	D-W-Sl	0.323	-	-	-
uaow487	19	1.14	8.60	0.00	0.50	255	-	-	-	W-Sl	0.267	-	-	-
uaow488	21	1.17	8.30	0.22	0.27	649	-	-	-	D-O-Sl	0.333	-	-	-
uaow489	21	1.15	8.40	0.33	0.16	520	-	-	-	D-O-Sl	0.402	-	-	-
uaow490	16	1.14	8.30	0.43	0.06	474	-	-	-	D-O-Sl	0.409	-	-	-
uaow491	25	1.18	12.10	0.51	0.00	536	-	-	-	O-Sl	0.353	-	-	-
uaow492	21	1.18	12.20	0.44	0.06	416	-	-	-	D-O-Sl	0.425	-	-	-
uaow493	21	1.18	12.30	0.36	0.13	392	-	-	-	D-O-Sl	0.354	-	-	-
uaow494	21	1.18	12.50	0.34	0.15	434	-	-	-	D-O-Sl	0.328	-	-	-
uaow495	22	1.20	12.40	0.28	0.22	508	-	-	-	D-O-Sl	0.225	-	-	-
uaow496	19	1.18	11.90	0.00	0.50	287	-	-	-	W-Sl	0.351	-	-	-
uaow497	22	1.14	8.10	0.44	0.06	665	-	-	-	D-O-Sl	0.369	-	-	-
uaow498	22	1.14	8.30	0.37	0.13	720	0.15	0.07	0.22	D-O-Sl	0.394	-	-	-
uaow499	21	1.15	8.20	0.34	0.15	723	0.15	0.08	0.23	D-O-Sl	0.396	-	-	-
uaow500	21	1.16	8.20	0.27	0.22	754	0.12	0.14	0.26	D-O-Sl	0.355	-	-	-
uaow501	22	1.16	8.20	0.21	0.28	784	0.10	0.18	0.28	D-W-Sl/D-O-Sl	0.356	-	-	-
uaow502	22	1.16	8.20	0.15	0.35	682	0.03	0.15	0.18	D-W-Sl	0.265	-	-	-
uaow503		1.15	8.30	0.21	0.29	756	-	-	-	D-W-Sl	0.287	-	-	-
uaow505	20	1.00	8.30	0.00	0.50	588	-	-	-	W-Sl	-	-	-	-
uaow506	23	1.16	7.90	0.23	0.27	553	0.12	0.20	0.31	D-O-Sl	0.333	-	-	-

File Name	T (°C)	P (bar)	$U_{a,s}$ (m/s)	$U_{o,s}$ (m/s)	$U_{w,s}$ (m/s)	Dp/dz (Pa/m)	ε_o	ε_w	ε_L	Flow Pattern	Mean Slug frequency (Hz)	Mean Slug Body Holdup	Mean Slug length (m)	Mean Slug velocity (m/s)
uaow507	23	1.15	6.70	0.21	0.27	375	0.08	0.18	0.26	D-W-Sl/D-O-Sl	0.257	-	-	-
uaow508	23	1.13	8.10	0.28	0.20	434	0.14	0.11	0.25	D-O-Sl	0.367	-	-	-
uaow509	23	1.14	6.80	0.26	0.23	392	0.15	0.16	0.31	D-O-Sl	0.311	-	-	-
uaow510	23	1.16	8.10	0.24	0.25	184	0.11	0.17	0.28	D-O-Sl	0.350	-	-	-
uaow511	24	1.15	6.80	0.23	0.26	401	0.14	0.18	0.32	D-W-Sl/D-O-Sl	0.295	-	-	-
uaow512	24	1.13	4.40	0.21	0.40	196	0.06	0.21	0.26	D-W-Sl	0.256	-	-	-
uaow513	24	1.14	4.20	0.25	0.67	190	0.04	0.24	0.28	D-W-Sl	0.367	-	-	-
uaow514	19	1.12	6.10	0.50	0.00	611	0.24	0.00	0.24	O-Sl	0.402	0.71	1.56	9.20
uaow515	19	1.13	6.40	0.44	0.05	627	0.23	0.02	0.25	D-O-Sl	0.392	0.67	1.17	8.16
uaow516	13	1.13	6.00	0.38	0.10	662	0.23	0.04	0.28	D-O-Sl	0.400	0.64	1.31	8.32
uaow517	19	1.13	6.00	0.35	0.14	731	0.22	0.07	0.29	D-O-Sl	0.389	0.66	1.49	8.33
uaow518	19	1.13	6.00	0.28	0.21	812	0.20	0.13	0.34	D-O-Sl	0.386	0.61	1.62	9.65
uaow519	19	1.13	6.00	0.23	0.25	688	0.16	0.15	0.31	D-O-Sl	0.298	0.614	2.00	8.27
uaow520	19	1.12	6.10	0.17	0.34	431	0.09	0.16	0.25	D-W-Sl	0.248	0.77	2.69	7.10
uaow521	19	1.12	6.10	0.11	0.40	317	-	-	-	D-W-Sl	0.190	0.78	3.30	7.52
uaow522	19	1.11	6.10	0.00	0.50	240	0.00	0.23	0.23	W-Sl	0.239	0.72	1.57	8.12
uaow523	18	1.14	6.00	0.28	0.23	843	0.15	0.17	0.32	D-W-Sl/D-O-Sl	0.325	0.63	2.69	10.45
uaow524	18	1.13	6.20	0.21	0.29	474	0.08	0.15	0.23	D-W-Sl	0.265	0.77	2.64	8.45
uaow525	18	1.13	6.20	0.24	0.25	579	0.11	0.13	0.24	D-W-Sl/D-O-Sl	0.288	0.70	2.49	10.56
uaow526	18	1.13	6.20	0.31	0.18	762	0.19	0.11	0.30	D-O-Sl	0.354	0.64	1.62	9.82
uaow527	18	1.14	6.20	0.27	0.22	857	0.18	0.15	0.34	D-O-Sl	0.364	0.61	1.38	9.38
uaow528	18	1.14	6.10	0.30	0.21	791	0.18	0.14	0.32	D-O-Sl	0.341	0.61	1.61	9.45
uaow529	18	1.11	4.30	0.00	0.49	368	0.00	0.22	0.22	W-Sl	0.186	0.87	2.89	6.58
uaow530	19	1.17	3.90	0.50	0.00	454	0.31	0.00	0.31	O-Sl	0.302	0.84	1.89	6.87
uaow531	19	1.17	3.90	0.26	0.24	444	0.16	0.17	0.34	D-W-Sl/D-O-Sl	0.301	0.78	2.15	6.88
uaow532	18	1.21	3.90	0.31	0.20	690	0.24	0.14	0.39	D-O-Sl	0.338	0.73	1.62	7.51
uaow533	19	1.12	4.10	0.45	0.04	544	0.30	0.01	0.31	D-O-Sl	0.325	0.81	1.51	7.50

File Name	T (°C)	P bar	$U_{a,s}$ m/s	$U_{o,s}$ (m/s)	$U_{w,s}$ m/s	Dp/dz (Pa/m)	ε_o	ε_w	ε_L	Flow Pattern	Mean Slug frequency (Hz)	Mean Slug Body Holdup	Mean Slug length (m)	Mean Slug velocity (m/s)
uaow534	19	1.12	4.20	0.40	0.09	609	0.27	0.05	0.32	D-O-Sl	0.372	0.79	1.51	7.10
uaow535	19	1.12	4.20	0.37	0.12	580	0.26	0.07	0.32	D-O-Sl	0.378	0.77	1.22	7.00
uaow536	18	1.12	4.20	0.26	0.23	511	0.16	0.14	0.30	D-W-Sl/D-O-Sl	0.272	0.79	1.71	6.88
uaow537	15	1.11	4.30	0.20	0.30	336	0.09	0.18	0.28	D-W-Sl/D-O-Sl	0.276	0.84	2.33	6.28
uaow538	18	1.12	4.40	0.24	0.26	427	0.14	0.15	0.29	D-W-Sl/D-O-Sl	0.261	0.83	2.02	6.4
uaow539	18	1.12	4.40	0.22	0.27	430	0.12	0.15	0.28	D-W-Sl/D-O-Sl	0.303	0.88	2.33	6.58
uaow540	18	1.12	4.40	0.21	0.28	418	0.11	0.16	0.28	D-W-Sl/D-O-Sl	0.291	0.86	2.86	6.41
uapw541	18	1.11	4.40	0.14	0.34	263	0.07	0.18	0.26	D-W-SL	0.222	0.86	2.86	6.41
uaow542	19	1.12	4.40	0.22	0.29	447	0.12	0.16	0.29	D-W-Sl/D-O-Sl	0.280	0.84	2.00	6.83
uaow543	19	1.13	4.10	0.29	0.21	812	0.22	0.17	0.40	D-O-Sl	0.384	-	1.63	7.75
uaow544	19	1.13	4.10	0.32	0.18	764	0.24	0.13	0.37	D-O-Sl	0.414	0.75	1.68	7.51
uaow545	19	1.13	4.20	0.29	0.20	743	0.22	0.15	0.37	D-O-Sl	0.395	0.75	1.42	8.18
uaow546	19	1.12	4.30	0.27	0.33	434	0.11	0.17	0.28	D-W-Sl/D-O-Sl	0.247	0.85	2.24	6.55
uaow547	17	1.12	4.30	0.59	0.00	551	0.32	0.00	0.32	O-Sl	0.376	0.84	1.37	6.68
uaow548	17	1.11	4.40	0.00	0.59	243	0.00	0.23	0.23	W-Sl	0.207	0.86	2.6	6.34
uaow549	18	1.11	4.30	0.19	0.41	354	0.08	0.20	0.27	D-W-Sl	0.232	0.87	3.2	6.37
uaow550	18	1.12	4.30	0.30	0.31	522	0.16	0.14	0.30	D-W-Sl/D-O-Sl	0.341	0.85	1.92	6.71
uaow551	18	1.12	4.30	0.33	0.27	639	0.17	0.14	0.31	D-O-Sl	0.379	0.78	1.6	7.83
uaow552	18	1.11	4.40	0.23	0.36	383	0.10	0.17	0.27	D-W-Sl	0.263	0.89	2.97	7.40
uaow553	17	1.12	4.10	0.44	0.05	536	0.32	0.01	0.33	D-O-Sl	0.356	0.78	-	-
uaow554	17	1.12	4.20	0.46	0.05	573	0.32	0.01	0.33	D-O-Sl	0.368	0.76	1.14	6.45
uaow555	17	1.12	4.10	0.38	0.10	617	0.31	0.04	0.35	D-O-Sl	0.359	0.75	1.14	6.65
uaow556	17	1.13	4.10	0.35	0.14	742	0.27	0.08	0.35	D-O-Sl	0.409	0.74	1.29	7.24
uaow557	17	1.13	4.10	0.34	0.16	776	0.28	0.09	0.37	D-O-Sl	0.425	0.73	1.29	7.03
uaow558	17	1.12	4.20	0.34	0.16	728	0.28	0.09	0.37	D-O-Sl	0.413	0.74	1.50	7.20
uaow560	17	1.12	4.10	0.41	0.09	634	0.31	0.03	0.34	D-O-Sl	0.386	0.76	-	-
uaow561	17	1.12	4.10	0.41	0.08	509	0.31	0.02	0.33	D-O-Sl	0.361	0.77	1.75	7.55
uaow562	17	1.12	4.10	0.46	0.03	550	0.31	0.01	0.32	D-O-Sl	0.356	0.78	1.21	6.98
uaow563	15	1.13	4.10	0.38	0.22	879	0.30	0.13	0.43	D-O-Sl	0.452	0.72	1.63	9.13
uaow564	17	1.12	4.20	0.43	0.16	768	0.31	0.07	0.37	D-O-Sl	0.467	0.78	1.16	6.802

File Name	T (°C)	P bar	$U_{a,s}$ m/s	$U_{o,s}$ (m/s)	$U_{w,s}$ m/s	Dp/dz (Pa/m)	ε_o	ε_w	ε_L	Flow Pattern	Mean Slug frequency (Hz)	Mean Slug Body Holdup	Mean Slug length (m)	Mean Slug velocity (m/s)
uaow565	17	1.12	4.10	0.53	0.07	661	0.33	0.02	0.34	D-O-Sl	0.419	0.83	-	7.12
uaow566	17	1.14	4.10	0.37	0.21	901	0.27	0.13	0.40	D-O-Sl	0.455	0.74	1.48	8.266
uaow568	17	6.04	4.30	0.00	0.49	189	0.00	0.23	0.23	W-Sl	0.273	0.70	-	-
uaow569	17	5.99	4.40	0.50	0.00	593	0.30	0.00	0.30	O-Sl	0.387	0.71	0.98	7.36
uaow570	17	6.03	4.30	0.21	0.28	310	0.16	0.18	0.35	D-W-Sl	0.114	0.66	-	-
uaow571	17	6.12	4.30	0.44	0.06	604	0.32	0.02	0.34	D-O-Sl	0.273	0.72	-	-
uaow572	17	6.03	4.30	0.40	0.10	625	0.27	0.05	0.32	D-O-Sl	0.300	0.74	1.16	6.5
uaow573	17	6.01	4.30	0.34	0.15	831	0.25	0.09	0.34	D-O-Sl	0.402	0.71	0.81	6.36
uaow574	18	6.09	4.20	0.29	0.20	992	0.25	0.14	0.38	D-O-Sl	0.341	0.68	0.82	7.21
uaow575	18	6.15	4.20	0.25	0.24	699	0.22	0.21	0.42	D-W-Sl/D-O-Sl	0.220	0.68	-	-
uaow577	18	11.14	4.10	0.50	0.00	960	0.30	0.00	0.31	D-O-Sl	0.392	-	0.86	5.86
uaow578	18	11.19	4.10	0.24	0.25	692	0.19	0.21	0.40	SStW	-	-	-	-
uaow579	18	11.14	4.20	0.39	0.10	575	0.36	0.08	0.44	D-O-St.A	-	-	-	-
uaow581	19	6.05	4.30	0.36	0.13	698	0.25	0.07	0.33	D-O-Sl	0.382	0.74	1.58	10.4
uaow582	18	6.16	4.10	0.32	0.19	872	0.25	0.11	0.36	D-O-Sl	0.425	0.69	1.13	7.28
uaow583	18	6.22	4.20	0.26	0.24	795	0.23	0.19	0.42	D-O-Sl	-	0.66	1.36	5.58
uaow584	16	6.16	2.26	0.21	0.05	303	0.35	0.05	0.40	D-O-Sl	0.211	-	-	-
uaow585	19	6.14	4.18	0.20	0.05	313	0.32	0.06	0.38	D-O-Sl	0.056	-	-	-
uaow586	18	6.09	6.11	0.20	0.05	290	0.28	0.05	0.33	D-O-St.A	-	-	-	-
uaow587	18	6.15	5.11	0.19	0.05	244	0.30	0.07	0.37	D-O-St.A	-	-	-	-
uaow588	18	6.07	4.38	0.19	0.05	251	0.32	0.07	0.39	D-O-St.A	-	-	-	-
uaow589	19	6.14	2.13	0.20	0.11	412	0.33	0.12	0.45	D-O-Sl	0.258	-	-	-
uaow590	19	6.12	6.09	0.20	0.10	552	0.23	0.09	0.32	D-O-Sl	0.079	-	0.93	3.27
uaow591	19	6.11	2.14	0.20	0.20	338	0.24	0.21	0.44	D-W-Sl/D-O-Sl	0.269	-	-	-
uaow592	19	6.03	7.08	0.20	0.05	363	0.25	0.05	0.30	D-O-St.A	-	-	-	
uaow593	19	6.02	7.04	0.20	0.09	481	0.23	0.08	0.31	D-O-St.A	-	-	-	
uaow594	19	6.19	7.01	0.20	0.16	852	0.21	0.12	0.32	DStW	-	-	-	
uaow595	19	6.15	7.09	0.21	0.19	848	0.19	0.15	0.35	D-StW	-	-	-	
uaow596	19	6.18	7.08	0.20	0.25	695	0.16	0.18	0.33	D-StW	-	-	-	
uaow597	19	6.09	5.08	0.20	0.24	638	0.17	0.21	0.38	D-StW	-	-	-	
uaow598	19	6.07	4.13	0.20	0.24	704	0.21	0.20	0.41	D-W-Sl/D-O-Sl	-	-	-	

File Name	T (°C)	P bar	$U_{a,s}$ m/s	$U_{o,s}$ (m/s)	$U_{w,s}$ m/s	Dp/dz (Pa/m)	ε_o	ε_w	ε_L	Flow Pattern	Mean Slug frequency (Hz)	Mean Slug length (m)	Mean Slug velocity (m/s)
uaow599	21	6.42	1.46	0.25	0.05	182	0.41	0.04	0.46	S.D-O-Sl	0.247	1.51	3.33
uaow600	21	6.37	1.29	0.18	0.10	285	0.39	0.12	0.51	S.D-O-Sl	0.305	-	-
uaow601	21	6.34	1.47	0.19	0.09	287	0.38	0.10	0.48	S.D-O-Sl	0.298	1.17	3.49
uaow602	21	6.40	1.52	0.14	0.15	262	0.32	0.20	0.52	S.D-O-Sl	0.218	1.52	3.94
uaow603	21	6.45	1.42	0.21	0.08	273	0.40	0.07	0.48	D-O-Sl	0.292	1.01	3.42
uaow604	23	1.12	6.36	0.20	0.04	366	0.23	0.01	0.24	D-O-Sl	0.222	1.62	11.11
uaow605	22	1.12	6.33	0.18	0.09	475	0.22	0.04	0.26	D-O-Sl	0.295	1.17	8.47
uaow606	23	1.13	6.19	0.21	0.16	574	0.22	0.09	0.31	D-O-Sl	0.311	-	-
uaow607	23	1.13	6.21	0.19	0.20	552	0.20	0.11	0.31	D-W-Sl/D-O-Sl	0.248	2.33	9.65
uaow608	23	1.13	6.27	0.21	0.25	487	0.16	0.12	0.27		0.267	2.17	9.31
uaow609	23	1.13	6.22	0.19	0.28	484	0.14	0.11	0.25	D-W-Sl	0.294	1.91	8.01
uaow610	24	1.12	4.01	0.21	0.17	555	0.25	0.12	0.37	D-O-Sl	0.294	1.19	6.95
uaow611	25	1.13	4.10	0.21	0.19	597	0.25	0.14	0.38	D-O-Sl	0.357	1.43	7.13
uaow612	21	11.07	2.04	0.19	0.05	194	0.36	0.06	0.42	S.D-O-Sl	0.187	-	-
uaow613	21	11.06	2.13	0.20	0.09	119	0.30	0.12	0.43	SSl	0.110	-	-
uaow614	21	11.02	2.16	0.19	0.15	167	-	-	-	SSl	0.105	-	-
uaow615	22	11.14	2.13	0.18	0.18	181	0.21	0.19	0.40	SSl	0.150	-	-
uaow617	21	6.00	1.47	0.20	0.04	184	0.41	0.05	0.46	S.D-W-Sl	0.217	-	-
uaow618	21	6.07	1.47	0.21	0.21	196	0.22	0.20	0.42	D-W-Sl	0.209	1.80	3.14
uaow619	20	6.13	2.13	0.21	0.21	270	0.20	0.21	0.41	D-O-Sl	0.255	1.64	4.29
uaow620	21	5.93	4.20	0.22	0.11	537	0.22	0.09	0.31	D-O-Sl	0.289	-	-
uaow621	20	6.05	5.11	0.22	0.10	537	0.23	0.07	0.29	D-W-Sl	0.218	1.09	5.78
uaow622	21	6.07	4.08	0.20	0.28	423	0.13	0.22	0.34	D-O-Sl	0.217	-	-
uaow623	21	6.11	4.13	0.20	0.19	826	0.22	0.16	0.38	D-O-StW	0.268	-	-
uaow624	20	-	6.10	0.20	0.20	953	0.21	0.15	0.35	D-W-StW/D-WSl	-	-	-
uaow625	21	-	6.10	0.20	0.30	341	0.13	0.20	0.33	D-W-Sl	-	-	-
uaow626	21	6.14	5.22	0.20	0.39	489	0.08	0.17	0.24	D-W-Sl	0.265	1.89	8.32
uaow627	22	6.02	1.47	0.20	0.30	135	0.20	0.22	0.42	D-W-Sl	0.211	-	-
uaow628	21	6.10	2.16	0.21	0.30	199	0.16	0.21	0.37	D-W-Sl	0.190	-	-
uaow629	21	6.11	3.17	0.21	0.05	301	0.30	0.04	0.35	D-O-Sl	0.175	-	-
uaow630	21	6.05	3.17	0.20	0.20	397	0.30	0.07	0.38	D-O-Sl	0.261	-	-
uaow631	21	6.08	3.11	0.20	0.20	491	0.25	0.19	0.44	D-O-Sl	0.189	-	-

File Name	T (°C)	P bar	$U_{a,s}$ m/s	$U_{o,s}$ (m/s)	$U_{w,s}$ m/s	Dp/dz (Pa/m)	ε_o	ε_w	ε_L	Flow Pattern	Mean Slug frequency (Hz)	Mean Slug length (m)	Mean Slug velocity (m/s)
uaow632	21	6.11	3.05	0.20	0.30	373	0.15	0.21	0.36	D-W-Sl	0.299	-	-
uaow633	21	1.12	3.07	0.22	0.03	250	0.35	0.01	0.36	D-O-Sl	0.211	-	-
uaow634	21	1.12	3.08	0.21	0.11	382	0.30	0.09	0.39	D-O-Sl	0.300	-	-
uaow635	21	1.12	3.14	0.19	0.22	341	-	-	-	D-W-Sl/D-O-Sl	0.241	-	-
uaow636	22	1.12	3.17	0.22	0.36	266	0.14	0.17	0.30	D-W-Sl	-	-	-

Flow Pattern Terminology

1. D-St.S Dispersed Stratified Smooth Flow
2. D-St.W Dispersed Stratified Wavy Flow
3. D-W-Sl Dispersed Water-Continuous Slug Flow
4. D-W-St.A Dispersed Water-Continuous Stratifying-Annular Flow
5. D-O-Sl Dispersed Oil-Continuous Slug Flow
6. D-O-A Dispersed Oil-Continuous Annular Flow
7. S.D-O-Sl Separated Dispersed Oil-Continuous Slug Flow
8. S-D-W-Sl Separated Dispersed Water-Continuous Slug Flow
9. D-O-St.A Dispersed Oil-Continuous Stratifying Annular flow

Appendix B:

Definition of Statistical Errors

A number of statistical parameters have been used to assess the performance of the correlations and these are explained here.

The Average Relative Error (ARE) is defined by the expression (B1) and gives an indication of whether the correlation over-predicts or under-predicts the entire data set.

$$ARE = \frac{1}{N}\sum_{i=1}^{N}\frac{P_i - M_i}{M_i} \tag{B1}$$

Where P_i is the predicted parameter for instance pressure gradient and M_i is the measured parameter

The drawback of using the Average Relative Error alone, is that the under-prediction and over-prediction of some of the data may cancel out, resulting in a deceptively smaller value in the average error. Use of the Average Relative Absolute Error (ARAE) eliminates this:

$$ARAE = \frac{1}{N}\sum_{i=1}^{N}\frac{|P_i - M_i|}{M_i} \tag{B2}$$

The Standard Deviation SD1 indicates the scatter of the data around the average relative error and is defined by:

$$SD1 = \sqrt{\sum_{i=1}^{N}\frac{\left[\frac{P_i - M_i}{M_i} - ARE\right]^2}{N-1}} \tag{B3}$$

The above-mentioned statistical parameters are based on the relative error instead of the absolute error. This makes the error dependent on the magnitude of the measurements. To avoid this, another set of statistical parameters have been used:

Average Error (AE)

$$AE = \frac{1}{N}\sum_{i=1}^{N}P_i - M_i \tag{B4}$$

Average Absolute Error (AAE), which is defined by the expression:

$$AAE = \frac{1}{N}\sum_{i=1}^{N}|P_i - M_i| \tag{B5}$$

And the standard deviation (SD2) based on the error is defined by:

$$SD2 = \sqrt{\sum_{i=1}^{N}\frac{[(P_i - M_i) - AE]^2}{N-1}} \tag{B6}$$

Brigham Young Univ.